Thermodynamic Optimization and Electromagnetic Control of the Adsorption Processes in the Refrigeration Technology

Dissertation

zur Erlangung des akademischen Grades

Doktoringenieur
(Dr. -Ing.)

vorgelegt der
Fakultät für Maschinenbau der
Technischen Universität Ilmenau

von Herrn
M. Sc. Majd Ali
Geboren am 20. 01.1986 in Tartous/Syrien

1. Gutachter: apl. Prof. Dr. -Ing. habil. Christian Karcher
2. Gutachter: Prof. Dr. -Ing. habil. Salman Ajib
3. Gutachter: Univ.-Prof. Dipl. -Ing. Dr. Wolfgang Streicher

Tag der Einreichung: 04.07.2018
Tag der wissenschaftlichen Aussprache: 14.12.2018

urn:nbn:de:gbv:ilm1-2018000523

Zusammenfassung

Das Ziel dieses Promotionsvorhabens ist es, die Adsorptionskälteanlage zu optimieren und die großen Entwicklungshindernisse der Adsorptionskältetechnik zu überwinden. Beispiele hierfür sind die geringe Leistungszahl und die lange Zykluszeit zur Erzeugung des Kältemittels, die sich je nach den verwendeten Arbeitspaaren und der Fahrtemperatur unterscheidet. Ein weiteres Problem stellt das intermittierende Arbeitsprinzip für den einfachsten Zyklus eines Adsorptionskühlsystems dar. Daher wird in dieser Arbeit eine analytische, thermodynamische und numerische Untersuchung eines Neubaus einer Adsorptionskälteanlage für Gefrieranwendungen vorgestellt. Dieses neuartige System, das in dieser Promotion als kombiniertes Adsorptions- Eisproduktionssystem (com-AIP-System) bezeichnet wird, verwendet zwei verschiedene Adsorptionsmaterialien zusammen in einer Maschine. Die Hauptziele der vorliegenden Arbeit sind: Erhöhung der pro Zyklus erzeugten Eismenge, Erzeugung von kontinuierlicher Kälteleistung, Verbesserung der Zykluszeit und Einsparung der erforderlichen Eingangswärme durch Erhöhung der Massenstromrate des Kältemittels. Dieses Kältemittel verlässt den Adsorptionsreaktor und fließt in Richtung des Kondensators. Um dies zu erreichen, umfasst das com-AIP-System zwei Adsorptionsreaktoren. Der erste Adsorptionsreaktor ist mit Silikagel und der zweite mit Aktivkohle als Adsorptionsmittel gefüllt. Methanol wurde als Adsorbat und Kühlmittel mit beiden Reaktoren verwendet. Das com-AIP-System ermöglicht die Nutzung der Vorteile der physikalischen Eigenschaften der Adsorbentien SG und AC. Diese vorgeschlagene Strategie des AIP-Systems unterscheidet sich vollständig von den herkömmlichen Adsorptionsreaktoren, die mit einem Adsorptionsmittel in einem oder in zwei Reaktoren gefüllt sind.

Im zweiten Teil dieser Arbeit wird eine numerische und analytische Untersuchung der Wirkung der HTF-Strömung vorgestellt. Die Desorption und Leistung des Adsorptionsreaktors wird ausgewertet. Die Wirkung der HTF-Natur wird für die gleichen Adsorptionsreaktoren (SG- und AC-Reaktoren) betrachtet, die zum Desorbieren von 1 kg Methanol erhitzt wurden. Um den HTF-Flow-Natur-Effekt zu untersuchen, wurde die Variation der Reynolds-, Nusselt- und Biot-Zahlen hinsichtlich ihrer Auswirkungen auf die Temperaturverteilung durch beide Reaktoren beobachtet.

Die Verwendung der thermischen Heizung, wie Abwärme oder Solarenergie der Industrie, hat einige schwerwiegende Nachteile bei der Entwicklung der Adsorptionstechnologie. Der größte Nachteil ist, dass der Adsorptionsreaktor eine lange Zeit von etwa einer Stunde benötigt um die erforderliche Menge des Adsorbats zu desorbieren. Darüber hinaus hat der Adsorptionsreaktor einen komplexen Aufbau, welcher aus Rohren mit heißem Wasser und einer Vielzahl an Heizrippen besteht. Um die Probleme konventioneller Methoden (thermisches Heizen) zu überwinden, wird im Rahmen dieser Arbeit ein neues Design vorgestellt. Dieses besteht aus zwei gleichen Adsorptionsreaktoren mit einer neuen Wärmequelle (Induktionserwärmung). Das Dissertationsprojekt behandelt auch eine mathematische Modellierung und numerische Simulation eines Induktionsheizsystems für zwei Adsorptionsreaktoren, gefüllt mit Silikagel und Aktivkohle als Adsorptionsmaterial sowie Methanol als Adsorbat. Der Zweck dieser Untersuchung war die Verwendung der elektromagnetischen Induktionstechnologie als eine neue Wärmequelle des Adsorptionseis-Produktionssystems. Die Induktionsheizung wird mit der thermischen Beheizung verglichen. Dazu werden die beiden thermischen und induktiven Adsorptionsreaktoren ausgelegt, um die gleiche desorbierte Kältemittelmenge von 1 kg zu erzeugen. Dieser Aufbau wurde unter gleichen Betriebs- und Randbedingungen getestet. Für die numerische und mathematische Modellierung werden die Programme **A**NSYS **E**lectronics, **A**NSYS **F**luent und **M**ATLAB verwendet.

Abstract

This PhD project is set out to optimize the adsorption refrigeration system and to overcome the big obstacles facing development of the adsorption refrigeration technology such as the low coefficient of performance, the intermittent work principle for the simplest cycle of an adsorption refrigeration system and the long cycle time to generate the refrigerant which differs based on the working pairs used and the driving temperature. Therefore an analytical, thermodynamic and numerical investigation of a new construction of an adsorption refrigeration system using for freezing applications is presented in this work. This novel system, named in this work as the combined **A**dsorption **I**ce **P**roduction system (com-AIP system), utilizes two different adsorption materials together in one machine. The main aims of the present work are: enhancing the amount of ice produced per cycle, producing continuous refrigeration power, improving the cycle time and saving of the required input heat by increasing the mass flow rate of the refrigerant, which leaves the adsorption reactor and flows toward the condenser. To achieve that, the com-AIP system comprises with two adsorption reactors, that the first adsorption reactor was filled by silica gel and the second by activated carbon as adsorbents. Methanol was used as adsorbate and refrigerant with both the reactors.

The com-AIP system allows using the advantages of physical properties of both the adsorbents SG and AC. This suggested strategy of com- AIP system is completely different from the conventional adsorption reactors, which are filled with one adsorbent in one reactor or in two reactors.

The second part of this theses presents a numerical and analytical investigation of effect of the flow nature and effect the adsorption reactor design on the desorption process and the performance. The effect of the HTF-nature has been studied for the same adsorption reactors (SG- and AC- reactors), which are heated to desorb $1\mathrm{kg}_{\mathrm{meth}}$ of methanol. In order to study the HTF- flow nature effect, the variation of the Reynolds, Nusselt and Biot numbers have been investigated to demonstrate their effects on the temperature distribution through both the adsorption medium.

Using the thermal heating such as industry waste heat or solar energy has some severe drawbacks in the development of adsorption technology. A major disadvantage is the adsorption reactor requires a long time of about one hour to desorb the required amount of the adsorbate. Moreover the adsorption reactor setup has a complex design, composed of tubes of hot water and many fins. In order to overcome the problems found with conventional methods (thermal heating), a new design of two adsorption reactors with a new heat source (induction heating) is studied and simulated in frame of this work. So that the PhD project deals also with a mathematical modeling and numerical simulation of an induction heating system for the same adsorption reactors filled by silica Gel and activated carbon as adsorption material and methanol as adsorbate. The purpose of this study was the use of electromagnetic induction technology as a new heat source of the adsorption ice production system. The induction heating technology has be compared with thermal heating, therefore, the two finned-tube heat exchangers using the thermal heating and the two adsorption reactors using the induction heating were designed in order to generate the same desorbed refrigerant amount of $1\mathrm{kg}_{\mathrm{meth}}$ and to work under the same operating and boundary conditions. Therefore, our investigation was carried out by a numerical and mathematical modelling with the **A**NSYS **E**lectronics, **A**NSYS **F**luent and **M**ATLAB Software, which can be help in this field.

Contents

Nomenclature

Symbol	SI Unit	Quantity
B	$[T]$	Magnetic flux density
B_f	$[m]$	Fin width
b_w	$[m]$	Winding width
COP	$[-]$	Coefficient of performance
C_p	$[J/kg.K]$	Specific heat capacity at constant pressure
C_v	$[J/kg.K]$	Specific heat capacity at constant volume
C_{ice}	$[J/kg.K]$	Ice specific heat capacity
C_{res}	$[F]$	Resonant capacitor
D_C	$[m^2/sec]$	Surface diffusion coefficient
D_{so}	$[1/sec]$	Mass transfer coefficient of adsorbent
D_a	$[m]$	Diameter of the adsorption container
D_i	$[m]$	Internal diameter of the induction coil
D_o	$[m]$	External diameter of the induction coil
E	$[V/m]$	Electric field intensity
E_a	$[J/kg]$	Activation energy of surface diffusion
E_{gen}	$[W]$	Energy generation within the Gr-ball
f_1 f_2	$[-]$	correction factors
$\dot{g}$	$[W/m^3]$	Heat generation per unit volume within adsorption-medium
H	$[A/m]$	Magnetic field intensity
H_f	$[m]$	Fin height
H_a	$[m]$	Height of the adsorption container
H_I	$[m]$	Height of the induction coil
h	$[J/kg]$	Specific enthalpy
H_{ads}	$[J/kg]$	Adsorption heat per unit mass of methanol
I	$[A]$	Electric current passing the coil (Inductor current)
I_E	$[A]$	Current passing the work- load
I_s	$[A]$	Secondary current of the transformer circuit
I_P	$[A]$	Primary current of the transformer circuit
i		Number of the Gr-balls
J	$[A/m^2]$	Electric current density (Induced current density in the Balls)
K_N	$[-]$	Nagaoka factor
L_{cond}	$[J/kg]$	Latent energy of condensation
L_{evap}	$[J/kg]$	Latent energy of vaporization
L_{ice}	$[J/kg]$	Latent heat of ice fusion
L	$[H]$	Inductance
L_t	$[m]$	Length of the HTF-channel
M	$[kg]$	Mass
$\dot{M}$	$[kg/s]$	Mass flow rate
N	turns	Number of the loops
N_s	turns	Turns in the secondary circuit
N_p	turns	turns in the primary circuit
n_f		Number of the fins
p	$[Pa]$	pressure
P_a	$[W]$	Active power
p_v	$[W/m^3]$	Heat generation per unit volume of Gr-ball/ Joule heat density
P_l	$[m]$	Coil pitch
P_E	$[W]$	Induced power inside Gr-balls
P_{in}	$[W]$	Total input power
Q	$[kJ]$	Heat amount
Q_r	$[V.A.R]$	Reactive power
$\dot{Q}$	$[W]$	Heat rate
Q_e	$[J]$	Refrigeration energy
R_a	$[J/kg.K]$	Gas constant of the adsorbate
R	$[\Omega]$	Ohmic resistance
R_1	$[m.K/W]$	Channel metal/secondary fluid convective heat transfer resistance
R_2	$[m.K/W]$	Conductive heat transfer resistance through the HTF- channel wall
R_3	$[m.K/W]$	Conductive heat transfer resistance through the adsorption particles
R_4	$[m.K/W]$	Channel metal/ fins metal heat transfer resistance
$R_{c,1}$	$[m.K/W]$	Contact resistance between the copper and the adsorbent

$R_{c,2}$	$[m.K/W]$	Contact resistance between the copper and aluminum
R_I	$[\Omega]$	Ohmic resistance of the coil
R_E	$[\Omega]$	Ohmic resistance of the work-load
r_i	$[m]$	Radius of Gr-ball/HTF-tube
r_o	$[m]$	Radius of spherical adsorption-medium
r_f	$[m]$	Fins radius
r_p	$[m]$	Adsorbent particle radius
S	$[V.A]$	Complex power (Appearance Power)
S_I	$[m]$	Thickness of the coil-wall
S_f	$[m]$	Fin spacing
SCP	$[W/kg]$	Specific cooling power
T	$[°C]$	Temperature
t	$[sec]$	time
U	$[W/m^2.K]$	Overall heat transfer coefficient
U_S	$[Volt]$	Voltages in the secondary circuit
U_P	$[Volt]$	Voltages in the primary circuit
u_z	$[m/s]$	Input fluid velocity
u_a	$[J/kg]$	Specific internal energy
U_a	$[J]$	Total internal energy
V	$[m^3]$	Emptied volume
V_a	$[m^3]$	Volume of the adsorption reactor
V_{Gr}	$[m^3]$	Volume of Gr-ball
V_S	$[m^3]$	Volume spherical adsorption-medium
V_0	$[m^3/kg]$	Maximum adsorption capacity of adsorbate
x	$[kg_a/kg_s]$	Uptake value of adsorbate (concentration)
X_E	$[\Omega]$	Work-load reactance
X_K	$[\Omega]$	Reactance of the air gab
X_R	$[\Omega]$	Reactance of the leakage flux
X_I	$[\Omega]$	Coil reactance
x_0	$[kg_a/kg_S]$	Initial of adsorbate concentration
Z	$[\Omega]$	Impedance
z	$[-]$	Wetness fraction
D, K, n	$[-]$	Dubinin-Astakhov constants
β	$[-]$	Porosity of the solid adsorbent medium
λ	$[W/m.K]$	Thermal conductivity
$\emptyset$	$[-]$	Adsorbate volume fraction
ω	$[rad/sec]$	Angular frequency
f	$[Hz]$	Heating frequency
μ	$[H/m]$	Absolute magnetic Permeability
μ_0	$[H/m]$	Permeability of free space
μ_r	[-]	The relative Permeability
δ	$[m]$	Skin depth
δ_f	$[m]$	Fin thickness
σ	$[S/m]$	Electrical Conductivity
ξ	$[m]$	Tube thickness
ρ	$[kg/m^3]$	Volumetric mass density
μ_m^s	$[-]$	Efficiency of refrigerant mass utilization
φ and Ψ	$[-]$	impedance correction factors
ϵ_r	$[-]$	Relative Error

Dimensionless Groups

Symbol		Description
A	$[-]$	Area ratio
Bi	$[-]$	Biot number
C_r	$[-]$	Conversion ratio
F_S	$[-]$	Fin spacing factor
F_L	$[-]$	Channel length factor
NTU	$[-]$	Number of transfer unit
Nu	$[-]$	Nusselt Number
Pr	$[-]$	Prandtl number
Re	$[-]$	Reynolds number
R_λ	$[-]$	Thermal conductivity ratio
R_G	$[-]$	Heat exchanger geometry ratio
R	$[-]$	Dimensionless distance
X	$[-]$	Dimensionless concentration
ξ_{metal}	$[-]$	Metal components factor
$\mathcal{E}$	$[-]$	Heat transfer effectiveness
ε_a	$[-]$	Adsorbate number
ε_F	$[-]$	Heat transfer fluid number
ε_v	$[-]$	Vapor adsorbate number
ε_{Gr}	$[-]$	Heat source number
ε_S	$[-]$	Adsorbent number
ε_r	$[-]$	Aspect ratio
ψ	$[-]$	Non-dimensional switching frequency of the adsorption reactor
θ	$[-]$	Dimensionless temperature
τ	$[-]$	Dimensionless time

Subscripts

h	Hot water to adsorption reactor	b	Bed/ Heat exchanger/Adsorber/desorber
ca	Cooling water to adsorption reactor	r	Reactor
co	Cooling water to condenser	a	Adsorbate phase of methanol
ch	Chilled water to evaporator	v	Vapor phase of methanol
evap	Evaporator	E	Work-load
cond	Condenser	res	Resonant
des	Desorption	sat	Saturation
ads	Adsorption	ave	Average
heat	Heating	max	Maximum
cool	Cooling	min	Minimum
SG	Silica gel	eq	Equivalent/ Equilibrium
AC	Activated carbon	tot	Total
Cu	Copper	amb	Ambient or atmospheric
Al	Aluminum	sim	Simulation
Gr	Graphite	exp	Experiment
S	Sorption material	s	Secondary
meth	Methanol	p	Primary
ref	Refrigerant	AIP	Adsorption Ice Production
ice	Ice	com	Combined
f	Fin	HTF/F	Heat Transfer Fluid
t	Tube	LDF	Linear driving force
mc	Metallic components of the generator	IH	Induction Heating
in	Inlet/Input	V.A.R	Volt-Amps-Reactive
out	Outlet/Output	div	Divergence Operator
add	Added	grad	Gradient operator
gen	Generated	req	Required

Chapter 1

Introductory Background

1.1 Introduction

Assuming that the earth has a human body and feelings, our earth looks old and tired, because the purpose of any research work is always achieving a comfortable indoor environment at the expense of the earth´s comfort. With the growth in people's living standards, the demand for refrigeration systems which is required for cold production and storage applications, food and vaccines transportation, comfort cooling, retails and supermarket display has been continuously increasing. So that, only in the US, the demand for commercial refrigeration equipment is forecast to increase 3.1 percent annually through 2020 to 11.3 $ billion [1].

Currently, most of the above demand is met by mechanical vapor compression systems driven by high grade electrical power inputs. Consequently, there has been a significant increase in electricity consumption, especially in high demand times. Refrigeration and air conditioning systems consume around 30 % of total worldwide energy consumption [2].

In addition, the traditional refrigeration systems utilize environmentally harmful refrigerants, because the refrigerants contain chlorofluorocarbons (CFCs) and hydrochlorofluorocarbons (HCFCs), which can act as catalytic agents and accelerate the depletion of the ozone layer. Based on the new environmental regulations (Kyoto protocol, Vienna Convention and Montreal Protocol) CFCs and HCFCs phase-out have been agreed. Moreover, countries may seek to limit the HFCs-use in order to meet its legally binding greenhouse gas emissions targets. Therefore, the need to develop the refrigeration technology by looking for alternative solutions to the current refrigeration technology is required [3-5].

In recent years the adsorption refrigeration technology, named green refrigeration technology, has been attracting more and more attention. The adsorption refrigeration systems will be the fastest growing types, because they have important advantages in comparing with the electrical driven air-conditioning and other refrigeration systems.

Their advantages are: **Low electricity consumption because of two reasons:** (1) The adsorption systems could be driven by low-grade energy such as industry waste heat or solar energy, unlike conventional systems which stress the electrical grid in summer whereas plenty of solar energy is available and could be used for refrigeration applications. (2) Lack of a pump from the system components, so electricity is only required for the switching valves and the control unit.

Environmentally friendly feasible technology: The adsorption refrigeration systems don’t have to use ozone-depleting CFCs and don’t need electricity or fossil fuels as driving sources, because adsorption cycles possess the advantage of employing natural and low global warming potential (GWP) refrigerants (water, methanol, ethanol, etc.).

Mechanical simplicity and high reliability because of their simple configuration, so they have no moving parts. The potential of maintenance effort and costs are low [3-8].

But on the other hand, the adsorption refrigeration systems have still some disadvantages such as slightly low coefficient of performance (COP) and careful design of the external hydraulic circuits because of the cyclic temperature variation. Furthermore, to date there are only a few manufacturers companies that design and develop adsorption systems for sale on the commercial market place and the commercially available machines are expensive and only some suppliers are on the market. In spite of these disadvantages, the adsorption technology will be the prospering technology and an excellent replacement for the conventional system in the foreseeable future.

In the last four decades, the adsorption refrigeration systems are laboratory and commercially developed to be applied in different applications. So that many researchers are still interested in the optimizing of the adsorption refrigeration system both numerically and experimentally. Therefore, the present study deals with a novel strategy of combined adsorption ice production system using two adsorption reactors, which utilizes two different adsorption materials in one machine. Using the induction heating technology as a new heat source in the adsorption system will be mathematically, physically and numerically investigated using a new design of two adsorption reactors filled with two adsorption materials.

1.2 Adsorption system

The adsorption systems generate refrigeration effect through the adsorption process on porous material. The adsorption refrigeration system is similar to the basic vapor compression refrigeration machines except that the power compressor is replaced by a thermally driven compressor which is the adsorption reactor (adsorption bed) [9].

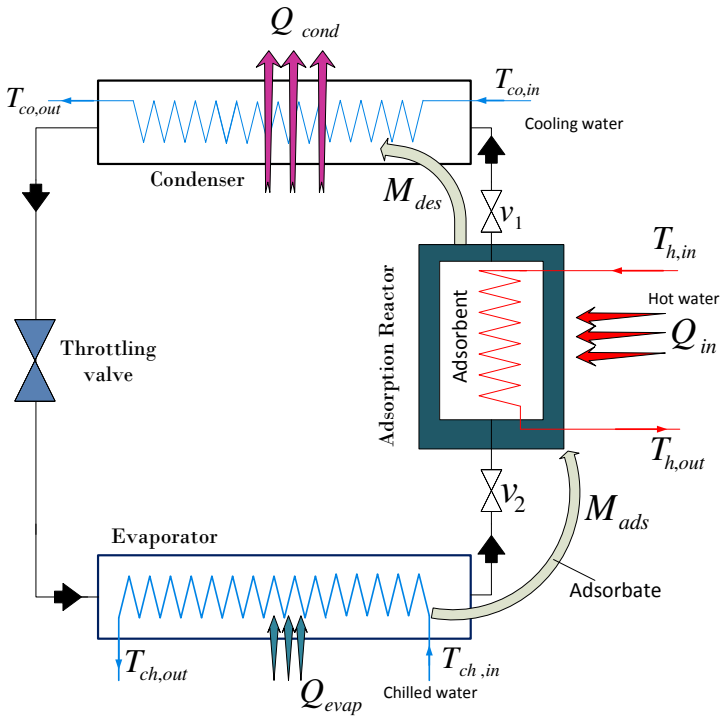

Figure 1.1: The simple adsorption refrigeration system

The adsorption reactor is composed of a working pair which consists of a solid adsorption medium (adsorbent) and refrigerant (adsorbate). **F**ig. 1.1 shows the schematic diagram of the conventional adsorption system which works using one working pair of adsorbent/adsorbate. The major components of the simplest adsorption system are one adsorption reactor, a condenser, an evaporator, a throttling device and 2 one-way control valves [10].

1.2.1 The thermodynamic cycle

The Adsorption refrigeration cycle is a thermodynamic cycle consisting of two cycles: the first is the adsorption/desorption cycle and the second is the refrigeration cycle. As shown in **F**ig. 1.2 the adsorption refrigeration cycle operates with two heat sources and two sinks using three temperature levels. The ambient temperature is considered as a heat source for the evaporator and as a heat sink for the adsorption reactor (adsorber) and the condenser [6,11].

Many thermodynamic adsorption cycles have been developed and investigated in order to enhance performance of the solid-adsorption system and to save the input heat supplied to the system. The thermodynamic adsorption cycles presented in the literature vary from the simplest cycles to more complex system utilizing mass or heat recovery, internal heat regeneration and thermal wave systems [6,10].

In the framework of this thesis a new thermodynamic cycle will be investigated in the third and fourth chapters. In order to know the new investigated cycle of the **A**dsorption **I**ce **P**roduction (AIP) system, which utilizes two adsorption reactors (two beds) using two adsorption materials together and one adsorbate, a brief thermodynamic analysis of the basic cycle is presented firstly here in this section. Usually the typical basic cycle of the simplest system is an intermittent cycle and produces an intermittent refrigeration effect. This is because the simplest adsorption system as shown in **F**ig. 1.1 consists of one adsorption reactor, which cannot work as desorber and adsorber at the same time.

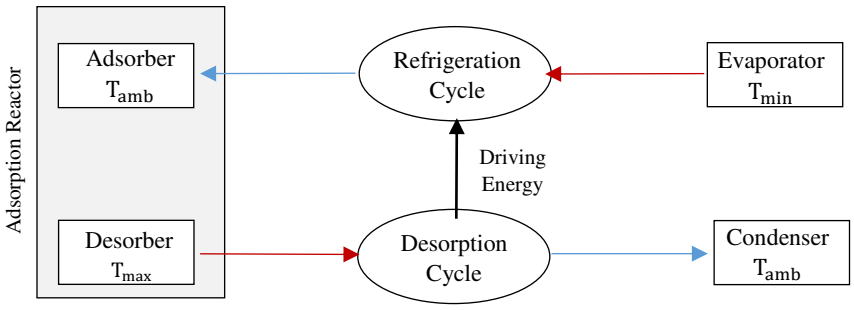

Figure 1.2: Basic thermodynamic cycle of the adsorption system

Fig. 1.3 presents the basic thermodynamic cycle of the simplest adsorption refrigeration system in a (p, T) diagram. The working principle of the idealized basic adsorption refrigeration cycle includes seven processes: Isosteric heating (1 → 2), Isobaric heating and desorption (2 → 3), Isosteric cooling (3 → 4), Isobaric cooling and adsorption (4 → 1), Condensation (A → B), Expansion (B → C) and Evaporation (C → D).

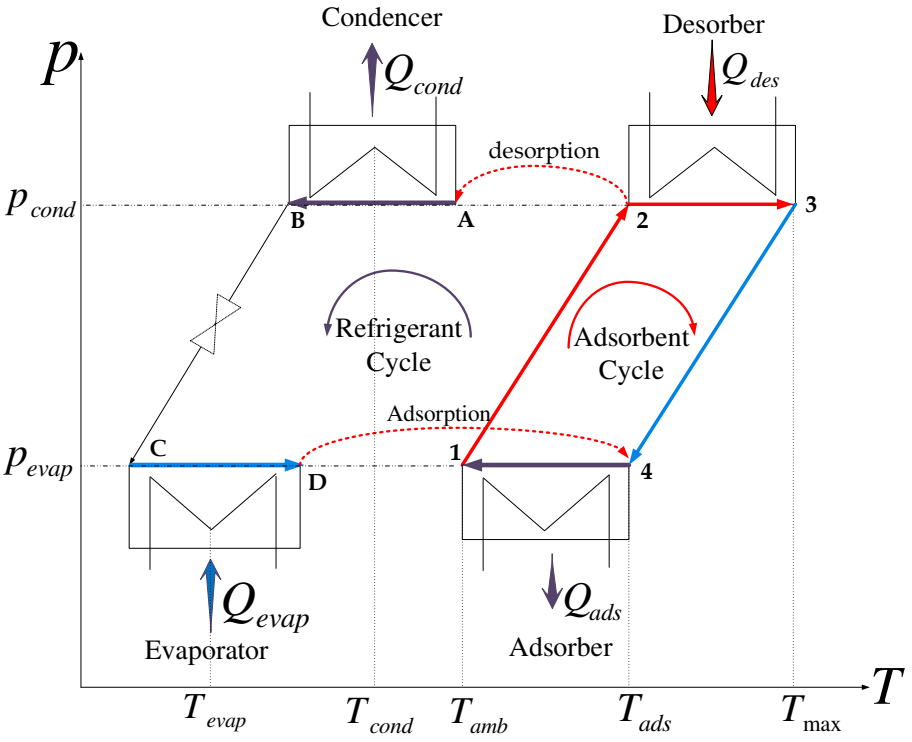

Figure 1.3: Clapeyron diagram for the basic adsorption refrigeration thermodynamic cycle

1.2.2 The working principle

The detailed description of the working principle of the simplest adsorption system is as follows:

Originally the adsorption reactor contains a maximum uptake of the refrigerant x $[kg_a/kg_S]$ and is disconnected from the condenser and the evaporator, where both the valves v_1 and v_2 are closed. During the process $1 \rightarrow 2$ the adsorption reactor receives heat using an external heat source T_{max} (the first heat source) thus both the temperature and pressure inside the reactor rises. During this stage the adsorbate mass is considered to remain unchanged ($x = const$) and the pressure of the adsorption reactor rises from the evaporation pressure to the condensation pressure (state 2), then the valve v_1 is opened and the condensing pressure dominates the adsorption reactor.

At state 2 the desorption process starts and the heating process continues as isobaric process. At this stage $2 \rightarrow 3$, while the temperature increases, the trapped adsorbate is gradually and continuously desorbed and the desorbed vapor is driven out from the adsorption reactor. In other words, in the process $2 \rightarrow 3$, the heat introduced to the reactor does not only to heat the reactor-components but also to drive the desorption of the adsorbate out of the adsorbent.

When the pressure of the adsorption reactor reaches the condenser pressure, the valve v_1 is opened and the adsorption reactor is connected to the condenser. The desorbed vapor coming from the reactor condenses and its heat rejected to the first heat sink T_{amb}. Then the evaporated adsorbate saturates into the liquid. The condensed liquid refrigerant goes to the throttling valve during the expansion process $B \rightarrow C$.

After the adsorption reactor has been heated to the maximum temperature fixed with the first heat source temperature, the valve v_1 is closed, and then the isosteric cooling process takes place from the

point 3 to the point 4 as shown in **F**ig. 3. In this stage, the sensible heat of the reactor is removed by an external cooling source (second heat sink) and the adsorbate concentration remains constant. Consequently, the adsorbent temperature decreases and this changes the pressure from the condensation pressure to the designed evaporating pressure. When the evaporator pressure prevails within the adsorption reactor, the valve v_2 is opened and the reactor is connected to the evaporator.

Meanwhile, the liquid refrigerant is transferred from the condenser through the expansion valve into the evaporator and the evaporation process $C \rightarrow D$ takes place inside the evaporator. Here, in the evaporator the useful refrigeration effect is produced, when the liquid refrigerant extracts the heat supplied by the heat source (the second heat source) at low temperature. Consequently, the refrigerant evaporates and the evaporated adsorbate flows toward the adsorption reactor, where the adsorbent temperature continues decreasing, which induces adsorption, where the adsorbate adsorbs on the surface of the adsorbent-particles. During this stage $4 \rightarrow 1$, the adsorbate mass increases as the temperature decreases from the initial adsorption temperature to the final adsorption temperature, which is the ambient temperature.

1.3 Physical and thermodynamic formulation

1.3.1 Adsorption and desorption equations

The adsorbate concentration $x\ [kg_a/kg_S]$ by the adsorbent particles depends on the pressure and the temperature of the adsorbate. The maximum value x_{max} is defined by the ambient temperature and designed evaporator pressure $x_{max} = f\left(T_{amb}, p_{evap}\right)$.

The adsorption and desorption concentrations x during the isobaric heating and cooling are usually determined by Dubinin-Astakhov equations [12-14]:

$$x_{(T,p)} = x_0 \exp\left\{-D.\left[T.\ln\left(\frac{p_{sat}}{p}\right)\right]^n\right\} \tag{1.1}$$

$$x_{(T,\,T_{sat})} = x_0 \exp\left\{-K.\left[\left(\frac{T}{T_{sat}} - 1\right)\right]^n\right\} \tag{1.2}$$

The initial adsorption concentration x_0 depends on the adsorbate density $\rho_a(T)$ and is related to the maximum adsorption capacity by this equation:

$$x_0 = \rho_a(T).V_0 \tag{1.3}$$

where V_0 is the maximum adsorption capacity $[m^3/kg]$. D, K and n are constants which can be determined experimentally depending on the adsorbate/adsorbent working pair.

$p_{sat}(T)$ and $T_{sat}(T)$ are saturation pressure and temperature corresponding to the reactor temperature. The relation between the pressure and temperature during the isosteric heating and cooling processes at steady state conditions is described by the following equations:

$$p = p_{sat}(T).\exp\left\{\frac{-1}{T}\left[\frac{1}{D}\ln\left(\frac{x_0}{x}\right)\right]^{1/n}\right\} \tag{1.4}$$

$$T = T_{sat}.\exp\left\{1 + \left[\frac{1}{K}\ln\left(\frac{x_0}{x}\right)\right]^{1/n}\right\} \tag{1.5}$$

For a given evaporator temperature T_{evap}, the corresponding evaporator pressure, p_{evap} is the saturation pressure of the refrigerant vapor $p_{sat}\left(T_{evap}\right) = p_{evap}$ corresponding to T_{evap}.

According to the previously mentioned equations, the processes cycle of the adsorption system can be displayed very well in (P-T) diagram as shown in **F**ig. 1.3. In this diagram the processes are plotted as a trapeziums between the isosteres x^{S}_{max} and x^{S}_{min} and the isobares p_{cond} and p_{evap}.

1.3.2 Adsorption kinetics

The kinetics of sorption dx/dt is assumed to be governed by well-known linear driving force (LDF) equation that could be used to describe internal mass transfer limitations with little error [15-17]. This equation is commonly used to estimate the adsorption rate of cylindrical/spherical adsorbent-adsorbate pairs given by:

$$\frac{dx}{dt} = D_{so}.(x_{eq} - x) \tag{1.6}$$

where x_{eq} is the equilibrium concentration at the corresponding pressure and temperature that is calculated by Dubinin-Astakhov **E**q. 1.1 and x represents the actual concentration of the adsorbate. The key parameter in the LDF model is the determination of the overall mass transfer coefficient D_{so} $[s^{-1}]$ for adsorption/desorption, which is expressed by Sakoda and Suzuki (1984) as a function of temperature as follows:

$$D_{so} = \frac{F_0.D_C}{r_P^2}.e^{(-E_a/R_a.T)} \tag{1.7}$$

where D_C is surface diffusion coefficient $[m^2/sec]$, r_p is the adsorbent particle radius. E_a and R_a are the activation energy of surface diffusion $[kJ/kg]$ and the adsorbate constant $[kJ/kg.K]$, respectively. It is found that the numerical value of F_0 is 11, considering the cylindrical shape of adsorption particles and 15 for spherical [18].

1.3.3 Isosteric heating and isobaric desorption processes

In the isosteric heating process, the adsorbate concentration in the heat exchanger (adsorption reactor) remains constant. The added energy Q_{heat} during this process is utilized to cause sensible heating of the adsorption reactor constituents. During the isobaric desorption process the adsorbate concentration decreases by increasing desorption temperature from the maximum value $x_{max}(p_{cond}, T_{cond})$ to the minimum value X_{min} (p_{cond}, T_{max}). The variation of the adsorbate concentration ratio along the isobaric desorption process is defined by the **E**q. 1.1. The amount of the added energy Q_{des} which is required during the isobaric desorption process causes also sensible heating of the adsorption reactor constituents, activates desorption of the refrigerant from the adsorbent media and generates the gas phase. As shown in **F**ig. 1.4, the summation of the isosteric heat together the desorption heat (isobaric heat) is called the input energy Q_{in} required form the external heat source for generation the adsorption reactor and is given as:

$$Q_{in} = \int_1^2 dQ_{heat} + \int_2^3 dQ_{des}, \tag{1.8}$$

$$Q_{in} = \int_1^2 [dQ_{mc} + dQ_s + dQ_a + dQ_v] + \int_2^3 [dQ_{mc} + dQ_s + dQ_a + dQ_v]$$

where Q_{mc}, Q_S, Q_a and Q_v are the introduced energy to the metallic components, adsorption material, adsorbate (refrigerant) and the adsorbate as vapor phase, respectively.

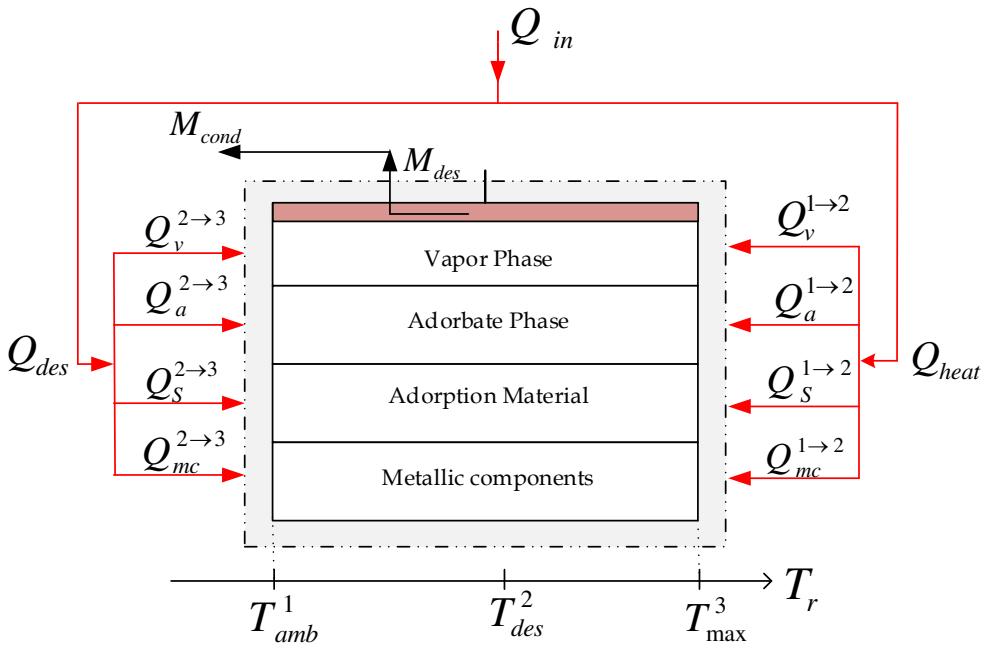

Figure 1.4: Energy flow diagram for the desorption reactor during the isosteric and isobaric heating processes

1.3.4 Isosteric cooling and isobaric adsorption processes

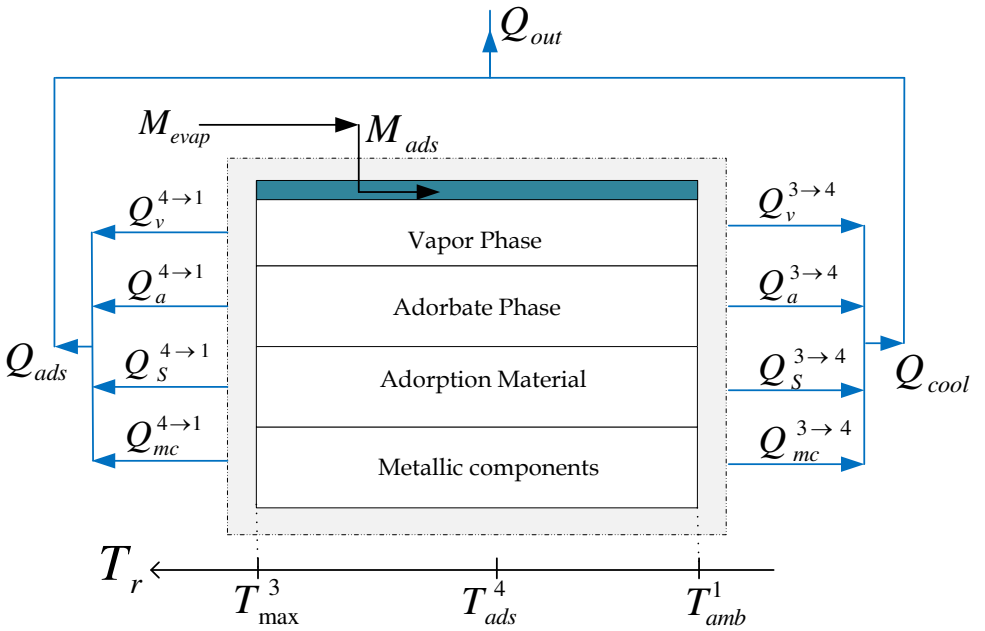

Figure 1.5: Energy flow diagram for the adsorption reactor during the isosteric and isobaric cooling processes

Using the same methodology which has been followed in the last section, the energy which is removed from the adsorption reactor to the ambient heat sink at T_{amb} is in a sensible form during isosteric cooling process Q_{cool} and consists of the reactor cooling energy in addition to the adsorption energy during the isobaric cooling process Q_{ads}. As shown in **F**ig. 1.5, the total amount of energy

removed from the reactor during isosteric and isobaric cooling is called the output energy Q_{out} and is given as follows:

$$Q_{out} = \int_3^4 dQ_{cool} + \int_4^1 dQ_{ads}, \tag{1.9}$$

$$Q_{out} = \int_3^4 [dQ_{mc} + dQ_s + dQ_a + dQ_v] + \int_4^1 [dQ_{mc} + dQ_s + dQ_a + dQ_v]$$

1.3.5 The condenser

As soon as the refrigerant vapor desorbs from the adsorption reactor, it enters the condenser. In the condenser, the refrigerant gas is being desuperheated first by removing sensible energy from the superheated vapor across a driving temperature difference of $T_{max} - T_{cond}$. By rejecting the latent energy of condensation L_{cond} to the ambient heat sink the refrigerant vapor starts to condense [19]. The condensation energy of Q_{cond} is given by:

$$Q_{cond} = M_{cond} . [h_v(p_{cond}, T_{max}) - h_{sat}(p_{cond}) + L_{cond}] \tag{1.10}$$

where $h_{sat}(p_{cond})$ is the refrigerant vapor saturation specific enthalpy at the condensation pressure and L_{cond} is the specific latent heat of condensation. The differential amount of adsorbate vapor dM_{cond} equals the total desorbed refrigerant mass and can be written as follows:

$$dM_{cond} = dM_{des}^{2\to3} \tag{1.11}$$

1.3.6 The evaporator

In the evaporator, the refrigeration effect takes place by the evaporation of the saturated liquid refrigerant. The evaporation effect Q_{evap} is calculated from the following equation [12,19-20]:

$$Q_{evap} = M_{evap} . [(1 - z) . L_{evap} + (h_{evap}(T) - h_{sat}(p_{evap}))] \tag{1.12}$$

where dM_{evap} is the differential mass of adsorbate vapor that leaves the evaporator, enters the adsorption reactor and is being adsorbed in the adsorption reactor. z is the wetness fraction.

The differential mass of adsorbate vapor dM_{evap} equals the total refrigerant mass, which adsorbs on the surface of the adsorbent-particles. This infinitesimal amount of adsorbate vapor can be written as follows:

$$dM_{evap} = dM_{ads}^{4\to1} \tag{1.13}$$

1.3.7 Coefficient of performance (COP)

To evaluate the efficiency of the adsorption refrigeration cycles, the coefficient of performance COP is used. The COP is defined as the ratio of the evaporative energy Q_{evap} to the amount of input energy Q_{in} to the adsorption reactor during the isosteric and isobaric heating processes [10, 19-20].

$$COP = \frac{Q_{evap}}{Q_{in}} \tag{1.14}$$

1.3.8 Specific cooling power (SCP)

It is defined as the ratio of evaporative energy to the mass of dry adsorption material multiplied by the cycle time [10]. The SCP represents the amount of refrigeration power produced per unit mass of dry adsorbent **E**q. (1.15).

$$SCP = \frac{Q_{evap}}{M_S . t_{cycle}} \tag{1.15}$$

1.3.9 Efficiency of the refrigerant utilization

In order to assess the effectiveness of refrigerant mass utilization on the adsorption system the efficiency of refrigerant mass utilization μ_m^S is used [12]. This parameter is defined as the ratio between the circulated refrigerant mass to the total refrigerant mass which is correspond to maximum value of adsorbate uptake and required to charge the adsorption reactor and is given by:

$$\mu_m^S = \frac{M_{des}}{M_S . (x_{max}^S - x_{min}^S)} \tag{1.16}$$

1.4 Research aims and objectives

The main aims of the present work are: enhancing the amount of ice produced per cycle, producing continuous cooling power, improving the cycle time and saving of the required input heat by increasing the mass flow rate of the refrigerant, which leaves the adsorption reactor and flows toward the condenser. To achieve the above mentioned research aims, the project objectives are set out below.

- Review of theoretical and experimental research works on adsorption refrigeration systems
- Review of various adsorbents and refrigerants to understand their advantages and disadvantages in order to select a working pair, which is an appropriate pair for the application of this work (ice production)
- Develop a cycle simulation computer program of the innovative combined adsorption ice production system (com-AIP system) studied in this work, which utilizes two adsorption materials silica gel (SG) and activated carbon (AC) in one machine. This program, which is written using **M**ATLAB Software, is flexible in changing both of the physical parameters and operating conditions. The written program allows to investigate the effect of desorption temperature T_{des}, adsorption temperature T_{ads} and the effect of difference of the required desorption/adsorption time on the system performance and on the amount of the ice produced per cycle M_{ice}.
- Study of the transient behavior of heat and mass transfer inside the adsorption reactor. The mass transfer limitations from the adsorption reactor and the heat transfer ability between the particles of adsorbents and heat exchanger fins are taken into account in the simulated model based on the linear driving force LDF model.
- To show the importance of this new strategy (com-AIP system), the performance and the needed driving energy are evaluated by comparing with two AIP systems, the first system

works using silica gel/methanol and the second works using activated carbon/methanol as working pairs. The boundary conditions used were similar between the three systems.

The next task of this work is studying the adsorption reactor as a heat exchanger in order to know effect of the flow type and design parameters on the desorption process. Therefore the following objectives are considered:

- Design and analytical investigation of two fined-tube heat exchangers *named SG- and AC-adsorption reactors* in order to generate the same desorbed refrigerant amount of $1\ \mathrm{kg_{meth}}$ and to contain two different adsorbents.
- Study by changing the adsorption reactor geometry such as the length and the diameter of the heat transfer fluid channels used including the fins spacing and dimensions.
- Study of Re, Nu and Bi in order to increase the heat transfer ability between the particles of adsorbents and heat exchanger fins.
- Discussion of a set of non- dimensional parameters, which are derived based on the parametric analysis, to show the effects of different non-dimensional parameters on the system performance and both the heat and mass transfer limitations during desorption process.

Another main task is using the induction heating technology as a new heat source in adsorption refrigeration systems. The following goals are considered in the context of this phase.

- Explore the possibility of heating nonmagnetic materials such as SG an AC, which are the adsorbents filled in the adsorption reactors, with the induction heating technology used to desorb the adsorbate CH_3OH loaded within the SG-and AC-particles.
- Design and simulating study of new two adsorption reactors.
- Investigation of a physical model.
- The solution of the induction heating problem by numerical modelling and simulation processes was implemented by the software **A**NSYS **E**LECTRONICS ®17.2.
- Using **A**NSYS **F**LUENT to study the temperature distribution at every point throughout the adsorption reactor during the desorption process.
- Study the structure of the induction heating system (calculation of the inductor and work-load) for the new application (desorption process).

1.5 Thesis structure

This thesis consists of 10 chapters. **The first chapter** introduces the general introduction about the importance of adsorption refrigeration technology and the research topic covered by this thesis, so that includes the project objectives and thesis structure. It includes also detail explanation of the simplest adsorption refrigeration system, thermodynamic cycle, working principle and the mathematical and physical formulation.

In **the second chapter**, adsorption historical background and the adsorption working pairs used in the adsorption technology are presented. Furthermore, the simulation and experimental previous works, that aim to improve the adsorption systems, are reviewed in this chapter over four last decades.

Chapter 3 and chapter 4 present an analytical, mathematical and numerical investigation of a new construction of the adsorption ice production system at different operating and boundary conditions. This system, named in this work as the combined **A**dsorption **I**ce **P**roduction system (com-AIP system), utilizes two different adsorption materials in one machine. The com-AIP system comprises of two adsorption reactors, such that the first adsorption reactor was filled by silica gel and the second by activated carbon as adsorbents. Methanol was used as adsorbate and refrigerant with both the reactors.

In **the third chapter** the SG-and AC-adsorption reactors as heat exchangers of the same size (same number of tubes, same number of fins and same emptied volume) were taken. Both the reactors were heated up to the same desorption temperature of 100 °C. The adsorption thermodynamic cycles of both the SG- and AC-adsorption reactors are considered to start at the same time (working simultaneously).

The com-AIP system in **the fourth chapter** has been studied to desorb $1\ \mathrm{kg_{meth}}$ from the AC-reactor and to desorb the same amount from the SG-reactor. Therefore, the reactors of different size were taken, so that the first adsorption reactor has to be filled by 3.31 kg activated carbon and 1.36 kg methanol and the second by 7.9 kg silica gel and 1.9 kg methanol. In contrast to the study in Chapter III, both the reactors are heated up to different desorption temperature but to same level of minimum adsorbate concentration rate. Another difference is also the working principle, in that the thermodynamic cycles for SG- and AC-reactors start one after the other.

In **the fifth chapter**, two finned-tube heat exchangers were designed (named SG-adsorption reactor and AC-adsorption reactor) in order to contain two different adsorbents and to generate the same desorbed refrigerant amount of $1\ \mathrm{kg_{meth}}$. This chapter focuses on the effect of the flow nature depending on varying the Reynolds number through the flow channels and the design parameters effect of the adsorption reactor on the thermal performance (coefficient of performance COP and specific cooling power SCP) of the AIP-system, the desorbed refrigerant amount $\mathrm{M_{des}}$, the produced amount of ice $\mathrm{M_{ice}}$, the evolution of temperature distribution throughout the adsorbent-adsorbate medium and the temperature difference $\Delta\mathrm{T}$ of the heat transfer fluid, which is directly related to the required input heat amount that must be supplied to the reactor in order to desorb $1\mathrm{kg_{meth}}$ of methanol as refrigerant.

The sixth chapter of this PhD-theses deals with a mathematical modeling and numerical simulation of an Induction Heating (IH) system for two adsorption reactors. This chapter studies the possibility of using the induction heating technology as a new heat source to heat and activate the adsorption materials such as silica gel and activated carbon. **The seventh chapter** presents the IH-system designed in this work for a new application for desorption process. This chapter is mainly focused on the design of the work-load and the induction coil, which is the most important one for the whole system to be efficient.

The eighth chapter is devoted to the verification and validation of the com-AIP system presented in this work. The verification is investigated by comparison of the com-AIP system with two separate systems: the first system works using one adsorbate/adsorbent pair (silica gel/methanol) in two beds and the second also works using also one adsorbate/adsorbent pair (activated carbon/methanol) in two beds. In addition, this chapter produces an experimental set up of ACS 08 system from the

manufacturer SorTech AG, which is built in Holzminden (Germany), is done to make validation of some simulation results of the AIP system. The comparison is conducted for the real processes inside the adsorption reactor, the coefficient of performance of the system, the refrigeration capacity and the required time to complete the processes of one cycle. Furthermore, this chapter presents a comparison between two methods the induction heating and thermal heating of both the SG-and AC-adsorption reactors.

The summary, conclusions and recommendations for improvement are presented in **the ninth chapter** and the references used in this work are displayed in **the tenth chapter**, which is the last chapter in this work.

Chapter 2

Literature Review

2.1 Adsorption historical background

Most applications now in use, and possibly many future developments, have their origins in earlier discoveries. The adsorption technology was applied for many applications at ancient times, where charcoal was only available and the dominant adsorption material. Egyptians and Sumerians in 3750 BC used the charcoal to reduce copper, zinc and tin ores for bronze manufacturing. Egyptians also used the charcoal for medical purposes in order to adsorb odorous vapors from putrefactive wounds and from intestine1in 550 BC [6,21].

In 460 BC, Hippocrates and Pliny introduced the use of charcoal to treat a wide range of afflictions including epilepsy, chlorosis and anthrax. Using charcoal for purification of drinking water was the first recorded application of charcoal, which was used by Phoenicians in 460 BC [21].

C. W. Scheele in 1773 and F. Fontana in 1777 were reported results associated with the first adsorption experiments. They heated charcoal and clay in a test tube and found that, charcoal and clay desorbed gases, then the gases adsorbed back when the adsorbent were cooled [6, 7, 21].

In 1814 De Saussure found out the exothermic character of adsorption processes. He started systematic studies of adsorption of various gases by porous substances as sea-foam, cork, charcoal, and asbestos [6,21]. The nature of adsorption/desorption has always been a widely discussed one throughout the nineteenth century. So many works and many papers have been implemented and introduced in this field.

In 1834 Faraday discussed, that the gases has ability to hold onto the surface by an electrical force and suggested that gases could react more easily once they were in the adsorbed state [7].

In 1836 Berzelius reported that the best adsorbent was highly porous materials. Therefore, Berzelius proposed that adsorption was a process where surface tension or some other force caused gas to be condensed into the pores of a porous media [22].

The first invention of an adsorption system was in 1848 and was demonstrated by Michael Faraday. He utilized ammonia and silver chloride as the working pair of this adsorption refrigeration system. In the 1850s to 1920s the idea, that most adsorption/desorption processes were really just pore condensations, was actively debated in the literature [6-7, 22-23].

The term ‘adsorption isotherm’ was introduced into literature in 1881 by Kayser. During the next few years, the term ‘isotherm’ was used to describe the results of adsorption measurements at constant temperature [24].

From 1879 to 1883 Chappuis measured adsorption of ammonia on charcoal and asbestos at a constant temperature. He also found that sulphur dioxide, carbon dioxide and air are taken up by charcoal depending on the pressure of the gas. He made the first calorimetric measurement of heat evolved during wetting of adsorbents by liquids.

In 1903, Selective adsorption phenomenon was found out by Tswett. He took advantage of this phenomenon to separate chlorophyll and other plant pigments by means of silica materials. This separation was possible due to different adsorption affinity of silica gel with regard to various pigments. This discovery was not only the beginning of a new analytical technique, but also the origin of a new field of surface science. Practical application of adsorption processes is based mainly on selective uptake of individual components from their mixtures by other substances [21,25] .

In 1915, a professor of Moscow University named Zelinsky was the first to suggest and apply the use of active carbons as the adsorption medium in gas mask. In the 1920s using silica gel and sulfur dioxide was the important key for the development and Industrial design of adsorption refrigeration systems [7, 21, 26-27].

In 1929, Hulse and Miller described an adsorption system in the United States for the air conditioning of railway carriages using silica gel and sulphur dioxide as the working pair [6, 23].

The method of zeolite synthesis was invented in 1956 by Barrer and Breck. In the same year the North American Linde Company started production of synthetic zeolites at a commercial scale [28-29].

Due to the low performance of adsorption systems compared to the vapor compression systems and because of the development of mechanical vapor compression, the adsorption systems was not as popular as the mechanical vapor compression driven cooling system. Therefore, research and development of adsorption refrigeration systems was reduced in the 1970s [6, 30].

The adsorption technology was abandoned until the 1970s, but the concerns over the ozone layer depletion due to CFCs, global warming due to HCFs and CO_2, due to the need of replacing the conventional vapor compression systems to meet the new environmental regulations, interest in adsorption systems has increased gradually since 1970s and up to the present date [7, 31-34].

In the last three decades, the adsorption cooling systems are laboratory and commercially developed to be used in different applications. A technical feasibility study of water vapor adsorption cooling system was conducted by IGT [7, 35].

Two design and development companies, Tchernev [36] and Meunier [37] started work on adsorption working pairs to be used in adsorption refrigeration systems. This was used for the cooling of vaccines in developing countries [7]. In Japan 1986 Nishiyodo Kuchou Manufacturing Company, designed and manufactured the first industrial adsorption cooling system. Since then, the adsorption chiller has been used and closely evaluated in a wide area of applications in Japan, Europe and USA with high initial acceptance. Due to its energy saving and environmental benefits, adsorption cooling systems could be an excellent replacement for traditional units in the foreseeable future [7].

2.2 Adsorption Working Pairs

The adsorbent/adsorbate working pair used in the adsorption refrigeration systems is an essential and critical element. The selection of the adsorption working pair has an important effect on the thermal performance (coefficient of performance and specific cooling power) of the adsorption systems. Most adsorption machines employ using silica gel/water, silica gel/methanol, activated carbon/methanol,

activated carbon/ethanol, activated carbon/ammonia and zeolite/water as working pairs. In investigations of common working pairs, wide range of possible adsorbent/adsorbate combinations have been applied [38]. The choice of any working pair should be dependent on certain characteristics and factors. So this section presents in details the characteristics of each type of the adsorbents, adsorbates and the working pairs.

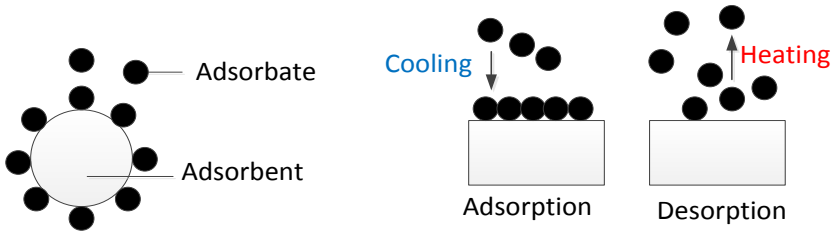

Figure 2.1: Idea of the adsorption and desorption processes

2.2.1 Porous Adsorbents Materials

Fig. 2.1 gives a short idea about the adsorption devices. The porous particles, which are called the adsorbents, have the ability to desorb moisture or gases by heating and the dry adsorbents can adsorb moisture or gases again by physical or chemical forces [39-40]. Therefore, the adsorbents materials are classified based on the adsorption process as: physical adsorbents and chemical adsorbents. In general, the choice of the adsorbent should be governed by the following criteria [40]:

- Significant and varied adsorbate uptake capacity corresponding with temperature range.
- Desorption of most of the adsorbate when exposed to thermal energy.
- Adsorption of large amount of the adsorbate under low temperature conditions.
- High specific power output (high density)
- Microspores of diameter less than 20Å.
- Good thermal conductivity.
- Low cost and widely available.

2.2.1.1 The physical adsorbents

Physical adsorption is caused by van der Walls force between the molecules of the adsorbent and the adsorbate [24,39]. The physical adsorbent has the advantage, that its original properties can be retained after desorption the refrigerant by the heating during the desorption process. This advantage makes the physical adsorbent be commonly used in the adsorption systems [6]. On the other hand most of the physical adsorbents have a disadvantage that the adsorption kinetics are low and hence low desorbed refrigerant flow rate. Usually the physical adsorbent used in the adsorption refrigeration systems are divided into three different classes: silica gel, zeolite and activated carbon [42-46].The characteristics of each type of these adsorbents are presented in details in this section.

Silica Gel

Silica gel structure made up by rigid and continuous net of colloidal silica connected to very small grains of hydrated SiO_4 [6,24]. Characteristics of silica gel such as the physical porous structure and large surface area make it popular in the adsorption systems. Silica gel is non-toxic, considered environmental friendly and has large adsorption ability of water vapor as adsorbate (50% of its mass without changing its volume) [39, 45-46]. Therefore, it has been the subject of many studies in adsorption systems in recent years. Despite the low porosity of silica gel, it can be regenerated using

low temperature sources $50-85\,°C$ and loses the adsorption ability by high temperatures above $120°C$ due to loss of its chemically bond [6]. Based on pore dimension there are three types of silica gel available commercially named; Type A silica gel of $2-3$ nm pore diameter and Type B of $15-20$ nm pore diameter [46-47]. Type A is used as an adsorbent in more practical for adsorption systems because of having a regular density and large internal surface area. It has also a high moisture-adsorption capacity at low humidity. Type B silica is known as macro-pored silica gel available in spherical. This type has a low density and also works as a good adsorbent in adsorption refrigeration system [7, 49-50]. Generally, silica gel is a porous material with high porosity $800\,[m^2/g]$, low density $0.003-0.35\,[g/cm^3]$, low thermal conductivity $0.14\,[W/m.K]$ and high adsorption heat $2500-2800\,[kJ/kg]$ [48].

Activated Carbon

The net structure of activated carbon has a larger surface area and its pores are more irregular [45-46]. Activated carbon is a substance of crystalline form having large internal pore structures with surfaces between 500 and $1500\,[m^2/g]$ [51-52]. Therefore, Activated carbon was a key adsorbent material in adsorption technology for many years and is still one of the best adsorption materials available on the market today. Activated carbon can be classified into 3 types based on the porous media: the first type is called microporous and its pore diameter of less than 20 nm, the second type is named mesoporous and the pore diameter is between 20 and 200 nm and the third type has the pore above 200 nm and is called macroporous activated carbon [7]. There are many forms of activated carbon such powders, granulated, molecular sieves and carbon fibers [7,51-52]. Activated carbon has a high level of the porosity, which is higher than silica gel, but the adsorption heat of the activated carbon types is relatively low among the other types of physical adsorbents $1800-2000\,[kJ/kg]$ [48]. There are many types of activated carbon, where Christoph et al [53] studied the adsorption performance of 26 types of activated carbon with ammonia. Activated carbon fiber is a fiber form of activated carbon that has many advantages over activated carbon in terms of mass and heat transfer performance. The disadvantages of the activated carbon are anisotropic thermal conductivity and high thermal resistance between the activated carbon particles and adsorbent-bed heat exchanger surface [6, 24].

Zeolites

There are more than 40 types of zeolite frameworks [7]. Most of zeolite types adsorb water vapor at low partial pressure with different capacities [6]. Zeolites have a crystalline structure which contains oxygen, silicon and aluminum [7,54]. These crystal are the fundamental construction for various zeolite such as zeolites A and X, the common adsorbents used in the application of adsorption cooling system. Compared to the other adsorbent zeolite has the highest adsorption heat of $3300-4200\,[kJ/kg]$. The investigations have shown, that silica gel and the zeolites have the same water vapour uptake capacity of $50\,\%$ of their own weight, but the zeolites are usually employed in adsorption refrigeration system that has a higher heat source between 250 and $300\,°C$. The porosity of the zeolite is between 0.2 and 0.5 [29]. Zeolite is a highly porous adsorbent material and can withstand high temperature treatment (up to $800\,°C$). 13X Zeolite adsorbent are the main types used for adsorption cooling system [14,46-54].

2.2.1.2 Chemical adsorbents

Chemical adsorbents mainly used in the adsorption cooling systems include:

- Metal chlorides such as calcium chloride, strontium chloride, barium chloride and magnesium chloride. Usually methanol, ethanol vapors and ammonia are the refrigerant used with metal chlorides [24, 39,55].
- Salt and Metal hydrides such as lithium hydrides, calcium hydrides, covalent high polymerized hydrides and non-metal molecular hydrides. Salt and Metal hydrides as adsorbent with hydrogen as refrigerant will be a promising working pair
- Metal oxides; the suitable refrigerant is Oxygen. Because of the large enthalpy of reaction between oxides and oxygen is the adsorption pair Metal oxides/oxygen suitable for heat pumps with temperature below 120 K [6, 24,39].

Chemical adsorbent adsorbs the refrigerant chemically by Valence force, where one layer of refrigerant reacts with the surface molecules of the adsorbent. Compared to physical adsorbent the advantage of the chemical adsorbents is that they can adsorb more adsorbate at a higher rate [56]. Whereas the stability of the chemical adsorbents is lower than a physical adsorbent and chemical pair molecules cannot keep their original state which limits its practical applications. Chemical adsorbents swell and agglomerate which negatively affect the heat and mass transfer performance, especially in cycles that operate under low pressure [57].

2.2.2 Refrigerants

The adsorbate or called refrigerant is the vital element in the adsorption working pairs, because the refrigerant is the element which produces the refrigeration effect when it flows within the evaporator. Many refrigerants can be utilized in the adsorption refrigeration systems, but the optimum refrigerant need to be carefully selected based on certain desirable characteristics. The adsorbate-characteristics range from its thermodynamic and physical properties to the chemical properties and even to their costs or availability. The refrigerants (adsorbate) should have some characteristics, are listed as following [6-7]:

- Large latent heat of vaporization and little adsorption heat.
- Thermally stability with the adsorbents over the operating temperature range.
- Evaporation temperature below 0 °C and low specific volume.
- Small size of molecules such that it can easily be adsorbed into the adsorbents.
- No flammability within certain concentration and at high desorption temperature obtained in the cycle.
- Environmentally friendly with non-ozone depletion and low global warming potential
- Non-corrosive, non-explosive and non- toxic
- Low saturation pressures (above atmospheric) at normal operating temperature.

Depending on the adsorption system application (freezing or air conditioning) and the cyclic operating conditions, the most useful refrigerant is the one that has the highest latent heat, low generation temperature and largest adsorbate concentration. This optimum refrigerant can give the better performance. Evaluating adsorbent or refrigerant independently is not sufficient, where the optimum adsorption working pair depend on the characteristics of both the adsorbent and adsorbate. **T**ab. 2.1 lists some common adsorption working pairs with some of their characteristics. From this table one can see, why water, ammonia and methanol are the commonly applied refrigerants in adsorption cycles [58-60].

Working pair	Adsorbate Latent Heat [kJ/kg]	Boling Temperature [°C]	Generating Temperature [°C]	Adsorption Concentration [kg/kg]	Adsorption Heat [kJ/kg]
AC/Ammonia	1368	-34	80-200	0.29	1800-2000
SG/Water	2258	100	50-85	0.30	2500-2800
AC/Methanol	1102	65	80-100	0.45	1800-2000
AC/Ethanol	842	79	80-120	0.19	1200-1400
Zeolite/Water	2258	100	250-300	0.17	3200-4200

Table 2.1: Characteristics of commonly used adsorption pairs [5, 63-66]

2.2.3 Types of the working Adsorbate and Adsorbent Pairs

At present, the most commonly utilized adsorption working pairs in the adsorption technology are the silica gel/water, zeolite/water, activated carbon/ammonia and activated carbon/methanol [7,24,38,59].

2.2.3.1 Silica Gel/Water

The adsorption refrigeration systems utilized silica gel/water can be driven by low heat sources of between 50 °C and 85 °C under low pressure [7,24,38]. Due to the water advantages as shown in Tab. 2.1 water is considered a very good adsorbate but it has the disadvantage, that it is impossible to get an evaporation temperature less than 0 °C [5,67]. Therefore, the adsorption systems utilized silica gel/water as working pair cannot be used for freezing applications. Other disadvantage of silica gel/water is the low adsorption capacity, which is about 0.2 [g/g] [24,67]. Silica gel/water as a working pair in the adsorption technology has been common since early 1980s. Many works in Japan were carried out using this working pair. Sakoda and Suzuki have tested a solar adsorption system. They used 1 kg of silica gel particles filled in solar collector $500 \times 500 \times 50$ m^3. The COP achieved is about 0.2 on a clear day with total solar insulation of 19.3 [MJ/m^2.day] [16]. The adsorption cooling system using silica gel/water and driven by waste heat was investigated by Ruud et al. [68]. The system achieved 0.62 of COP and 208 [W/kg] of SCP. The system tested the chilled water outlet temperature at 12 °C. De Lieto Vollaro et al. [69] studied the thermodynamic behavior of the adsorption system used silica gel/water that heated by vacuum solar collector to provide 2 kW of cooling capacity to satisfy the cooling requirement of one apartment $70 - 80$ m^2 during summer. With 20 m^{2}of the collector, the obtained chilled water temperature reached 10 °C.

2.2.3.2 Zeolite/Water

The heat adsorption is in range of $3200 - 4200$ [kJ/kg] and the generation temperature of zeolite/water pair is about $250 - 300$ °C but the adsorption temperature might be lower than 80 °C [7,24]. The zeolite/water adsorption systems are suitable for the air conditioning because the evaporation temperature of water cannot be below 0 °C and the latent heat of water is much larger than ethanol, methanol or other traditional refrigerants and the high desorption temperature increases the sensible heat of the adsorber [37-38, 66-71]. The equilibrium adsorption capacity of water on a natural zeolite has been experimentally determined by Ismail, Cemil et al [14]. The experiment implanted at different zeolite temperatures and water vapor pressures in the range $40 - 150$ °C and $0.87 - 7.38$ [kPa], respectively. The results showed that the maximum water concentration by zeolite is nearly 0.12 [kg/kg]. Because of low evaporating pressure of water which this causes a slow adsorption process. Therefore, SCP of the zeolite/water system is not very high. The zeolite/water adsorption refrigeration system is used where the speed of temperature variation inside the adsorbent bed is slow, such as in the intermittent adsorption air conditioning using a tubular solar collector as an adsorber [24,37,70-71]. Design and performance prediction of a novel zeolite/water adsorption air

conditioner has been investigated by Wang et al. [72]. The system was driven by 350–450 °C exhaust gas. The cooling power of this machine was up to 10 kW and supplied 8–12 °C chilled water for the fan coil with an evaporating temperature of 6.5 °C. The designed refrigerating power and COP were 5 [kW] and 0.25 respectively. The cycle time was 1320 s and the SCP reached 200 [W/kg]. In another research conducted an adsorption air-conditioning system has been experimental investigated by Lu et al. [73]. The aim of this experiment was to provide chilled water for air-conditioning in the driver's cab of the locomotive and to study the practical performance of this system which was powered by exhausted heat from a diesel locomotive and was incorporated with one adsorbent bed and utilizes zeolite/water as a working pair. Under typical running conditions, their experimental results showed, that the average refrigeration effect ranging from 3.0 to 4.2 [kW] was obtained. They also gave an idea, that the adsorption system is technically feasible and can be applied for space air conditioning. However, this system may not be suitable for automobile application due to its size and high regenerative temperature.

2.2.3.3 Activated carbon/Ammonia

The latent heat of ammonia is a relatively high about 1365 [kJ/kg] at −30 °C but less than half the latent heat of water. Therefore, ammonia cannot be considered thermodynamically efficient as water [38-39]. In spite of environmentally friendly characteristic of ammonia, but it cannot be normally used within residential or office spaces because of its drawbacks of toxicity and corrosive pungent smell [6,24]. So it may not be used together with copper or its alloys, although steel and aluminum are acceptable. However ammonia has the advantage of high adsorption in range of 2000 to 2700 [kJ/kg] [39] and the large adsorption capacity in activated carbon is 0.29 [g/g] [74]. Another advantage is that, the activated carbon/ammonia pair works at high desorption pressure, which reaches 1.6 [MPa]. The relatively high pressure makes the time of adsorption process short and enhances the desorbed mass of ammonia from activated carbon. Consequently, the SCP of the system rises [75]. The activated carbon/ammonia adsorption systems may be used for cooling down to about −40 °C. Another advantage of activated carbon/ammonia is the possibility of using heat sources at 200 °C or above.

26 various activated carbon/ammonia pairs for three cycles (single bed, two-bed and infinite number for adsorption refrigeration applications of beds) have been investigated by Tamainot-Telto et al. [53]. In this study the driving temperature varied from 80 °C to 200 °C. The simulation results showed, that considering a two-bed cycle, the best thermal performances based on power density were obtained with the monolithic carbon, with a driving temperature of 100 °C; the cooling production was about 66 [MJ/m] (COP = 0.45) and 151 [MJ/m] (COP = 0.61) for ice making and air conditioning respectively.

2.2.3.4 Activated carbon/methanol

Both the activated carbon/methanol and the activated carbon/ammonia working pairs have almost the same adsorption heat. In comparing to activated carbon/methanol, the operating pressure of activated carbon/ammonia adsorption systems is much higher (about 1600 [kPa] when the condensing temperature is 40 °C) [3976-77]. The high operating pressure leads to rather small pipe diameters and relatively compact heat exchangers, as compared to activated carbon/methanol. Activated carbon/methanol is one of the most common and more promising working pairs in practical adsorption applications, because activated carbon/methanol has a large adsorption capacity about 0.45 [kg/kg] and low adsorption heat about 1800 to 2000 [kJ/kg] [55-57]. Low adsorption heat leads to enhancing in the coefficient of performance of the adsorption system and saving in the input required heat, because the majority of heat consumption in the desorption phase is the adsorption heat.

Low desorption temperature (between 65 and 100 °C) is another advantage of activated carbon/methanol, which makes the adsorption systems that utilized the activated carbon/methanol as a working pair suitable for using the solar energy as a heat source [39,77]. A solar-powered ice-maker using activated carbon /methanol has been developed by Li and Sumathy [78]. The experimentally results showed that, the system produced about 4-5 kg ice per day at an evaporator temperature of −6 °C and obtained COP about 0.1– 0.12. Pons et al. [79] also experimented on activated carbon/methanol adsorption ice maker, which produced around 30– 35 kg of ice on sunny days. The system was filled with 130 kg of activated carbon and employed flat-plate collector having exposed area of 6 m^2. It was reported that the system COP was about 0.12.

2.3 State of the previous works

The adsorption refrigeration systems in comparison with traditional refrigeration systems still have some technology problems such as low values of the coefficient of performance, large size, and intermittently working principles. The research efforts by previous investigators have therefore been focused on improving the performance, finding new composite adsorption materials [7] and design multi-bed adsorption systems to produce continuous refrigeration power [6].

A brief discussion of the researchers' efforts and their attempts to obtain an ideal adsorption refrigeration system with good efficiency and costs will be presented in the following section of this literature review. The investigation works in field of the adsorption refrigeration system over the last four decades will be produced in two groups: the first for the experimental and analytical researches and the second group for the theoretical and simulation works.

All of the numerical, thermodynamic, experimental, analytical studies of the adsorption refrigeration system were done with the objective of optimizing its performance and investigation of the adsorption refrigeration system with the different working pairs of adsorbent/adsorbate [8, 21].

2.3.1 Experimental analysis

Tchernev (1979) was the first to build a solar assisted adsorption cooling machine to produce ice, using a zeolite/water system featuring maximum temperature of a generator ranging from 250 to 300 °C. The operating principle of the zeolite system and experimental results demonstrated, that the zeolite system was capable of providing refrigeration and ice production with very good engineering efficiency. This system utilizes natural zeolites as the solid adsorber and water vapor as the working fluid, to produce on a sunny day two pounds of ice per each square meter of solar zeolite collector [80].

In 1983, Tanaka and Hasegawa [81] designed and carried out an experimental study on a compact silica gel/water adsorption cooling system which they concluded, had a good performance. There has also, been several cycles proposed to reduce heat inherent in batch cycle operation and hence improve cycle efficiency.

In 1984, Sakoda and Suzuki [5] investigated the silica gel/water working pair and its ability to use the adsorption cooling systems. Then Sakoda and Suzuki in 1986 [6] designed and built a small silica gel /water cooling system. They proposed a simple CFD simulation model which could explain the experimental results. The results of their study showed, that the heat transfer between the adsorbent particles filled in the bed and its heat exchanger had an important effect on the coefficient of performance.

Pons and Guilleminot have experimentally designed a prototype of adsorption ice production system powered using 6 m^2 of solar collectors. This ice maker with the activated carbon/methanol pair, was built in Orsay in 1986. The adsorption bed was filled with 130 kg of activated carbon, the condenser was air-cooled. The machine could produce up to $30 - 35$ kg ice with solar insolation of 22000 [kJ/m^2 . day] and the solar COP was 0.12, which makes this machine one of the most efficient solar ice makers [79].

Kluppel and Gurgel (1987) constructed two units on solar operated adsorption cooling system using silica gel/water as the working pair. The first unit was designed for use as a small house hold refrigerator and the second unit for the cooling of drinking water at temperatures around 12 °C. Their experimental results showed, that the mean solar COP obtained from both the units were 0.055 and 0.077, respectively [82].

N. Medini, B. Marmottant and S. El Gollia (1991) studied and constructed a solar ice maker using AC-methanol with a $0.8\ m^2$ collection surface. The results showed that, with a collection efficiency of 0.41 and a thermal COP of 0.40, it is possible to obtain a gross solar COP of 0.15 (as a function of the quantity of methanol). The system produced 4 kg of ice per day, during summer [83].

In 1992, Cho and Kim performed theoretical and experimental studies on a silica gel/water adsorption cooling system. They designed and developed a CFD simulation code to study the effects of heat exchangers and heat transfer rate on the cooling capacity of a silica-gal/water adsorption cooling system. The heat transfer rate of the condenser was found to be the most sensitive parameter having influence on the cold generation capacity [84].

Hajji and Khalloufi (1995) investigated a theoretical and experimental analysis to analyze the effect of some operating and design parameters on a constant-pressure adsorption process. Their model was validated by comparison and experimental results. The thermal fluid had the strongest effect on adsorption kinetics and on the refrigerating capacity of adsorption systems and correlated in terms of solid adsorbent thickness and heat transfer coefficient [85].

Oertel and Fischer (1998) have experimentally investigated two adsorption cooling systems, the first employs silica gel/water and the second employs silica gel/methanol as working pairs. They found the lower operation temperature and the faster operation period is for the silica gel/methanol system [86].

A design scheme of a new continuous combined solid adsorption refrigeration/heating hybrid system driven by solar energy was proposed by Zhang and Wang in 2002. They constructed the thermodynamic theory of this system and investigated the performance simulation and analysis under normal working conditions. From the experimental results, the system had a refrigerating capacity of 0.15 [MJ] per kg zeolite in the day-time and a refrigeration capacity of 0.34 [MJ] per kg zeolite in the evening. During the day-time, when the system works on the heating mode, it produced 290 kg of hot water at about 45°C for family use [87].

L.W. Wang, J.Y Wu, R.Z Wang, Y.X Xu, S.G Wang and X.R Li (2003) studied three types of adsorption beds and two types of activated carbon/methanol adsorption systems. They compared the structure of adsorption beds, performance of adsorbents, performance of different adsorption beds and different systems. Their results showed: (1) The heat transfer coefficient of a solidified bed are much higher than that of a granular bed. (2) The design of gas flow channels in adsorption beds is very important to the performance of mass transfer and the performance of the whole system [76].

Yeung and Sumathy (2003) presented a work about the functioning of a solar operated hybrid adsorption ice-making machine utilizing AC fiber/methanol as the working pair. Their study indicated

that using multi adsorption beds instead of the conventional single adsorber, the system performance could be improved. They employed an ETC collector with an uncovered area of 2 m^2. Consequently 6 kg of ice was produced per day with a COP of 0.56 [88].

Design, construction and set run of an activated carbon/methanol adsorption solar refrigerator was presented by Anyanwu and Ezekwe in 2003. According to them, the experimental set-up and results were as follows: "In this flat plate type collector-generator-adsorber used a clear plane glass sheet of exposed effective area of 1.2 m^2. The steel condenser tube with a square plan view was immersed in a pool of stagnant water contained in reinforced cement concrete tank. The evaporator was a spirally coiled copper tube immersed in stagnant water. Adsorbent cooling, during the adsorption process is both by natural convection of air flow over the collector plate and tubes. The night sky radiation was facilitated by removing the collector box end cover plates. During the study the ambient temperatures varied for adsorbate generation and adsorption process over 18.5– 34 °C. The refrigerator yielded evaporator temperatures was ranging over 1.0–8.5°C from water initially in the temperature range 24– 28°C. Accordingly, the maximum daily useful cooling produced was 266.8 [kJ/m^2] of collector area" [89].

Khattab (2004) presented the description and operation of a simple structure, low cost solar-powered adsorption refrigeration module with the solid adsorption pair of local domestic type charcoal and methanol. The testing of the module was mainly focused on the adsorption bed. Therefore, four types of bed techniques and four reflector arrangements to heat the adsorption bed had been proposed and tested under climatic condition of Cairo (30 °C latitude). The daily ice production was ranging from 6.9 to 9.4 [kg/m^2] and COP solar of 0.136 and 0.159 for cold and hot conditions respectively. His test results showed that, the time duration during which the bed temperature is above 100 °C was found to be 5 h, with a maximum temperature of 120 °C in winter. In summer, the corresponding values 6 h and 133 °C. During cooling, the minimum bed temperature recorded in either winter or summer time is very close to the ambient temperature due to the absence of bed insulation [90].

Wang and Oliveira (2006) designed and carried out a study on the energy efficiency of a new solar energy adsorption cooling system. Their system is described as follows. "The chiller consisted of four subsystems such as a solar water heating unit with 49.4 m^2 solar collecting area, a silica gel/water adsorption chiller, a cooling tower and a fan coil unit. In order to achieve continuous refrigeration, two adsorption units are operated out-of-phase with mass recovery cycle in the adsorption chiller. Test results showed that, under climatic conditions of daily solar radiation of about 16– 21 [MJ/m^2] , the chiller can furnish $14-22°C$ chilled air with an average cooling output ranging from 3.2 – 4.4 [kW]and solar cooling COP was about 0.13". They found that the new system had a higher solar energy conversion efficiency than the conventional solar thermal power generation system. The energy efficiency increased to 58 % from 10.2 %, and the energy efficiency increased to 15.2 % from 12.5 % [91].

Lambert (2007) described the design and performance of a solar powered adsorption heat pump for residential cooling. The adsorption device utilizes economical, robust configurations (shell-and-tube) and components (helical annular finned tubes, multi-lumen tubes) commonly employed in heat exchangers in a manner heretofore untried, as well as other enhancements (metal wool to diffuse heat throughout the adsorbent). The system utilized carbon/ammonia as a working pair, provided ice 24 hour cooling under high heat source temperature of 170 °C and the specific cooling power 264 [W/ kg] was expected [92].

In 2008, Dr. Uli Jakob and Walter Mittelbach [79] developed a system consisting two identical modules. Each module contains a heat exchanger for the adsorption material and a second heat exchanger for evaporation and condensation of the process water. Both heat exchangers are assembled into one single vacuum tight container forming a sealed unit that is connected to the surroundings only by hydraulic piping. This type of design configuration helped to lower the material, weight and volume of the adsorption cooling system which is one of the problems affecting the development of this type of system. At the present stage of development the adsorption design heat exchanger surface is coated with silica gel using epoxy resin as adhesive this helps them with a faster heat transfer, another recognized problem in this type of system.

W.S. Chang et al [93] designed and tested an adsorption cooling system with silica gel as the adsorbent and water as the adsorbate. This was experimentally studied to reduce the manufacturing costs and simplify the construction of the adsorption cooling system. A vacuum tank was designed to contain the adsorption bed and evaporator/condenser. Flat-tube type heat exchangers were used for adsorption beds in order to increase the heat transfer area and improve the heat transfer ability between the adsorbent and heat exchanger fins. Under the standard test conditions of 80 °C hot water, 30 °C cooling water, and 14 °C chilled water inlet temperatures, a cooling power of 4.3 [kW] and a coefficient of performance (COP) for cooling of 0.45 was to be achieved. It provided a specific cooling power (SCP) of about 176 [W/ (kg adsorbent)] with lower hot water flow rates, a higher COP of 0.53 was achieved

Thermal analysis of an activated carbon solar icemaker has been experimentally studied by Naef, Qasem, Maged and Shaarawi. The results showed that the system performance in winter is better than in summer under the climate conditions for the city Dhahran [94].

A computational fluid dynamics (CFD) transient simulation of finned tube type adsorber/desorber employing activated carbon/ethanol was analytically and experimentally studied by Skandar, Takahiko, Bidyut and Shigeru. Simulation results showed that temperature and pressure profiles agree fairly with experimental data at lower adsorbent thicknesses. Moreover, it is found that adsorption kinetics restricted the amount adsorbed to 45% possible amount for adsorption/desorption time of 350 s [18].

2.3.2 Simulation studies

Hu et. al. (1994) developed a numerical code using FORTRAN language in order to simulate and optimize a solar refrigeration unit. The system works discontinuously using activated carbon/methanol as a working pair. They found, that the efficiency of the adsorption bed can be improved with an increase in solar insolation. They predicted the existence of an optimum outside diameter for the adsorption tube that depended on the local climatological conditions [95]. In 1994, Watabe and Yanadori [96] designed and studied the cooling characteristic of silica gel /ethanol.

A three-stage silica-gel/water adsorption cooling system was studied by Saha et al. [97]. They proposed an analytically study of the performance. Their adsorption system was driven by the waste heat temperature between 55 °C to 85 °C as the heat source.

Boelman et al. [98] studied the influence of thermal capacitance of the adsorber/desorber and heat exchanger U-values (adsorber/desorber, evaporator, and condenser) on the cooling capacity, power density, and COP of a silica gel/water chiller. The system is driven by low-grade waste heat 85 °C and

cooled by water at $31\,°C$ and operates on relatively short cycle times (420 seconds adsorption/desorption; 30 second adsorber/desorber sensible cooling and heating).

The effect of heat exchanger design on the system performance of silica gel adsorption refrigeration systems has been also investigated by Alam et al. [40].

Li and Wang (2003) proposed theoretically a prototype of freezer using solar plate. They studied the mass and heat transfer in the adsorption bed of system at constant pressure. They concluded, that the studied prototype is a good optimization system for the solar assisted freezer and the dynamic response of the solar solid-adsorption refrigerator had obtained $14.4\,\%$ accuracy [76].

Li and Wang studied theoretically and experimentally heat and mass transfer in an adsorbent bed for a flat plate solar adsorption ice-maker. 10 kg of methanol and 42 kg of activated carbon were used in a rectangular adsorbent bed of $1.5\,m^2$ solar collector. The experimental analysis was done by constructing a device in lab and simulating the solar radiation by means of quartz lamps. The investigation showed that the numerical results from the theoretical study were in agreement with the experimental results at COP of 0.125 and 0.132 and the amounts of produced ice were 8 and 7.8 kg for 30.24 and 29 [MJ] of incident solar radiation, respectively [99].

Khan, Sultana, Akisawa and Kashiwagi have investigated a numerical simulation of advanced adsorption chiller and they could improve the performance of the chiller using the mass recovery [100].

Anyanwu et al [101] investigated the effects of the heat transfer of a new heat exchanger design parameter on the switching frequency, and the results showed that the optimum switching frequency was very sensitive to the heat exchanger's design parameters, and increases with the increase of adsorbent granules packing. They presented also a thermodynamic design procedure for solid adsorption solar refrigeration and applied to systems using activated carbon/methanol, activated carbon/ammonia and zeolite/water adsorbent/adsorbate pairs. The results obtained showed that zeolite/water is the best pair for the air conditioning application while activated carbon/ammonia is preferred for ice making, deep freezing and food preservation. In all cases, the system depends strongly on adsorption and condensation temperatures and weakly on the evaporator temperature.

Liu and Leong (2008) have investigated a new transient two-dimensional numerical model utilizing zeolite/water. They studied this model with non-constant condensation pressure for different types of solar collectors compared under certain conditions. Their work was focused on study the heat and mass transfer behavior inside the adsorber and effect of mass flow rate of condenser cooling water on system performance. Although the generation phase was considered as an isobaric process, they claimed, that the simulated pressure during the isobaric generation phase is not constant and changes with time. Their result also showed, that both COP and SCP increase with increasing the mass flow rate of cooling water in the condenser. Liu and Leong have analytically investigated the influence of operating conditions on the performance of an adsorption cooling system based on the zeolite 13X-water working pair [102].

Using FORTRAN language, A.El Fadar, A. Mimet and M. Perez-Garcia (2009) simulated a two beds adsorption refrigeration system powered by parabolic trough solar collector. They selected activated carbon/ammonia as working pair. In their work the heat balance in the solar collector components and instantaneous heat and mass transfer in adsorbent bed have been studied and the temperature, pressure and adsorbed mass profiles in the two beds have been shown. Under the climatic conditions of daily solar radiation being about $17.5\,[MJ/m^2]$ (Heat source temperature of $100\,°C$), the system could

achieve a promising performance COP of 0.43 and could produce a daily useful cooling of 2515 [kJ] per 0.8 m^2 of collector area [103].

The analysis of the cooling and adsorption processes was investigated by Ogueke and Anyanwu. Their study showed that low condenser pressure increases the adsorption process while the evaporator pressure should be high to increase the adsorption process. They found also the optimum value of initial concentration of methanol was 0.21 [kg/kg] to obtain the best adsorbing of adsorbate (the maximum concentration was about 0.29 [kg/kg]). The produced ice increased from 0 to about 0.4 $[kg_{ice}/kg_{sorbent}]$ [104].

H. Z. Hassan, A. A. Mohamad and R. Bennacer (2011) developed a computer program written in C++ in order to produce a more realistic theoretical simulation study for adsorption refrigerating system using activated carbon/methanol as working pair. Their simulation technique taken into account the heat and mass transfer inside the adsorption bed, the condenser, and the evaporator. They further studied the local thermal conductivity and pressure variation of the reactor on transient. It revealed that an improvement in COP to 0.211 [105].
Matlab–Simulink was used to simulate the operating characteristics of the adsorption chiller by Zhang et. al. (2011). They investigated the operating characteristics of a lumped parameter model of a silica gel/water adsorption chiller driven by solar energy. Effects of the cycle time, the capacity of hot water tank and the initial hot water temperature on the performance of the chiller were analyzed. The system could be obtained an average cooling capacity of 6.04 [kW] and average coefficient of performance COP of 0.458 [106].
Suleiman et.al. (2012) carried out a modeling and simulation study of a solar powered adsorption refrigeration system using flat plate solar collector, with activated carbon/methanol as the adsorbent/adsorbate pair. This study was implemented to determine the effects of generation, evaporation and condensation temperatures on the performance of the cooling system using the TRNSYS software over a period of a typical year. The evaporation and condensation temperature considered in this study were 0 °C and 25 °C, respectively. Their simulation results showed, that the system using the Flat plate collector can be able to achieve a refrigeration effect of 4815 [kJ] and cooling coefficient of performance (COP) of 0.608 [107].

A new approach for the performance analysis of a single-stage solar solid-adsorption cooling system using AC-R134a as working pair was proposed by Baiju and Muraleedharan (2012). Artificial neural network has been used to determine the performance parameters of the system, namely, coefficient of performance, specific cooling power, adsorbent bed discharge temperature and solar cooling coefficient of performance. They say; “The ANN used in the performance calculation was made in MATLAB background using neural network tool box. In this study the temperature, pressure and solar intensity were used as an input layer. The back propagation algorithm was developed by considering three different variants namely scaled conjugate gradient, Pola-Ribiere conjugate gradient, Levenberg-Marquardt (LM) and logistic sigmoid transfer function were used for finding performance (COP, SCP, COP solar and desorption temperature). After training, it was observed that LM algorithm with 9 neurons is best suitable for modelling the solar adsorption refrigeration system” [108].

A simple thermodynamic differential analysis for ice machine working with activated carbon/methanol has been developed by H. Z. Hassan. It is found that the system attains a refrigeration performance of 61 % with a refrigeration effect produced inside the evaporator estimated 12.15 MJ per cycle [12].

We have noticed that many researchers have been interested in the study of the adsorption refrigeration system both numerically and experimentally with the different working pairs. The popular typical working pairs were silica gel/water, silica gel/methanol, zeolite/water, activated carbon/ammonia, and activated carbon/methanol. The effectiveness of the adsorption systems using the different working pairs were investigated and assessed.

Based on the previous investigation works, it is found, that the big obstacle to development of adsorption refrigeration technology is the low coefficient of performance and the long cycle time to generate the refrigerant which differs based on the working pairs used and the driving temperature. Another problem is that the simplest cycle of an adsorption refrigeration system works intermittently, because the adsorption reactor can't work as desorber and adsorber at the same time, which requires time to desorb and adsorb the circulated refrigerant into the condenser and from the evaporator. This means the amount of cold produced per cycle is smaller compared with the refrigeration systems which work continuously. Research efforts by previous investigators have therefore been focused on improving the performance and finding new composite adsorption materials. But the adsorption working pairs used don't have ideal characteristics and although the physical properties of the adsorption materials are limited, most of the published studies on the adsorption systems utilized one adsorbent in their adsorbent beds to simulate the system and to enhance its performance.

To produce continuous refrigeration power, the analytical, thermodynamic and numerical investigation of a new adsorption ice production system using two different adsorbents together in one machine was presented in this work. The system in this study comprises with two adsorption beds, that the first adsorption bed was filled by silica gel and the second by activated carbon as adsorbents. Methanol was used as adsorbate and refrigerant with both the reactors. This research presents a simulation of silica gel - / activated carbon -methanol finned tube adsorption reactor and the present work aims to enhancing the amount of ice produced, improving the cycle time and saving of the required input heat by increasing the mass flow rate of the refrigerant. This suggested strategy is completely different from the conventional adsorption systems which work using one working pair of adsorbent/refrigerant.

Using the thermal heating such as industry waste heat or solar energy has some severe drawbacks in the development of adsorption technology. A major disadvantage is the adsorption reactor requires a long time of about one hour to desorb the required amount of the adsorbate. Moreover the setup has a complex design, composed of tubes of hot water and many fins. In order to overcome the problems found with conventional methods (thermal heating), a new design of two adsorption reactors with a new heat source has been studied and simulated in frame of this work. Our work deals also with a mathematical modeling and numerical simulation of an induction heating system for two adsorption reactors filled by silica gel and activated carbon as adsorption material and methanol as adsorbate. The purpose of this study is the use of electromagnetic induction technology as a new heat source of the adsorption ice production system. The induction heating will be compare with thermal heating, therefore, two finned-tube heat exchangers were designed (named SG-adsorption reactor and AC-adsorption reactor) in order to contain two different adsorbents and to generate the same desorbed refrigerant amount of 1 kg_{meth} and also to increase the heat transfer ability between the particles of adsorbents and heat exchanger fins.

Chapter 3

Combined Adsorption Ice Production System Using Two Adsorption Elements

3.1 Introduction

In this chapter, the transient modelling for a new construction of an adsorption refrigeration system was investigated. This adsorption system utilizes both silica gel (SG) and activated carbon (AC) together in one adsorption reactor and is named in this work the combined **A**dsorption **I**ce **P**roduction system (com-AIP system). The new strategy of the com-AIP system operates with silica gel/methanol as the first working pair in the SG-bed and operates with activated carbon/methanol as the second working pair in the AC-bed. This strategy (com- AIP system) is completely different from the conventional adsorption reactors, which are filled with one adsorbent in one bed or in two beds.

A fined-tube heat exchanger was designed *(named combined adsorption reactor)* in order to contain two different adsorbents and increase the heat transfer ability between the particles of adsorbents and heat exchanger components (tubes and fins). A cycle simulation computer program of this innovative system was developed to analyze the refrigeration energy Q_e and coefficient of performance COP variations by varying the inlet temperature of the heat transfer fluid (HTF) and adsorption/desorption cycle time. The transient behavior of heat and mass transfer fluids has been also studied. Moreover, the simulation study will focus on study the impact of the amounts of methanol desorbed M_{des}, adsorbed M_{ads} and the desorption temperature inside the com-adsorption reactor on the performance and on the amount of produced ice M_{ice}.

The new technique of the com-AIP system aims to save the input energy required from the external heat source and improve the refrigeration energy Q_e by increasing the mass of the desorbed refrigerant M_{des}, which leaves from the com-adsorption reactor (both the SG-and AC-beds) into the condenser. Consequently, the coefficient of performance COP of the com-AIP system rises.

The com- adsorption reactor allows using the advantages of physical properties of both the adsorbents SG and AC. Consequently, this innovative com-AIP system utilizes effectively low-temperature heat sources of temperature, because of the inferior thermodynamic properties of methanol and the low regeneration temperature from silica gel and activated carbon as adsorbents.

3.2 Thermodynamic cycle of the com-AIP system

The schematic diagram of the combined **A**dsorption **I**ce **P**roduction system and its components are shown in **F**ig 3.1. The main components of the system studied are the com- adsorption reactor, a condenser, an evaporator, a throttling device and 4 one-way control valves. The com- adsorption reactor consists of two adsorption elements (SG-bed and AC-bed). The configuration of these adsorption elements (two beds) is taken as identical design and same size. In the proposed design the effect of metallic components of the com-adsorption reactor is taken into account. The basic

adsorption thermodynamic cycle is illustrated on the conceptual clapeyron diagram, **F**ig. 3.2. The cycle of the com-AIP system consists mainly of these processes:

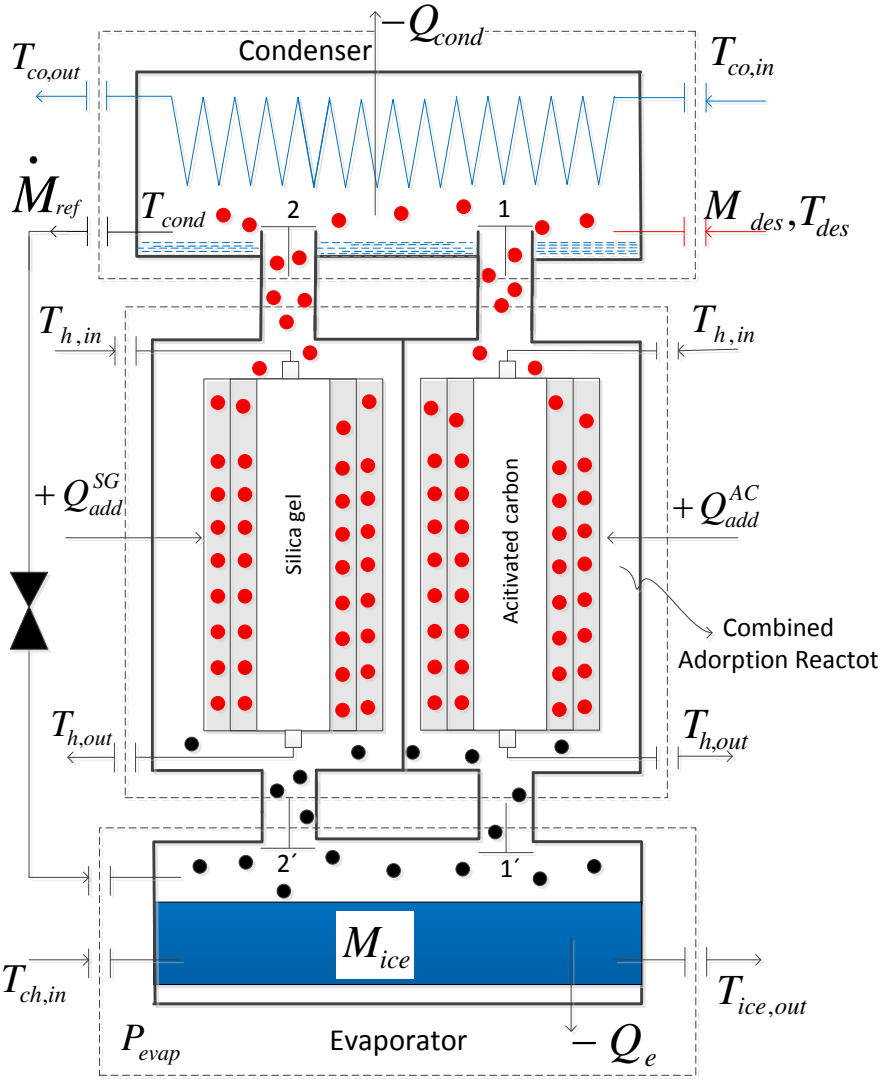

Figure 3.1: Schematic diagram of com- AIP system

1→2	Isosteric heating and pressurization process at the constant higher concentration x_{max}^{SG} in the SG-bed (pre-heating).
1→2`	Isosteric heating and pressurization process at the constant higher concentration x_{max}^{AC} in the AC-bed (pre-heating)
2→3	Isobaric heating and desorption process from the silica gel particles.
2`→3`	Isobaric heating and desorption process from the activated carbon particles.
3→4	Isosteric cooling and depressurization process at the constant lower concentration x_{min}^{SG} in the SG-bed (pre-cooling)
3`→4`	Isosteric cooling and depressurization process at the constant lower concentration x_{min}^{AC} in the AC-bed (pre-cooling).
4 →1	Isobaric cooling and adsorption process for the SG-adsorbent.
4`→1	Isobaric cooling and adsorption process for the AC-adsorbent.
A→B	Condensation process at constant condenser pressure p_{cond}.
C →D	Evaporation process at constant evaporator pressure p_{evap}.

3.2.1 Adsorption working pairs used

Usually the conventional adsorption systems work using one adsorption material with adsorbate as working pair, but the com-AIP system in this study comprises with two adsorption beds using two different adsorption materials, that the first bed was filled by silica gel as adsorbent and the second by activated carbon. Methanol was used as adsorbate and refrigerant with both the beds. This section presents the selection criteria of the two adsorption working pairs. According to working pair comparisons in the literature and in the labor market, for low-grade temperature sources, heights adsorbate concentration and largest evaporation latent heat, the appropriate pairs for refrigeration purposes are activated carbon/methanol and zeolite/water [109]. However the zeolite/water pair is not utilized for freezing application. So the suitable pair that can be used to produce ice (function of the com-AIP system) is activated carbon/methanol. Methanol has a higher operation pressure compared with water under the same temperature [109]. Activated carbon with methanol as a working pair is broadly used in adsorption refrigeration systems due to the high adsorption/desorption concentration, which reaches 0.45 [kg/kg] and low desorption heat, which is about $1800 - 2000$ [kJ/kg]. Moreover, adsorbate uptake capacity of activated carbon is more than that of silica gel. But due to a lower specific heat capacity C_P and a faster sorption kinetic of the silica gel particles [86], the silica gel was utilized in the com-AIP system.

The other important factor is volumetric mass density of the adsorption material $\rho_S[kg/m^3]$ which affects the volume of adsorption reactor. Density of activated carbon is about 500 $[kg/m^3]$, whereas density of silica gel is about 750 $[kg/m^3]$. Therefore, the needed amount of activated carbon is smaller than the amount of silica gel inside the same volume of adsorption reactor [13]. The system of activated carbon/methanol and silica gel/methanol needs low grade heat source, because of the inferior thermodynamic properties of methanol and the low regeneration temperature from silica gel and activated carbon as adsorbents [38-39]. On the other hand, methanol operates at sub atmospheric pressure; the low-pressure system is suitable to utilize the adsorption cold system as ice maker [110].

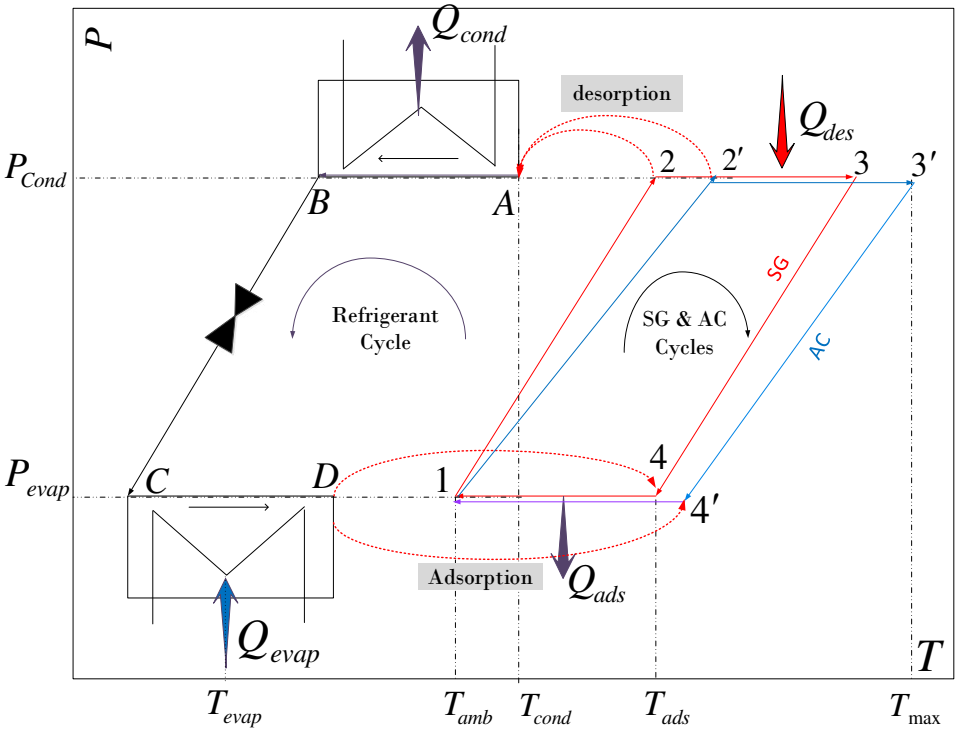

Figure 3.2: Clapeyron diagram for the basic **A**dsorption **I**ce **P**roduction thermodynamic cycle

3.2.2 Working principle of the com- AIP system

To complete a full cycle for the proposed system, the system needs 8 modes A, B, C, D, E, F, G and H. In **T**ab. 3.1 is shown for one cycle the operational strategy of the proposed com-AIP system. The working processes are described in the following:

In the **mode A** the com-adsorption reactor works in the isosteric pre-heating process. Hot water flows into SG-bed and AC-bed. The both beds are heated up by the hot water from a driving heat source. When the pressure of both the beds are nearly equal to the pressure of condenser, both the AC-bed and the SG-bed are connected to the condenser in order to start the desorption process.

In the **mode B** the com–adsorption reactor works in the isobaric desorption process. The desorption-condensation process takes place at the condenser pressure. In this mode only SG-bed is heated up to the end desorption temperature $T_{des,max}$ by the heat input Q_{des}^{SG} provided by the driving heat source. The resulting refrigerant (methanol vapor) from SG-bed is cooled down by the temperature T_{cond} in the condenser by the cooling water. The cooling water flows through the condenser and carries away the condensation heat Q_{cond}. The condensate passes through expansion device into the evaporator.

Mode	A	B	C	D	E	F	G	H
SG-bed	Heating	Desorption	Cooling	Adsorption	Heating	Desorption	Cooling	Adsorption
AC-bed	Heating	Desorption	Desorption	Desorption	Heating	Desorption	Desorption	Desorption
v_1	●	○	○	○	●	●	●	●
v_2	●	○	●	●	●	○	●	●
$v_{1'}$	●	●	●	●	●	○	○	○
$v_{2'}$	●	●	●	○	●	●	●	○

Heating Desorption Cooling Adsorption ○ Open ● Closed

Table 3.1: The states of valves in operation and working processes of the com- AIP system

In the **Mode C** the SG-bed is in the isosteric pre-cooling process and the AC-bed is still in the desorption process. During pre-cooling process the SG-bed is isolated from the evaporator and the condenser. The operating states of the valves are shown in **T**ab. 3.1. The cooling water is supplied to the SG-bed for short time t_{cool}^{SG} and is cooled down to the adsorption temperature T_4 as shown in **F**ig. 3.2.

In the **Mode D** the SG-bed is connected with the evaporator in order to start the adsorption process. While the SG-bed begins the adsorption process, the AC-bed is still in the desorption process. The adsorption-evaporation process is obtained completely inside SG-bed, which is the last process for the SG-bed. After this mode the SG-cycle will return to its initial position. AC-bed is at the end position of desorption-condensation process. The AC-bed is heated up to the end desorption temperature $T_{des,max}$ by the heat input Q_{des}^{AC} provided by the driving heat source.

In the **Mode E** the AC-bed begins the pre-cooling process, whereas the SG-bed begins again the pre-heating. Cooling water is supplied to the AC-bed for short time t_{cool}^{AC}. This time, the AC-bed is isolated from evaporator and condenser and is connected with cooling water.

In **mode F** the SG-bed works as a desorber and AC-bed works as an adsorber. In this mode the SG-adsorber is at the end position of desorption-condensation process.

In **mode G**, the pre-cooling process for SG-bed starts and the AC-bed is still in the adsorption process.

In **mode H**, Both the SG-bed and AC-bed work as an adsorber. Because of the adsorption speed, the concentration level of SG-adsorber reaches in nearly equilibrium faster than the concentration level of

AC-adsorber. In this mode the AC-adsorber reachs at the end position of adsorption-evaporation process, which is the last process for the AC-bed.

3.2.3 Geometry model parameters of the com-adsorption reactor

Fig. 3.3 shows the schematic view of the finned tube heat exchanger developed in this study. It mainly consists of:

1. four tubes of copper having inner diameter 17.3 [mm] and length 450 [mm];
2. fins of aluminum characterized by fin height $H_f = 200$ [mm], fin thickness $\delta_f = 1$ [mm] and fin spacing $S_f = 4$ [mm];
3. Activated carbon of type Maxsorb packed between the fins of two tubes and silica gel packed between the fins of another two tubes.
4. Mesh sheet covering the material of com-heat exchanger.

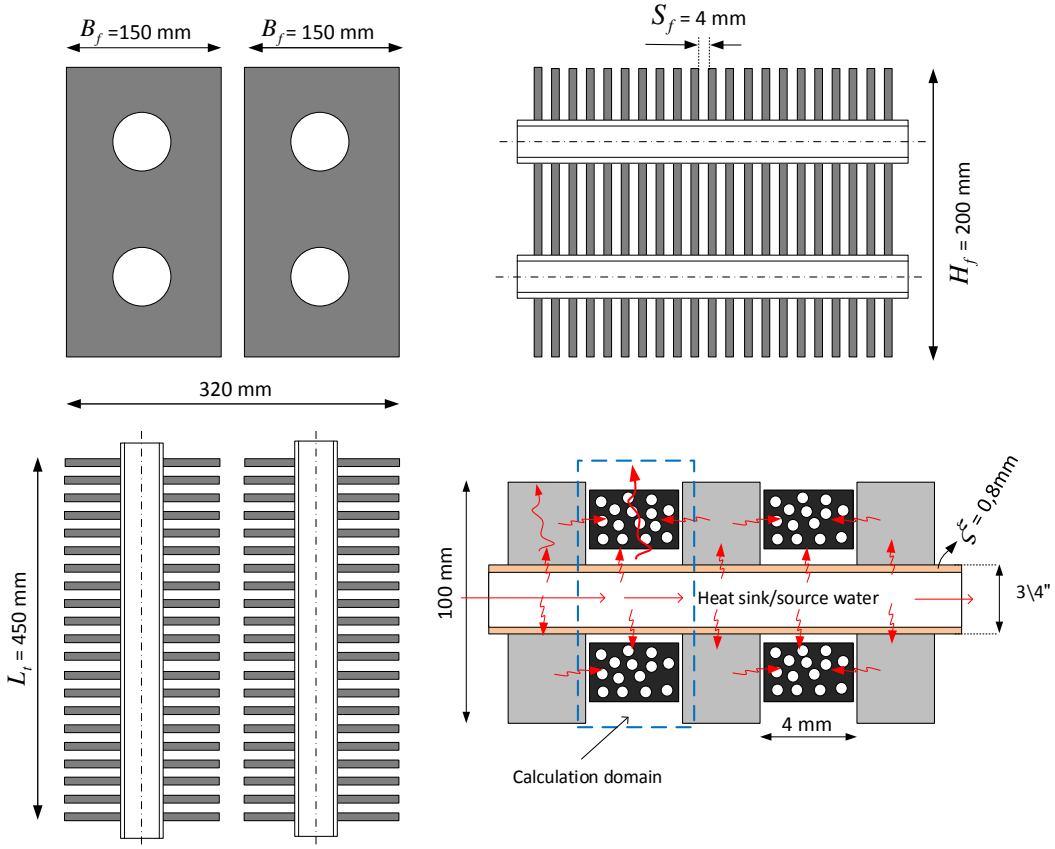

Figure 3.3: Schematic diagram for the rectangular finned tube adsorption reactor

This com-heat exchanger is composed of flat tube with rectangular fins. There are 4 tube horizontally and 90 fins vertically arranged adsorption heat exchanger in all, between 3.9 kg silica gel and 3.3 kg activated carbon are employed. The AC-and SG-bed are taken as same size and the AC-and SG-particles are taken as same diameter (Ø 1.15 mm). This com-heat exchanger is used as desorber during desorption cycles and as an adsorber during adsorption cycles. The characteristics of the fined–tube heat exchanger used is listed in **T**ab. 3.2.

Parameter	Value	Unit
Dimension	$450 \times 320 \times 200$	[mm]
Number of flat tube	4	[−]
Tube diameter	17.3	[mm]
Tube thickness (ξ)	0.8	[mm]
Number of fins	90	[−]
Fin width (B_f)	150	[mm]
Fin spacing (S_f)	4	[mm]
Heat transfer area	10.68	[m^2]

Table 3.2: Characteristics of the fined –tube combined heat exchanger

3.3 Mathematical formulation and thermodynamic analysis approach

A schematic of the com-adsorption reactor is shown in Fig. 3.3. The modelling of this heat exchanger involves heat and mass conversation equations for the adsorbent particles of both SG and AC, the adsorbate refrigerant (methanol), the heat exchanger fluid (water) and the metallic components of the reactor (the metal tubes and the fins). The following assumptions are utilized:

- The average granules diameters of adsorbents SG and AC are similar.
- The temperature of refrigerant and adsorbents at the same point is the same.
- The adsorbed phase is considered as a liquid and the vapor methanol behaves as an ideal gas.

3.3.1 Adsorption and desorption equations

The methanol concentrations (adsorbate uptake) x [kg/kg] by the SG- and AC-particles depends on the pressure and the temperature of the adsorption reactor. The variation of the methanol concentration ratio along the isobaric heating process (desorption) is defined for SG-bed and AC-bed by the following equations:

$$x_{2\to3}^{SG} = x_0^{SG} \exp\left\{-D^{SG}.\left[T_{2\to3}.\ln\left(\frac{p_{sat}(T_{2\to3})}{p_{cond}}\right)\right]^n\right\} \tag{3.1}$$

$$x_{2'\to3'}^{AC} = x_0^{AC} \exp\left\{-D^{AC}.\left[T_{2'\to3'}.\ln\left(\frac{p_{sat}(T_{2'\to3'})}{p_{cond}}\right)\right]^n\right\} \tag{3.2}$$

The variation of the methanol concentration ratio for SG-bed and AC-bed along the isobaric cooling process (adsorption) is defined by the following equation:

$$x_{4\to1}^{SG} = x_0^{SG} \exp\left\{-D^{SG}.\left[T_{4\to1}.\ln\left(\frac{p_{sat}(T_{4\to1})}{p_{evap}}\right)\right]^n\right\} \tag{3.3}$$

$$x_{4'\to1}^{AC} = x_0^{AC} \exp\left\{-D^{AC}.\left[T_{4'\to1}.\ln\left(\frac{p_{sat}(T_{4'\to1})}{p_{evap}}\right)\right]^n\right\} \tag{3.4}$$

where $p_{sat}(T)$ is saturation pressure corresponding to the reactor temperature. For a given evaporator temperature T_{evap}, the corresponding evaporator pressure p_{evap} is the saturation pressure of the refrigerant vapor $p_{sat}(T_{evap}) = p_{evap}$.

The relation between the pressure and temperature during the isosteric pre-heating processes inside both the SG-and AC-beds is described by following equations:

$$p_{1\to2}^{SG} = p_{sat}(T_{1\to2}).\exp\left\{\frac{-1}{T_{1\to2}}\left[\frac{1}{D^{SG}}\ln\left(\frac{x_0^{SG}}{x_{max}^{SG}}\right)\right]^{1/n}\right\} \tag{3.5}$$

$$p_{1\to2'}^{AC} = p_{sat}(T_{1\to2'}).\exp\left\{\frac{-1}{T_{1\to2'}}\left[\frac{1}{D^{AC}}\ln\left(\frac{x_0^{AC}}{x_{max}^{AC}}\right)\right]^{1/n}\right\} \tag{3.6}$$

The maximum value x_{max} is defined by the ambient temperature T_{amb} and evaporation pressure $x_{max} = f(T_{amb}, p_{evap})$. The relation between the pressure and temperature during the isosteric pre-cooling processes inside both the SG-and AC-beds is described by following equations:

$$p_{3\to4}^{SG} = p_{sat}(T_{3\to4}).\exp\left\{\frac{-1}{T_{3\to4}}\left[\frac{1}{D^{SG}}\ln\left(\frac{x_0^{SG}}{x_{min}^{SG}}\right)\right]^{1/n}\right\} \quad (3.7)$$

$$p_{3'\to4'}^{AC} = p_{sat}(T_{3'\to4'}).\exp\left\{\frac{-1}{T_{3'\to4'}}\left[\frac{1}{D^{AC}}\ln\left(\frac{x_0^{AC}}{x_{min}^{AC}}\right)\right]^{1/n}\right\} \quad (3.8)$$

The minimum value x_{min} is defined by the maximum cyclic temperature T_{max} and condenser pressure $x_{min} = f(T_{max}, p_{cond})$.

According to the above mentioned equations, the processes cycle of com-AIP system can be displayed very well in (P-T) diagram, **F**ig. 3.2. In this diagram the processes are plotted as two trapeziums. The first trapezium for SG-bed is plotted between the isosteres x_{max}^{SG} and x_{min}^{SG} and the isobares p_{cond} and p_{evap}. Another trapezium for AC-bed, that is bigger than the first (simulation results) is too plotted at the same diagram with different values of x_{max}^{AC} and x_{min}^{AC} and with same evaporator and condenser pressure.

3.3.2 Isostatic heating and pressurization process

Fig 3.4 shows the energy flow diagram for the com-adsorption reactor during the isosteric and isobaric heating processes. In the isosteric heating the com-adsorption reactor which is filled with silica gel and activated carbon particles is preheated at two constant highest isostere lines, because the refrigerant concentration for SG and AC particles has different values.

In this process, the methanol concentration in the heat exchanger remains constant. The added energy Q_{heat}^{add} during the preheating process of the com-adsorption reactor is utilized to cause sensible heating of the adsorption reactor constituents. The isosteric heat added Q_{heat}^{add} is expressed as:

$$dQ_{heat}^{add} = dQ_{1\to2}^{SG} + dQ_{1\to2}^{AC}, \quad (3.9)$$

$$dQ_{1\to2}^{SG} = (dQ_{mc}^{SG} + dQ_{s}^{SG} + dQ_{a}^{SG} + dQ_{v}^{SG})_{1\to2} \quad (3.10)$$

$$dQ_{1\to2}^{AC}, = (dQ_{mc}^{AC} + dQ_{s}^{AC} + dQ_{a}^{AC} + dQ_{v}^{AC})_{1\to2}, \quad (3.11)$$

where dQ_{mc}^{S}, dQ_{s}^{S}, dQ_{a}^{S} and dQ_{v}^{S} are the differential sensible energies absorbed by the metallic components of the adsorption reactor, the solid adsorbent media, the adsorbate (refrigerant) and the adsorbate vapor phase, respectively. S indicates the SG adsorbent or the AC adsorbent.

The energy, which is introduced to the metallic components (copper tubes and aluminum fins) of the com-reactor, causes a step temperature increase.

$$dQ_{mc}^{SG} = \left(M_{t,cu}.C_{Cu} + M_{f,Al}.C_{Al}\right).dT_{1\to2}^{SG} \quad (3.12)$$

$$dQ_{mc}^{AC} = \left(M_{t,cu}.C_{Cu} + M_{f,Al}.C_{Al}\right).dT_{1\to2}^{AC}, \quad (3.13)$$

where $M_{t,cu}$ and $M_{f,Al}$ are the mass of the copper tubes and the aluminum fins. C_{Cu} and C_{Al} are the specific heat capacity of the metallic materials (copper and aluminum) used in the adsorption reactor.
The thermal energy consumed in sensible heating of the solid adsorbent media causes a step temperature rise from T_1 to T_2 for the SG-adsorbent bed and from $T_1$to T_2, for the AC-adsorbent bed.

$$dQ_s^{SG} = M_{SG}.C_{SG}.dT_{1\to2}^{SG} \tag{3.14}$$

$$dQ_s^{AC} = M_{AC}.C_{AC}.dT_{1\to2'}^{AC} \tag{3.15}$$

During the preheating process, there is no desorption taking place and therefore, the mass of the adsorbate phase M_a[kg] remains constant. The differential amount of energy input to the adsorbate phase (methanol liquid) appears in the increase of the specific adsorbate internal energy u_a [kJ/kg] and is given by:

$$dQ_a^{SG} = (M_a.du_a)_{1\to2}^{SG} = x_{max}^{SG}.M_{SG}.C_{V,a}.dT_{1\to2}^{SG} \tag{3.16}$$

$$dQ_a^{AC} = (M_a.du_a)_{1\to2'}^{AC} = x_{max}^{AC}.M_{AC}.C_{V,a}.dT_{1\to2'}^{AC} \tag{3.17}$$

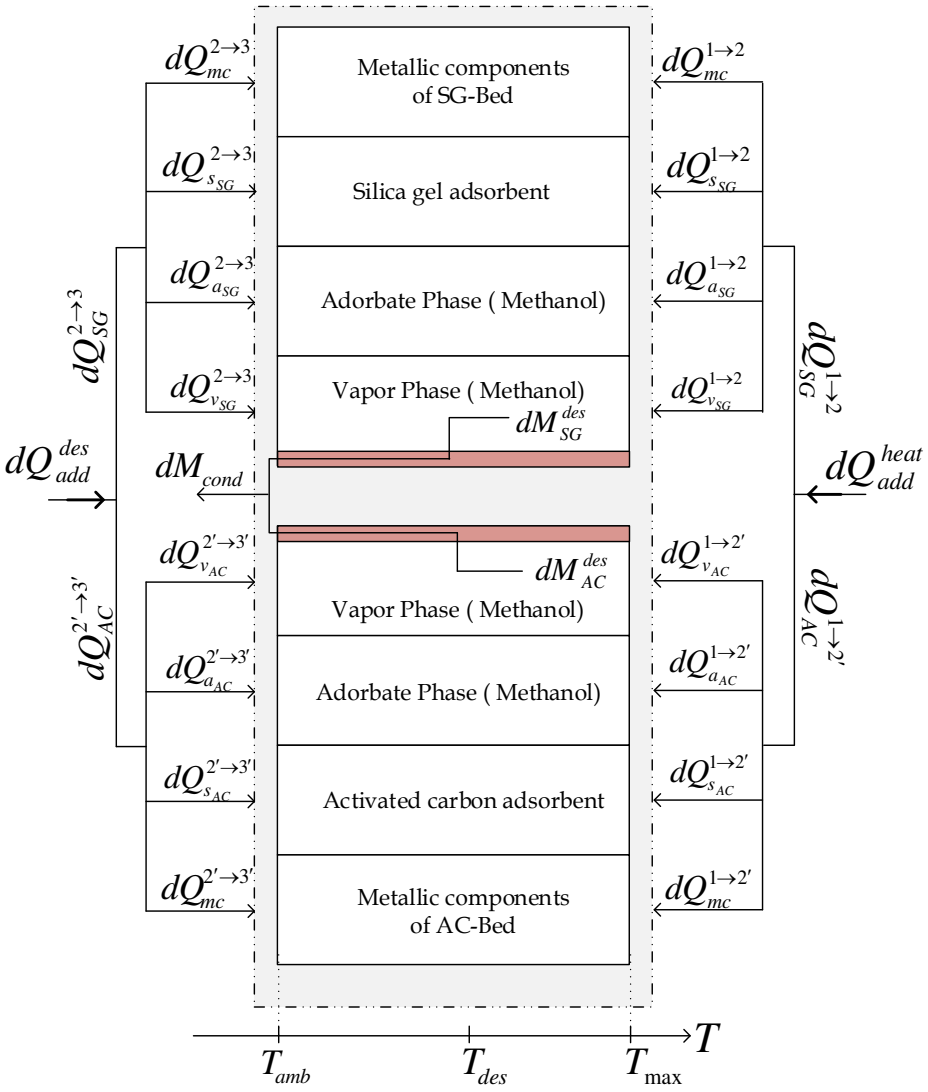

Figure 3.4: Energy flow diagram for the com-adsorption reactor during the isosteric and isobaric heating processes.

The differential amount of energy required by the refrigerant vapor phase is calculated as follows:

$$dQ_v^{SG} = (M_v.du_v)_{1\to2}^{SG} = M_v.C_{V,v}.dT_{1\to2}^{SG} \tag{3.18}$$

$$\delta Q_v^{AC} = (M_v.du_v)_{1\to2'}^{AC} = M_v.C_{V,v}.dT_{1\to2'}^{AC} \tag{3.19}$$

where u_v is the specific adsorbate internal energy of the vapor phase. M_v [kg] is the mass of the vapor phase which remains constant during pre-heating process and is given by:

$$M_v = \rho_v(p_{evap}, T_1).(\beta - \emptyset).V \tag{3.20}$$

The variation of the adsorbate volume fraction $\emptyset$ along the highest concentration path can be determined from the following equation [12].

$$\emptyset = x_{max}.\frac{\rho_s}{\rho_{a(T)}}.(1-\beta) \tag{3.21}$$

where β and ρ_s are the porosity and the density of the adsorption material, respectively. V is the emptied volume inside the adsorption reactor.

3.3.3 Isobaric heating and desorption process

Both the SG the AC adsorbents during the isobaric heating undergoes the desorption phase at the same constant condenser pressure. The methanol concentration by the SG-particles decreases by increasing the desorption temperature from the maximum value $x_{max}^{SG}(p_{cond}, T_{cond})$ to the minimum value x_{min}^{SG} $(p_{cond}, T_{des,max})$ and the methanol concentration by the AC-particles decreases during this process from $x_{max}^{AC}(p_{cond}, T_{cond})$ to x_{min}^{AC} $(p_{cond}, T_{des,max})$.

The amount of the added energy Q_{des}^{add} which is required during the isobaric heating process causes sensible heating of the com-adsorption reactor constituents, activates the desorption of the refrigerant from the adsorbent media (SG and AC) and generates the gas phase. This added energy can be expressed as follows:

$$dQ_{des}^{add} = dQ_{2\to3}^{SG} + dQ_{2'\to3'}^{AC} \tag{3.22}$$

$$dQ_{2\to3}^{SG} = (dQ_{mc}^{SG} + dQ_s^{SG} + dQ_a^{SG} + dQ_v^{SG})_{2\to3} \tag{3.23}$$

$$dQ_{2`\to3`}^{AC} = (dQ_{mc}^{AC} + dQ_s^{AC} + dQ_a^{AC} + dQ_v^{AC})_{2`\to3`} \tag{3.24}$$

The energy introduced to the metallic components (copper tubes and aluminum fins) of the com-adsorption reactor causes a step temperature rise.

$$dQ_{mc}^{SG} = \left(M_{t,cu}.C_{Cu} + M_{f,Al}.C_{Al}\right)dT_{2\to3}^{SG} \tag{3.25}$$

$$dQ_{mc}^{AC} = (M_{t,cu}.C_{Cu} + M_{f,Al}.C_{Al})dT_{2`\to3`}^{AC} \tag{3.26}$$

The thermal energy consumed in sensible heating of the solid adsorbent media causes a step temperature rise from T_2 to T_3 for SG-bed and from $T_{2`}$ to $T_{3`}$ for AC-bed.

$$dQ_S^{SG} = M_{SG}.C_{SG}.dT_{2\to3}^{SG} \tag{3.27}$$

$$dQ_S^{AC} = M_{AC}.C_{AC}.dT_{2`\to3`}^{AC} \tag{3.28}$$

The differential amount of energy input to the adsorbate phase appears in the increase of the adsorbate (liquid methanol) and refrigerant vapor internal energy.
By applying in this case the conservation of energy principle on the adsorbate and refrigerant vapor phase, we get:

$$dQ_a^{SG} = (dU_a^{SG})_{2\to3} = d(M_a.u_a)_{2\to3}^{SG} = M_{SG}.C_{p,a}.d(x.T)_{2\to3}^{SG} \tag{3.29}$$

$$dQ_a^{AC} = (dU_a^{AC})_{2`\to3`} = d(M_a.u_a)_{2`\to3`}^{AC} = M_{AC}.C_{p,a}.d(x.T)_{2`\to3`}^{AC} \tag{3.30}$$

where dU_a is the step change in the total internal energy of the adsorbate refrigerant phase. Regarding the mass of the refrigerant vapor phase is varying during the desorption process. The differential amount of energy input to the vapor phase appears in the increase of the refrigerant vapor internal energy.

$$dQ_v^{SG} = (dU_v^{SG} + dM_{des}H_{ads})_{2\to3}^{SG} = d(M_v.u_v) + d(M_{des}.H_{ads})_{2\to3}^{SG} \quad (3.31)$$

$$dQ_v^{AC} = (dU_v^{AC} + dM_{des}H_{ads})_{2`\to3`}^{AC} = d(M_v.u_v) + d(M_{des}.H_{ads})_{2`\to3`}^{AC} \quad (3.32)$$

where H_{ads}, the adsorption heat per unit mass of adsorbate, which can be determined in depending on the adsorption material used. The amount of methanol that leaves the com-adsorption reactor and flows towards the condenser can be written as follows:

$$dM_{cond} = dM_{des} = (dM_a + dM_v)_{2\to3}^{SG} + (dM_a + dM_v)_{2`\to3`}^{AC} \quad (3.33)$$

3.3.4 Isostatic cooling and depressurization process

Like the pre-heating process, the methanol concentration remains constant. In this process, the com-adsorption reactor is precooled at two constant isostere lines $x_{min} = f(T_{max}, p_{cond})$ for AC-bed and SG-bed. The rejected energy Q_{cool}^{reject} during the precooling process of com-adsorption reactor causes sensible cooling of the adsorption reactor constituents. This differential amount of energy which lost from the adsorption reactor to the ambient surroundings is given by:

$$dQ_{cool}^{reject} = dQ_{3\to4}^{SG} + dQ_{3`\to4`}^{AC} \quad (3.34)$$

$$dQ_{3\to4}^{SG} = dQ_{mc}^{SG} + dQ_s^{SG} + dQ_a^{SG} + dQ_v^{SG} \quad (3.35)$$

$$dQ_{3`\to4`}^{AC} = dQ_{mc}^{AC} + dQ_s^{AC} + dQ_a^{AC} + dQ_v^{AC} \quad (3.36)$$

By the same methodology which has been followed in preheating process, the energy is lost from the metallic components of the generator is calculated from following equations:

$$dQ_{mc}^{SG} = \left(M_{t,cu}.C_{Cu} + M_{f,Al}.C_{Al}\right).dT_{3\to4}^{SG} \quad (3.37)$$

$$dQ_{mc}^{AC} = \left(M_{t,cu}.C_{Cu} + M_{f,Al}.C_{Al}\right).dT_{3`\to4`}^{AC} \quad (3.38)$$

The thermal energy which is lost in sensible form of the solid adsorbent media causes a drop temperature from T_3 to T_4 for SG- bed and from $T_{3`}$ to $T_{4`}$ AC-bed.

$$dQ_s^{SG} = (M_{SG}.C_{SG}.dT)_{3\to4} \quad (3.39)$$

$$dQ_s^{AC} = (M_{AC}.C_{AC}.dT)_{3`\to4`} \quad (3.40)$$

The differential amount of energy output from the adsorbate refrigerant appears in the decrease of the adsorbate internal energy. During the pre-cooling process, there is no desorption/adsorption taking place and therefore, the mass of the adsorbate phase M_a[kg] remains constant and is given by:

$$dQ_a^{SG} = (M_a.du_a)_{3\to4}^{SG} = x_{min}^{SG}.M_{SG}.C_{V,a}.dT_{3\to4}^{SG} \quad (3.41)$$

$$dQ_a^{AC} = (M_a.du_a)_{3`\to4`}^{AC} = x_{min}^{AC}.M_{AC}.C_{V,a}.dT_{3`\to4`}^{AC} \quad (3.42)$$

The differential amount of energy losses from the refrigerant vapor phase is calculated as follows:

$$dQ_v^{SG} = (M_v.du_v)_{3\to4}^{SG} = M_v.C_{V,v}.dT_{3\to4}^{SG} \quad (3.43)$$

$$dQ_v^{AC} = (M_v.du_v)_{3`\to4`}^{AC} = M_v.C_{V,v}.dT_{3`\to4`}^{AC} \quad (3.44)$$

where M_v[kg] is the mass of the vapor phase which remains constant during precooling process and is given by:

$$M_v = \rho_v(p_{cond}, T_{max}).(\beta - \emptyset_{3\to4}).V \tag{3.45}$$

The variation of the adsorbate volume fraction $\emptyset_{3\to4}$ along the lowest concentration path can be determined from the following equation [12].

$$\emptyset_{3\to4} = x_{min}.\frac{\rho_s}{\rho_a(T_{3\to4})}.(1-\beta) \tag{3.46}$$

3.3.5 Isobaric cooling and adsorption process

The com-adsorption reactor during isobaric cooling undergoes the adsorption phase at the same constant evaporator pressure and is cooled at the ambient temperature.

By decreasing the temperature the methanol concentration by the SG-particles increases from the minimum value $x_{min}^{SG}(p_{cond}, T_{des,max})$ to the maximum value $x_{max}^{SG}(p_{evap}, T_{amb})$ and the methanol concentration by the AC-particles increases during this process from $x_{min}^{AC}(p_{cond}, T_{des,max})$ to $x_{max}^{AC}(p_{evap}, T_{amb})$.

The amount of the rejected energy Q_{ads}^{reject} which is lost during the isobaric cooling process causes sensible cooling of the com-adsorption reactor constituents and activates the adsorption of the refrigerant on the adsorbents media (SG and AC). This rejected energy can be expressed as follows:

$$dQ_{ads}^{reject} = dQ_{4\to1}^{SG} + dQ_{4`\to1}^{AC} \tag{3.47}$$

$$dQ_{4\to1}^{SG} = (dQ_{mc}^{SG} + dQ_s^{SG} + dQ_a^{SG} + dQ_v^{SG})_{4\to1} \tag{3.48}$$

$$dQ_{4`\to1}^{AC} = (\delta Q_{mc}^{AC} + dQ_s^{AC} + dQ_a^{AC} + dQ_v^{AC})_{4`\to1} \tag{3.49}$$

The energy which is lost from the metallic components of the generator is calculated from following equations:

$$dQ_{mc}^{SG} = \left(M_{t,cu}.C_{Cu} + M_{f,Al}.C_{Al}\right).dT_{4\to1}^{SG} \tag{3.50}$$

$$dQ_{mc}^{AC} = \left(M_{t,cu}.C_{Cu} + M_{f,Al}.C_{Al}\right).dT_{4`\to1}^{AC} \tag{3.51}$$

The thermal energy which is lost in sensible form of the solid adsorbent media causes a drop temperature from T_4 to T_1 for SG-bed and from $T_{4`}$ to T_1 AC-bed.

$$dQ_S^{SG} = M_{SG}.C_{SG}.dT_{4\to1}^{SG} \tag{3.52}$$

$$dQ_S^{AC} = M_{AC}.C_{AC}.dT_{4`\to1}^{AC} \tag{3.53}$$

The differential amount of energy output from the adsorbate phase appears in the decrease of the adsorbate and refrigerant vapor internal energy. By applying in this case the conservation of energy principle on the adsorbate and refrigerant vapor phase, we get:

$$dQ_a^{SG} = (dU_a^{SG})_{4\to1} = d(M_a.u_a)_{4\to1}^{SG} = M_{SG}.C_{P,a}.d(x.T)_{4\to1}^{SG} \tag{3.54}$$

$$dQ_a^{AC} = (dU_a^{AC})_{4`\to1} = d(M_a.u_a)_{4`\to1}^{AC} = M_{AC}.C_{P,a}.d(x.T)_{4`\to1}^{AC} \tag{3.55}$$

Regarding the mass of the refrigerant vapor phase is varying during adsorption process. The differential amount of energy output from the vapor phase appears in the decrease of the refrigerant vapor internal energy.

$$dQ_v^{SG} = (dU_v^{SG} + dM_{ads}.H_{ads})_{4\to1}^{SG} = (d(M_v.u_v) + dM_{ads}.H_{ads})_{4\to1}^{SG} \quad (3.56)$$

$$dQ_v^{AC} = (dU_v^{AC} + dM_{ads}.H_{ads})_{4`\to1}^{AC} = (d(m_v.u_v) + dM_{ads}.H_{ads})_{4`\to1}^{AC} \quad (3.57)$$

The amount of methanol which leaves the evaporator and enters the com-adsorption reactor can be written as follows:

$$dM_{evap} = dM_{ads} = (dM_a + dM_v)_{4\to1}^{SG} + (dM_a + dM_v)_{4`\to1}^{AC} \quad (3.58)$$

3.3.6 The evaporator

The refrigeration energy is associated with a differential amount of refrigerant liquid $dM_{evap} = dM_{ads}$, which is coming from the condenser and is being adsorbed in the com-adsorption reactor. The differential evaporation effect dQ_{evap} is calculated from following equation:

$$dQ_{evap} = dM_{evap}.[(1-z).L_{evap} + (h_{evap}(T) - h_{sat}(p_{evap}))] \quad (3.59)$$

In this work, the com-AIP system is used for freezing applications. In the evaporator, the ice production takes place by the evaporation of the saturated liquid refrigerant. The total amount of the ice produced from the com-AIP system per cycle is given by:

$$M_{ice} = \frac{Q_e}{[C_{ch,in}.(T_{ch,in} - 273) + L_{ice} + C_{ice}.(273 - T_{evap} + \Delta\varphi_e)]} \quad (3.60$$

Here Q_e is the refrigeration effect. Assume, there is no losses in the evaporator device used $\Delta\varphi_e = 0$, therefore it can be considered $Q_{evap} = Q_e$.

where $C_{ch,in}$ and $T_{ch,in}$ are the specific heat capacity and the initial temperature of the chilled water. L_{ice} and C_{ice} are the ice specific heat and the latent heat of ice fusion.

3.4 Calculation Procedure

The analysis of the combined adsorption ice production system has been investigated using a simulation program written in **MATLAB**. This program is designed to analyze the thermodynamic cycle parameters of this technique. The above mentioned set of coupled equations is solved by finite difference approximation with a temperature step of one grad Celsius and with a time step of one second. The investigation focused on the effect of the adsorption reactor temperature, the desorbed refrigerant mass from com-adsorption reactor M_{des}, the adsorbed mass from the evaporator into the com- adsorption reactor M_{ads}, cycle time t_{cycle} and the amount of produced ice M_{ice}.

The case investigated in the present study is an ice maker at an evaporation temperature of -3 °C. The configuration of both the SG- and AC- adsorption elements as heat exchangers is taken as identical design and same size (same number of tubes, same number of fins and same emptied volume). Both the beds were heated up to the same desorption temperature of 100 °C. The characteristics of activated carbon and silica gel, packed in this adsorption reactor, are shown in **T**ab. 3.3.

Parameter	Activated carbon	Silica gel
Absolute density ρ_s	$400-600\ [kg/m^3]$	$700-750\ [kg/m^3]$
BET surface area	$2250\ [m^2/gr]$	$800\ [m^2/gr]$
Specific heat capacity C_p	$0.93\ [kJ/kg.K]$	$0.85\ [kJ/kg.K]$
Porosity β	0.858	0.5
x_0	$1.24\ [kg_{meth}/kg_{AC}]$	$0.35\ [kg_{meth}/kg_{SG}]$
n	2,0	1,7
D	4.022×10^{-6}	9.08×10^{-6}
E_a	306.766[kJ/kg]	1310.76[kJ/kg]

Table 3.3: The characteristics of Maxsorb activated carbon and silica gel used in this study. (Data reported by Kanasi Coke and Chemical, Japan)

The base parameters used in this case study are summarized in Tab. 3.4. The liquid and vapor thermodynamic properties of methanol have been calculated from the methanol equations [111]. The simulation uses embedded **Refprop** thermophysical properties of methanol.

Parameter	Value	Parameter	Value
T_{evap}	-3 °C	T_{amb}	27 °C
T_{cond}	32 °C	$T_{des,max}$	100 °C
p_{evap}	3.313[kPa]	p_{cond}	24[kPa]

Table 3.4: The base parameters used in this case study

3.5 Results and discussions of the case study

Based on the analysis for thermodynamic processes of the com-AIP system, it is found that the total input energy of the whole system equals 5766 [kJ]. Whereas, the total output energy of the system equals 5866 [kJ]. Therefore, the relative error in the calculations is nearly 1.75 % , this is an acceptable numerical error and validates the calculation accuracy. Based on the simulation results it is found that the com-AIP system attains a refrigeration COP of 73 % with a refrigeration energy produced Q_e inside the evaporator estimated to 2168 [kJ] per cycle. This refrigeration effect corresponds to ice production of 5.34 kg per cycle at a temperature of −3 °C from water at a source temperature of 15 °C. Therefore, every 1 kg of silica gel-particles inside this com-adsorption reactor produces ice mass of 0.4 kg per cycle and every 1 kg of activated carbon-particles inside the com-adsorption reactor produces ice mass of 1.13 kg per cycle under the hot water inlet temperature of 100 °C.

3.5.1 Pressure profile

The adsorbate (refrigerant) inlet condition during the adsorption process is performed at pressure of 3.31 kPa corresponding to evaporation temperature of −3 °C, and the adsorbate outlet condition during desorption process is done at pressure of 24 kPa corresponding to condensation temperature of 32 °C. Plotting a variation of the pressure inside the com-system, which is filled with two different adsorbents silica gel and activated carbon, is demonstrated along the cycle time Fig. 3.5.

Based on the simulation results, it is found that the desorption and adsorption processes of the SG-bed begin before the same processes inside the AC-bed. Because of the properties of silica gel such as the specific heat capacity and the speed desorption, the duration of desorption process inside the SG-bed is about 100 sec, whereas the desorption process inside the AC-bed is about 240 sec. Consequently, both of the adsorbents work under the same pressures (p_{evap} and p_{cond}) but with the different time.

The pressure level for isosteric pre-heating and pre-cooling is calculated by variation of the temperature in the heat exchanger of the com-adsorption reactor. **F**ig. 3.6 shows the simulated pressure profile for all of the cycle processes, the result corresponds to the ideal cycle displayed in **F**ig. 3.2.

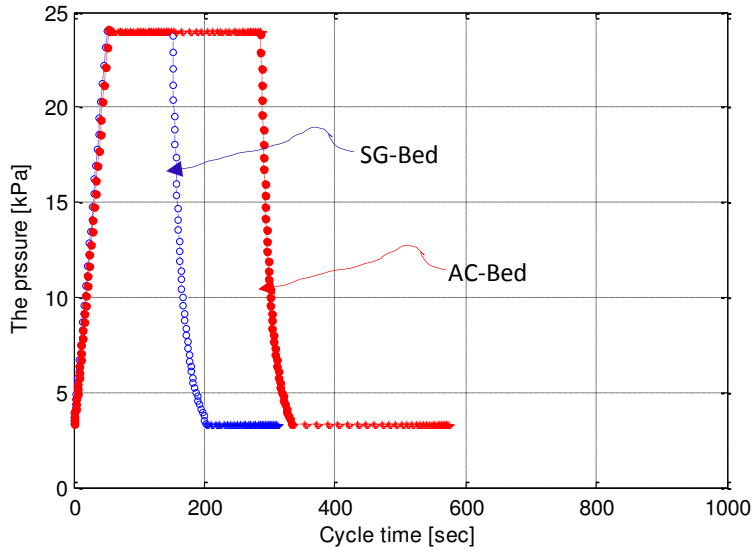

Figure 3.5: Variation of the com- adsorption reactor pressure along the cycle time

Although the com- AIP system use two adsorbents, we can notice that the variation of the pressure inside both the AC- and SG-beds related to the temperature remains identical. The adsorption reactor pressure rises from the evaporator pressure at 3.31 kPa to the highest cycle pressure at the condenser of 24 kPa during the isosteric pre-heating process. It can be also seen that the AC and SG adsorbents start the generation process at same temperature of about 67 °C. Then the reactor pressure remains steady during the generation process (desorption) till the maximum cycle temperature 100 °C is approached. Not only both the adsorbents start the desorption process at same temperature of 67 °C but also begin the adsorption process at same adsorption temperature of about 57 °C.

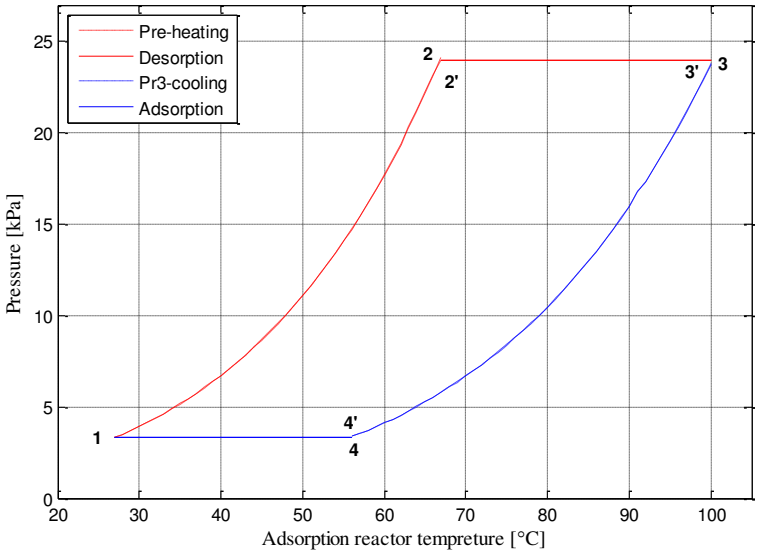

Figure 3.6: Variation of the com-reactor pressure versus the temperature along the cycle processes

3.5.2 Adsorption uptake profile

The **F**ig. 3.7 illustrates the variation of the adsorbate (methanol) concentration ratio with the temperature of the both adsorption elements along the cycle. From this plot, the adsorbate concentration ratio of SG-bed varies between its maximum value of 0.24 to its minimum value of 0.11 $[kg_{meth}/kg_{SG}]$ during the cycle and the adsorbate concentration ratio of AC-be varies between its maximum value of 0.42 to its minimum value of 0.021 $[kg_{meth}/kg_{AC}]$ during the cycle.

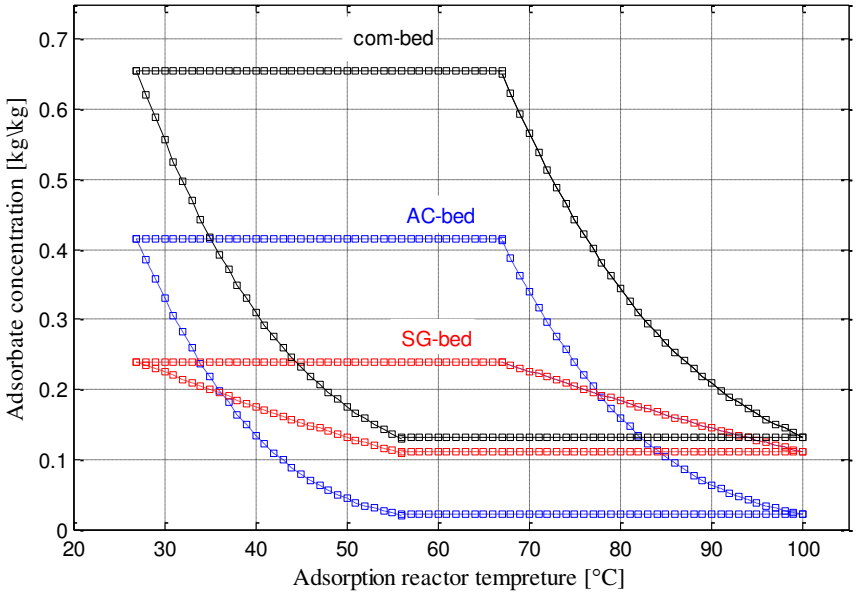

Figure 3.7: Variation of the adsorbate concentration with temperature along the cycle processes

The variation of the methanol concentration inside the SG- and AC- particles is demonstrated for all of the working processes along duration of three consecutive cycles in **F**ig. 3.8.

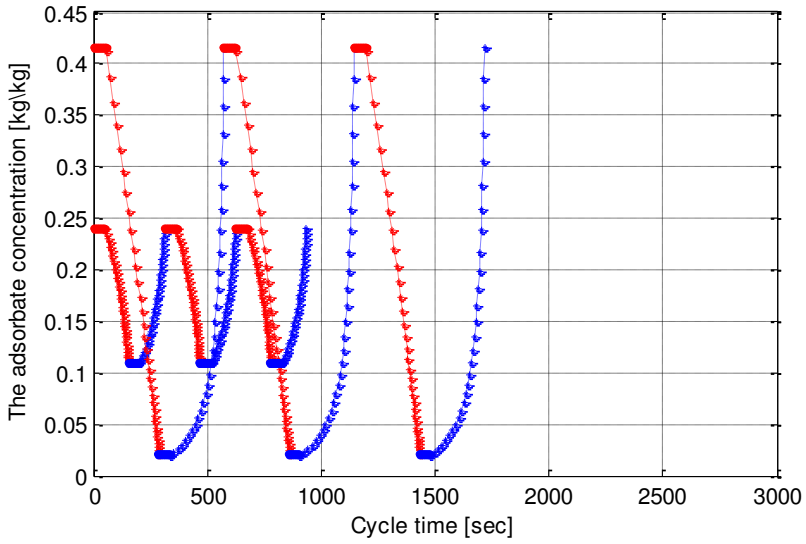

Figure 3.8: Variation of the adsorbate concentration along duration of three consecutive cycles.

Based on the properties of the adsorbents and simulation study it is found, that the maximum adsorbate concentration of Activated carbon x_{max}^{AC} is considerably larger by half than that of silica gel x_{max}^{SG} at the same ambient temperature T_{amb} and the same evaporator pressure p_{evap}. Hence it has the potential to provide higher refrigeration effect. Because of the large value of the methanol

concentration by the AC-particles compared with the methanol concentration by the SG-particles, the desorption process inside the AC- bed takes more time until the end under the same desorption temperature of 100 °C.

Tab. 3.5 shows the required time of the cycle processes for both the SG- bed and AC- bed inside the com-adsorption reactor.

	Preheating	Desorption	Precooling	Adsorption	Total cycle time
Silica gel	46 sec	100 sec	46 sec	100 sec	292 sec
Activated carbon	50 sec	240 sec	50 sec	240 sec	580 sec

Table 3.5: The required time for all the cycle processes

Depending on the speed adsorption, the SG-bed reaches in equilibrium value of adsorption capacity faster than the AC-bed. This is also because of the minimum adsorbate concentration of silica gel x_{min}^{SG}, which is bigger by 6 times than the minimum adsorbate concentration of Activated carbon x_{min}^{AC} at the same highest cycle temperature of 100 °C. That means the amount of methanol must be adsorbed by AC-bed is larger. Therefore, the cooling water supplied to the AC-bed takes more time about 240 sec during adsorption process until the AC particles can be adsorb the methanol vapor and reaches at the equilibrium adsorption capacity x_{max}^{AC} of 0.42 $[kg_{meth}/kg_{AC}]$ at the initial temperature T_1.

3.5.3 Adsorbate refrigerant mass

Fig. 3.9 presents the evolution of the adsorbate mass inside the com-adsorption reactor with the adsorption reactor temperature for all of the working processes.

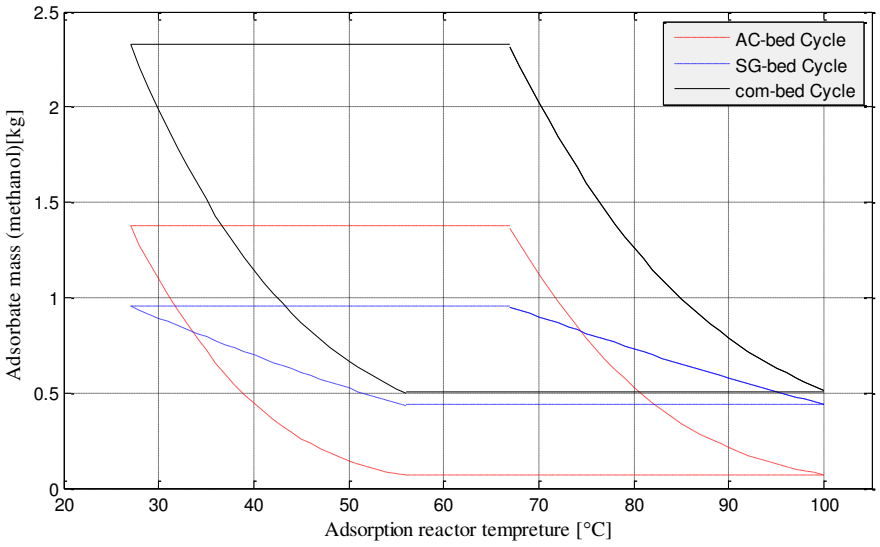

Figure 3.9: Variation of the adsorbate mass with adsorption reactor temperature along the cycle

During the isobaric heating process, the mass of the adsorbate phase (methanol) in the SG-particles M_a^{SG} and in the AC-particles M_a^{AC} are continuously decreasing since the refrigerant is being freed from the com-adsorption reactor and flows towards the condenser and the mass of the refrigerant vapor phase is varying during this process, because the concentration ratio is continuously decreasing along the process.

During the isobaric cooling process, the mass of the adsorbate phase is continuously increasing, because the refrigerant leaves from the evaporator and flows into the com-adsorption reactor. Hence, the concentration ratio is continuously increasing along this process. As noticed from the **F**ig. 3.9, no

changes of the adsorbate refrigerant mass are observed during both of the isosteric processes (preheating and precooling). In the isobaric desorption phase, the desorbed methanol mass increases with temperature due to the decrease in refrigerant density with increasing temperature.

3.5.4 Variation of the desorbed refrigerant mass

Using the com-AIP system will increase the adsorbate mass content M_a inside the adsorption reactor. Consequently the desorbed mass of methanol M_{des}^{com}, that leaves the com-reactor and flows towards the condenser, is higher than this mass M_{des}^{SG} when only silica gel and higher than M_{des}^{AC} when only activated carbon is used in the adsorption reactor. Therefor the refrigerant mass through the evaporator increases and this has important effect on the refrigeration energy Q_e.

The adsorbate mass of SG-adsorption bed attains its minimum cyclic value at the end of the desorption process about 0.44 kg. The decreasing trend in the adsorbate mass during the isobaric desorption process is obtained due to the decrease in its density with the increasing temperature. It attains its highest value at the end of adsorption process about 0.952 kg.

For the AC-adsorption bed varies between its maximum value of 1.4 kg to its minimum value of 0.071 kg during the cycle. The development of the total desorbed mass with the desorption temperature from the com-adsorption reactor (from both the SG- and AC- particles) along the cycle is demonstrated in **F**ig. 3.10. It can be seen that the maximum desorbed mass from the SG-bed and from AC-bed equal to 0.52 kg and 1 .33 kg, respectively. As a result, the total refrigerant mass which is circulated through the com-AIP system increases to 1.85 kg.

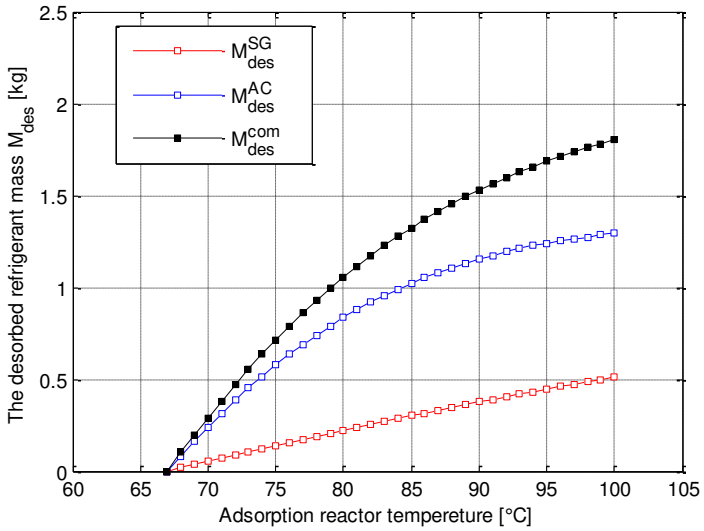

Figure 3.10: Evolution of the desorbed refrigerant mass that leaves the SG-particles, AC-particles and the com-adsorption reactor during isobaric desorption processes.

Fig. 3.11 presents the evolution of the total refrigerant desorbed mass from the com-adsorption reactor along the cycle time of the desorption process. It is noticed that the rate of the generated refrigerant has its minimum value at the beginning of the desorption process, when the bed temperature reaches the value of the generation temperature at 67 °C. This rate, as depicted in the **F**ig. 3.11, is continuously increasing with the increase of the temperature and it reaches the maximum value at the end of the desorption process with the maximum cyclic temperature and the minimum concentration. The total desorbed refrigerant vapor mass at the end of this process equals1.85 kg.

Based on the simulation results, it found that the SG-bed reaches the end of desorption process faster than AC-bed. This has a significant impact on saving the input energy required from driving heat source and the system could produce ice before the end of desorption process inside the AC-bed. But the desorbed amount from AC-bed is more by about 61.5 % than this amount desorbed from the SG-bed. This has a significant impact on increasing the refrigeration energy.

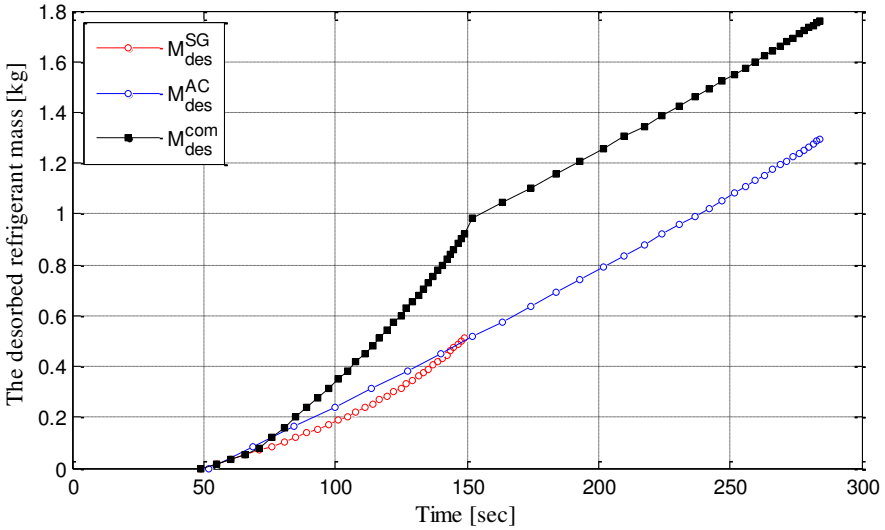

Figure 3.11: Evolution of the total desorbed refrigerant mass that leaves the SG-particles, AC-particles and com-adsorption reactor along the time of the desorption process

As a result of using this technique, it is found that the refrigerant desorbed mass, that leaves from adsorption reactor into the condenser, has been increased to high value, which has important effect on the mass flow rate circulated through the condenser and the evaporator. This improved the COP and increased the mass of ice produced from the com-AIP system.

3.5.5 Variation of the adsorbed refrigerant Mass

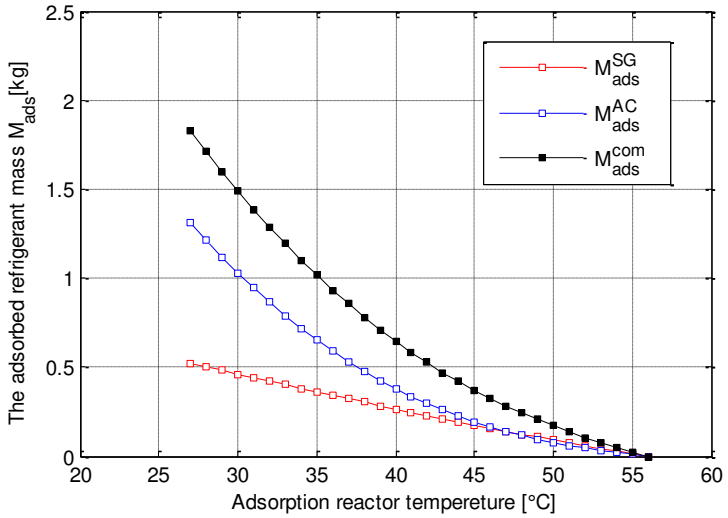

Figure 3.12 Evolution of the adsorbed refrigerant mass that flows toward the SG-particles, AC-particles and the com-adsorption reactor during the isobaric adsorption processes

Fig. 3.12 shows the effect of the adsorption reactor temperature on the amount of adsorbed refrigerant M_{ads} during the isobaric adsorption process. The adsorbate concentration ratio increases with cooling

of the com-adsorption reactor, which means a larger amount of methanol, can be adsorbed with decreasing temperature during the adsorption process. It achieves a maximal value under initial temperature of 27 °C with SG-bed cycle of about 0.52 kg, and 1.33 kg with AC-bed cycle. As a result the total amount of methanol, adsorbed with this proposed technique, achieves a value of 1.85 kg at the end position of adsorption process under ambient temperature of 27 °C and evaporation pressure of 3.31 kPa.

The adsorbed refrigerant mass evolution with the cycle time during isobaric adsorption processes is demonstrated in **F**ig. 3.13.

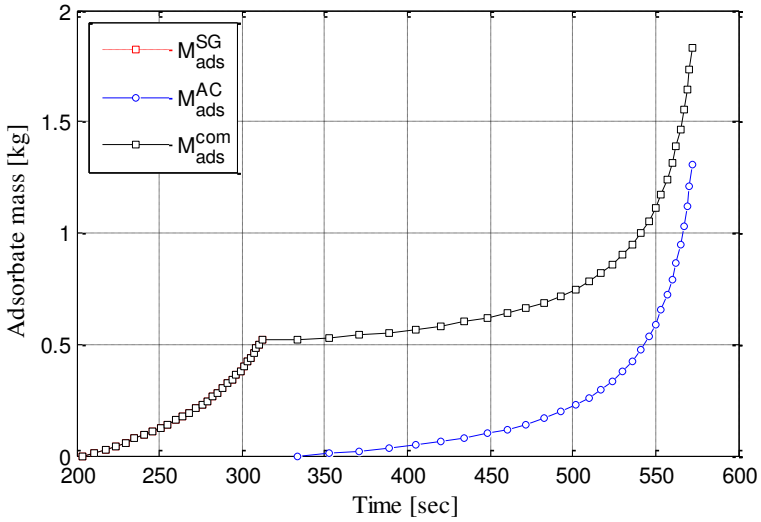

Figure 3.13 Evolution of the desorbed refrigerant mass that leaves the SG-particles, AC-particles and the com-adsorption reactor along the time of the adsorption process

Based on the simulation results and properties of the adsorption materials, it was found that the adsorption process inside AC-bed takes more time than the same process inside the SG-bed. This is because the amount of refrigerant (methanol) inside the AC-particles at start of the adsorption process is larger than this amount inside the SG-particles and also because of the faster kinetic adsorption of silica gel. Therefore, the duration of supplying with the cooling water to the AC-bed is about 240 sec during adsorption process until the AC particles can adsorb the methanol vapor and reach at the equilibrium adsorption capacity x_{max}^{AC}. Because the time of adsorption process is different for SG-bed and AC-bed, this technique could work nearly as permanent system in order to produce the ice.

3.5.6 The amount of produced ice and the refrigeration energy

Fig. 3.14 shows the effect of desorption temperature on the ice production M_{ice} .The trend shows considerable increasing in M_{ice} with increasing desorption temperature over the range shown from 67 °C to 100°C. It can be seen also that the larger fraction from the produced ice about 72 % is produced from the AC-particles whereas the remaining part of the total amount ice produced 28 % is created from the SG-particles. This is because of the large adsorption quantity of the activated carbon particles compared to silica gel as adsorbent. The **E**q. 3.60 shows that the ice produced is proportional to the refrigeration energy.

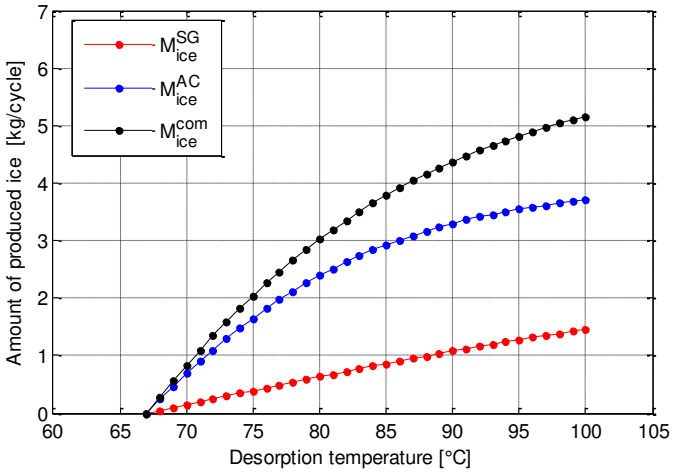

Figure 3.14: Effect of the desorption temperature on the amount of produced ice

The effect of desorption temperature on the refrigeration energy of the system is shown in the **F**ig. 3.15. When desorption temperature increases, the refrigeration energy also increases. Based on simulation results and physical properties of the adsorbents it was found that the cycled refrigerant mass $M_a(x_{max} - x_{min})$ increases with higher desorption temperature. Thus an increase in M_{evap} will result in improvement of the refrigeration energy.

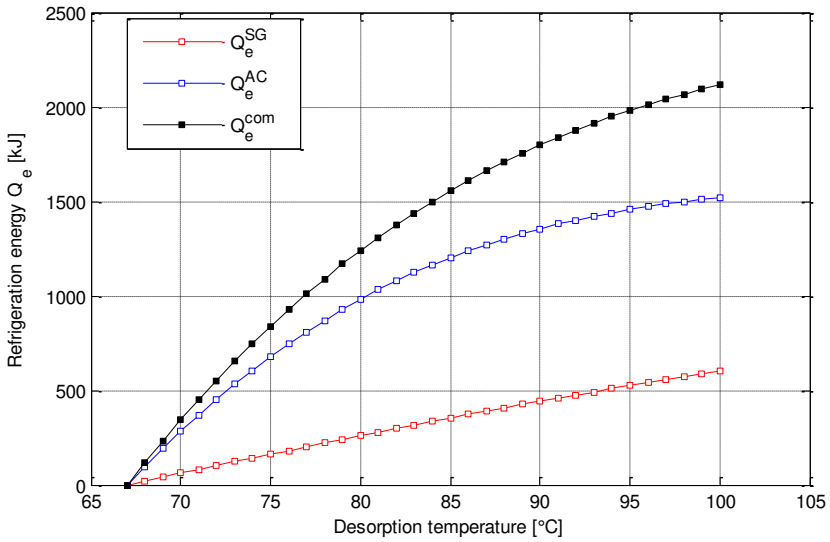

Figure 3.15: Variation of the refrigeration energy with the desorption temperature

3.6 Evaluation of the com-AIP system

In order to assess the effectiveness of the com-AIP system proposed on the driving energy required from external heat source Q_{in} , a comparison with two AIP systems is made under the same operating conditions, taking into account the produced ice amount M_{ice} and performance COP. The first system works using silica gel/methanol and the second works using activated carbon/methanol as working pair. The modeling of both the two systems has been simulated also using a **MATLAB** program.

The comparison with two AIP systems is made under the same operating conditions. The inlet temperature of the heat transfer fluid are 100 °C for hot water, 24 °C for cooling water, and 15 °C for chilled water. The standard operating conditions are shown in **T**ab 3.6.

Parameter	Value	Unit
Hot water inlet temperature	100	[°C]
Hot water inlet flow rate	0.232	[kg/sec]
Cooling water inlet temperature	24	[°C]
Cooling water inlet flow rate	0.4	[kg/sec]
Chilled water inlet temperature	15	[°C]

Table 3.6: Standard operating conditions

Fig. 3.16 shows the influence of adsorption reactor temperature on COP for the SG-, AC- and com-AIP systems. It is seen that COP increases as the adsorption reactor temperature is increased from 67 to 100°C. This is because the amount of refrigerant (methanol) circulated increases, due to increased refrigerant desorption with higher driving source temperature. The COP remains almost steady for large values of $T > 90$ °C. This linear slight increase happens due to the fact that most of the methanol had desorbed below 90 °C, so the increase in heat input produces negligible methanol and hence the COP remains constant.

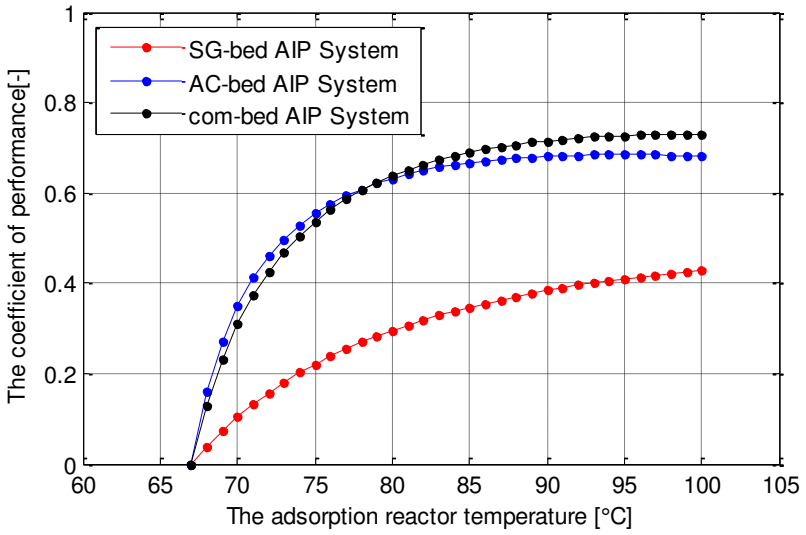

Figure 3.16: Effect of the adsorption reactor temperature on the coefficient of performance COP for the three AIP systems

Based on the comparison with the silica gel/methanol AIP system the simulation results showed that, the COP of this novel com-AIP system was improved by 30 % and that of activated carbon/methanol AIP system by 6 %.

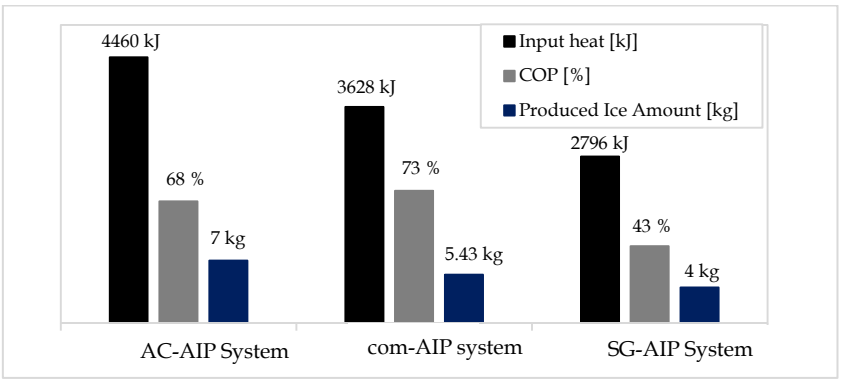

Figure 3.17: Comparison between the three AIP systems, the first is filled only by silica gel/methanol, the second is filled only by activated carbon/methanol and the third is filled by combined adsorbents by silica gel-activated carbon/ methanol

From **F**ig. 3.17 it is found, that the input heat required from the external heat source of this novel com-heat exchanger could be lowered by 19 % compared with AC-AIP system and the amount of ice produced increases by 25 % compared with SG-AIP system although the operating conditions were similar.

Due to a lower specific heat capacity of the silica gel particles, smaller density of activated carbon and higher adsorption quantity of the activated carbon particles, the com-adsorption reactor has a higher COP and lower heat input Q_{in} compared to SG-bed and AC-bed.

Consequently the com-adsorption reactor has an important advantage that can save the heat required from the heat source and have efficient performance.

3.7 Summary and Conclusions

This work was done to improve the refrigeration energy and save the driving energy. To achieve that, a novel com-AIP system with both silica gel and activated carbon as adsorbents and methanol as refrigerant theoretically and thermodynamically is investigated. The analytical model is simulated using **MATLAB** software.

The analysis of the cooling processes and adsorption/desorption processes for com-adsorption reactor theoretical were studied by using 3.9 kg of silica gel, 3.3 kg of activated carbon and 4 kg of methanol. The main feature of the proposed com-AIP system is the ability to be driven by relatively low temperature heat source. So that, this com-AIP system can utilize the fluctuated heat source temperature between 65 and 100 °C to produce effective cold (ice) at a temperature of − 3 °C with a coolant inlet 15 °C.

The com- adsorption reactor allows using the advantages of physical properties of both the adsorbents SG and AC as follows:

The SG-cycle takes about half of time compared with the time required by the AC-cycle. So that the SG-bed reaches the end of desorption process faster than AC-bed. The desorbed amount from the AC-bed is more by about 61.5 % than this amount desorbed from the SG-bed.

As a result of using this technique, it is found that the refrigerant desorbed mass has been increased to high value by saving the required input energy and the cycle time. This improved the COP and increased the mass of ice produced from the com-AIP system. Based on the simulation results it is found that the com-AIP system attains a refrigeration COP of 73 % with a refrigeration energy produced Q_e inside the evaporator estimated to 2168 [kJ] per cycle. This refrigeration effect corresponds to ice production of 5.34 kg per cycle.

Although the SG-reactor achieves two cycles when the AC-reactor achieves only one cycle, the amount of ice produced from the AC-reactor works is more by about 22.5 % compared to the amount produced from SG-reactor.

The performance of this technique and the needed driving energy are evaluated by comparing with two AIP systems, the first system works using silica gel/methanol and the second works using activated carbon/methanol. The boundary conditions used were similar between the three systems.

The comparison results showed, that the amount of ice produced of ice per cycle (5.34 kg) decreases to 4 kg with using only silica gel in the adsorption reactor and increases to about 7 kg, if the adsorption reactor is filled with only activated carbon as adsorbent, but in this case the required heat

input is about 20 % higher. Consequently, this innovative com-AIP system allows using the advantages of physical properties of both the adsorbents SG and AC.

Chapter 4

Application to a Standard com-AIP System

4.1 Introduction

Just as in the last chapter, this presented chapter deals with a theoretical investigation of the thermal performance (coefficient of performance COP and specific cooling power SCP) of a two bed **A**dsorption **I**ce **P**roduction AIP system based on the silica gel/methanol as adsorbent/refrigerant in the first bed and activated carbon/methanol in the second bed. But the different aspects here in this study are as follows:

i. The fined-tube heat exchangers *(named SG-bed and AC-bed)* were designed in order to generate the same desorbed refrigerant amount of 1 kg_{meth}
ii. Both the SG-and AC-beds were heated up to the same level of minimum adsorbate concentration rate.
iii. Both the SG-and AC-beds were heated up during desorption process to different maximum temperatures, so that the SG-bed is heated to 100 °C, whereas the AC-bed is heated only to 84 °C.
iv. In terms of desorption the same amount of methanol, the SG-and AC-reactors must have different sizes and configurations of the heat exchanger (number of HTF-tubes and mass of the adsorption material). So the size of the SG-reactor as heat exchanger has a double size in comparison with the AC-reactor as heat exchanger.
v. Another difference is also the working principle, in that the thermodynamic cycles for SG- and AC-reactors start one after the other. So that, the desorption process inside the AC-reactor starts after the end of the desorption process inside SG-reactor. So the AIP-system can produce continuous refrigeration power.

This study also allows using the advantages of physical properties of both the adsorbents SG and AC. Consequently, this innovative AIP system utilizes effectively low-temperature heat sources of temperature between 65 and 100 °C for SG-reactor and between 65 and 84 °C for AC-reactor. The schematic diagram of the **A**dsorption **I**ce **P**roduction system and its components are shown in **F**ig 4.1.

To desorb 1 kg_{meth} from the SG-bed as well from the AC-bed a cycle simulation computer program of the AIP system was developed to investigate the effect of desorption temperature T_{des}, adsorption temperature T_{ads} and the effect of difference of the required desorption/adsorption time on the system performance and on the amount of the ice produced per cycle M_{ice}. In the present simulations, the variation of the chilled water temperature from 15 °C to 25 °C is taken.

This research presents a simulation of silica gel - /activated carbon-methanol finned tube adsorption system. This chapter will focus on enhancing the specific cooling power SCP, the coefficient of performance COP and saving of the required input heat by increasing the desorbed mass of refrigerant M_{des} from 0 to 1 kg_{meth} to achieve higher performance. Moreover, the impact of difference time for

SC-cycle and AC-cycle and the desorption temperature inside the adsorption reactor on the performance and on the amount of produced ice M_{ice} are considered. The mass transfer limitations from both the two beds and the heat transfer ability between the particles of adsorbents and heat exchanger fins are taken into account in the simulated model based on the linear driving force LDF model.

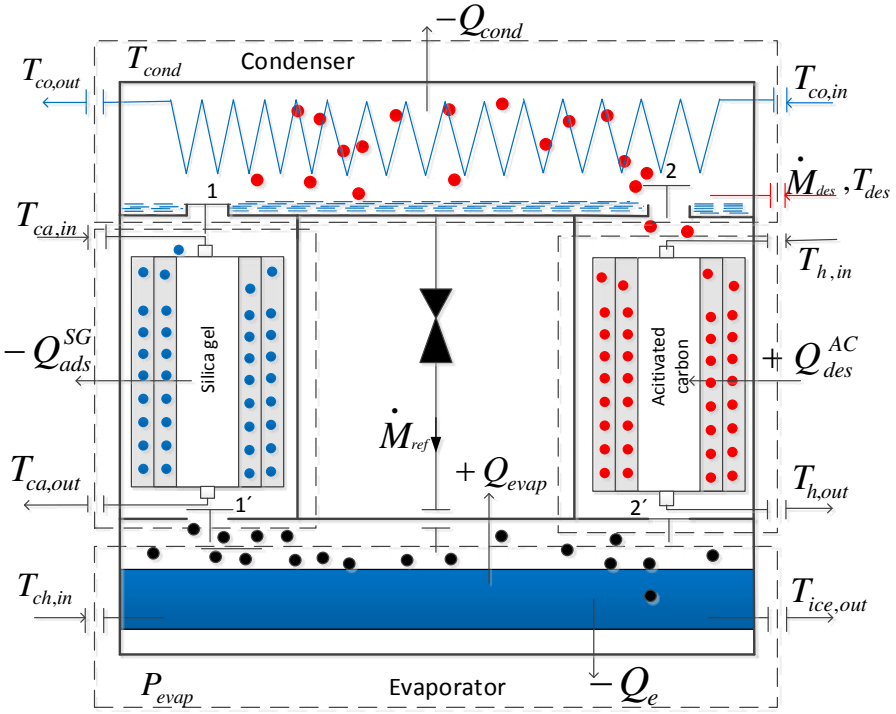

Figure 4. 1: Schematic diagram of two-bed AIP system

4.2 Thermodynamic cycle and working principle of AIP system

The basic adsorption refrigeration thermodynamic cycle is illustrated on the conceptual Clapeyron diagram, shown in **F**ig. 4.2. The cycle of the AIP system consists mainly of these processes:

1→2	Isosteric heating and pressurization process at the constant higher concentration x_{max}^{SG} in the SG-bed (pre-heating).
1`→2`	Isosteric heating and pressurization process at the constant higher concentration x_{max}^{AC} in the AC-bed (pre-heating)
2→3	Isobaric heating and desorption process from the silica gel particles.
2`→3`	Isobaric heating and desorption process from the activated carbon particles.
3→4	Isosteric cooling and depressurization process at the constant lower concentration x_{min}^{SG} in the SG-bed (pre-cooling)
3`→4`	Isosteric cooling and depressurization process at the constant lower concentration x_{min}^{AC} in the AC-bed (pre-cooling).
4 →1	Isobaric cooling and adsorption process for the SG-adsorbent.
4`→1`	Isobaric cooling and adsorption process for the AC-adsorbent.
A→B	Condensation process at constant condenser pressure p_{cond}.
C →D	Evaporation process at constant evaporator pressure p_{evap}.

At the beginning of the cycle for SG-adsorption reactor, state **1**, the SG-adsorption reactor is isolated from both the condenser and the evaporator by the valves v_1 and $v_{1`}$ and the SG-bed is completely charged with the adsorption material of silica gel and saturated with the refrigerant (methanol). The pressure inside the heat exchanger initially equals the evaporator pressure P_{evap} and its temperature is

uniform and equals the ambient temperature T_{amb}. When the hot water flows, both pressure and temperature inside the heat exchanger are elevated due to the adsorbate (methanol) desorption from the adsorbent particles.

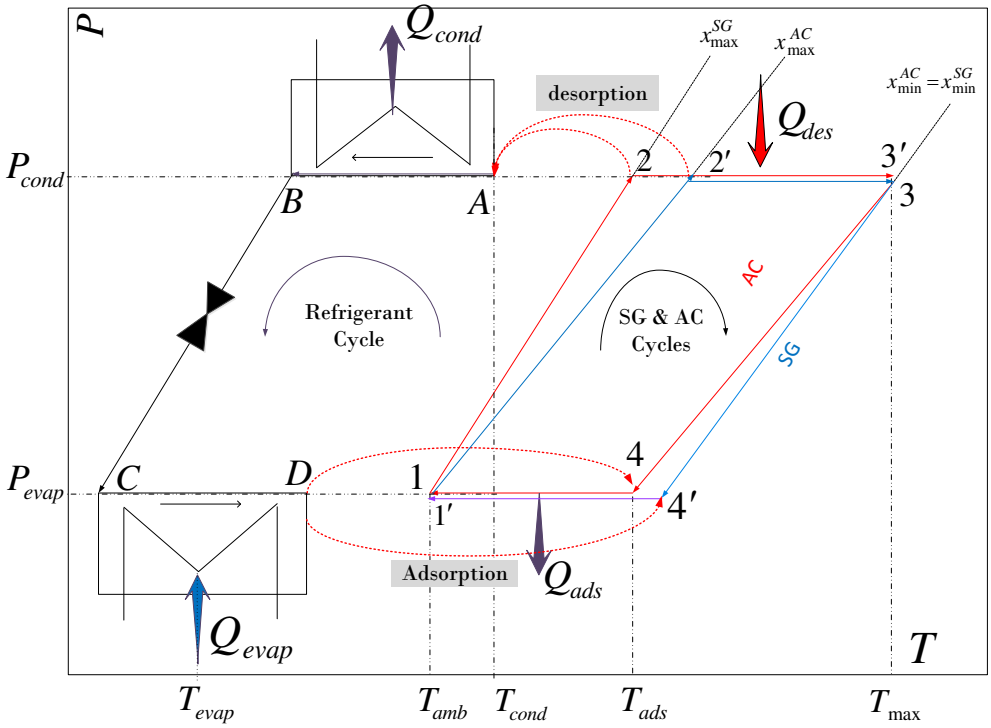

Figure 4.2: Clapeyron diagram for the basic **A**dsorption **I**ce **P**roduction thermodynamic cycle

During the step 1 → 2, the SG-heat exchanger through an isosteric pre-heating process absorbs heat in amount of Q^{SG}_{12} from an external heat source. During the step 1′ → 2′, the AC-heat exchanger through an isosteric pre-heating process also absorbs heat in amount of $Q^{AC}_{1`2`}$ from the same external heat source. The constant concentration preheating process continues until the pressure of SG-adsorbent bed and AC-adsorption bed reach the pressure of condenser P_{cond}.

At the time, the entrance valves v_1 and v_2 to the condenser are opened. In the next step the external heat source continuously heats both the SG- and AC-adsorption reactors during an isobaric desorption process 2 → 3 for SG-cycle and 2` → 3` for AC-cycle. In this process the adsorbate (methanol) leaves the adsorption reactor and is condensed inside the condenser at isobaric cooling process A → B. In this time, the valves v_1 and v_2 between the adsorption reactors and condenser are closed in order to disconnect the reactor from the condenser and start the pre-cooling process. In the condenser the refrigerant vapor losses both sensible heat and latent heat.

In parallel with the desorption process, the adsorption reactor is still being heated and the pressure inside the bed is fixed at the condenser pressure. The temperature continues to increase until the desorption temperature T_{max}. The adsorbate content inside the SG- and AC-particles continues to decrease as more adsorbate is being freed from the SG-reactor and AC-reactor. This operation continues for a certain period of time until both the reactors enable to generate the same desorbed refrigerant amount of 1 kg_{meth}.

During an isosteric pre-cooling process 3 → 4, the SG-adsorbent loses its heat Q^{SG}_{34} in contact with a heat sink and the AC-adsorbent loses its heat $Q^{AC}_{3`4`}$ during the process 3` → 4`. In the step B → C the

refrigerant (methanol from the SG and AC particles) passes through the expansion valve and enters to the evaporator. During step $C \rightarrow D$ the refrigerant absorbs heat in amount of Q_{evap} from the environment of interest converts to the vapor. At the same time, the entrance valves $v_{1`}$ to the SG-adsorption reactor and $v_{2`}$ to the AC-adsorption reactor are opened and the adsorbents (silica gel and activated carbon) adsorb the vapor refrigerant (methanol) during an isobaric adsorption processes $4 \rightarrow 1$ and $4` \rightarrow 1`$respectively. During an isobaric adsorption process release the SG-reactor and AC-reactor the heat Q_{ads}^{SG}, Q_{ads}^{AC}. The reactor is being cooled during this period in order to remove the generated heat from the exothermic adsorption. The evaporation-adsorption process takes place at the constant evaporator pressure.

4.3 Geometry model parameters of the finned tube-adsorption reactor

Fig. 4.3 shows the schematic view of the finned tube heat exchangers developed in this study. This heat exchanger is composed of flat tubes with rectangular fins.
To desorb/adsorb 1 kg_{meth} of circulated refrigerant mass from the SG-adsorption reactor, there are 4 tubes horizontally and 90 fins vertically arranged adsorption heat exchanger in all, between 7.95 kg silica gel and 1.9 kg methanol are employed. To desorb also the same masse of circulated refrigerant, there are 2 tubes horizontally and 90 fins vertically arranged adsorption heat exchanger in all, between 3.31 kg activated carbon and 1.36 kg methanol are employed. This heat exchanger is used as desorber during desorption cycles and as an adsorber during adsorption cycles.
Silica gel and activated carbon particles are taken as same diameter (Ø 1.15 mm). The characteristics of the fined–tube heat exchanger used in both the SG-and AC-adsorption reactors have been calculated and listed in the **T**ab. 4.1.

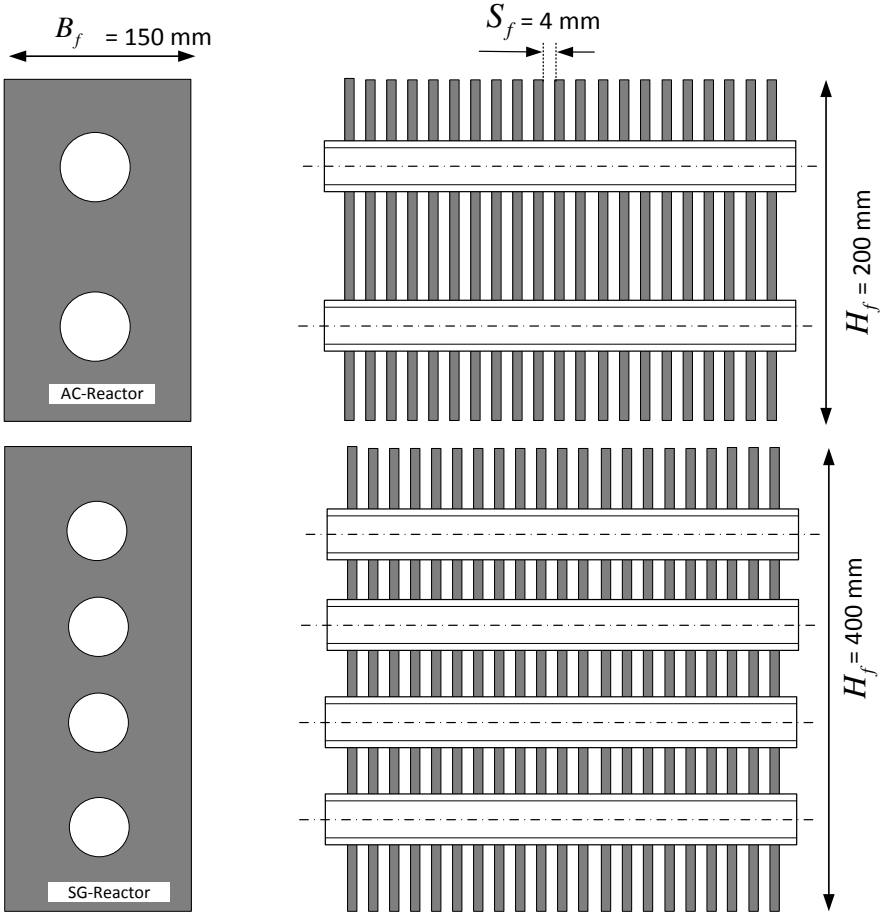

Figure 4.3: Schematic diagram for the rectangular finned tube adsorption reactors of the AIP system

Parameter	SG- heat exchanger	AC- heat exchanger	Unit
Dimension	$450 \times 150 \times 400$	$450 \times 150 \times 200$	[mm]
Number of flat tube	4	2	[−]
Tube diameter	17.3	17.3	[mm]
Tube thickness (ξ)	0.8	0.8	[mm]
Number of fins	90	90	[−]
Fin width (B_f)	150	150	[mm]
Fin spccing (S_f)	4	4	[mm]
Heat transfer area	10.68	5.34	[m^2]
Emptied volume (V)	0.0212	0.0106	[m^3]

Table 4.1: Characteristics of the fined –tube heat exchanger

4.4 Calculation Procedure

The analysis of the **A**dsorption **I**ce **P**roduction AIP system with two-heat exchangers has been investigated using a simulation program written in **MATLAB.** This program is designed to analyze the thermodynamic cycle parameters of this technique. The required equations is solved by finite difference approximation with a temperature step of one grad Celsius and with a time step of one second. The investigation focused on the effect of the difference time of desorption and adsorption processes for SG and AC as adsorbents, the adsorption reactor temperature, the thermal performance (coefficient of performance COP and specific cooling power SCP) and the amount of produced ice M_{ice}.

The case investigated in the present study is an ice maker at an evaporation temperature of -3 °C. The characteristics of activated carbon and silica gel, used in the studied system, are shown in **T**ab. 3.3. To adsorb or desorb the same amount of the circulated refrigerant through the AIP system in case the AC-bed is working or the SG-bed is working, the analysis of the cooling processes and adsorption/desorption processes were simulated by using 3.31 kg of activated carbon, 1.36 kg of methanol in the AC-adsorption reactor of 5.34 m^2 heat transfer area and by using 7.95 kg of silica gel, 1.9 kg of methanol in the SG-adsorption reactor of 10.68 m^2 heat transfer area. Therefore the configuration of these adsorption elements isn't identical. In the proposed design the effect of metallic components of both the adsorption beds is taken into account.

Parameter	Value	Parameter	Value
T_{evap}	-3 °C	T_{amb}	27 °C
T_{cond}	32 °C	T_{max}^{SG}	100 °C
P_{evap}	3.3[kPa]	T_{max}^{AC}	84 °C
P_{cond}	24[kPa]	$x_{min}^{AC} = x_{min}^{SG}$	0.11 [kg/kg]

Table 4.2: The base parameters used in this case study

The base parameters used in this case study are summarized in **T**ab. 4.2. The liquid and vapor thermodynamic properties of methanol have been calculated from the methanol equations [111]. The simulation uses embedded **Refprop** thermophysical properties of methanol.

4.5 Results and discussion

4.5.1 Pressure profile

The pressure of both the SG-bed and AC-bed rises from the evaporator pressure at 3.31 kPa corresponding to evaporation temperature -3 °C to the highest cycle pressure at the condenser of

24 kPa corresponding to condensation temperature 32 °C. In **F**ig. 4.6 the various modes of the AIP system are designated by numbers: 1 2 3 4 cycle processes of SG-adsorbent bed and 1` 2` 3` 4` cycle processes of AC-adsorbent bed. The result corresponds to the ideal cycle displayed in **F**ig. 4.2 based to the equations from (3.1) to (3.8). Although each of adsorbent bed was filled by different adsorption material, we can notice the pressure variation inside the SG-bed and AC-bed related to the temperature remains identical.

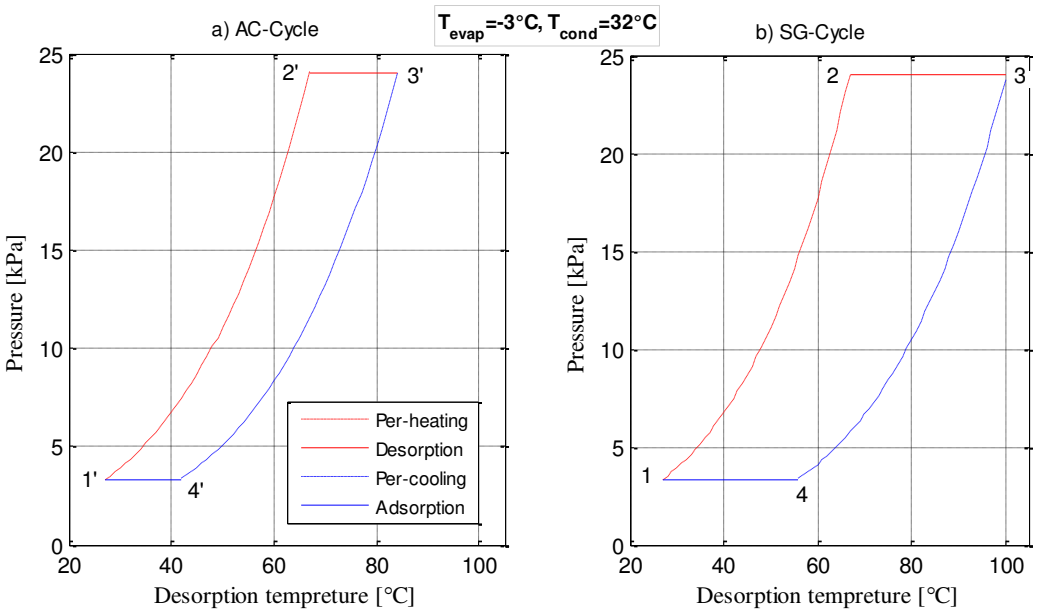

Figure 6: Variation of the pressure versus the temperature along the cycle processes for (a) AC-bed and (b) SG-bed

The pressure variation of one complete cycle with time inside the SG-adsorbent bed and AC-adsorbent bed have also been studied and demonstrated in **F**ig. 4.7. During the adsorption process the pressure in the SG- and AC-bed is set with regard to the evaporation pressure of methanol in the evaporator $P_{evap\ (T_{evap}=-3\ °C)} = 3.31$ kPa, which gives the lower limit. During the desorption process the pressure is set with regard to the condensation pressure in the condenser $P_{cond\ (T_{cond}=32\ °C)} = 24$ kPa, which gives the upper limit. By the isosteric heating and cooling the pressure changes by variation the temperature in the heat exchangers of the AIP system.

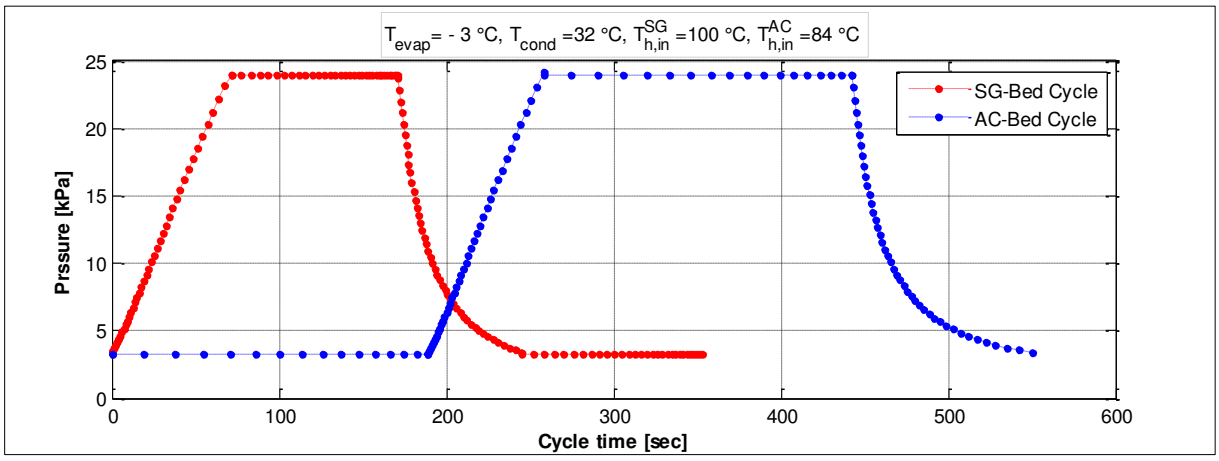

Figure 4.7: Variation of the SG- and AC-adsorption reactor pressure along the cycle time

In **F**ig. 4.7 the cycle processes of both the SG- and AC-adsorption reactors are displayed. Both the adsorption and desorption processes of SG-cycle take about 100 sec, whereas the adsorption and desorption processes of AC-cycle are completed in about 185 sec. Consequently, both of the adsorbents work under the same pressures but with the different time.

4.5.2 Adsorption uptake profile

The adsorbate concentration of activated carbon reaches 0.42 [kg/kg], whereas the equilibrium adsorbate concentration of silica gel is rather low and usually doesn't exceed 0.24 [kg/kg]. Therefore the second adsorption reactor was filled by activated carbon as adsorbent. The variation of the adsorbate concentration by particles of the different adsorbents inside both the SG-bed and AC-bed has been simulated and demonstrated versus the temperature along the cycle processes in **F**ig. 4.8.

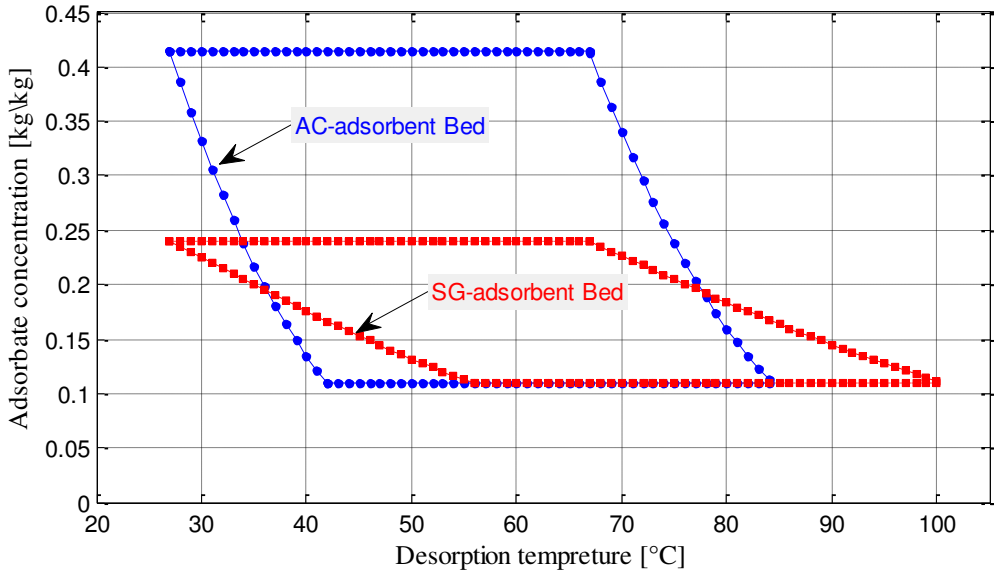

Figure 4.8: Variation of the adsorbate concentration with temperature along the cycle processes

From this plot, the adsorbate concentration ratio x_{SG} of SG-bed varies between its maximum value of 0.24 [kg/kg] to its minimum value of 0.11[kg/kg] during the cycle and the adsorbate concentration ratio x_{AC} of AC-bed varies between its maximum value of 0.42 [kg/kg] to its minimum value of 0.11 [kg/kg] during the cycle.

Based on the properties of the adsorbents and calculations **E**q. (3.1) to **E**q. (3.4) and **E**q. (1.6), it is found that the SG-bed reaches the end of desorption process faster than AC-bed. The different characteristic times for adsorption and desorption processes during the SG-bed and the AC-bed results from different mass transfer coefficient D_{so} $[s^{-1}]$ in **E**q. (1.7). **F**ig. 4.9a shows plotting of the adsorbate concentration inside both the SG-and AC-adsorption reactors, which is demonstrated along the cycle time.

As noticed from the **F**ig. 4.9b, the adsorbate mass is continuously varying throughout the cycle operations. No changes of the adsorbate refrigerant mass are observed during both isosteric preheating and precooling processes. In the isobaric desorption phase, the desorbed methanol mass M_{des} increases with temperature due to the decrease in the refrigerant density with increasing temperature. During the isobaric heating process, the mass of the adsorbate phase (methanol) in the SG-particles M_a^{SG} and in the AC-particles M_a^{AC} are continuously decreasing since the refrigerant is

being freed from the adsorption reactor and flows towards the condenser. During the isobaric cooling process, both the M_a^{SG} and M_a^{AC} are continuously increasing, because the refrigerant leaves from the evaporator and flows into the adsorption reactors. Hence, the concentration ratio is continuously increasing along this process.

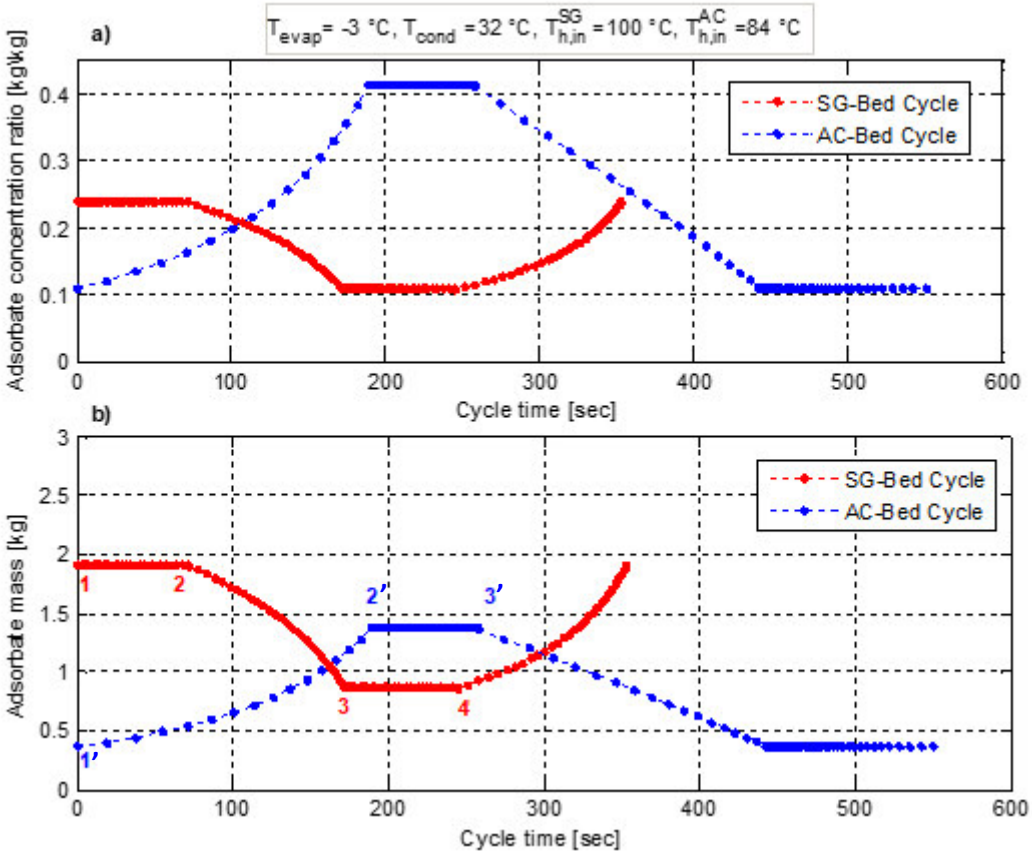

Figure 4.9: **a)** Variation of the adsorbate concentration ratio along the cycle time.
b) Variation of the adsorbate mass during cycle processes of SG-/AC-bed along the cycle time

Fig. 4.9b shows variation of the adsorbate refrigerant mass inside both the SG- and AC- reactors along the cycle time. The maximum and minimum values of the adsorbate concentration by SG-bed correspond to a maximum and minimum contents of an adsorbate mass of 1.9 kg and 0.9 kg, respectively, whereas by AC-bed this corresponds to a maximum and minimum contents of an adsorbate mass of 1.36 kg and 0.36 kg, respectively.

As a result, the refrigerant mass utilization efficiency is estimated to be 73% by AC-bed and 53% by SG-bed, although $1kg_{meth}$ circulated refrigerant mass was used for both reactors. The results are simulated for $1kg_{meth}$ of circulated refrigerant amount, therefore the minimum adsorbate concentration of SG-bed is limited by the heat source temperature 100 °C and the minimum adsorbate concentration of AC-bed is limited by the heat source temperature 84 °C.

4.5.3 Variation of the desorbed refrigerant mass

Both the SG-bed and the AC-bed start the desorption process at a temperature of about 67 °C, but the SG-bed starts the adsorption process at a temperature of about 56 °C, whereas the AC-bed starts that at a different temperature of 42 °C.

Fig. 4.10 shows the evolution of the desorbed refrigerant mass that leaves the SG-particles and AC-particles with the temperature and along the time of the desorption process.

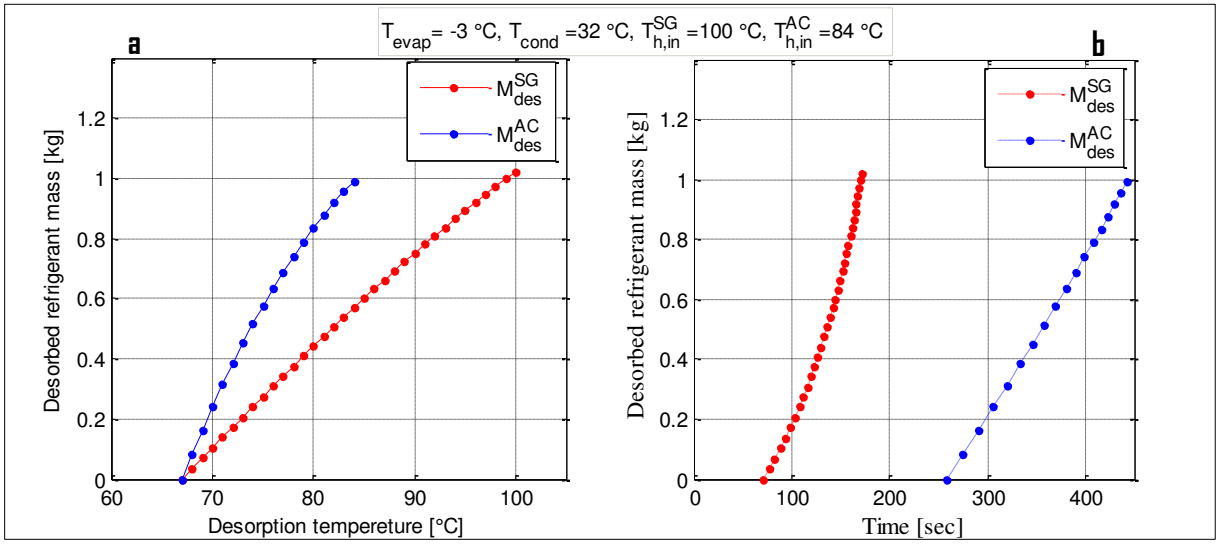

Figure 4.10: Evolution of the desorbed refrigerant mass during desorption process

For operating the AIP system (SG-bed and AC-bed) at same the circulated refrigerant mass through the system of 1kg_{meth}, at same the evaporator temperature of $T_{evap} = -3\,°C$ and at same the condenser temperature of $T_{cond} = 32\,°C$ it is found, that the SG-bed reaches the minimum value of the adsorbate concentration after a period of time about 100 sec and during this process the SG-bed is heated up to the maximum desorption temperature of 100 °C. Whereas the AC-bed reaches the minimum value of the adsorbate concentration after 185 sec and during this process the AC-bed is heated up to only 84 °C.

4.5.4 Variation of the adsorbed refrigerant mass

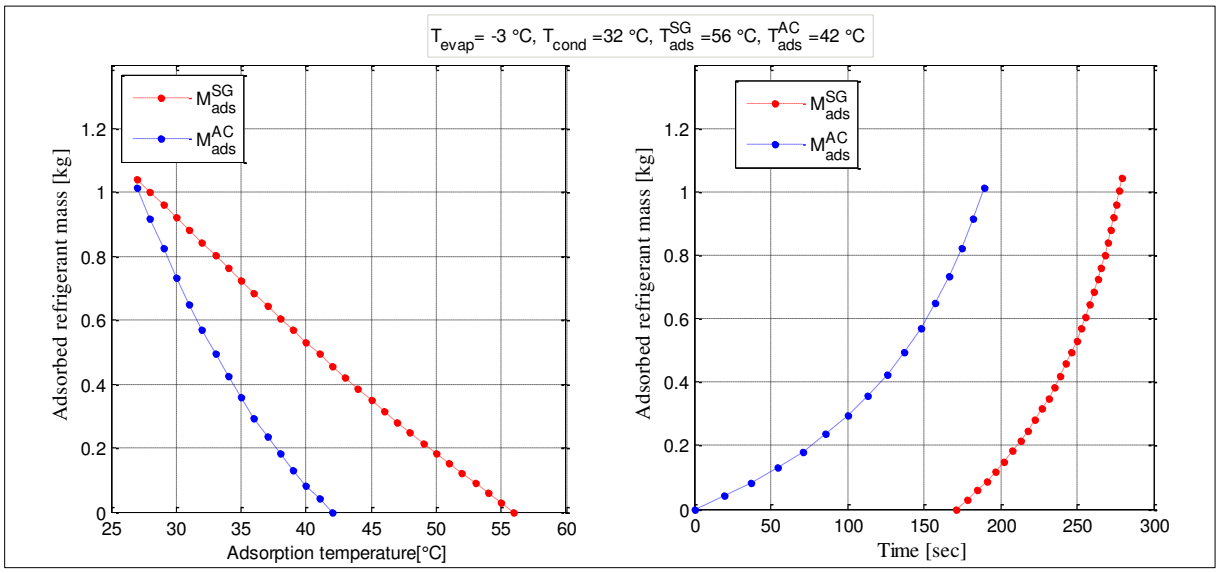

Figure 4.11: Evolution of the adsorbed refrigerant mass during adsorption process

Fig. 4.11 shows the variation of the adsorbed refrigerant mass from the SG-bed and from the AC-bed. To adsorb 1kg_{meth} of the methanol refrigerant the SG-bed starts with adsorption process at 56 °C and

reaches the maximum value of adsorbate uptake 24% after 100 sec at the ambient temperature of 27 °C. To adsorb the same mass of methanol refrigerant $1\,kg_{meth}$ the AC-bed starts with adsorption process at 42 °C and reaches the maximum value of adsorbate uptake 42% after 185 sec at the ambient temperature of 27 °C.

The time difference is mainly caused by the temperature dependence of the mass transfer coefficient D_{so}. Including the isosteric heating and cooling processes a complete cycle for SG-bed takes about 350 sec, whereas a complete cycle for AC-bed takes about 550 sec.

4.5.5 Effect of desorption temperature on COP and SCP

Fig. 4.12 shows the influence of desorption temperature on the two bed AIP system COP. It is seen that COP increases as desorption temperature is increased. This is because the amount of refrigerant (methanol) circulated increases from 0 to 1 kg_{meth}, due to increased refrigerant desorption with higher driving source temperature.

Nevertheless the desorbed methanol amount from both the beds is similar and the refrigeration energy produced Q_e inside the evaporator estimated to 1200 kJ with using not only SG-bed but also AC-bed, it is found based on the simulation results, that the COP for the AIP system in case of using SG-bed at the selected point of operation ($T_{evap} = -3$ °C, $T_{cod} = 32$ °C, $T_{h,in} = 100$ °C) is about 44 %, whereas the COP for the AIP system using AC-bed at the selected point of operation ($T_{evap} = -3$ °C, $T_{cond} = 32$ °C, $T_{h,in} = 85$ °C) is about 66 %.

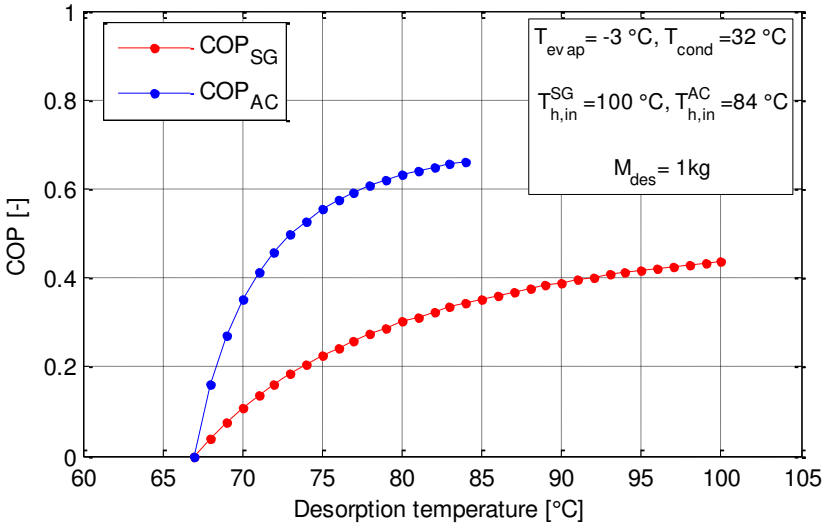

Figure 4.12: Effect of the desorption temperature on the coefficient performance of the AIP system

The difference in the values of the coefficient performance for the AIP system is caused by variations in the driving energy required Q_{in} by SG-adsorption reactor and by AC-adsorption reactor. To desorb 1 kg_{meth} of refrigerant mass, the driving energy required by SG-bed is more than that required by AC-bed. This is because the SG-bed must been heated up to desorption temperature of 100 °C, whereas the SG-bed must be heated up to 84 °C from AC-bed.

In **F**ig. 4.13 the specific cooling power SCP is depicted with the variation of desorption temperature inside both the SG- and AC-adsorption reactors. It is seen that SCP of the proposed cycle is also increased with increase of desorption temperature as we observed for COP. Although the sorption

kinetic with silica gel is faster, the much higher power density SCP of the AIP system is mainly reached by activated carbon. This is because of the adsorption material density, which affects the used amount of adsorbent M_S.

SCP is inversely proportional to the amount of the adsorption material **E**q. (1.15). The used amount of activated carbon is smaller than the amount of silica gel to desorb or adsorb the same circulated refrigerant through the AIP system.

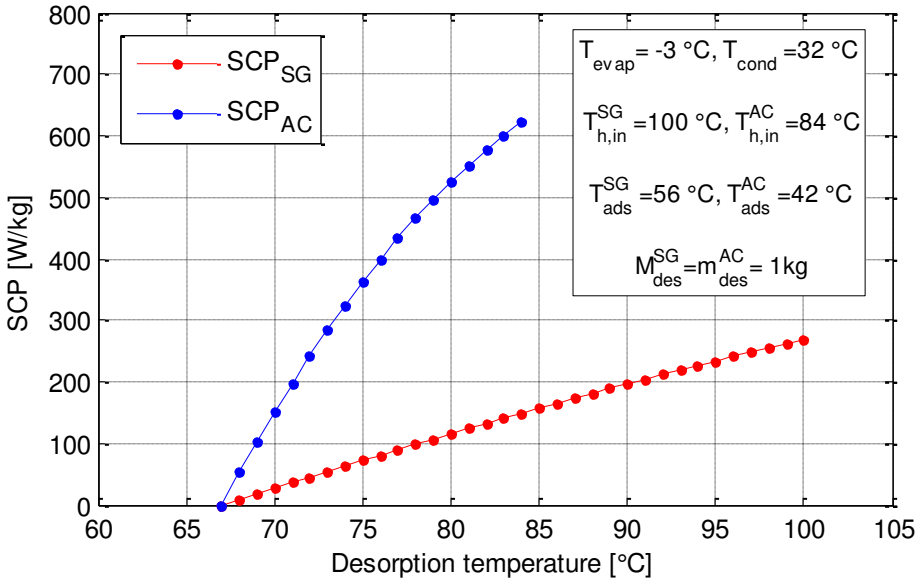

Figure 4.13: Effect of the desorption temperature on the specific cooling power of the AIP system

4.5.6 The amount of produced ice and the refrigeration capacity

When desorption temperature increases, the cycle refrigerant mass $M_{ref} = M_{des}$ will increase and the refrigeration capacity $\dot{Q}_e$ produced in the evaporator will increase as seen in **F**ig. 4.14,

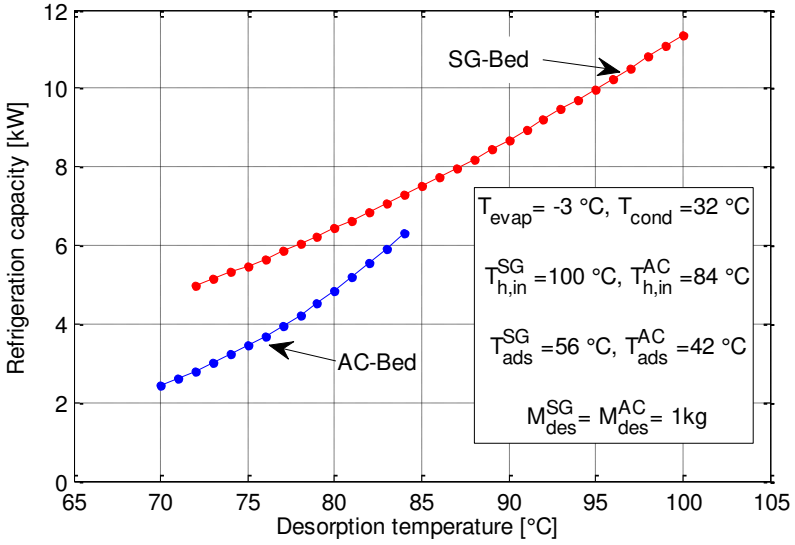

Figure 4.14: Effect of the desorption temperature on the refrigeration capacity of the AIP system

Whereas the amount of circulated refrigerant mass through the AIP system is same for both adsorbents, the resulting refrigeration energy Q_e is same due to the same heat of vaporization which corresponds to the same methanol mass by the different adsorbents and the same evaporator temperature. But the refrigeration capacity $\dot{Q}_e[kW]$ is different. This is caused by the different adsorption time. SG-bed takes about half of the adsorption time for the AC-bed. Comparing the resulting refrigeration capacity from the SG-bed with the results from the AC-bed shows that $\dot{Q}_e^{SG}$ is about 11.34 kW , whereas $\dot{Q}_e^{AC}$ is only 6.29 kW.

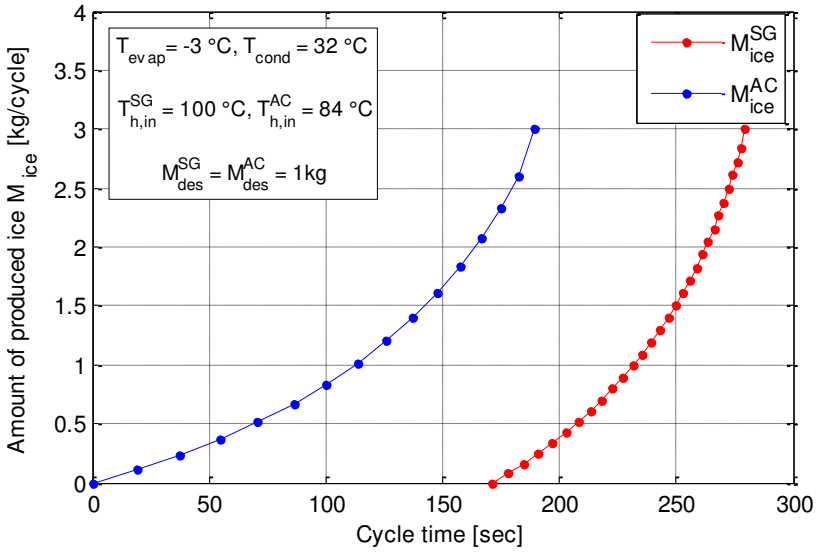

Figure 4.15: Evolution of the amount of ice produced during the time of one cycle

The **E**q. (3.60) shows that the ice produced is proportional to the refrigeration energy. The amount of ice produced per one complete cycle of the AIP system is shown in the **F**ig. 4.15.

If the SG-bed or the AC-bed works, the system produces the same amount of ice of 3 kg at -3 °C from water at a source temperature of 15 °C. Therefore the amount of the ice produced from this system estimated to 6 kg per cycle. Based on the simulation results it is found, that every 1 kg of silica gel-particles inside the SG-adsorption reactor produces ice mass of 0.38 kg per cycle under the hot water inlet temperature of 100 °C and every 1 kg of activated carbon-particles inside the AC-adsorption reactor produces ice mass of 0.9 kg per cycle under the hot water inlet temperature of 84 °C.

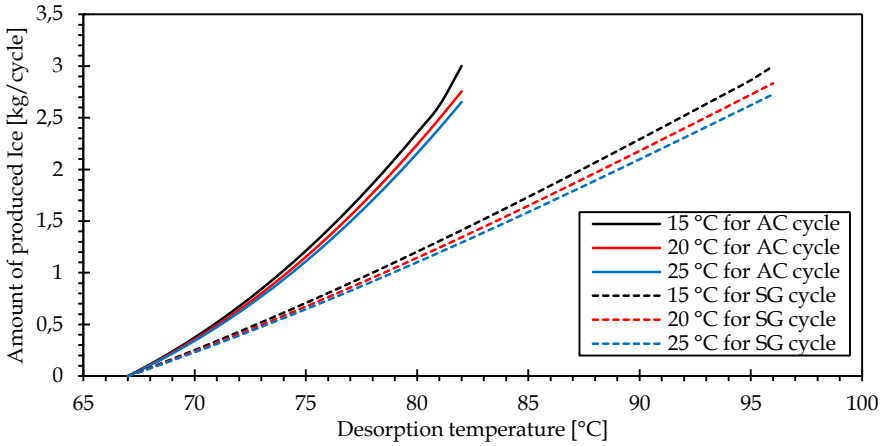

Figure 4.16: Effect of the inlet chilled water and desorption temperature on the amount of ice produced

The amount of produced ice is shown in **F**ig. 4.16 versus the desorption temperature for a given inlet chilled water temperature $T_{ch,in}$. As a result of using this technique we can note that AIP–system works effectively, because the increasing the inlet chilled water temperature slightly reduces the rate of increase in the amount of produced ice. As noticed from the **F**ig. 4.16, the decrease in the amount of ice produced per cycle with variation of the inlet chilled water temperature from 15 °C to 25 °C is estimated to be 11% by AC-cycle and 9 % by SG-cycle.

4.6 Importance of the AIP system

The theoretical and thermodynamic investigation of the two bed AIP system that works using silica gel/methanol in the first adsorption bed and activated carbon/methanol in the second bed was done to improve the cycle time and save the driving energy based on using the advantages of physical properties of both the adsorbents SG and AC. To achieve that, two finned tube-heat exchangers for each adsorption reactor are investigated to desorb/adsorb the same amount of the refrigerant (methanol). The analytical model was simulated using **MATLAB** software.

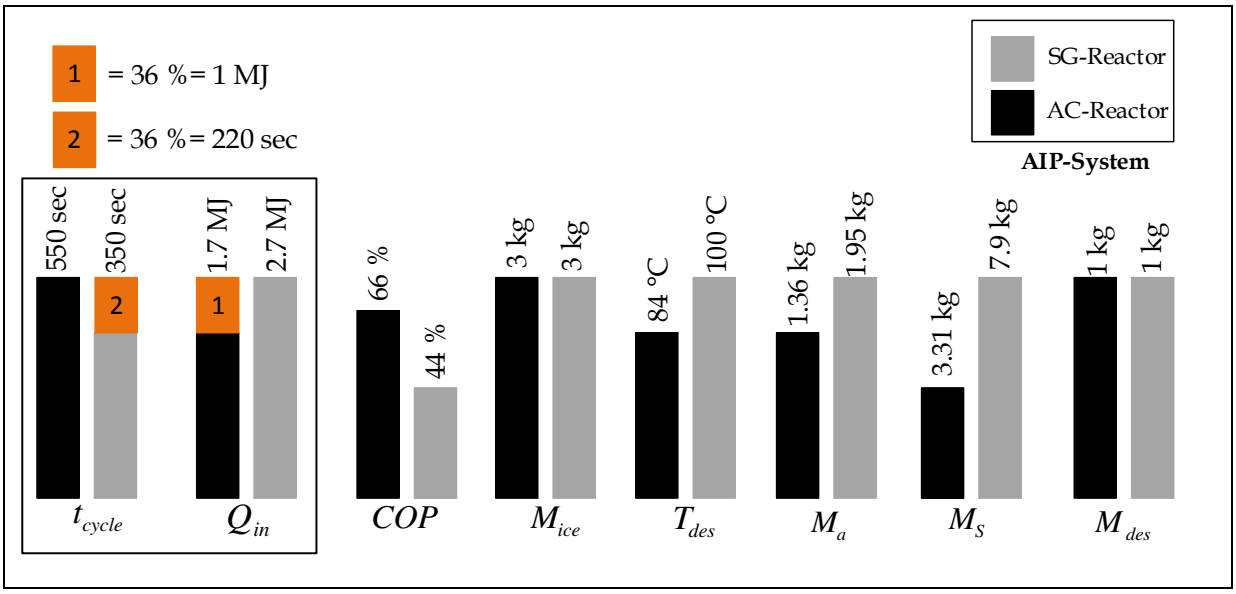

Figure 4.17: The importance of the AIP-system

To desorb the same amount 1 kg of the refrigerant, the SG-reactor has to be filled with 7.95 kg of silica gel and 1.9 kg of methanol, whereas the AC-reactor has to be filled by 3.31 kg of activated carbon and 1.36 kg of methanol. During the desorption process the SG-reactor has to be heated up to the maximal desorption temperature of 100 °C whereas the AC-reactor only to 84 °C.

The simulation results showed that 6 kg of ice per cycle could be produced from the AIP system. If the SG-reactor or the AC-reactor works, the system produces the same mass of ice of 3 kg, but the system attains a coefficient of performance of 66 %, when the AC-reactor works and attains of 44 %, when the SG-reactor works.

The importance of the AIP-system is as follows: The adsorption reactor employed by activated carbon as adsorbent can save the required energy about 36 % and the adsorption reactor employed by silica gel as adsorbent takes about half of the desorption/adsorption time compared with the AC-bed, which can save the cycle time by about 36 %. This is because of the physical properties of silica gel as adsorbent compared with the physical properties of activated carbon such as the activation energy E_a [kJ/kg] and the mass transfer coefficient D_{so} [1/sec].

Consequently, The utilization of silica gel and activated carbon as adsorbents together in an adsorption machine make it possible to produce more amount of ice with saving required energy.

Chapter 5

Effect of Physical and Design parameters on the Adsorption Reactor Performance and Enhancing technique

5.1 Introduction

In this chapter we will focus on the effect of the flow type depending on varying the Reynolds number through the flow channels and the design parameters effect of the adsorption reactor on the thermal performance (coefficient of performance COP and specific cooling power SCP) of the AIP-system, the desorbed refrigerant amount M_{des}, the produced amount of ice M_{ice}, the evolution of temperature distribution throughout the adsorbent-adsorbate medium and the temperature of the heat transfer fluid (HTF). These effects will be studied by changing the adsorption reactor geometry such as the length and the diameter of the used HTF- channels including the fins spacing and dimensions. Depending on these changes, the overall heat transfer coefficient of the adsorption reactor will also be discussed, thus the possibility of absorbing the reactor to different amounts of the adsorption material can be taken into account and studied based on these changes.

The primary objective of this chapter, which studies the effect of the flow type on desorption process, will provide fundamental understandings of two-adsorption reactors silica gel/methanol and activated carbon/methanol and give useful guidelines regarding designs of adsorbent bed reactors. Both the adsorption reactors will be heated to desorb $1kg_{meth}$ of methanol, which is used as an adsorbate with both the reactors. So each reactor should be filled with a quantity of the adsorption material to ensure that $1kg_{meth}$ is released. Based on this quantity, the installation of both reactors will be constructed in terms of the number of HTF-channels needed, furthermore the dimensions and the number of fins.

In the other objective the non-dimensional numbers, which are derived based on the parametric analysis; present the different physical design and operating parameters of the system. Therefore, the presented study analyzes a set of non- dimensional parameters such as thermal conductivity ratio R_λ, heat exchanger geometry ratio R_G, channel length factor F_L, fin spacing factor F_S, heat transfer fluid number ε_F, metal components number ξ_{metal}, adsorbate number ε_a, vapor adsorbate number ε_v, adsorbent number ε_s, area ratio A and adsorption reactor Biot number Bi. The parametric study is conducted to show the effects of different non-dimensional parameters on the system performances and both the heat and mass transfer limitations are taken into account in this study.

5.2 Adsorption reactor description

5.2.1 Adsorption reactor construction

Fig. 5.1 shows the SG- and AC-adsorption reactors as a heat exchanger. This heat exchanger is composed of flat tubes with rectangular fins and designed in order to desorb/adsorb 1 kg_{meth} of circulated refrigerant mass. The SG-adsorption reactor consists of 4 copper tubes horizontally and 90 aluminum fins vertically. The gaps between the fins were filled by 7.95 kg silica gel and 1.9 kg methanol. Whereas to desorb also the same mass of circulated refrigerant, the AC-adsorption reactor is constructed from 2 horizontal copper tubes with 90 vertical aluminum fins. The AC-adsorption reactor was employed with 3.31 kg activated carbon granules and 1.36 kg methanol. The characteristics of the fined –tube heat exchanger used in SG- and in AC-adsorption reactors have been calculated and listed in the **T**ab. 5.1.

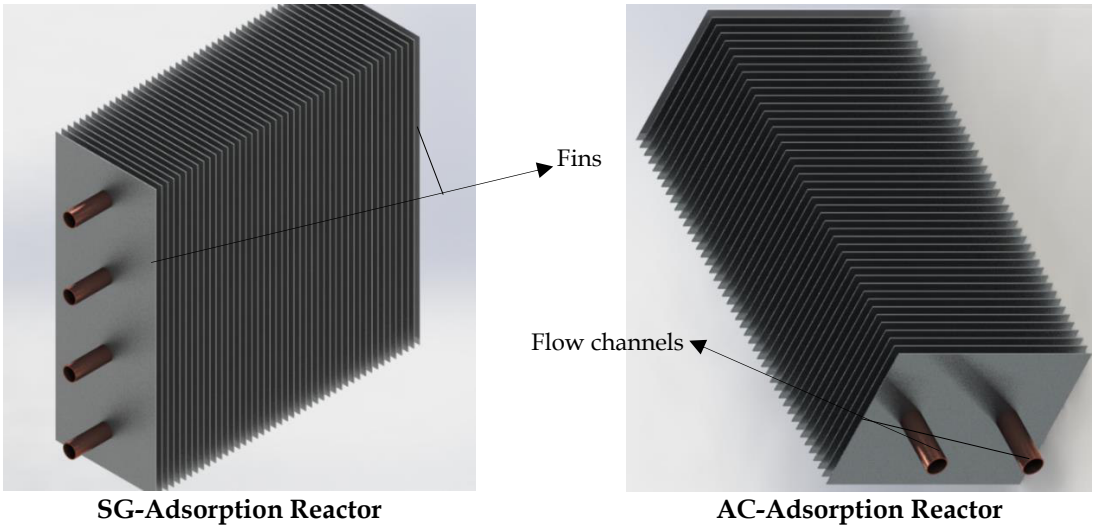

Figure 5.1: View of both the SG-and AC- heat exchangers used as adsorption reactors in this work

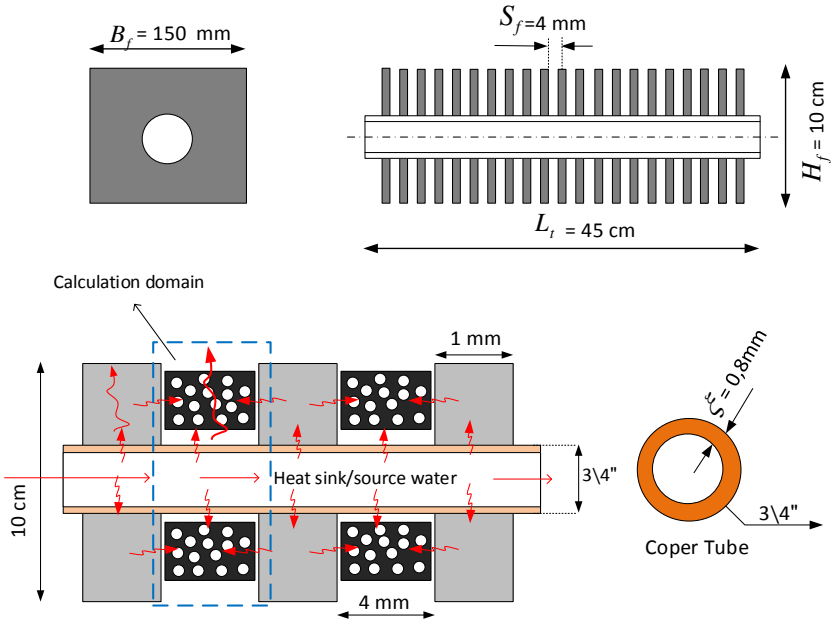

Figure 5.2: Schematic diagram for the one rectangular finned tube adsorption reactor of the AIP system

Fig. 5.2 shows the schematic view of the one finned tube heat exchanger developed in this study and also displays the main design parameters such as; the inner radius of the HTF-cannel r_i , length of the HTF-channel L_t, fin height H_f , fin thickness δ_f, fin width B_f and fin spacing S_f.

Parameter	SG- heat exchanger	AC- heat exchanger	Unit
Dimension	$450 \times 150 \times 400$	$450 \times 150 \times 200$	[mm]
Number of flat tube	4	2	[−]
Tube diameter	17.3	17.3	[mm]
Tube thickness (ξ)	0.8	0.8	[mm]
Number of fins (n_f)	90	90	[−]
Fin width (B_f)	150	150	[mm]
Fin spacing (S_f)	4	4	[mm]
Heat transfer area	10.68	5.34	$[m^2]$
Emptied volume (V)	0.0212	0.0106	$[m^3]$

Table 5.1: Characteristics of the finned–tube heat exchanger

5.2.2 Heat transfer in the adsorption reactor

One of the important factors controlling heat transfer is the resistance to heat flow through the adsorption reactor. In the adsorption reactors presented in this work the adsorption and desorption heat are introduced by means of secondary heat transfer fluid (HTF), water. The driving force for the heat transfer is the difference in temperature levels between the hot water and the adsorption particles, the greater the difference the higher the rate at which the heat will flow between them. **F**ig. 5.3 shows schematic diagram for the heat transfer resistances in the adsorption reactor. The resistance to heat flow depend greatly on the nature of the fluids but also, crucially, on the geometry of the heat transfer surfaces they are in contact with. These resistances could vary depending on the heat exchanger design, but generally named:

1- Secondary fluid/channel metal wall convective heat transfer resistance R_1.
2- Conductive heat transfer resistance through the thickness of the HTF- channel wall R_2.
3- Conductive heat transfer resistance through the adsorption medium R_3.
4- Conductive heat transfer resistance through the fins metal R_4.
5- Contact resistance between the copper and the adsorbent $R_{c,1}$.
6- Contact resistance between the copper and aluminum $R_{c,2}$.

The convective heat transfer resistance is inversely proportional to the fluid velocity. The conductive heat transfer resistance throughout the adsorption medium is directly proportional to the thickness of the medium and inversely proportional to the adsorbent thermal conductivity. The conductive heat transfer resistance is very small through the HTF-tube wall but relatively high through the adsorbent medium and has a strong effect on the heat transfer performance of the adsorption cycle [112].

5.3 Mathematical modelling

A Side view of the main portion of the adsorbent heat exchanger is traced in **F**ig. 5.3. The adsorption reactor is divided into two parts. One is the adsorbent side, which is filled with the adsorbent particles and the other is the heat transfer fluid side. The role of the HTF is either to heat up or to cool down the adsorbent particles, which causes the heat exchanger to desorb the refrigerant to the condenser or to adsorb refrigerant vapor from the evaporator [40,54,113].

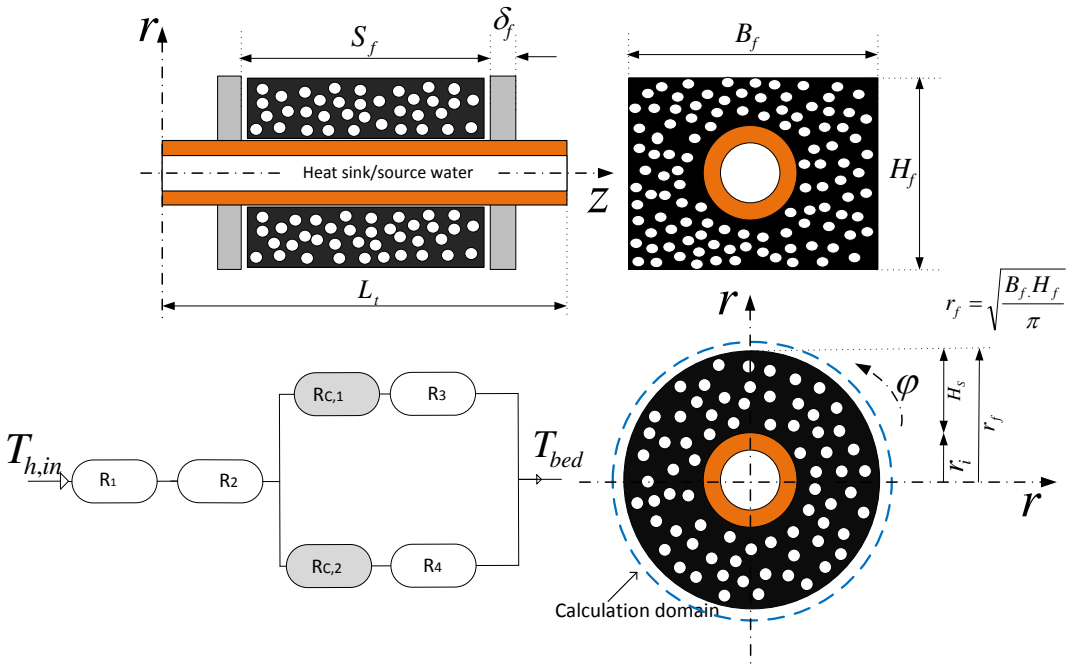

Figure 5.3: Schematic diagram for the heat transfer resistances in the adsorption reactor, Side view of the portion of the adsorbent heat exchanger and the circular equivalent fin to the rectangular fin

The modelling of the adsorption reactor involves heat and mass conservation equations for the heat transfer fluid, the metal components (copper tubes and aluminum fins) and the adsorption materials (silica gel or activated carbon). The following assumptions are taken in account to analyze and simulate the adsorption reactor:

- The adsorbed phase is considered as a liquid, and the adsorbate vapor is assumed as an ideal gas.
- The adsorption reactor is composed of uniformly sized particles with isotropic properties.
- The properties of the fluid and the metal components are constant (constant the physical properties).
- There are no heat losses during the desorption process.
- The thermal contact resistance between the metal tube and the adsorbent bed is neglected.
- The particles are small enough to be regarded as saturated

5.3.1 Conservation of energy

The HTF-side is an absolutely important part of the adsorption reactors. Therefore, it is desirable to find out more about the design parameters of the HTF-side on the system performance in more detail. However, very little works have been found on the parametric study on the fluid sides. From this context, in the present investigation, three-dimensional heat equations are considered for both the fluid and adsorbent sides.

The energy balance on the heat transfer fluid (water):

$$\rho_F.C_F.\frac{dT_F}{dt}=\frac{1}{r}.\frac{\partial}{\partial r}\left(\lambda_F.r.\frac{\partial T_F}{\partial r}\right)+\frac{1}{r^2}.\frac{\partial}{\partial \varphi}\left(\lambda_F.\frac{\partial T_F}{\partial \varphi}\right)+\frac{\partial}{\partial z}\left(\lambda_F\frac{\partial T_F}{\partial z}\right),$$

$$M_F.C_F\frac{\partial T_F}{\partial t}+\dot{M}_F.C_F.L_t\frac{\partial T_F}{\partial z}=\lambda_F.A_F.L_t.\left(\frac{\partial^2 T_F}{\partial r^2}+\frac{1}{r^2}\frac{\partial^2 T_F}{\partial \varphi^2}+\frac{\partial^2 T_F}{\partial z^2}\right) \quad (5.1)$$

where M_F, C_F, $\dot{M}_F$, λ_F and T_F are the mass, specific heat capacity, mass flow rate, thermal conductivity and temperature of the HTF. L_t is the length of the HTF-channel and A_F is the cross section surface of the HTF channel.

The energy balance for the adsorption particles SG or AC and the adsorbate (methanol) can be described by:

$$(M_S.C_S+M_S.C_a.x+M_v.C_v)\frac{\partial T_S}{\partial t}+M_S.H_{ads}.\frac{\partial x}{\partial t}=\lambda_S.A_S.L_S.\left(\frac{\partial^2 T_S}{\partial r^2}+\frac{1}{r^2}\frac{\partial^2 T_S}{\partial \varphi^2}+\frac{\partial^2 T_S}{\partial z^2}\right) \quad (5.2)$$

where M_S, C_S, λ_S and T_S are the mass, specific heat capacity, thermal conductivity and temperature of the adsorption-medium (silica gel or activated carbon). L_s is the length of non-finned HTF-channel and gives as $L_S = (n_f - 1).S_f$. A_S is the contact surface between the adsorption particles and the fins. C_a is the specific heat capacity of the adsorbate (methanol).

The energy balance for the metal components (aluminum fins):

$$(M_f.C_f)\frac{\partial T_f}{\partial t}=n_f.\lambda_f.A_f.S_f.\left(\frac{\partial^2 T_f}{\partial r^2}+\frac{1}{r^2}\frac{\partial^2 T_f}{\partial \varphi^2}+\frac{\partial^2 T_f}{\partial z^2}\right) \quad (5.3)$$

where λ_f, A_f and T_f are the thermal conductivity, surface area and temperature of the fins. n_f is number of the fins used in the adsorption reactor.

The energy balance for the bed, which consists of adsorbent, adsorbate and the metal components (aluminum fins+ copper tubes):

$$(M_S.C_S+M_S.C_a.x+M_v.C_v+M_f.C_f+M_t.C_t)\frac{\partial T_b}{\partial t}+M_S.H_{ads}.\frac{\partial x}{\partial t}=\lambda_{tot}.V_a.\left(\frac{\partial^2 T_b}{\partial r^2}+\frac{1}{r^2}\frac{\partial^2 T_b}{\partial \varphi^2}+\frac{\partial^2 T_b}{\partial z^2}\right) \quad (5.4)$$

where T_b, λ_{tot} and V_a are the temperature, total thermal conductivity and the volume of the adsorption bed.

5.3.2 Conservation of mass

In this study, it is assumed that the rate of change of the refrigerant content in the adsorption reactor is proportional to the difference between the equilibrium x_{eq} and the actual adsorbate content x. Therefore, the refrigerant mass balance can be expressed as [40,54]:

$$\frac{dx}{dt}=D_{so}.(x_{eq}-x) \quad (5.5)$$

where D_{so} is the overall mass transfer coefficient for adsorption/desorption.

5.3.3 Dimensionless system

The following groups of transformation are introduced into the equations from (1-5) to (5-5) to normalize the governing equations,

$z = L_t.Z$	$r = r_f.R$	$\varphi = 2\pi.\emptyset$
$T = \Delta T.\theta$	$x = x_{eq}.X$	$t = t_{des}.\tau$

These non-dimensional numbers allow us to study the effect of adsorption reactor configuration on the performance. Therefore, the resulting non-dimensional equations are as follows:

Energy equation for the heat transfer fluid:

$$\psi.\epsilon_F.\frac{\partial\theta_F}{\partial\tau}+\frac{\partial\theta_F}{\partial Z}=\frac{NTU.R_\lambda.F_L}{B_i.(1+R_G)}.\left(\frac{\partial^2\theta_F}{\partial R^2}+\frac{1}{{L_t}^2}\frac{\partial^2\theta_F}{\partial\emptyset^2}+\frac{1}{F_L^2}.\frac{\partial^2\theta_F}{\partial Z^2}\right) \tag{5.6}$$

Energy equation for the adsorbate and adsorbent:

$$(1+\varepsilon_a.X+\varepsilon_v)\frac{\partial\theta_S}{\partial\tau}+\varepsilon_S.\frac{\partial X}{\partial\tau}=\frac{NTU.A.F_S}{\psi.B_i.(1+R_G)}.\left(\frac{\partial^2\theta_S}{\partial R^2}+\frac{1}{{L_t}^2}\frac{\partial^2\theta_S}{\partial\emptyset^2}+\frac{1}{F_L^2}.\frac{\partial^2\theta_S}{\partial Z^2}\right) \tag{5.7}$$

Energy equation for the adsorption reactor (adsorbent bed):

$$\left(1+\varepsilon_a.X+\varepsilon_v+\xi_{metal}\right)\frac{\partial\theta_b}{\partial\tau}+\varepsilon_S.\frac{\partial X}{\partial\tau}=\frac{NTU.A.F_L}{\psi.B_i.(1+R_G)}.\left(\frac{\partial^2\theta_b}{\partial R^2}+\frac{1}{L^2}\frac{\partial^2\theta_b}{\partial\emptyset^2}+\frac{1}{F_L^2}.\frac{\partial^2\theta_b}{\partial Z^2}\right) \tag{5.8}$$

The mass balance equation can be expressed as:

$$\frac{dX}{d\tau}=\varphi`.(1-X),$$

$$\varphi`=D_{so}.t_{des} \tag{5.9}$$

Where $\varphi`$ is a constant and t_{des} is the required time to desorb 1 kg_{meth}.

5.3.4 Dimensionless Factors

The following non-dimensional factors are used in this analysis:

- Heat transfer fluid number ϵ_F:

$$\varepsilon_F=M_F.C_F.(M_S.c_S)^{-1} \tag{5.10}$$

- Number of transfer unit NTU :

$$NTU=\lambda_F.(\rho_F.C_F.u_z.L_t)^{-1} \tag{5.11}$$

where u_z and α_F are the inlet velocity and the convective coefficient of the HTF, respectively.

- Switching frequency of the adsorption reactor ψ :

$$\psi=M_S.C_S.(\rho_F.C_F.u_z.A_F.t_{des})^{-1},$$

$$\psi=M_S.C_S.(\dot{M}_F.C_F.t_{des})^{-1} \tag{5.12}$$

- Thermal conductivity ratio R_λ:

$$R_\lambda=\lambda_F.{\lambda_{tot}}^{-1} \tag{5.13}$$

- HTF-channel length factor F_L:

$$F_L=L_t.{r_f}^{-1} \tag{5.14}$$

- Heat exchanger geometry R_G:

$$R_G = r_i . r_S^{-1} \tag{5.15}$$

Here $r_S = r_f - r_i$

- Adsorption reactor Biot number Bi:

$$Bi = r_S . \alpha_F . (\lambda_{tot})^{-1} \tag{5.16}$$

- Adsorbate number ε_a:

$$\varepsilon_a = x_{eq} . C_a . . C_S^{-1} \tag{5.17}$$

- Vapor adsorbate number ε_v:

$$\varepsilon_v = M_v . C_v . (M_S . C_S)^{-1} \tag{5.18}$$

- Adsorbent number ε_s:

$$\varepsilon_s = H_{ads} . x_{eq} . (\Delta T . C_S)^{-1} \tag{5.19}$$

- Area ratio A:

$$A = \frac{A_S}{A_F} \tag{5.20}$$

- Fin spacing factor or Adsorbent thickness factor F_S

$$F_S = \frac{L_s}{r_f} = \frac{(n-1).S_f}{r_f} \tag{5.21}$$

- Metal components number ξ_{metal} :

$$\xi_{metal} = (M_f . C_f + M_t . C_t) . (M_S . C_S)^{-1} \tag{5.22}$$

5.3.5 The initial and boundary conditions

The initial and boundary conditions for the present problem are as follows:

During isosteric and isobaric heating

Initial conditions (t=0)

$$T_F(z, \varphi, r, 0) = T_b(z, \varphi, r, 0) = T_0$$
$$\theta = \frac{T - T_0}{T_{h,in} - T_0} = 0$$
$$\theta_F(Z, \emptyset, R, 0) = \theta_b(Z, \emptyset, R, 0) = 0$$

$$x = x_{eq} = x_{max}$$
$$X = 1$$

where $T_{h,in}$ is the inlet temperature of the hot water and T_0 is the initial temperature of the adsorption reactor

Boundary conditions

$z = 0$	$z = L_t$
$T_F = T_{h,in}$ $\frac{\partial T_b}{\partial z} = T_F - T_{h,in} = 0$ $\theta_F = 1$ $\frac{\partial \theta_b}{\partial Z} = 0$	$\frac{\partial T_b}{\partial z} = \frac{\partial T_F}{\partial z} = 0$ $\frac{\partial \theta_b}{\partial Z} = \frac{\partial \theta_b}{\partial Z} = 0$ $Z = 1$

$r = 0$	$r = r_i$	$r = r_f$
$\frac{\partial T_F}{\partial r} = 0$ $\frac{\partial \theta_F}{\partial R} = 0$ $R = 0$	$\lambda_F . \frac{\partial T_F}{\partial r} = \alpha_F . (T_b - T_F)$ $\frac{\partial \theta_F}{\partial R} = \frac{B_i . (1 + R_G)}{R_\lambda} . (\theta_F - \theta_b)$ $\lambda_{tot} . \frac{\partial T_r}{\partial r} = \alpha_F . (T_b - T_F)$ $\frac{\partial \theta_b}{\partial R} = B_i . (1 + R_G) . (\theta_b - \theta_F)$ $R = \frac{R_G}{1 + R_G}$	$\frac{\partial T_b}{\partial r} = 0$ $\frac{\partial \theta_b}{\partial R} = 0$ $R = 1$

During Isosteric and isobaric cooling

Initial conditions:

$t = 0$	$z = 0$	$z = L_t$
$T_F = T_{h,in}$ $\theta_F = \frac{T - T_0}{T_{h,in} - T_0} = 1$	$T_b = T_{h,in}$ $\frac{\partial T_b}{\partial z} = T_S - T_{h,in} = 0$ $\theta_b = 1$	$\frac{\partial T_b}{\partial z} = \frac{\partial T_F}{\partial z} = 0$ $\frac{\partial \theta_b}{\partial Z} = \frac{\partial \theta_F}{\partial Z} = 0$ $Z = 1$

5.3.6 System performance equations

The system performance of an adsorption refrigeration system can be characterized by the coefficient of performance COP which is defined as [54,113]:

$$COP = \frac{\dot{Q}_{evap}}{\dot{Q}_{in}} \tag{5.23}$$

The heat extracted from the evaporator is

$$\dot{Q}_{evap} = \int_0^{t_{des}} M_S \frac{\partial x}{\partial t} \left[L_{evap} + C_a (T_{cond} - T_{evap}) \right] . \partial t \tag{5.24}$$

The energy input during the isosteric and isobaric heating

$$\dot{Q}_{in} = \dot{M}_F . C_F . \int_0^{t_{des}} (T_{h,in} - T_{h,out}) . \partial t \tag{5.25}$$

5.4 Results and Discussions

5.4.1 Influence of the flow type

The analytical and numerical investigation of the flow type effect on desorption process have been implemented by study Reynolds number Re, which is one of the important factors controlling the heat transfer. Variation of Re is considered at different temperature $T_{h,in}$ and velocity values u_z of the hot water as a HTF, which is supplied to both the reactors. The role of the HTF is to heat up the adsorbent particles, which causes the heat exchange to desorb the refrigerant to the condenser. In this study the size, installation and composition of the adsorption reactor (number and dimensions of the fins as well as HTF-channels) including the filled adsorbent amount were kept constant in order to desorb $1k_{meth}$. This means, that regardless of flow type the required input heat, which is consumed from the HTF, must be obtained and introduced to the adsorption reactors.

Parameter	SG-Bed	AC-Bed
$T_{h,in}$	100 °C	84 °C
T_0	27 °C	27 °C
T_{cond}	32 °C	32 °C
T_{evap}	−3 °C	−3 °C
ξ_{metal}	1.839	2.040
ε_a	0.44	0.69
ε_s	4.239	8.591

Table 5.2: Base run parameters

In the present analysis, in order to desorb a constant amount of the refrigerant, a set of non-dimensional parameters is presented and discussion. Tab. 2 shows the base run parameters, which related to the adsorbent and adsorbate amounts and to the adsorption reactor geometry to desorb $1kg_{meth}$.

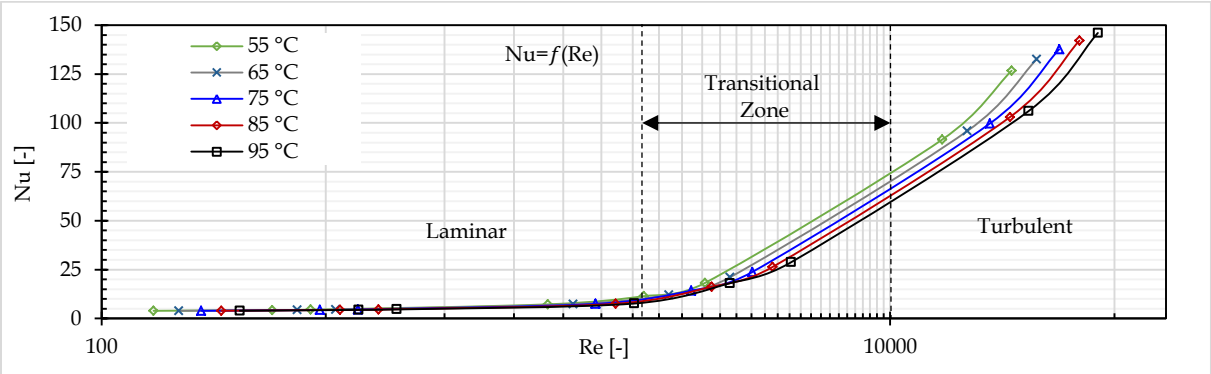

Figure 5.4: Relation between Reynolds number Re and Nusselt number Nu for different temperatures of the flowed water.

By the simulation results shown in Fig. 5.4 and as it is known, that Reynolds numbers of less than 2300 describe the condition which is termed laminar flow. At values of Reynolds number between 2300 and 10^4 is the transitional zone. At Reynolds numbers above 10^4 the condition is described as turbulent [114]. Consequently, the Reynolds number was discussed and it is worth noting, that the values of the input fluid velocity u_z were carefully selected after Reynolds analysis and the calculation of the critical values to study the effect of flow type on the desorption process throughout flow channels of both the SG-and AC-adsorption reactors. Six values of the input fluid velocity u_z were selected, two for each flow type as follows:

Laminar flow $\mathrm{Re} < 2300$ at $u_z = 0.01$ and 0.04 [m/s]

Transition flow $2300 < \mathrm{Re} < 10^4$ at $u_z = 0.07$ and 0.1 [m/s]

Turbulent flow $\mathrm{Re} > 10^4$ at $u_z = 0.4$ and 0.6 [m/s]

As is common, it is observed from **F**igs. 5.5 and 5.6 that the Reynolds number increases significantly with increasing the fluid velocity u_z and slightly with increasing the fluid temperature $T_{h,in}$. This is known as the result of the direct proportion between the Reynolds number and the fluid velocity as shown in the relationship $Re = u_z . d_i / \vartheta$.

Where d_i and ϑ are the inner diameter of the HTF-channel and the kinematic viscosity, respectively.

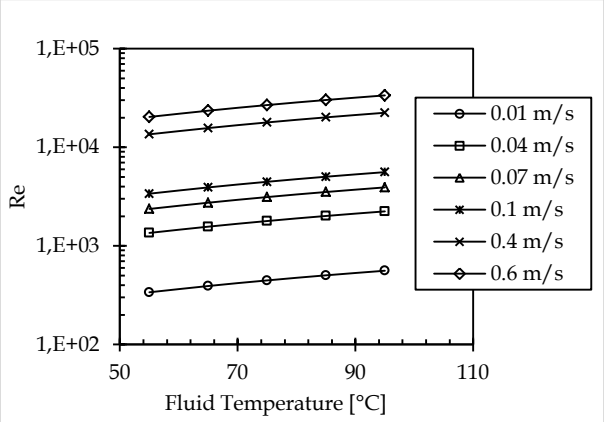

Figure 5.5: Relation between Reynolds number Re and temperature of the flowed water for different velocities

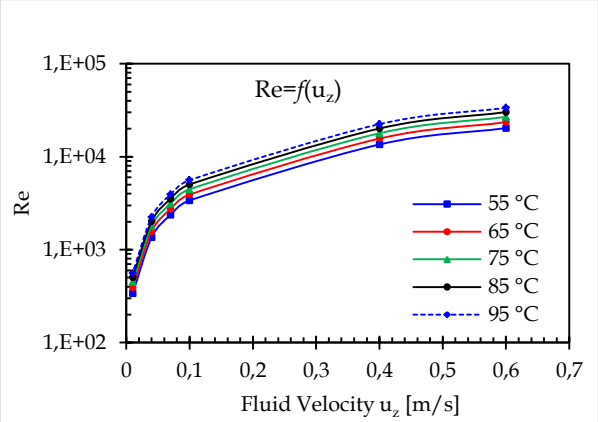

Figure 5.6: Relation between Reynolds number Re and the velocity of the flowed water for different temperatures

The driving temperature $T_{h,in}$ and velocity u_z of the HTF were found to have important effect on the desorption process in order to activate the reactor and desorb $1k_{meth}$. **F**ig. 5.7 shows evolution of temperature field throughout both the SG-and AC-reactors with increasing of Reynolds number. It can be seen, that temperature distribution by $\mathrm{Re} = 23511$ is higher than one by $\mathrm{Re} = 392$. When the HTF flows with high velocity 0.6 m/s ($\mathrm{Re} = 23511$), the intense mixing of the fluid in turbulent flow enhances the heat and momentum transfer between fluid particles, which in turn increases the friction force and the convection heat transfer coefficient. When the velocity is lower 0.01 m/s ($\mathrm{Re} = 392$), the heat transfer fluid spends more time in the channel, hence the heat exchange needs more time in order to activate the adsorption materials and to heat the adsorption reactor components. When the operating in a laminar flow regime, the physical properties of the HTF are the determining factors for the heat transfer in this case which is inefficient in heat transfer terms.

The study of the temperature distribution as shown in **F**ig 5.7 was implemented using **MATLAB** software on symmetry plane $x - y$ throughout the SG-and AC-adsorption reactors. This symmetry plane $x - y$ has the same dimensions for both the SG-and AC-adsorption reactors.

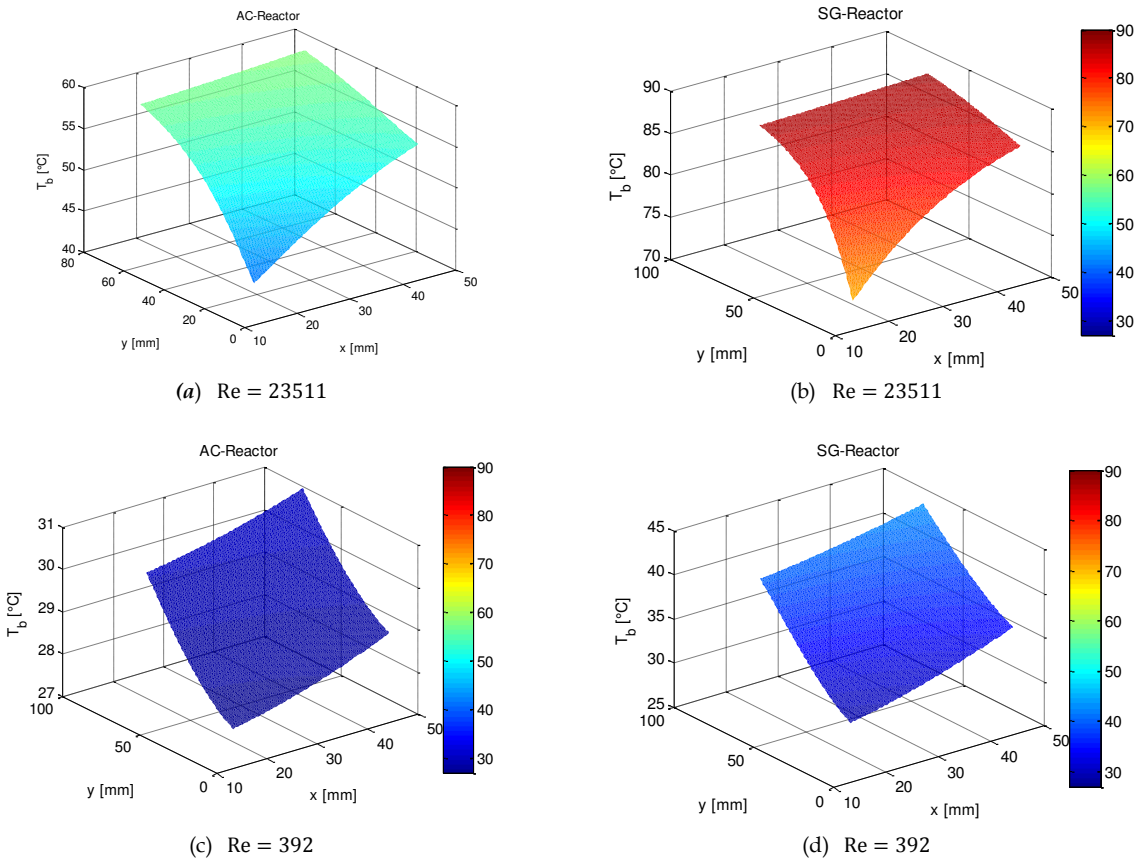

(a) Re = 23511 (b) Re = 23511

(c) Re = 392 (d) Re = 392

Figure 5.7: Effect of Reynolds number on temperature distribution throughout the SG-and AC-adsorption reactors (a, b) Re = 23511, (c, d) Re = 392

In other words when the operating in a laminar flow regime Re = 392, the velocity of HTF-flow is lower and therefore, the heat transfer among the fluid particles is poor. Whereas, in case of turbulent flow Re = 23511 the higher velocity of fluid flow causes higher collision among the fluid particles. Due to higher collision among fluid particles, heat transition rate increases [114-115].

5.4.2 Effect of Biot number

The simulation results presented in **F**ig. 5.7 can be explained based on analysis the non-dimensional number Bi. In the context of the presented problem analysis, the Biot number Bi can be used to characterize the heat transfer resistance inside the adsorption reactor, because Bi is defined as ratio of internal resistance of the reactor components which is conduction resistance to external resistance which is heat convection. This ratio determines whether or not the temperatures inside the reactor will vary significantly in space, while the adsorption reactor is heated over time, from a thermal gradient applied to its surface [114-116].

As explained in **F**ig. 5.8 one can easily by calculating the Biot number understand that temperature gradients should be taken in to consideration or not in the studied problem. **F**ig. 5.8 gives us idea about the relation between the flow type and temperature distribution through the reactor [114-116].

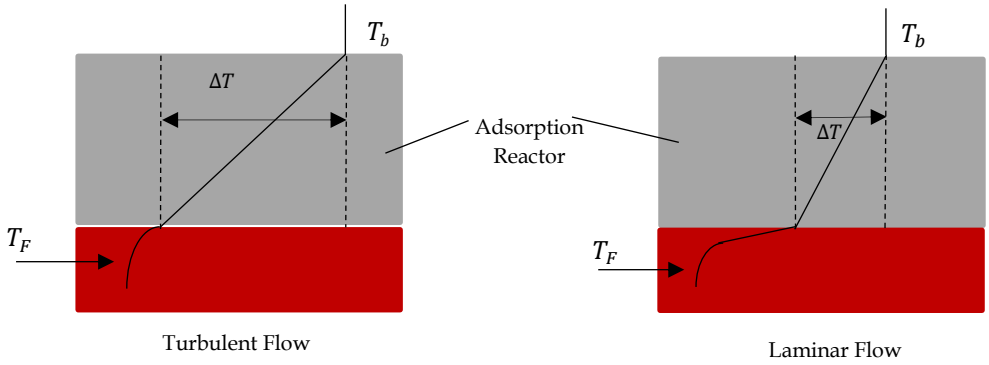

Figure 5.8: Temperature gradient based on the flow type

It can be observed from **F**ig. 5.9 two cases: In the first case if $\mathrm{Bi} > 1$, variation of temperature is significant inside the adsorption reactor. In the second case if $\mathrm{Bi} < 1$ which means the external convective resistance is more high when compared to the internal conductive resistance, so smaller significant temperature variation inside the adsorption reactor in comparison with the first case. By turbulent flow $\mathrm{Re} > 10^4$ it is found, that Biot numbers larger than 1, which means the internal conductive resistance exceeds that external convective resistance. If $\mathrm{Bi} > 1$ is signal more temperature distribution within the adsorption reactor as shown in **F**ig 5.7a and b for $\mathrm{Re} = 23511$. In case of laminar flow the problem involving small Biot numbers (smaller than 1) is thermally simple, due to uniform temperature field inside the adsorption reactor, which implies that temperature gradients are there slightly inside of adsorption reactor as shown in **F**ig 5.7c and d for $\mathrm{Re} = 392$.

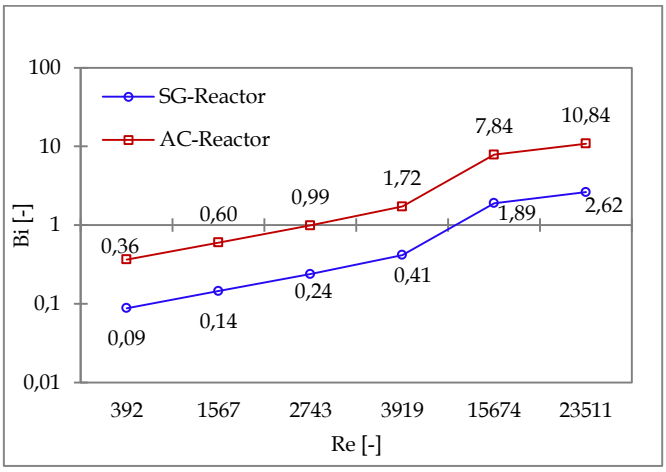

Figure 5.9: Relation between Reynolds number Re and Biot number Bi for the SG- and AC-adsorption reactors

5.4.3 Effect of Nusselt number

In the context of the presented problem analysis, which is involved the conductive and convective heat transfer (conduction inside the adsorption reactor components and convection throughout the adsorption reactor HTF-channels), the Nusselt Number Nu is also an important factor. Nu shows how much is the heat is transfered due to fluid motion as compared to the heat transferred by fluid by the process of conduction. Nusselt number Nu gives us idea about the quality of heat transfer rather than its quantity [112].

Fig. 5.4 shows how to change the Nusselt number Nu with Reynolds number Re for different temperatures. Based on the results, it is found, that Nusselt number Nu for different Reynolds number values remains larger than 1, which means more effective convection, because the convective

resistance of the heat transfer fluid is less than that the conductive resistance. With $Nu > 3.66$, the fluid motion enhances heat transfer by advection. If $Nu = 3.66$ then, the fluid is stationary and all heat transfer is by conduction. It is also shown in **F**ig. 5.4 that there is a small change of Nusselt number with respect to laminar flow regimes $Re < 2300$.

We know that Nusselt number is a function of the convection coefficient α_F. In order to find the overall heat transfer coefficient for both the adsorption reactors, the non-dimensional number Nu is required based on its relationship with the following [112, 116]:

$$Nu = f(Re, Pr, Geometry, T_F/T_t)$$

where Pr, T_F and T_t are Prandtl number, HTF-temperate and the temperature of the tube wall, respectively.

Turbulent Flow: $Re > 10000$

$$Nu_{turb} = \frac{(\xi/8)\, Re\, Pr}{1 + 12.7\sqrt{\xi/8}\,(pr^{2/3} - 1)}\, f_1\, f_2 \tag{5.26}$$

$$\xi = [1.8\log(Re) - 1.5]^{-2} \quad \text{(Darcy friction factor [116])}$$

where $f_1 = 1 + (d_i/L_t)^{2/3}$ and $f_2 = (Pr/Pr_t)^{2/3}$ are correction factor [116].

Laminar Flow $Re < 2300$

$$Nu_{lam} = \sqrt[3]{3.66^3 + 0.644^3 Pr(Re\ d_i/L_t)^{3/2}} \tag{5.27}$$

Transition Flow $2300 < Re < 10000$

$$Nu_{trans} = (1 - \gamma)\, Nu_{lam}(Re = 2300) + \gamma\, Nu_{turb}(Re = 10^4) \tag{5.28}$$

$$\gamma = \frac{Re - 2300}{7700}$$

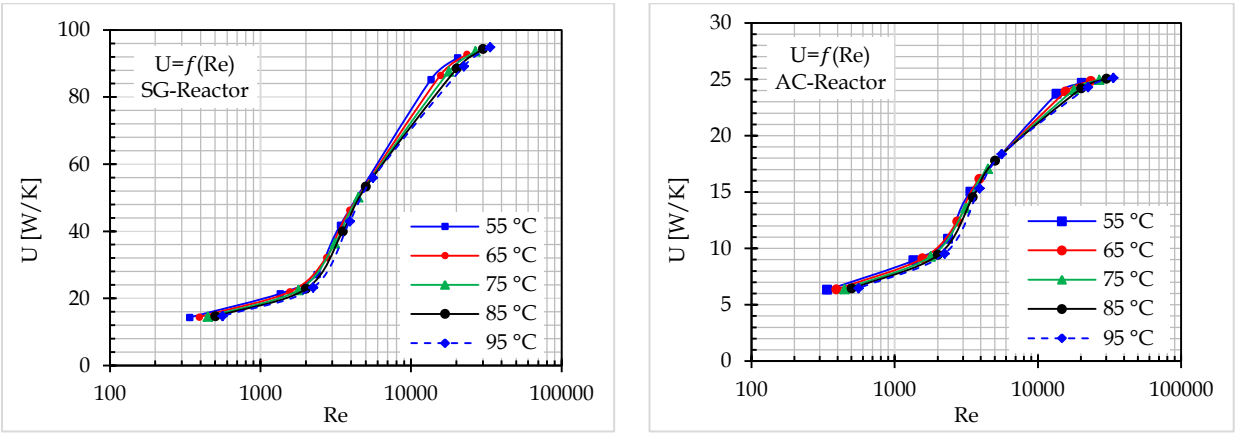

Figure 5.10: Effect of Reynolds number Re on the overall heat transfer coefficient of the SG- and AC- adsorption reactors

At the governing equation of the overall heat transfer coefficient of both the SG- and AC- adsorption reactors, only the convection coefficient of fluid α_F is used in this study as a variable and other parameters, which are related to the size and components the reactor, are constant. According to **F**ig. 5.10, it is observed, that the overall heat transfer coefficient U [W / K] improves with increasing

values of Reynolds number Re. When the inlet velocity of the flow increases, we notice that the fluid motion always results in increase in heat transfer (**F**ig. 5.10) and hence Nu is always greater than 1 for convection **F**ig. 5.4. Here, it is shown based on **F**ig. 5.10 that there is a small change of overall heat transfer coefficient with lower Reynolds number because of laminar flow analysis.

Due to the laminar flow, the velocity of HTF flowed through the channel is small and therefore, the interaction among fluid particles is also low. Due to low velocity, the heat transfer among fluid particle occurs very slowly. This is why the overall heat transfer coefficient and Nusselt number become approximately similar at different Reynolds number. This graph shows that the overall heat transfer coefficient of both the adsorption reactors in turbulent flow regimes has a significant enhancing effect for Reynolds numbers range $\mathrm{Re} > 10^4$. This can be explained as follow: The higher velocity of fluid flow causes higher collision among the fluid particles. Due to higher collision among fluid particles, heat transition rate increases and it is possible in case of turbulent flow [114].

It can be shown from the **F**ig. 5.10, how increasing of Reynolds number can effect of the overall heat transfer coefficient. For $\mathrm{Re} > 10^4$, we find $\mathrm{U_{SG}} > 70\ [\mathrm{W/K}]$ and $\mathrm{U_{AC}} > 20\ [\mathrm{W/K}]$. It can be also seen, that for a mean hot water temperature of $65\,^{\circ}\mathrm{C}$ it is found, that the value of the heat transfer coefficient varies from 14.5 to $92\ [\mathrm{W/K}]$ with an increase in Nusselt number from 4.5 to $132\ [\mathrm{W/K}]$ for the SG-adsorption reactor.

Why $\mathbf{U_{SG} > U_{AC}}$?

It is known that the dimensions of the heat exchanger (the length and number of the tubes, the dimensions and number of fins as well as the amount of material filled in the reactor) has an important effect on the overall heat transfer coefficient. The study of the adsorption reactor is interested in finding a relation between the overall heat transfer coefficient of the adsorption reactor and the geometry parameters. **F**ig. 5.11 shows variation of the overall heat transfer coefficient through the fin dimension.

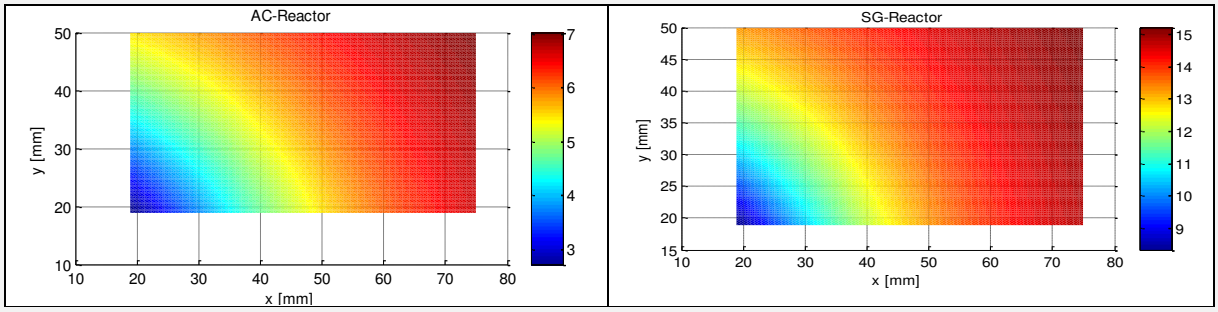

Figure 5.11: Variation the overall heat transfer coefficient U [W / K] through the fin dimension of the SG- and AC-Reactors

The extended surfaces of fins increase the overall heat transfer coefficient by increasing the heat transfer area. It is noticed, that the overall heat transfer coefficient of the SG- adsorption reactor $\mathrm{U_{SG}}$ is higher than $\mathrm{U_{AC}}$ of the reactor filled with activated carbon, because the dimension of SG-reactor contained four tubes larger than the dimension of AC-reactor reactor which contains only two tubes. Another reason is the thermal conductivity of SG as adsorbent is higher than the thermal conductivity of AC $\lambda_{SG} > \lambda_{AC}$.

The other objective of this task is to know the effect of the flow type on the time required to desorb $1\ \mathrm{kg_{meth}}$ from both the reactors. It can be observed from **F**ig. 5.12, a brief summary of the comparison between the SG-and AC- reactors in terms of Nusselt number, the required heating time as well as the overall heat transfer coefficient depending on the flow type determined by different values of Reynolds number. The results in **F**ig. 5.12a shows, that when the HTF in the channel flows with $\mathrm{Re} = 392$ as laminar, the SG-adsorption reactor requires a longer desorption time of about 81 min than the required time in the case of a turbulent flow $\mathrm{Re} = 23511$, where requires only about 7 min, to desorb the same amount of methanol $1\mathrm{kg_{meth}}$ during desorption process.

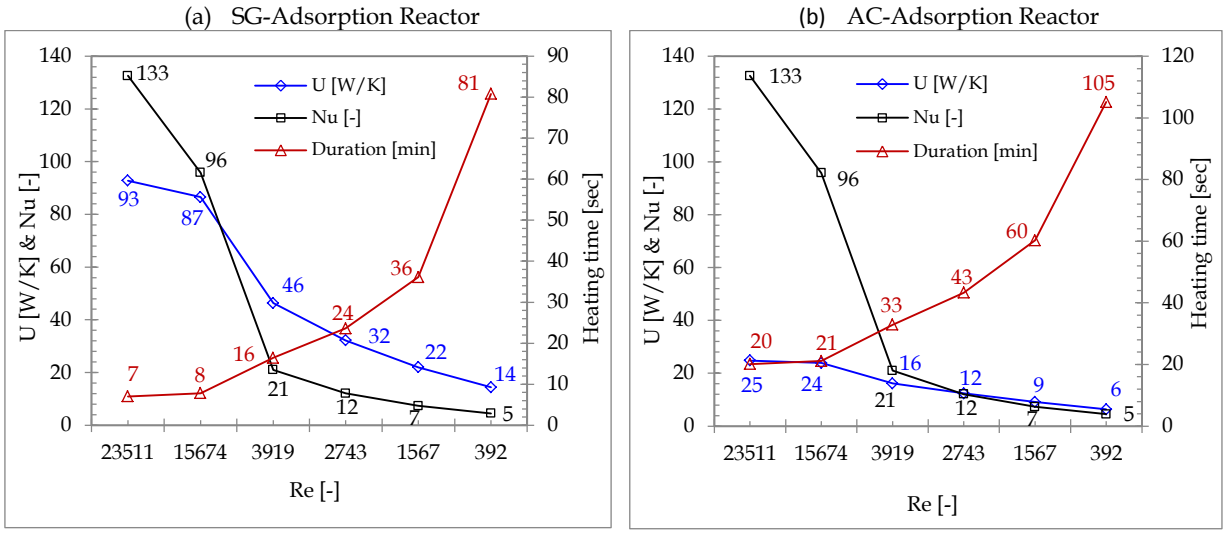

Figure 5.12: Nusselt number Nu, overall heat transfer coefficient and required heating time as function of Reynolds number Re to desorb $1kg_{meth}$ from both the SG- and AC- adsorption reactors

While Re = 392 throughout the channels of the AC-adsorption reactor the desorption process takes longer desorption time than it throughout the SG-adsorption reactor. As shown from **F**ig. 5.12b, the AC-adsorption reactor takes 105 min when Re = 392, whereas takes about 20 min for turbulent flow Re = 23511 to desorb $1kg_{meth}$. This is because of the low overall heat transfer coefficient, the installation of the reactor and the properties of the activated carbon as adsorbent.

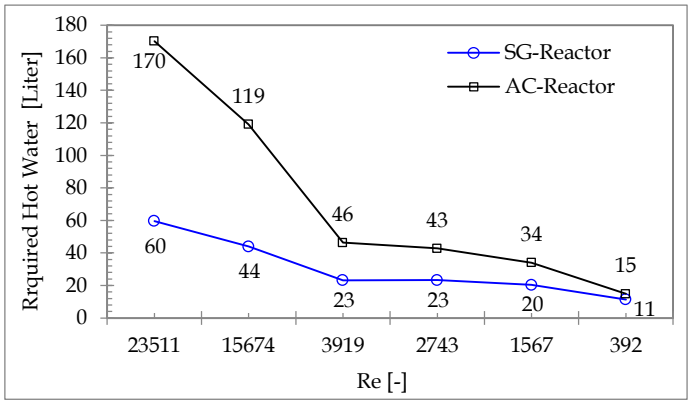

Figure 5.13: Comparison of the required amount of hot water to desorb $1kg_{meth}$ varying different flows based on different velocities and temperatures

By knowing the required desorption time and the mass flow rate required, the amount of hot water needed to secure it from the heat source in order to achieve completely desorption process (desorbing 1 kg_{meth}) can be easily calculated. Based on **F**ig. 5.13, we find that the reactor in the case of high values of Reynolds number ($Re > 10^4$) requires more amount of hot water than it required in the case of laminar flow ($Re < 2300$) due to the long of desorption time required.

5.4.4 Flow nature effect on the temperature difference of HTF

This section presents flow type effect at different values of Reynolds number on the required heating duration and variation the HTF-temperature during desorption process.

In order to determine the effect of the flow type on the heat exchanger's efficiency, the temperature difference of the HTF between the inlet and outlet channel of the both reactors was simulated and

demonstrated with the needed heating time (desorption time) for the different values of Re. In other studies the temperature difference can be considered as a measure of how much heat is consumed from the hot fluid and absorbed by the reactor as well as can be a measure of the wasted heat, which remains with the HTF. But in our study the adsorption reactor regardless of the flow type, must absorb the same amount of the heat in order to desorb same amount of the refrigerant $1\ \mathrm{kg_{meth}}$. In other words the HTF must obtain the required desorbing heat.

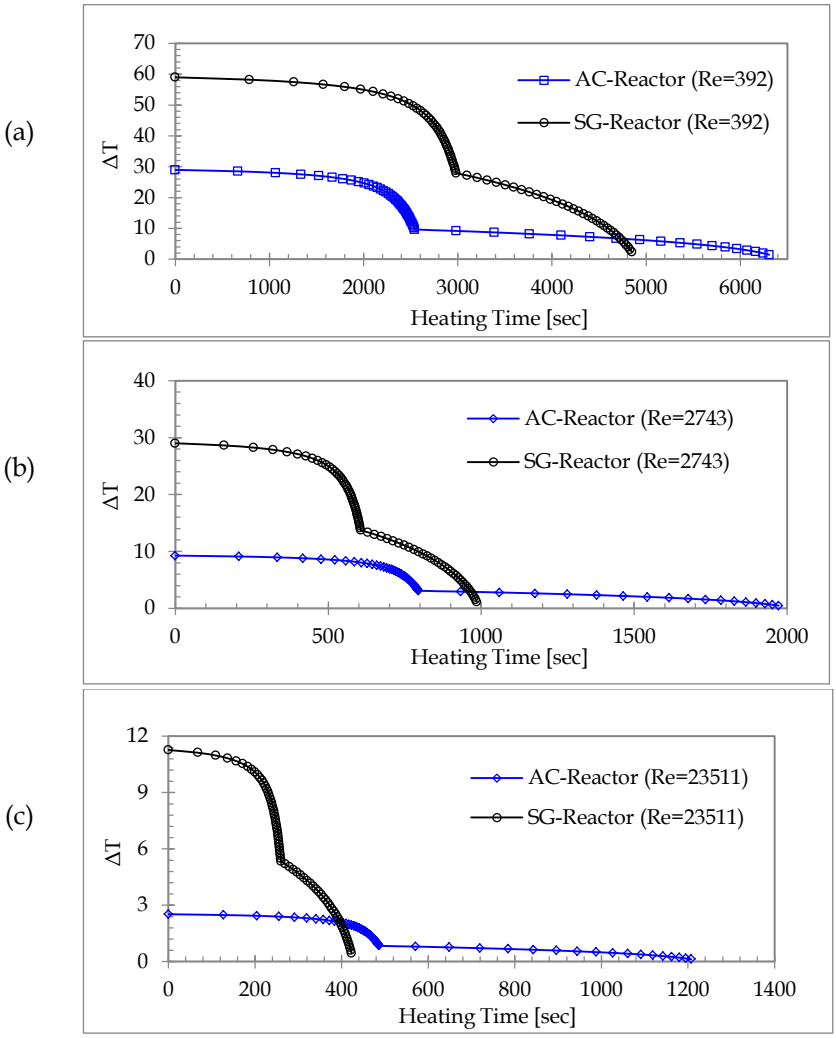

Figure 5.14: Variation of the temperature difference with the required heating time based on different flow types inside the channels of both the SG-and AC-Reactors.

Based on the results demonstrated in **F**ig. 5.14, which focus on the change in the fluid temperature of the SG- and AC-reactors with the heating time required to desorb a similar amount of adsorbate $1\mathrm{kg_{meth}}$ for $\mathrm{Re} = 392$ **F**ig. 14a, $\mathrm{Re} = 2743$ **F**ig. 14b and $\mathrm{Re} = 23511$ **F**ig. 14c. It is found that a longer time leads to higher drop of the HTF-temperature as observed in laminar flow regimes.

In spite of the absorbing the same amount of the heat, the short heating time with $\mathrm{Re} > 10^4$ leads to low temperature difference. So the water exits at a very high temperature $\mathrm{T_{h,out}} > 90\ ℃$ as shown in **F**ig. 5.14c. In the conducted results, the input temperature was kept constant at $100\ ℃$.

As noticed from **F**ig. 5.14a the large difference is noticed with low values of Re. Here it is needed less hot water but the HTF spends longer time inside the channel for $\mathrm{Re} = 392$. From **F**ig. 5.14b we note for the transient flow $\mathrm{Re} = 2743$, that the results are located between the results of the turbulent and the laminar flow.

However, we observe that the temperature difference of the SG-reactor is reduced to lower levels over a longer period than the AC-reactor due to the activated carbon properties. **F**ig. 5.14 gives also a comparison between both the reactors. The reactor filled with activated carbon requires a longer time and less heat $(\Delta T_{out}^{SG} > \Delta T_{out}^{AC})$ in order to desorb the same amount of methanol.

5.5 Temperature Field

The numerical study of the temperature field $T(x, y, z, t)$ is necessary to know the homogeneity of the temperature distribution throughout the adsorption reactor. **F**ig. 5.15 tell us about how much the heat transfer is enhanced due to fluid motion and also exhibits the temperature distribution from our simulation study throughout the adsorption reactor, which is filled by adsorbent materials (SG-particles).

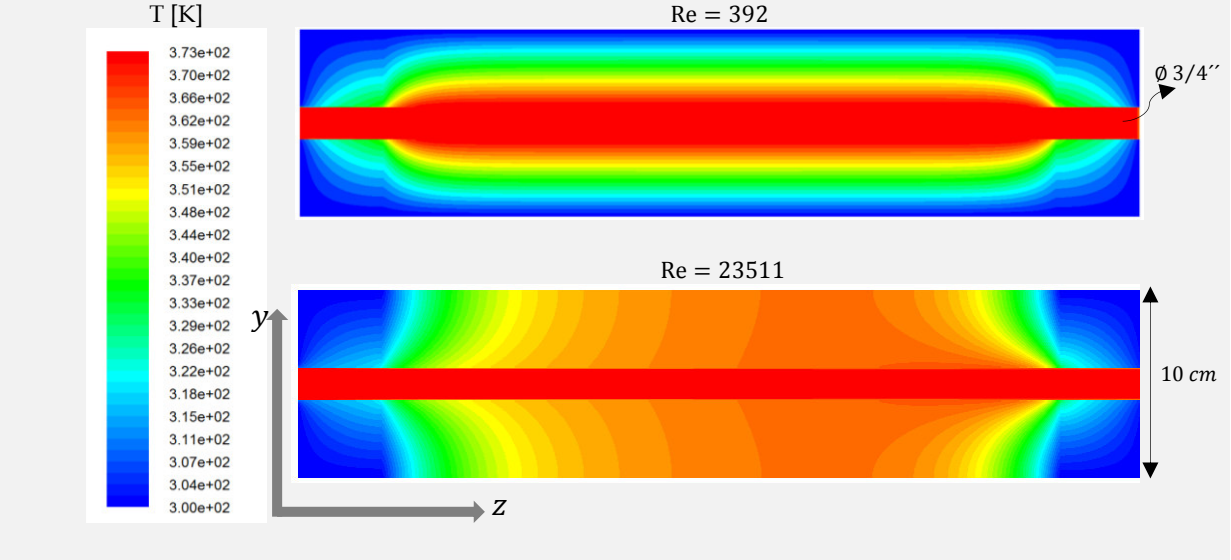

Figure 5.15: Temperature distribution plot on $z - y$ symmetry plane throughout the adsorption reactor during desorption process for (a) $\mathrm{Re} = 392$ and (b) $\mathrm{Re} = 23511$

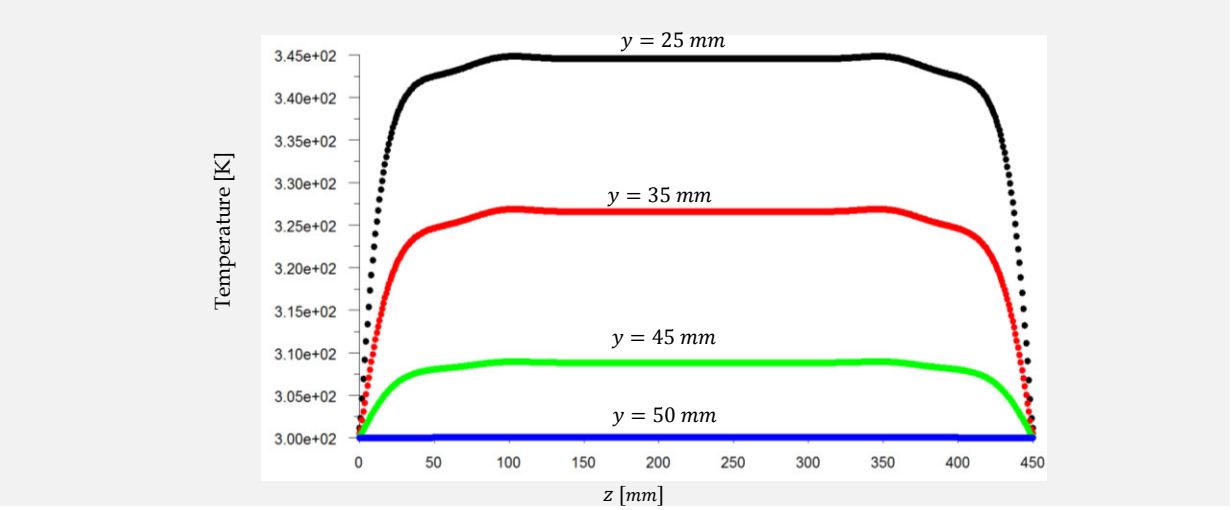

Figure 5.16: Profile of the temperature variation along the z axis throughout the adsorption reactor during desorption by $\mathrm{Re} = 392$ and at $y = 25, y = 35, y = 45$ *and* $y = 50\ mm$

When $\mathrm{Re} = 392$, it can be seen that temperature rises slowly, gradually and homogenously from the HTF-channel inside adsorbent-adsorbate medium and then toward the outer boundaries. Whereas the temperature distribution is non homogeneous throughout the adsorption reactor with high values of

Reynolds number Re = 23511, Because the heat transfer rate increases with the increase of Reynolds number and increased mixing and shearing occur in turbulent flow. This results in increased viscous losses which affects the efficiency of hydraulic machines. However, for lower to higher velocity range the temperature reaches at every point to the desired desorption temperature. **F**ig. 5.17 shows also temperature distribution for other symmetry plane throughout the adsorption reactor in laminar flow regimes.

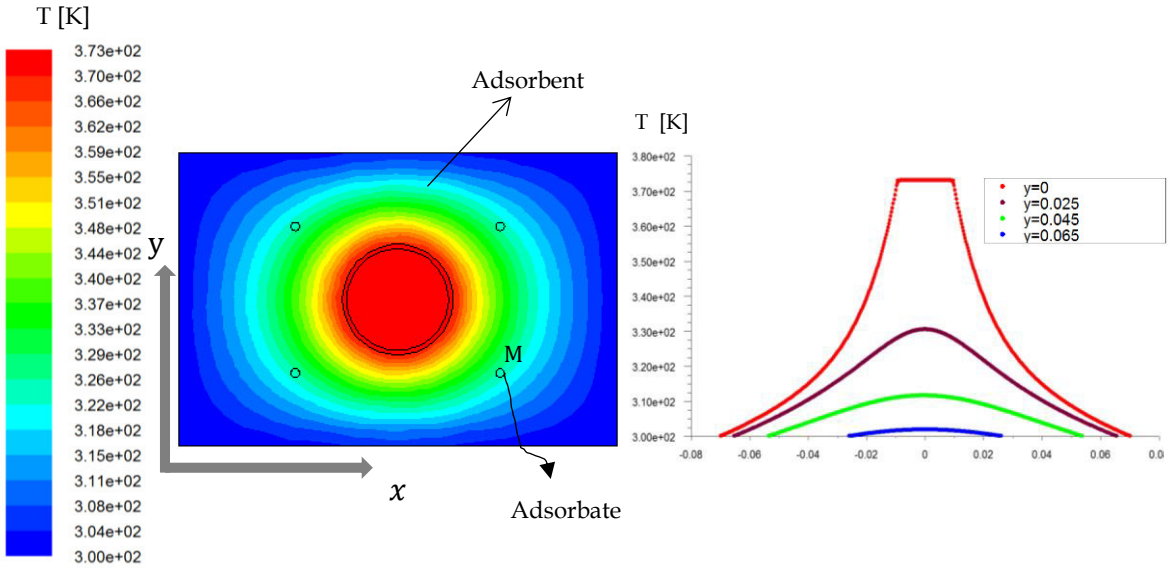

Figure 5.17: Temperature distribution plot on $x - y$ symmetry plane (left) and Temperature profile along x axis at $y = 0,\ y = 25, y = 45\ and\ y = 65mm$ (right) throughout the adsorption reactor during desorption process for Re = 392

In order to study the behavior of the adsorbate (methanol), which is fixed on the adsorbent, during desorption process in the cases of laminar and turbulent flows, we considered methanol as a circle shape of 1 mm diameter as geometry inside the adsorption medium as shown in the **F**ig. 5.17 above labelled M. Therefore the simulation study with the help of the software **A**NSYS **F**LUENT is implemented during desorption process, so that we considered that the methanol particle has a couple wall as a boundary condition. This means, that the temperature of the methanol border has the same adsorbent temperature and this border allows the heat transfer between the adsorbate (methanol) and the adsorbent.

This study of methanol-behavior is an assumption (allegation) study, because there is no bulk motion inside the adsorption medium and the pore diameter of the adsorption material doesn't exceed 100 nm.

During the desorption process both the temperature of the adsorbent particles and temperature of methanol, which is loaded on the adsorbent, also rises to the desorption temperature. As a result, the methanol that is used as a refrigerant in the adsorption system, evaporates and leaves from the adsorption reactor. **F**ig. 5.18 shows the methanol-behavior, fixing on the SG-particles during desorption process and gives the variation in its velocity resulting from the absorption of the heat by SG-particles. When the adsorbent temperature rises from 27 °C to the maximum desorption temperature of 100 °C, it is observed, that the velocity of the methanol as an adsorbate changes from 0 to only 0.03 m/s in the case of laminar flow. Whereas in the case of the turbulent flow the velocity of methanol changes from 0 to 0.08 m/s. Therefore, the desorption process with a laminar regime requires longer time.

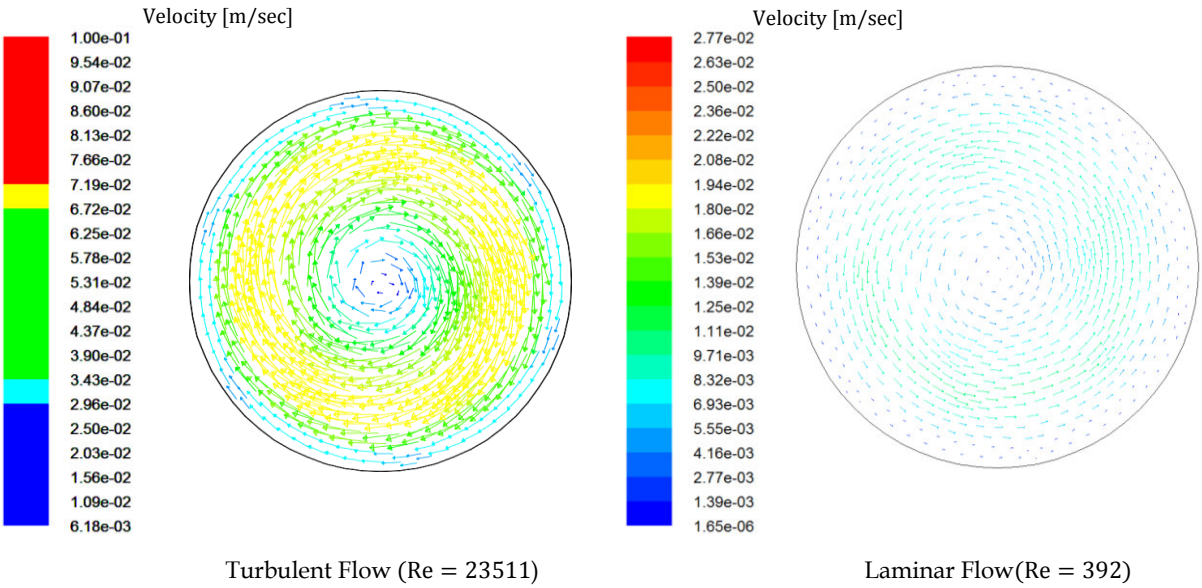

Figure 5.18: Methanol behavior inside the adsorption reactor during the desorption process in case of laminar and turbulent flow

5.6 Effect of the non-dimensional adsorption reactor design factors

The other main goal of this work is to analyze the effect of heat exchanger design parameters of the **A**dsorption **I**ce **P**roduction **AIP** system containing two different substances (two adsorption materials) together, each in a reactor

In this study, the effect of the non-dimensional heat exchanger design factors, which are derived based on the parametric analysis such as the area ratio A, factor of the length channel factor F_L, reactor geometry ratio R_G and fin spacing factor F_S, on the system performance (COP and SCP), desorbed methanol mass M_{des} and the amount of produced ice M_{ice}, have been geometrical and thermal investigated on the two adsorption reactors. The first adsorption reactor contains a silica gel and the second contains activated carbon as adsorption materials.

The factors A, F_L, R_G and F_S allow us to study the effect of using different geometries of the fins, fin spacing, adsorbent thickness as well as effect of variation the number of fins or the channels, used in adsorption reactor. The effect of these factors has been studied and discussed in the case of a constant heat source which means same temperature and the velocity of the HTF at the entrance of the heat exchanger.

5.6.1 Area ratio

The area ratio A of the studied adsorption reactor is defined as the ratio of the contact surface A_S between the adsorption particles and the fins to the cross section surface of the HTF channel A_F. An increase in A is equivalent to increasing the fins' surface (contact surface) or decreasing of the diameter of the HTF-channel.

Not only the area ratio factor A but also the length channel factor F_L, the reactor geometry R_G and the fin spacing factor F_S are related to the fins' dimensions as well as play an important role in the heat transfer design. In the following **T**ab. 5.3 it can be seen that the fins' dimensions which were discussed and how change the other mentioned factors with use of different fins for both the SG-reactor and AC-reactor.

	$H_f \times B_f$	A	F_L	R_G	F_S
SG-Reactor	**(1)** 50 × 75 mm	14,76	52,09	0,33	42,14
	(2) 100 × 150 mm	62,62	26,04	0,14	21,07
	(3) 200 × 300mm	254,06	13,02	0,06	10,53
	(4) 200 × 675 mm	573,14	8,68	0,04	7,02

	$H_f \times B_f$	A	F_L	R_G	F_S
AC-Reactor	**(1)** 50 × 75 mm	14,76	26,05	0,33	21,07
	(2) 100 × 150 mm	62,62	13,02	0,14	10,54
	(3) 200 × 300mm	254,06	6,51	0,06	5,27
	(4) 200 × 675 mm	573,14	4,34	0,04	3,51

Table 5.3: Relationship between the dimensions' values of the studied fins and the non-dimensional numbers A, F_L, R_G and F_S for both the SG-and AC-adsorption reactors

The analyze factor A has been discussed in the present work with two cases. In the first case the fins' dimension is extended by contestant adsorbent amount M_S. In the second case the factor A has been studied also by increasing the fins' dimension but by changing the adsorbent amount filled inside the adsorption reactor, where the adsorbent amount is related to the fins' geometry used. Both the cases were implemented for constant diameter of the heat transfer fluid channel A_F.

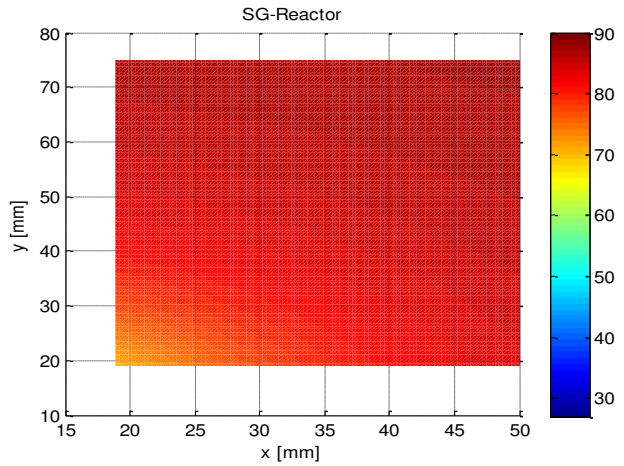

(a) $50 \times 75\ mm$

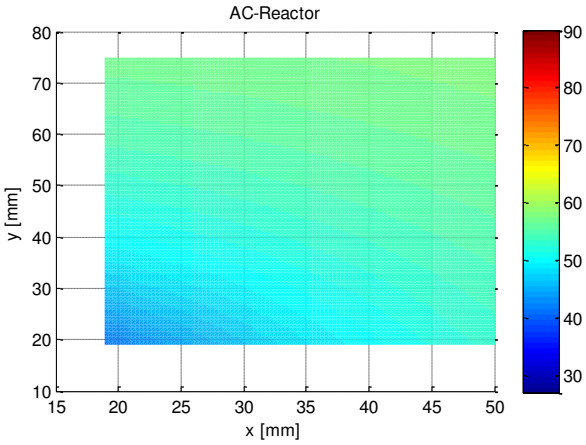

(b) $50 \times 75\ mm$

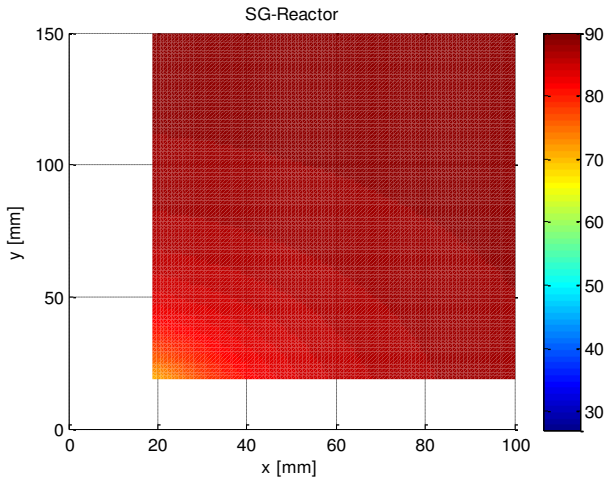

(c) $100 \times 150\ mm$

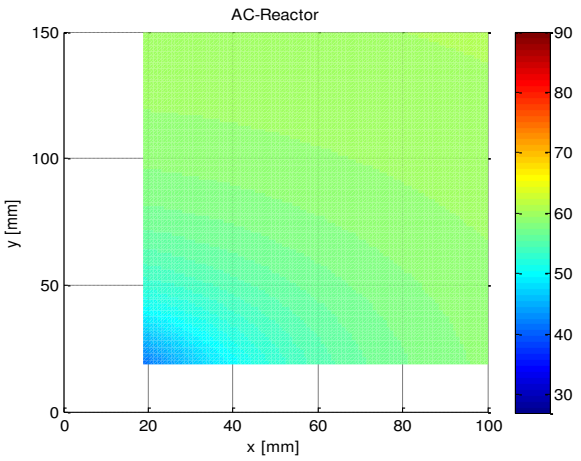

(d) $100 \times 150\ mm$

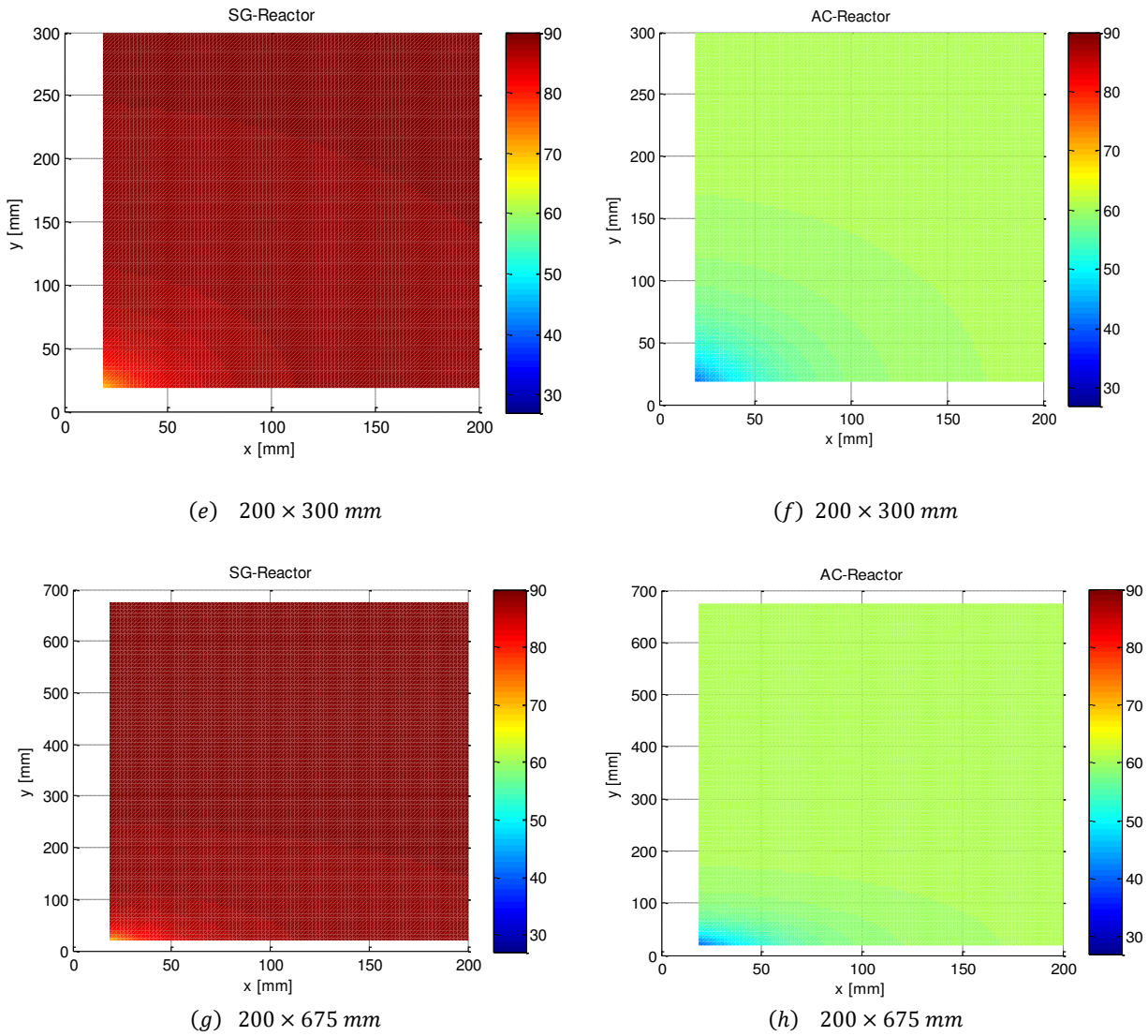

Figure 5.19: Two dimensional view in the x-y plane of the temperature distribution throughout the SG-and AC-adsorption reactors during desorption process at Re = 392 by varying the fins' dimensions
(a, b) 50 × 75 mm (c, d) 100 × 150 mm (e, f) 200 × 300 mm (g, h) 200 × 675 mm

Fig. 5.19 shows the simulation results of investigation of fin dimension effect on temperature field in $x - y$ plane throughout both the SG-and AC-reactors during desorption process. In the conduct simulations, the Reynolds number was kept constant (Re = 392) and the adsorbent amount increased in order to employ the new spaces. As it is obvious, in spite of increasing the adsorbent amount M_S, temperature distribution inside the adsorption medium rises because of extend the heat transfer surface.

The effect of the area ratio **A** on COP has been presented in **F**igs. 5.20a and b for both the cases and for the SG- and AC-adsorption reactors. When the fin dimension is extended from 50 × 75 mm to 200 × 675 mm and the adsorbent amount remains constant, the coefficient of performance COP decreases by about 57 % for the AC-reactor and by about 39 % for the SG-reactor. Whereas the same increase of the fin geometries in the second case $M_S \neq$ constant leads to slight enhancement of 1.78 % and 1.57 % in COP for AC-and SG-reactors, respectively.

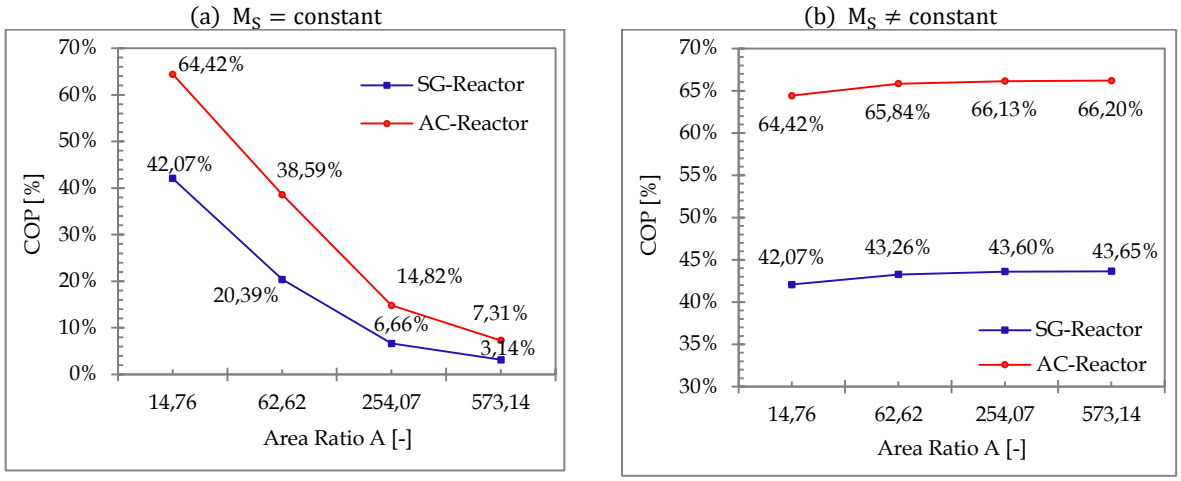

Figure 5.20: Effect of the area ratio A on the coefficient of performance COP of both the SG- and AC- adsorption reactors in case of (a) M_S = constant and (b) $M_S \neq$ constant

The change of the COP in both the cases can be explained by analyzing the metal components factor ξ_{metal}, which is related to both the metal components mass and the adsorption material amount as shown in **F**ig. 5.21. Although the metal components mass for both the cases has the same increase of about 128 kg for SG-reactor and 65 kg for the AC-reactor, the factor ξ_{metal} increases clearly from 2.27 to 80.47 for AC-reactor and from 2.09 to 74.13 for SG-reactor, whereas a slight decrease in the factor ξ_{metal} of about 11 % is observed by increasing the adsorbent amount for both the reactors.

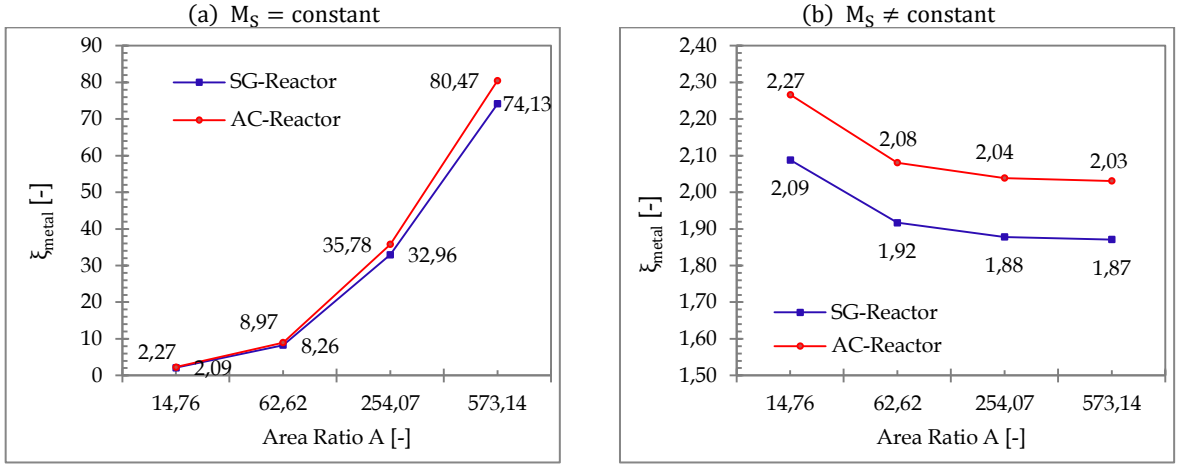

Figure 5.21: Relation between the area ratio **A** and the metal components factor ξ_{metal} by (a) constant adsorbent amount and (b) varying the adsorbent amount

The evolution of the desorbed refrigerant amount, the produced amount of ice and the specific cooling power have been simulated during desorption process for different values of the factor A inside both the SG-and AC-reactors and demonstrated versus adsorption reactor temperature in **F**ig. 5.22.

In the present second case, increasing the fin geometries is associated with the ability to employ more of the adsorbents amount and adsorbate quantity, which is loaded on the adsorbents particles. Thus the desorbed refrigerant mass M_{des} which leaves from the adsorption reactor increases by about 9 kg during the desorption process as shown in **F**ig. 5.22. The Increase of the desorbed amount which goes into the evaporator improves the refrigeration energy Q_e and this leads to an enhancement in the amount of produced ice of about 25 kg as shown in same **F**ig 5.22.

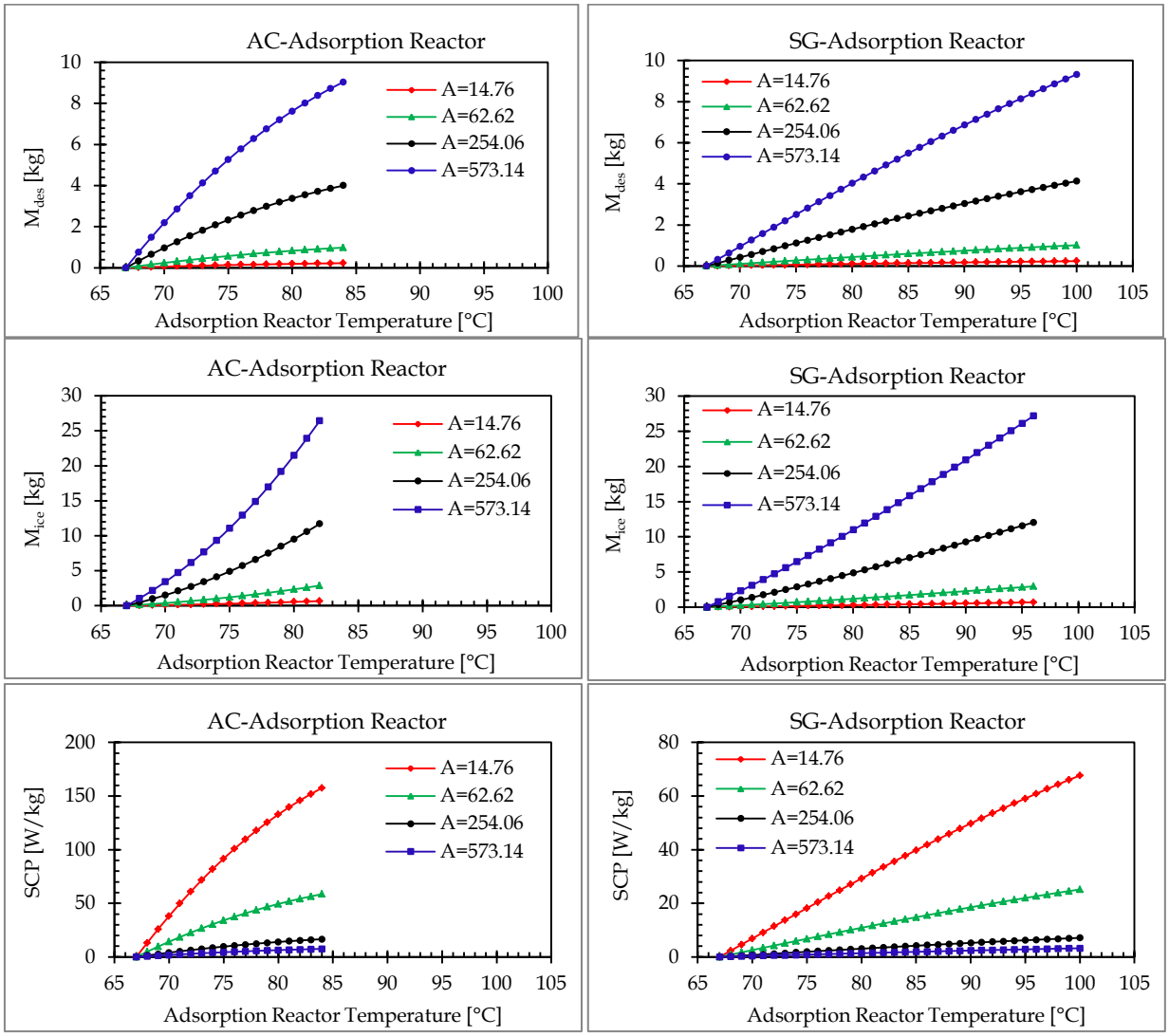

Figure 5.22: Variation the desorbed refrigerant mass, the produced amount of ice and the specific cooling power with temperature throughout the AC- and SG-adsorption reactors during desorption process for different fin geometries.
(1) $50 \times 75\ mm$, (2) $100 \times 150\ mm$, (3) $200 \times 300\ mm$, (4) $200 \times 675\ mm$

Based on the simulation results it is found that, the doubling of the fin geometries from 50×75 mm to 100×150 mm increases the amount of the produced ice amount by about only 3kg, whereas the doubling from 100×150 mm to 200×300 mm increases the amount of produced ice by 9kg.

The enlargement of the factor A leads to an improvement of the evaporative energy Q_e and allows the use of more amount of the adsorbent M_S. Hence, these two parameters M_S and Q_e have opposing effects on the specific cooling power SCP of the AIP system. According to the results shown in **F**ig. 5.23, SCP of the AC-system decreases by about 92 $[W/kg_{AC}]$ with extending the fin geometries from $50 \times 75\ mm$ to $200 \times 675\ mm$, whereas SCP of SG-system decreases by about 40 $[W/kg_{SG}]$.

It is observed, that the increase of the adsorbent amount has stronger effect on SCP than the improvement of the evaporative energy Q_e. Nevertheless, the interference of the effects doesn't prevent the observation of the fin geometries effect independently. However, it shows that the selection of the fin geometries should be carefully done, considering that the increase of COP and the reduction of SCP in order to utilize effectively the increase of the filled adsorbent amount inside the adsorption reactor.

In comparison with the first case, which was studied with increasing the fins' dimension by constant adsorbent amount M_S filled between the fins, it is found, that the area ratio factor A plays no effect on the desorbed refrigerant amount M_{des} and the produced amount of ice M_{ice}.

As noticed from the **F**ig. 5.24, no changes of both M_{des} and M_{ice} can be observed during desorption process throughout the SG-and AC-reactors, because of using the same adsorbent amount by increasing the fins' geometries.

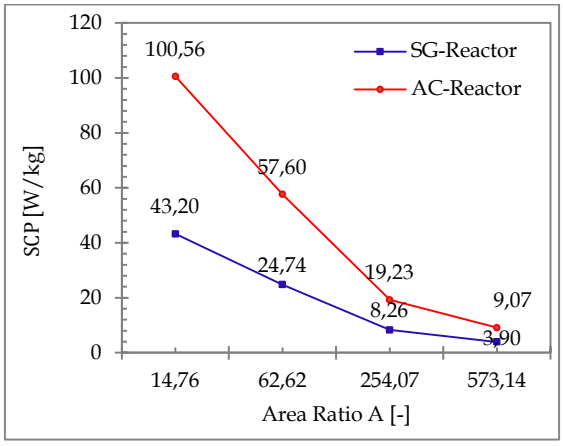

Figure 5.23: Effect the area ratio A on the SCP throughout SG-and AC-adsorption reactors

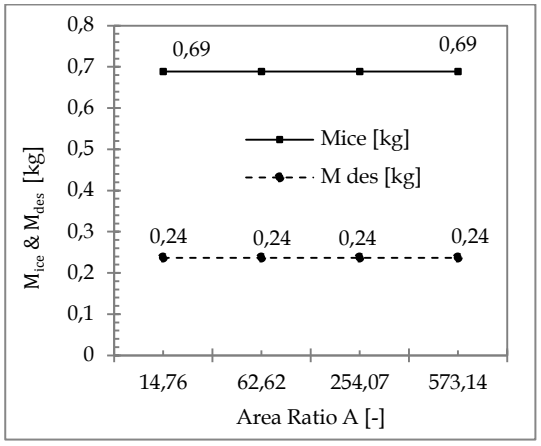

Figure 5.24: Effect the area ratio A on the M_{des} and M_{ice} throughout SG-and AC-adsorption reactors

The required energy Q_{in}, which is introduced to the SG- and AC-adsorption reactors by $M_S =$ constant, and the required energy, which is needed by second case $M_S \neq$ constant are demonstrated in the **F**ig. 5.25 versus the variation of the area ratio factor. In both the cases the energy is used to heat the increase in fins' mass, but in the second case the input heat is introduced to activate more amount of the SG-and AC-adsorbents and to desorb more amount of the refrigerant.

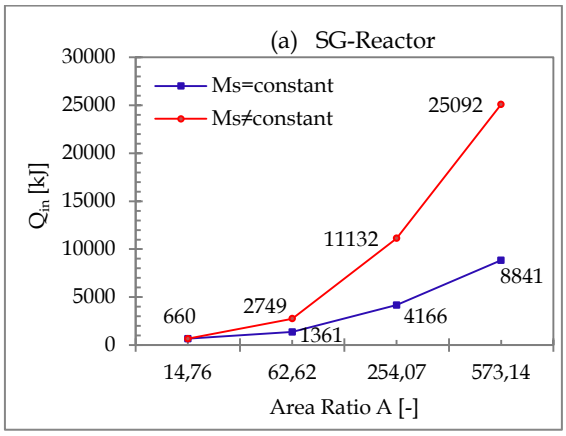

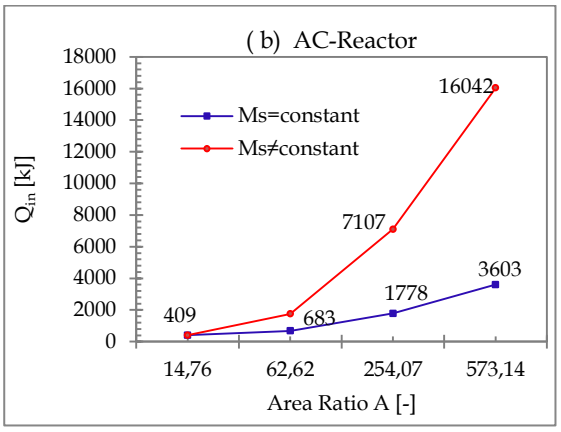

Figure 5.25: Effect the area ratio A on the required input heat introduced to (a) SG-reactor and (b) AC-reactor by constant adsorbent amount and by varying the adsorbent amount

5.6.2 Effect of the adsorbent thickness factor

The non-dimensional factor F_S is defined here as ratio of the adsorbent thickness L_S (length of the non-finned fluid channel) to the radius of the fins r_f. The adsorbent thickness factor F_S can also be named fin spacing factor because of the relation between the adsorbent thickness and the fin spacing as follows: $L_S = (n_f - 1).S_f$ where n_f is number of the used fins and S_f is fin spacing. Analyzing the

factor F_S is crucial to study the effect of fin spacing (non-finned surface) and the adsorbent thickness on the desorption process which takes place inside the adsorption reactor. The study of different F_S has been done at different fin spacing values $2\ mm$, $4\ mm$ and $8\ mm$ for both the SG- and AC- reactors as shown in the **T**ab. 5.4. An increase in the factor F_S is equivalent to increasing of L_S or decreasing of r_f. The factor F_S analysis was studied by constant the radius of fins r_f. Therefore, no changing of the factors A, F_L and R_G is noticed from the **T**ab. 5.4. It can also be shown how the factor F_S relates to the fin spacing and the fins' number. Doubling of the fin spacing, where the adsorbent-particles are located, from $S_f = 2\ mm$ to $4\ mm$ and then from $S_f = 4\ mm$ to $8\ mm$ increases the non-dimensional number F_S firstly from 8.68 to 10.53 and then to 11.57 for AC-reactor and from 17.36 to 23.159 for SG-reactor.

	S_f	A	F_L	R_G	F_S	n_f
SG-Reactor	**(1)** $2\ mm$	62.62	26.04	0.14	17.3	150
	(2) $4\ mm$	62.62	26.04	0.14	21.07	90
	(3) $8\ mm$	62.62	26.04	0.14	23.15	50

	S_f	A	F_L	R_G	F_S	n_f
AC-Reactor	**(1)** $2\ mm$	62.62	13.02	0.14	8.68	150
	(2) $4\ mm$	62.62	13.02	0.14	10.53	90
	(3) $8\ mm$	62.62	13.02	0.14	11.57	50

Table 5.4: Relationship between the different fin spacing values and the non-dimensional numbers A, F_L, R_G and F_S for both the SG-and AC-adsorption reactors

Increasing of the fin spacing from $S_f = 2\ mm$ to $8\ mm$ allows us to fill more of the adsorbent amount by about $2.25\ kg$ (25%) inside the SG-adsorption reactor and about $0.93\ kg$ (34%) inside the AC-reactor as shown in **F**ig. 5.26. Thus, the adsorbate mass (methanol) which is fixed on the adsorbents increases. Consequently, the desorbed amount which leaves from the reactors rises during the desorption process and the amount of ice produced from the system enlarge by about 34.29 % for SG- and AC-reactors by raising the desorbed refrigerant mass also by about 34.29 % for both the reactors.

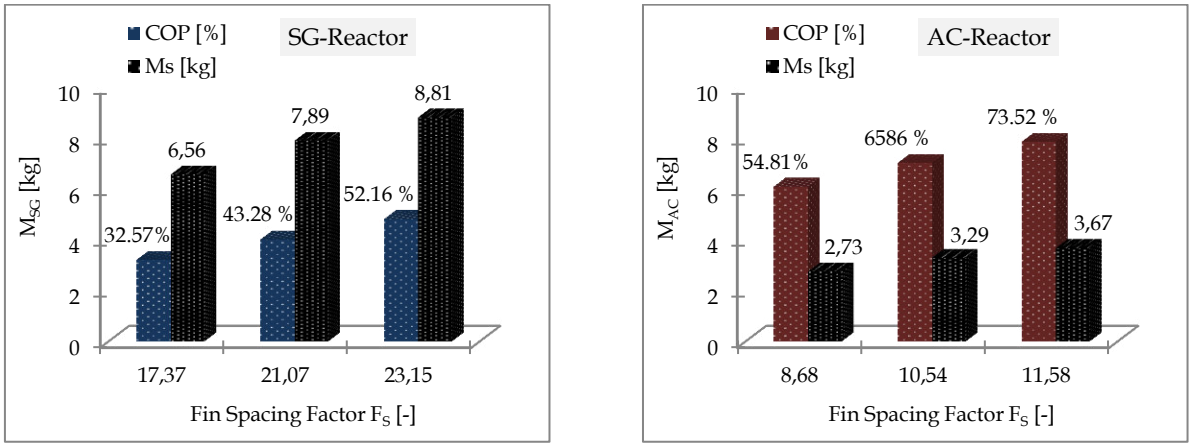

Figure 5.26: Effect of the fin spacing factor on the adsorbent amount and the coefficient of performance throughout (a) SG-reactor and (b) AC-Reactor

The effect of different F_S on the thermal performance COP of the AIP-system, the desorbed methanol amount and the produced amount of ice are illustrated in **F**ig. 5.27. It is seen that an increase in F_S from 8.68 to 11.57 leads to enhancement in the coefficient of performance by about 19 % for the AC-reactor, but the largest increasing friction is related to the first doubling of about 12 %, whereas the

coefficient of performance for the SG-Reactor improves about 20 % by doubling the adsorbent thickness twice.

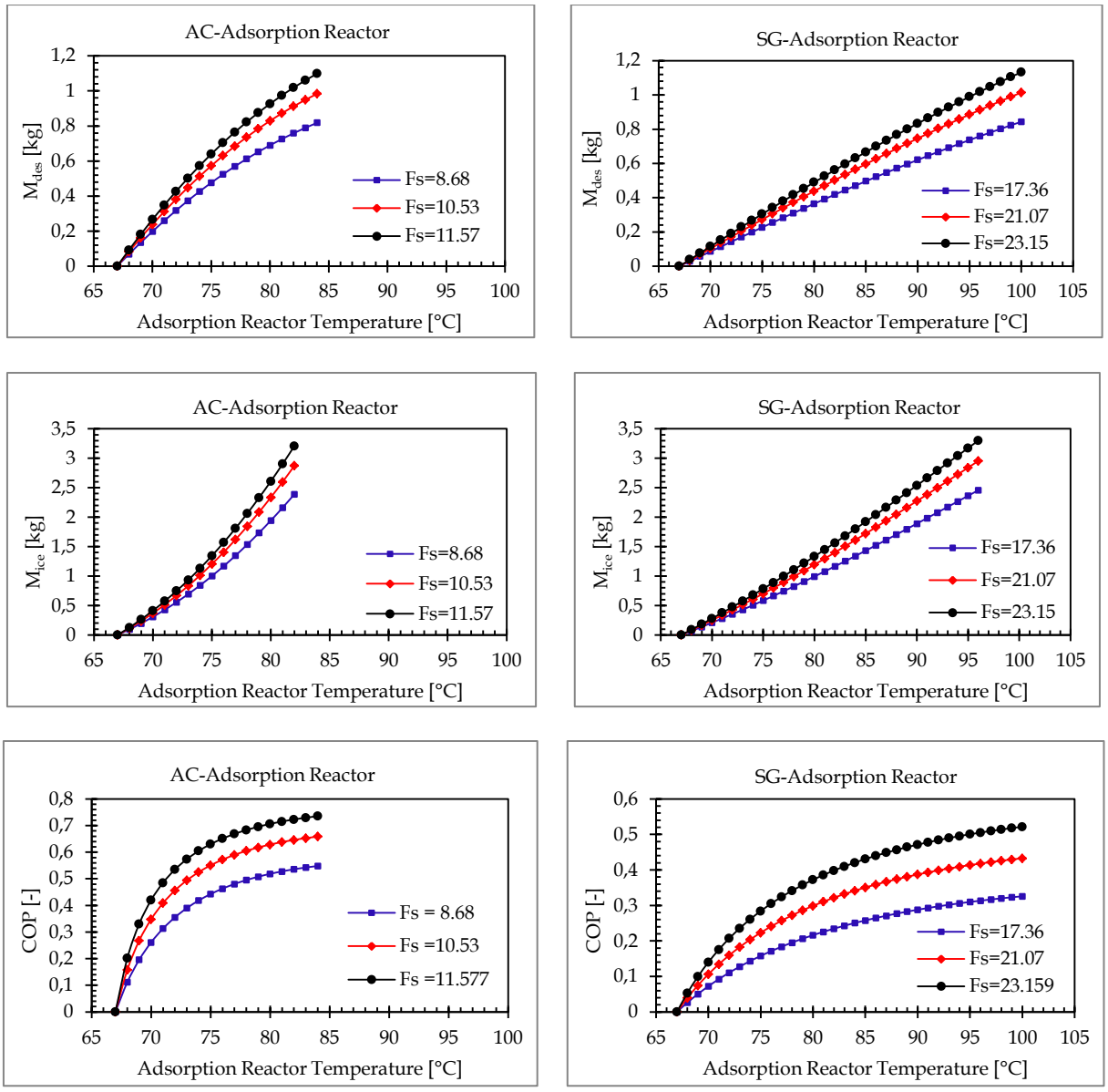

Figure 5.27: Evolution the M_{des}, M_{ice} and COP throughout the AC- and SG-adsorption reactors during desorption process for different fin spacing. (1) $S_f = 2\ mm$, (2) $S_f = 4\ mm$, (3) $S_f = 8\ mm$

On the design hand by increasing the fin spacing, the fins' number used for the same size of the adsorption reactor lowers, so the mass of the used metal components shrinks and the heat transfer area becomes less. As shown in **F**ig. 5.28a and b, although the adsorbent amount inside both the reactors increases by about 26 %, the metal components factor ξ_{metal} decreases by about 75 % because of shrinking of the metal components by about 16 kg for SG-reactor and 8 kg for the AC-reactor.

Based on the simulation results for both the SG- and AC-reactors it's found that, the thermal conductivity ratio R_λ increases to about 4 times when the fin spacing changes from $2\ mm$ to $8\ mm$, which causes a decrease in the heat transfer area to 65 %. Consequently, the required input heat, which is needed to desorb more of the adsorbate amount, becomes slightly less with increasing the factor F_S (increasing of the adsorbent amount). The fins' number decreases from 150 to 50 with increasing of the fin spacing from $S_f = 2$ to 8 mm. Therefore the design of the adsorption reactor

must be studied carefully to determine how the input energy can be lowered and the evaporation energy produced can be improved.

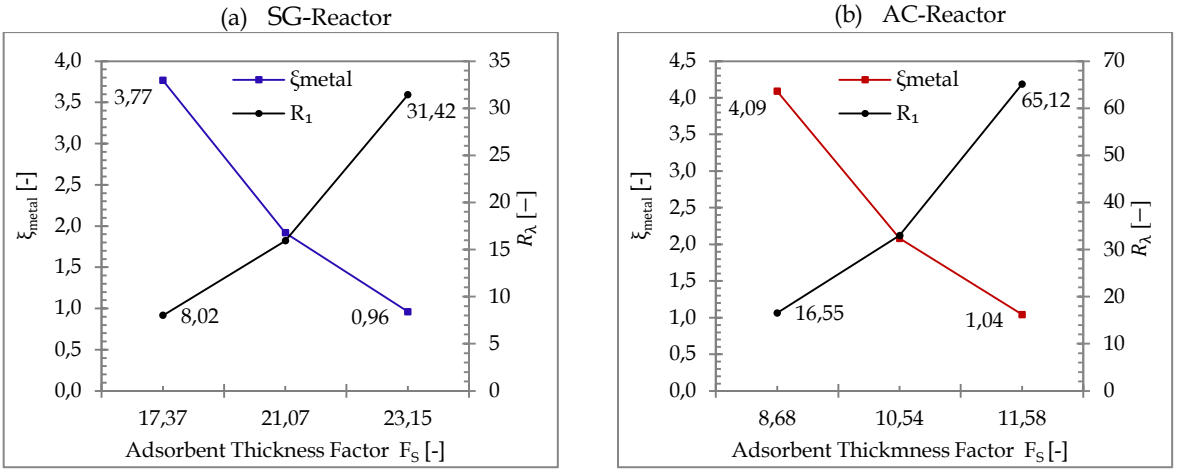

Figure 5.28: Relationship between the non-dimensional factors ξ_{metal} , R_λ and the factor F_S for (a) SG-reactor and (b) AC-Reactor

In the first case the parametric analysis has been studied by changing both the fin spacing and the adsorbent amount, where the adsorbent amount is related to the fin spacing. But one can't increase the factor F_S with increasing the fin spacing value and employ more adsorbent amount without limit. Therefore, the adsorbent thickness (fin spacing) factor has been also studied in another case that the adsorbent thickness will not increase by increasing the fin spacing value, which means the adsorbent amount remains constant but occupies more space (larger surface). The SG-reactor was filled with 6.56 kg of SG-particles and the AC-reactor was filled with 2.73 kg of AC-particles by increasing S_f from 2 mm to 8 mm as shown in **F**ig. 5.29.

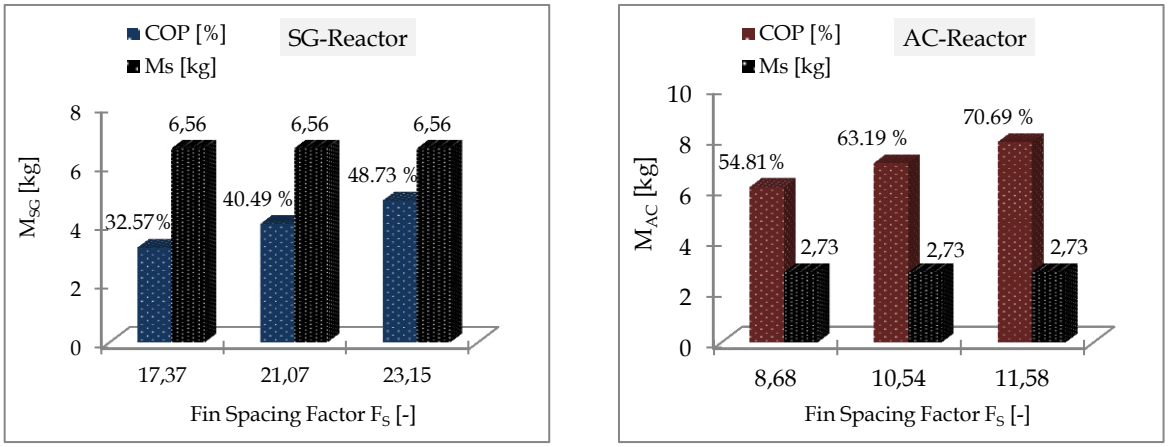

Figure 5.29: Effect of the fin spacing factor on the adsorbent amount and the coefficient of performance throughout (a) SG-Reactor and (b) AC-Reactor

As a result of changing the fin spacing $S_f = 2$ to 8 mm with constant adsorbent amount it is found, that both the SG-and AC-reactors desorb the same amount of refrigerant and produce the same amount ice. **F**ig. 5.30 shows evolution the desorbed amount of methanol and the produced amount of ice during desorption process throughout both the SG-and AC-reactors. Due to similar values of the adsorbent amount, desorbed refrigerant and produced ice amounts also show similar values.

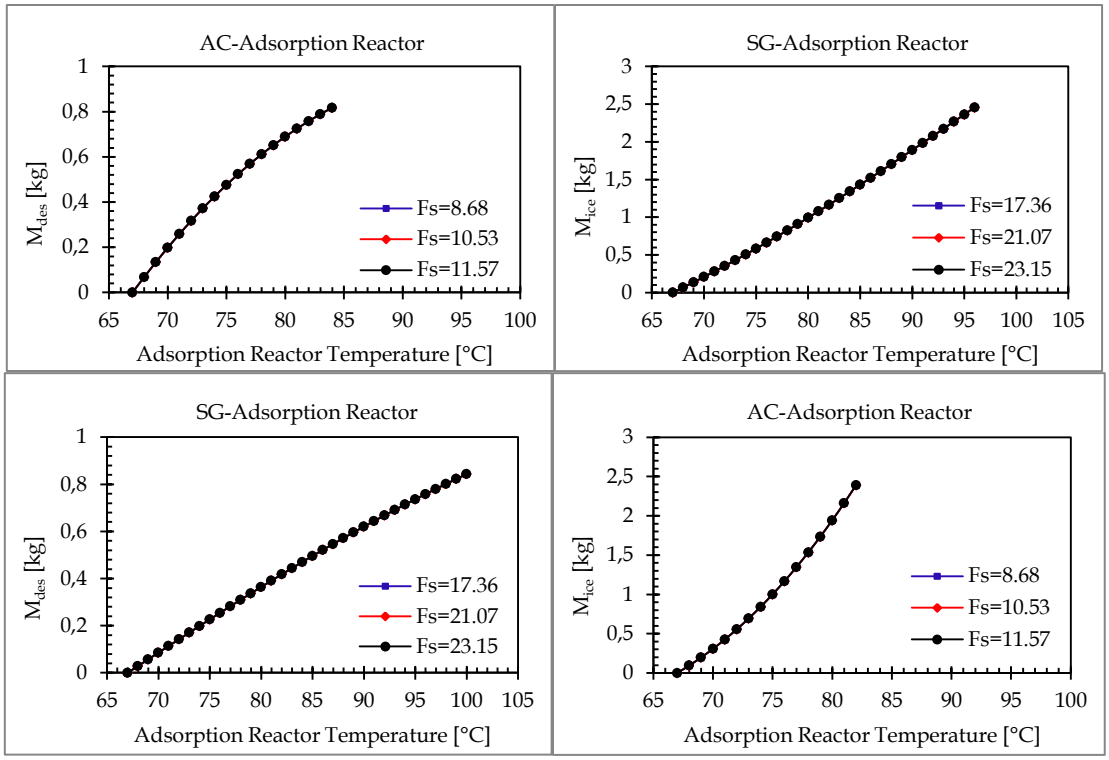

Figure 5.30: Evolution the M_{des} and M_{ice} throughout the AC- and SG-adsorption reactors during desorption process for different fin spacing. (1) $S_f = 2\ mm$, (2) $S_f = 4\ mm$, (3) $S_f = 8\ mm$

In comparison with the first case (increase both the fin spacing and the adsorbent amount) we can notice, that the coefficient of performance improves by about only 16 % for SG-and AC-adsorption reactors, whereas the first case leads to improvement by about 20 %. As shown in **F**ig. 5.31 the required input heat, which is introduced to SG-reactor by constant adsorbent amount, is lowered by about 33 % (1008.23 kJ), whereas the required input heat needed by increasing adsorbent amount, is lowered by about only 16 % (491 kJ).

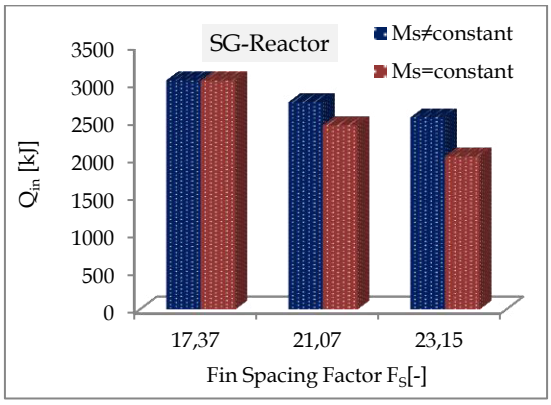

Figure 5.31: Comparison of the required input heat for different values Fs by varying and constant adsorbent amount.

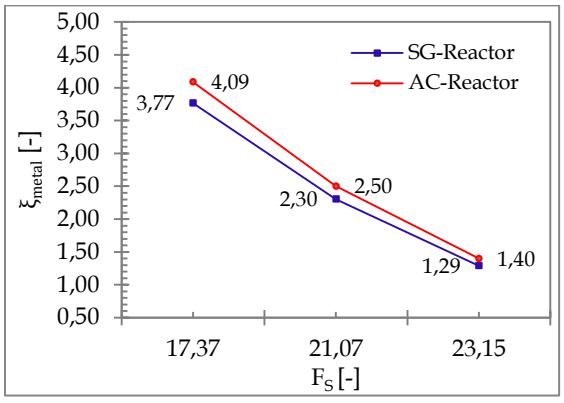

Figure 5.32: Relationship between the non-dimensional factors ξ_{metal} and the factor Fs for SG-reactor and AC-Reactor

As shown in **F**ig. 5.32 when the fin spacing increases with the same adsorbent amount, the metal factor increases by about 65% for SG-and AC-adsorption reactors and the input heat of about 1008.23 kJ and 394 kJ is lowered for SG-and AC-adsorption reactors, respectively.

5.6.3 Effect of the HTF-channel length factor

The analysis of the HTF-channel length factor F_L, which is related to the HTF-tube length L_t of the heat exchanger and to the equivalent radius r_f of the rectangular fin, has been studied by varying the tube lengths L_t used in SG-adsorption reactor.

Tab. 5.5 displays the different values of the channel lengths which were varied, discussed and how the previously mentioned factors change with the use of different tubes for the SG-reactor. Now, it can be seen from this table that no change of A and R_G with varying L_t.

	L_F	A	F_L	R_G	F_S
SG-Reactor	**(1)** 45 *cm*	62,62	6,51	0,14	5,26
	(2) 90 *cm*	62,62	13,02	0,14	10,53
	(3) 135 *cm*	62,62	19,53	0,14	15,80
	(4) 180 *cm*	62,62	26,05	0,14	21,07

Table 5.5: Relationship between the different values of the channel lengths and the non-dimensional numbers A, F_L, R_G and F_S for both the SG-and AC-adsorption reactors

In this section, it is focused on the effect of the HTF- channel length by same fins' dimension, same fin spacing as well as varying the adsorbent amount on the desorbed mass which leaves from the reactor and on the ice amount which can be obtained from the system.

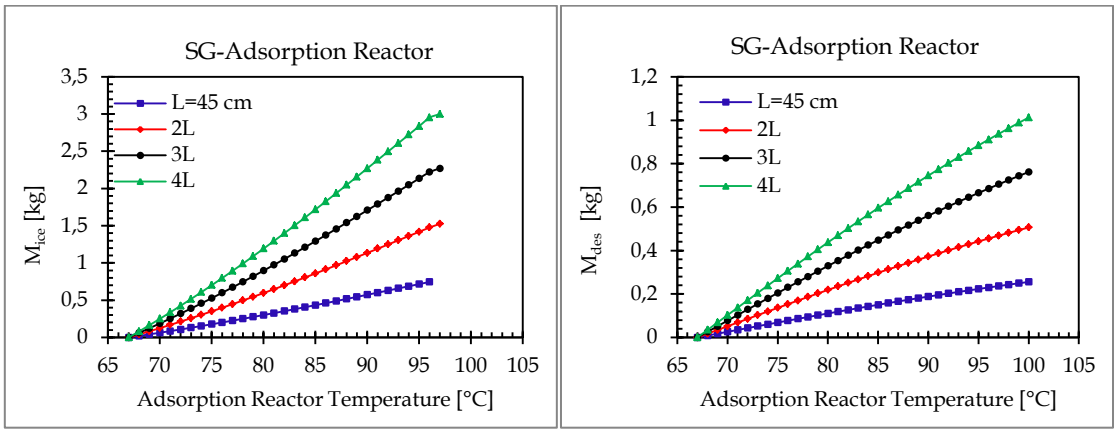

Figure 5.33: Evolution of the produced ice amount and desorbed methanol mass against the adsorption reactor temperature during desorption process for different tube-lengths

Lengthening the channel length from 45 *cm* to 180 *cm* improves the produced ice amount from 0.79 to 3 kg, because of improving the evaporation energy by about 4 times. Increasing the desorbed methanol mass has an important effect on the evaporation energy, which increases also by 4 times as shown in **F**ig. 5.33.

Nevertheless, varying the channel length by about 4 times increases the adsorbent mass, improves the evaporative energy (**F**ig. 5.34) and enhances the produced ice amount, but it is noticed from **F**ig. 5.35, that the coefficient of performance cannot improve and remains at a constant of 44 %, because increasing the channel length requires more input heat, which is directly proportional to the increase of the evaporator energy.

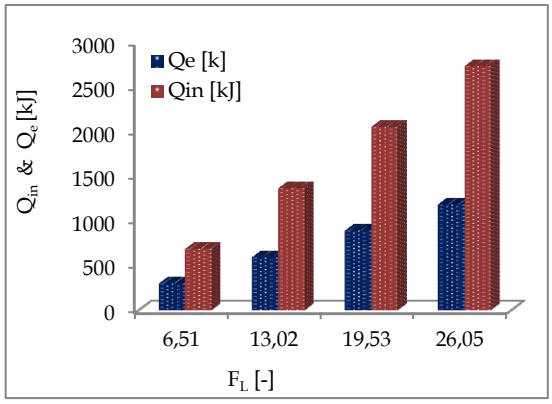

Figure 5.34: Numerically obtained input and evaporation energy against the factor F_L

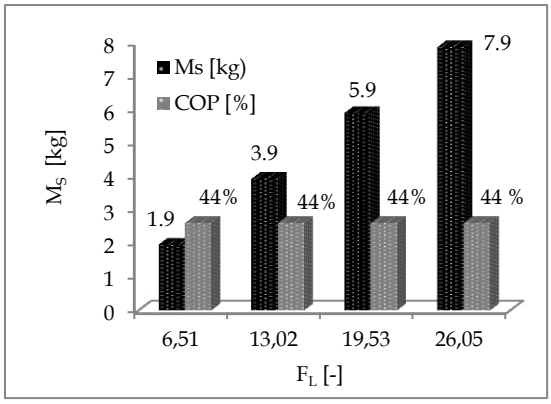

Figure 5.35: Numerically obtained coefficient of performance and desorbed refrigeration mass against the factor F_L

*In the case of using constant channel lengths, the analysis of the factor F_L allows us also to study the variation fins' dimension effect on the coefficient of performance COP, desorbed amount M_{des}, produced amount of ice M_{ice} and the specific cooling power SCP. **F**igs. 5.36 and 5.37 display evaluation of the COP, SCP, M_{des} and M_{ice} during desorption process for $L_t = 45$ cm.*

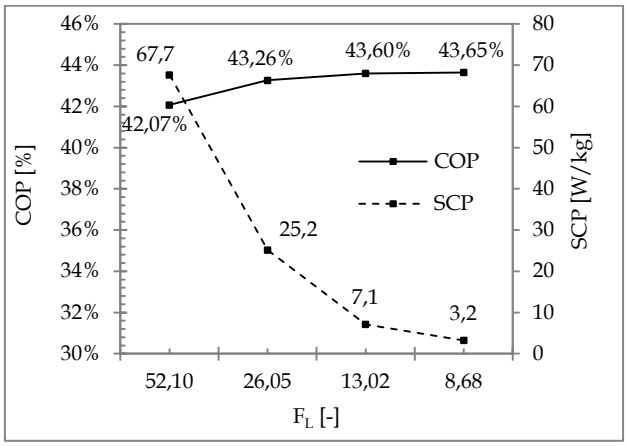

Figure 5.36: Effect of F_L on the coefficient of performance COP and the specific cooling power SCP

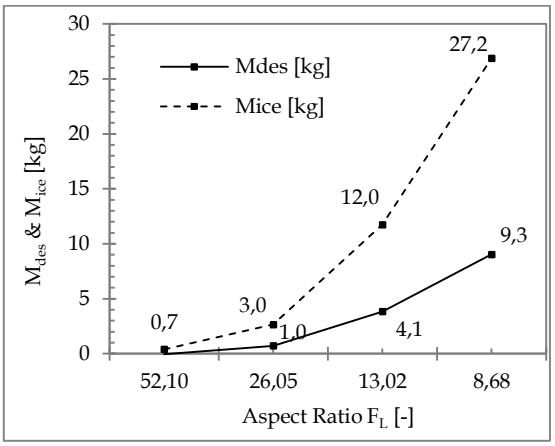

Figure 5.37: Effect of F_L on the desorbed amount M_{des} and produced amount of ice M_{ice}

5.6.4 Effect of the heat exchanger geometry ratio

Fig. 5.38 shows the investigation results of the effect of the adsorption reactor geometry factor R_G on coefficient of performance COP, desorbed amount M_{des} and produced amount of ice M_{ice}. The factor R_G relates the radius of the HTF-channel r_i to the radius of the fin-adsorbent contact surface r_S. In case of constant heat source a decrease in the factor R_G from 0.334 to 0.043 (which agrees with increasing the fin dimension about 6 times) leads to 2 %, 27 kg and 9 kg decease in coefficient of performance, desorbed amount and ice mass, respectively. It can be observed, that the same results can be obtained which have been discussed in section analysis of area ratio A.

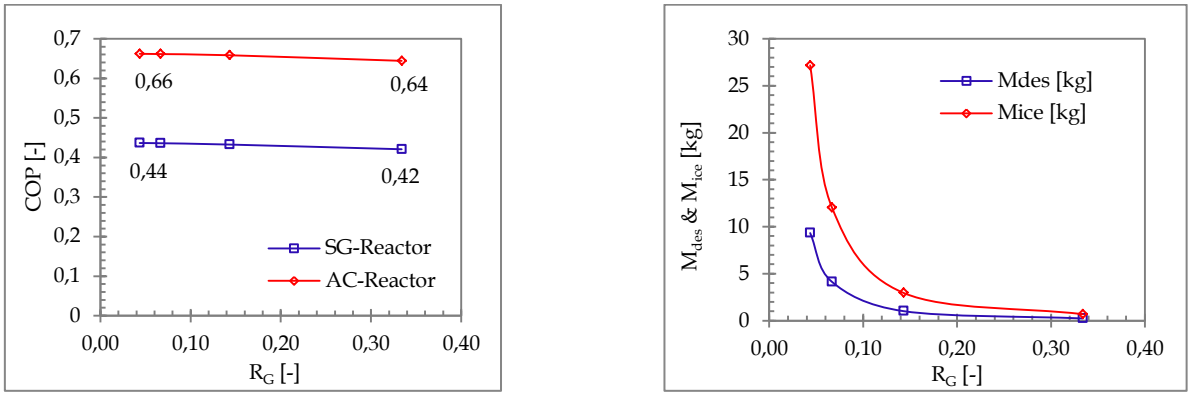

Figure 5.38: Effect of the heat exchanger geometry ratio R_G on the coefficient of performance COP, desorbed amount M_{des}, produced amount of ice M_{ice}

5.7 Summary and conclusion

This chapter presented a numerical and analytical investigation of effect of the HTF-flow nature and effect the adsorption reactor design on the desorption process and the performance of two bed adsorption system.

The effect of the HTF-nature has been studied for two adsorption reactors, which were heated to desorb $1kg_{meth}$ of methanol, which is used as an adsorbate with both the reactors. So each reactor was filled with a quantity of the adsorption material to ensure that $1kg_{meth}$ is released. Based on this quantity it is found, that the installation of both the reactors has different construction in terms of the number of HTF-channels needed, furthermore the dimensions and the number of fins. So the dimension of SG-reactor contained four HTF-tubes is larger than the dimension of AC-reactor which contains only two HTF-tubes. To study the HTF-nature effect, the variation of the Reynolds, Nusselt and Biot numbers have been investigated to demonstrate their effects on the temperature distribution through both the reactors. The following conclusions were drawn from this study:

1. When operating in a turbulent flow regime $Re > 10^4$, the temperature distribution through the adsorption reactor is higher than in the laminar flow regime $Re < 2300$. The HTF-flow with lower velocity spends more time in the channel, hence the heat exchange needs more time to active the adsorption materials and to heat the adsorption reactor components. Whereas the intense mixing of the fluid in turbulent flow enhances the heat transfer between fluid particles and also improves the heat transfer through the adsorption reactor.

2. It was seen based on analysis of the Biot number, that variation of temperature is significant inside the adsorption reactor when $Bi > 1$, so the internal conductive resistance is higher when compared to the external convective resistance, which can be obtained when the operating in a turbulent flow regime $Re > 10^4$. Whereas it is found by $Bi < 1$ when the operating in a laminar flow regime $Re < 2300$, that the temperature variation inside the adsorption reactor is significantly smaller when comparison to the first case.

3. Based on the simulation results, it is found, that Nusselt number Nu for different Reynolds number values remains larger than 1, which means more effective convection, because the convective resistance of the heat transfer fluid is less than that the conductive resistance. With $Nu > 3.66$, the fluid motion enhances heat transfer by advection.

4. It may be concluded that the cycle time of the adsorption system is strongly dependent on the HTF-flow nature. So that the desorption process inside the SG-reactor takes a shorter time by about 91% when the operating in a turbulent flow regime ($R_e = 23511$) in comparison with the laminar flow regime $R_e = 392$. Whereas the required desorption time for the AC-reactor can be lowered about 81%.

5. Due to the activated carbon properties The AC-reactor requires a less desorption heat ($\Delta T_{out}^{SG} > \Delta T_{out}^{AC}$), but requires a longer time because of the slower kinetic desorption in comparison with SG- kinetic desorption.

6. An assumption (allegation) study was numerically implemented with help of the **A**NSYS **F**luent Software. Based on this study it is observed, that the velocity of the methanol as an adsorbate changes from 0 to only $0.03\ m/s$ in the case of laminar flow. Whereas in the case of the turbulent flow the velocity of methanol changes from 0 to $0.08\ m/s$. Consequently, when operating in a turbulent flow regime, the methanol can be desorbed from the adsorption material faster in comparison with the laminar flow regime.

In the influence study of the HTF-nature on the desorption process, the size, installation and composition of both the adsorption reactors (number and dimensions of the fins as well as HTF-channels) including the filled adsorbent amount were kept constant in order to desorb $1kg_{meth}$. Whereas the influence study of the design parameters of the adsorption reactor on the thermal performance of the adsorption system was be investigated by geometrical and thermal study a set of non- dimensional factors A, F_L, R_G, ξ_{metal}, R_λ and F_S. The analysis factors allows us to change the adsorption reactor geometry such as the length and the diameter of the HTF- channels used including the fins spacing and dimensions.

Depending on these changes it can be noticed, that the possibility of absorbing the reactor to different amounts of the adsorption material can be taken into account and studied based on these changes. The influence study of the design parameters of the adsorption reactor had been discussed in the present work with two cases.

I. **First case:** Changing the adsorption reactor geometry at contestant adsorbent amount M_S. So that the adsorbent amount remains constant but occupies more space (larger surface).

II. **Second case:** Changing the adsorption reactor geometry but the adsorbent amount changes in order to employ the new spaces, where the adsorbent amount is related to the changed geometry used.

The following conclusions were drawn based on the influence study of the design parameters of the adsorption reactor:

1. The same increase of the fin geometries leads to slight enhancement of COP when the adsorbent amount $M_S \neq constant$ but the COP decreases clearly in the first case when the adsorbent amount $M_S = constant$. This was explained by analyzing the metal components factor ξ_{metal}, which is related to both the metal components mass and the adsorption material amount.

2. Increasing the area ratio A (increase the fins' dimension), which is associated with the ability to employ more of the adsorbents amount and adsorbate quantity, leads to increase in the desorbed refrigerant mass M_{des} and leads to an enhancement in the amount of produced ice M_{ice}.

3. Increasing the area ratio A by constant adsorbent amount M_S filled between the fins plays no effect on the desorbed refrigerant amount M_{des} and the produced amount of ice M_{ice}.

4. In the second case ($M_S \neq$ constant), the adsorption reactor requires more input energy, because this input energy is introduced to activate more amount of the adsorption amount and to desorb more amount of the refrigerant.

5. In spite of increasing the adsorbent amount M_S, temperature distribution inside the adsorption medium rises because of extend the heat transfer surface.

6. Opposite to the effect of area ratio A, the increasing adsorbate thickness factor F_S in both the cases ($M_S \neq$ constant and $M_S =$ constant) leads to clear enhancement in the coefficient of performance. This can be explained by analyzing the metal components factor ξ_{metal}, so that the mass of the used metal components shrinks by increasing the fin spacing (increasing the factor F_S).

7. Also opposite to the area ratio A, the required input heat by increasing the adsorbate thickness factor F_S is saved in both the cases by about 33 % when $M_S =$ constant and about 16 % when $M_S \neq$ constant.

8. Increasing the channel length factor F_L (lengthening the HTF-channel length) increases the adsorbent mass, improves the refrigeration heat and enhances the produced ice amount. But the coefficient of performance cannot improve and remains at a constant because increasing the channel length requires more input heat, which is directly proportional to the increase of the evaporator energy.

Chapter 6

Numerical and Mathematical Modelling of Electromagnetic Induction in Adsorption Systems

6.1 Introduction

It is common to heat conductors by subjecting them to an alternating magnetic field. The changing electromagnetic flux induces eddy currents that heat the conductor by the Joule effect. This method is called Induction Heating (IH) [117].

Induction heating is a complex combination of electromagnetic and heat transfer phenomena involving many factors such as the skin depth and properties of the materials [118]. Usually it is used extensively for melting metals and for hardening and forging steel. The power used ranges from watts to megawatts, and the frequencies used from 60 Hz to several hundred kilohertz [119]. A large number of papers on use the thermal heating of the adsorption reactors using industry waste heat or solar energy have been written. However, no research has been carried out on the adsorption materials such as silica gel and activated carbon in an attempt to generate the refrigerant (adsorbate) at the adsorption refrigeration systems using the induction heating technology.

The method of the induction heating in this study will be used to heat both the SG-and AC -adsorption reactors, which were studied in the fifth chapter using the thermal heating. The new adsorption reactors using IH would be filled with the same amount of adsorbent and adsorbate but with new design. So that the final purpose is comparing both the methods (thermal and induction heating) in terms of the desorption process of the same adsorption reactors.

In order to overcome the problems found with the conventional methods (thermal heating), the new process IH was considered with the following approach:

No contact between the adsorbents and the heat source	Good performance
Heat can be generated within the material	High energy density
Simply design of the adsorption reactor	Safety procedure
Exact temperature distribution in the material	Less environmental impact
High temperature if required	Lower energy consumption

Given these different conditions, induction heating seems to be an appropriate method of generating the adsorbates which are fixed on the adsorbents [120].

IH -technology is based on well-known physical phenomena: electromagnetic induction discovered by Maxwell's equations (Faraday's, Lenz's and Ampere's laws) and the Joule effect [121]. There is not much research available on induction heating at relatively low temperatures of the reactors which packed with granular materials (SG and AC) with a bad electrical conductivity. Therefore, our

investigation into the generation of the adsorbents granular was carried out with incorporation of graphite (Gr) balls into the adsorbents, because of the bad electrical conductivity of SG and AC as adsorbents. The induction heating and desorption processes are tightly interrelated because the physical properties of the heated materials depend strongly on magnetic field intensity and temperature.

6.2 Description of the IH-system for the adsorption reactor

6.2.1 Geometry and component of the model

Just as in the SG-and the AC-adsorption reactors studied using the thermal heating in the last chapter (fifth chapter), also both the SG-and AC-adsorption reactors using the induction heating have been designed to desorb the same amount of the desorbed refrigerant of 1 kg_{meth}. So the desorption process using the induction heating technology for both the adsorption reactors was simulated by using 3.31 kg of activated carbon, 1.36 kg of methanol in the AC-adsorption reactor and by using 7.95 kg of silica gel, 1.9 kg of methanol in the SG-adsorption reactor.

We consider an induction heating system consisting of one inductor (induction coil) and the work-load in order to desorb 1 kg of methanol as an adsorbate loaded with the SG- or AC- adsorbents, The work-load, which is the adsorption reactor in this model, consists of the adsorption medium (adsorbent particles + adsorbate) and the Gr-balls, which are used as a heat generation source. **F**ig. 6.1 shows the induction heating system together with the adsorption reactor. The adsorption reactor is considered as a cylindrical container of height H_a and diameter D_a , which is filled by an amount of the adsorbent M_S and the adsorbate M_a. The geometric characteristics of the induction heating setup for the SG- and the AC-adsorption reactors are shown in **T**ab. 6.1.

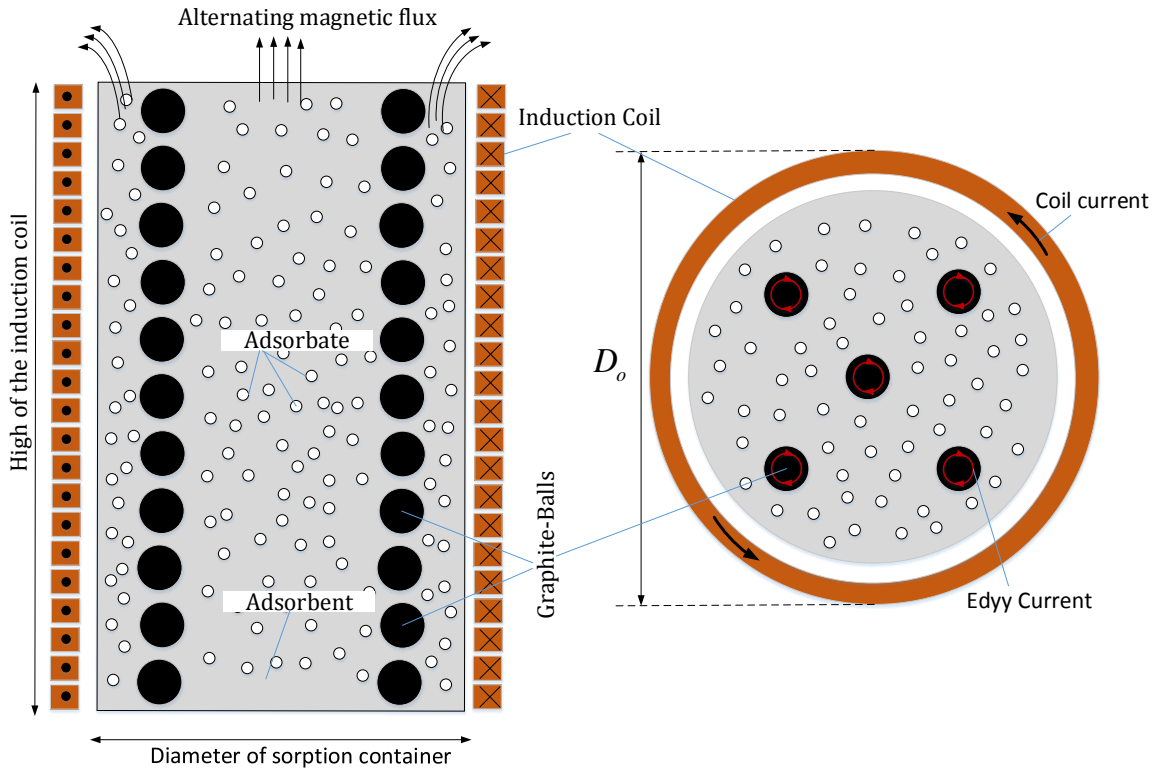

Figure 6.1: Cross section of the induction heating system together with the adsorption reactor

Because of the dielectric properties of the adsorption materials $\sigma_{SG} = 10^{-12}$ and $\sigma_{AC} = 10^{-3}$ [S/m] we can't heat them by the IH -technology. The idea is to place graphite balls, in which the required heat Q_{req} will be generated. The incorporation of Gr-balls into the adsorption reactor improves the heating desorption processes (the simulation results will be presented).

The adsorption reactor, containing the Gr- balls, is placed inside the induction coil, which has an outer diameter D_o, an inner diameter D_i and a height of H_I. The coil used is made of copper, which is usually used because of its very good electric conductivity reducing thus the ohmic losses in the coil [122]. The material chosen for the balls is graphite that has a lower electrical conductivity, thus resulting higher ohmic losses in the balls.

Adsorption Reactor	Symbol	SG-Reactor	AC-Reactor
Height of the adsorption container	H_a	450 mm	220 mm
Diameter of the adsorption container	D_a	250 mm	250 mm
Height of the induction coil	H_I	460 mm	230 mm
Internal diameter of the induction coil	D_i	260 mm	260 mm
External diameter of the induction coil	D_o	280 mm	280 mm
Radius of the Gr-ball	r_i	10 mm	10 mm
Number of the loops	N	10	5
Number of the Gr-balls	i	75	35

Table 6.1: Geometric characteristics of the SG- and AC- induction heated adsorption systems studied

6.2.2 Operating Principles

The induction heating usually is comprised of three basic factors: The electromagnetic induction, the skin effect and the heat transfer [123], which would be analyzed detailed in this study. The heat, conducted in the adsorption medium is a result of conversion of the inductive heat in the thermal energy, which makes the Gr-balls a source of heat generation that supplies the converted heat to the adsorbent-adsorbate medium (S-medium).

The operating principle of the IH-system for the desorption reactor, which is considered in this study is based on four physical principles. These principles are as follows:

- Transfer of energy from the induction coil to the Gr-balls to be heated by means the electromagnetic field $\vec{E}$.
- Transformation of the electric energy into heat due to Joule effect.
- Transmission of the heat inside the geometry of the Gr-balls by means of the thermal conduction and the skin effect.
- Transfer of the energy from the Gr-balls to the S-medium in order to generate and to desorb the methanol from the adsorption materials.

The electrical and thermal properties of the base parameters used in this study are shown in the **T**ab. 6.2. In the general case, a space-time temperature distribution within a heated workpiece is described by a highly complicated system of interrelated Maxwell's and Fourier equations for electromagnetic and temperature field [120]:

$$\nabla \times \vec{H} = J + \frac{\partial \vec{D}}{\partial t} \qquad (6.1)$$

$$\nabla \times \vec{E} = -\frac{\partial \vec{B}}{\partial t} \qquad (6.2)$$

$$\nabla \cdot \vec{B} = 0 \tag{6. 3}$$

$$\nabla \cdot \vec{J} = 0 \tag{6. 4}$$

$$\mathrm{div}(\lambda . \mathrm{grad}\ T) - \rho . C(v . \mathrm{grad}\ T) - \rho . C . \frac{\partial T}{\partial t} = -\mathrm{div}(\vec{E} . \vec{H}) \tag{6. 5}$$

where $\vec{H}$, $\vec{E}$, $\vec{B}$ and $\vec{J}$ are the magnetic field intensity, the electric field intensity, magnetic flux density and the eddy currents density, respectively.

The Gr-balls as a heat generation source will convert the electromagnetic energy into heat and this heat conducted in the S-medium. Therefore, the power consumption of the induction coil must be equal to the rate of heat generation in the Gr-balls in order to provide the required heat conduction absorbed by the S-medium.

Material	Electrical Conductivity $\boldsymbol{\sigma}$ $[\mathbf{S . m^{-1}}]$	Thermal Conductivity $\boldsymbol{\lambda}$ $[\mathbf{W . m^{-1} . K^{-1}}]$
Silica gel (SG)	10^{-12}	0.17
Activated carbon (AC)	10^{-3}	0.082
Graphite (Gr)	10^{5}	168
Copper (Cu)	5.8×10^{7}	237
Aluminum (Al)	35×10^{6}	398
Iron (Fe)	10×10^{6}	80

Table 6.2: Electrical and thermal properties of the materials used in the numerical and mathematical study

The technique of providing the required absorbed energy Q_{req} and calculating the electromagnetic fields depends on the ability to solve Maxwell's equations (**E**q. 6.1 through **E**q. 6.4) and Fourier's equation (**E**q. 6.5) for general time-varying electromagnetic field. Therefore, our investigation was carried out by a numerical and mathematical modelling with the **A**NSYS **M**axwell and **A**NSYS **F**luent Software, which can be help in this field.

6.3 Basic thermal phenomena in the IH-System

This section deals with the theoretical and mathematical aspects of the heat transfer throughout the medium of silica gel and activated carbon during the induction heating and desorption processes.

The heat transfer in this case is defined as the transfer of thermal energy from the Gr-balls, which are more energetic particles because of the eddy currents induced inside it, and flow to less energetic adjacent adsorption medium. This study does not cover the radiation and convection because there is no bulk motion involved in the adsorption reactors. The driving force for the heat transfer is the temperature difference between the Gr-balls and the temperature of S-medium, and the larger the temperature difference means the larger the rate of heat transfer.

The temperature field is determined based on the Kirchhoff-Fourier equation (**E**q. 6.5) supplemented by the right-hand term, which represents the internal heat source taken from electromagnetic calculations [124].

To analyze the heat transfer (conduction) in the S-medium, consider, a coordinate system in which the temperature distribution is three-dimensional and time dependent, because the conduction in all dimensions of the S-medium is significant in order to activate the adsorbents (SG and AC) and desorb the adsorbate (methanol).

The heat is conducted throughout S-medium in the direction of decreasing temperature from the surface of the Gr-balls T_{max} into the outer boundaries of the cylindrical container T_o.

The temperature distribution throughout at a specified time as well as the heat transfer rate at any location in the S-medium will be described by a set of the rectangular coordinate system. The temperature distribution in the S-medium is expressed as $T = T(x, y, z, t)$ (**E**q. 6. 6) [125].

$$\frac{\partial}{\partial x}\left(\lambda_S.\frac{\partial T}{\partial x}\right)+\frac{\partial}{\partial y}\left(\lambda_S.\frac{\partial T}{\partial y}\right)+\frac{\partial}{\partial z}\left(\lambda_S.\frac{\partial T}{\partial z}\right)+\dot{g}=[\rho.C.\frac{\partial T}{\partial t}]_{S\text{-medium}} \quad (6.\ 6)$$

where λ_S is the thermal conductivity of the S-medium. The Gr-balls are used in our induction heating system as a heat generation source, through which the induction heat E_{gen} is converted into thermal energy and conducted the heat Q_{req} in the S-medium in order to desorb methanol from the adsorption-particles.

The differential equation in the spherical coordinate that describes the variation of temperature in the Gr-balls during the induction heating and the desorption processes, can be considered to be one dimensional since the heat transfer occurs predominantly in a radial direction, because of symmetry [125]. The temperature variation inside the Gr-balls can be expressed as $T = T(r, t)$, **E**q. (6. 7).

$$\frac{1}{r^2}.\frac{\partial}{\partial r}\left(\lambda_{Gr}.r^2\frac{\partial T}{\partial r}\right)+p_v=[\rho.C.\frac{\partial T}{\partial t}]_{Gr-balls} \quad (6.\ 7)$$

where λ_{Gr} is the thermal conductivity of the Gr-balls. Here $p_v[W/m^3]$ is the power density induced inside the Gr-balls (named ohmic loss in **A**NSYS **M**axwell). The temperature of the Gr-balls rises rapidly when the induced current passes through it as a result of the electromagnetic induction energy being converted to heat at a rate per unit volume p_v.

The energy equation for the adsorption reactor, consisting of the Gr-balls, the adsorption materials SG or AC and the adsorbate is expressed as:

$$V_a\left[\frac{\partial}{\partial x}\left(\lambda_{tot}.\frac{\partial T}{\partial x}\right)+\frac{\partial}{\partial y}\left(\lambda_{tot}.\frac{\partial T}{\partial y}\right)+\frac{\partial}{\partial z}\left(\lambda_{tot}.\frac{\partial T}{\partial z}\right)\right]+\frac{|\vec{J}|^2.V_{Gr}}{\sigma V_S}=(M_S.C_S+M_S.C_a.X+M_v.C_v+M_{Gr}.C_{Gr})\frac{\partial T}{\partial t}+M_S.H_{ads}.\frac{\partial x}{\partial t}$$

where M_S, M_a, M_v and M_{Gr} are the mass of the adsorbent, mass of the adsorbate, mass of the adsorbate vapor phase and mass of the Gr-balls respectively. V_a is the volume of adsorption reactor, λ_{tot} the total thermal conductivity, H_{ads} the desorption heat per unit mass of adsorbate, x [kg/kg] the adsorbate concentration by the adsorbent particles and T, the temperature of the adsorption reactor.

6.4 Basic electromagnetic phenomena in IH-System

The alternating current $I = I_0.\cos\omega t$ [A] applied to the induction coil circuit will produce in its surroundings a time-variable magnetic field $\vec{B}$ [T] that has the same frequency f [kHZ] as the same coil current. The magnetic field strength depends on the current flowing in the induction coil, the coil geometry and the distance from the coil and it is calculated according to Ampere's law as [118]:

$$\oint \vec{H}.\vec{dl}=\mu.N.I_0.\cos\omega t \quad (6.\ 9)$$

$$\vec{B}=\mu_0.\mu_r.\vec{H} \quad (6.\ 10)$$

where H [A/m] and ω [rad/sec] are the magnetic field intensity and the angular frequency. $\mu_0[H/m]$ and $\mu_r[-]$ are the permeability of free space and the magnetic permeability of the material, respectively.

The changing magnetic field produces an electric field $\vec{E}$ [V/m] in the area where such changes take place, which can be expressed according to Faraday's Law as [126]:

$$\nabla \times \vec{E} = -\frac{\partial \vec{B}}{\partial t} \tag{6.11}$$

Consequently, eddy currents $\vec{J}$ [A/m^2] are induced inside the Gr-balls placed in the core of the coil. These induced currents have the same frequency as the coil current; however, their direction is opposite to the coil currents, which are described by Lenz's Law. The ability of the Gr-balls, used as a heat generation to conduct the electrical current, is specified by its electric conductivity σ [S/m]. From Ohm's Law we get [127]:

$$\vec{J} = \sigma . \vec{E} \tag{6.12}$$

The alternating currents induced in the Gr-balls produce heat by the Joule effect. Since the Gr-balls conducting materials, the current density heats up the balls due to the Joule dissipation. The power loss by the Joule heating per unit volume is [140]:

$$p_v = \frac{J^2}{\sigma} \tag{6.13}$$

As a result, the total electric power caused by the eddy currents, which is converted to heat energy to provide the required desorption heat, can be calculated by integrating over the volume of the Gr-balls V_{Gr}.

$$P_{tot} = \sum_{i=1}^{i} \int_{V_{Gr}} p_v . dV \tag{6.14}$$

where i is the number of the Gr-balls. The current density will decrease from the surface of the Gr-balls toward its center. Consequently, the induced power will be concentrated in the surface layer of the Gr-balls, as shown in **E**q. 6. 15. This is called the skin effect. From this effect, it can be inferred that the heat energy converted from electric energy is concentrated on the skin depth δ [mm] [128].

$$\delta = (\pi . f . \sigma . \mu)^{-0.5} \tag{6.15}$$

6.5 Mathematical modeling of the IH- System

While the objective of the heat transfer analysis through the adsorption reactor is to know the required energy absorbed by the adsorbent-particles SG or AC in order to desorb CH_3OH, it is necessary to determine the maximum rate of the heat transfer from the Gr-balls and ohmic losses generated in the Gr-balls. The ohmic losses in the balls is determined by considering the Joule effect and the heat transfer from the balls is studied under transient state for an extended period of time which named desorption time.

Mathematical modeling is one of the major factors in the successful design of IH-systems. The specification of the local rate heat transfer inside the adsorption reactor requires firstly choosing a suitable coordinate system depending on the geometry of the model studied. For the sake of simplicity, we consider a spherical adsorption reactor consisting of one Gr-ball. As shown in the **F**ig. 6.2 the S-medium has an inner radius r_i and an outer radius of r_o. The Gr-ball, which is placed in the center of adsorption reactor, has the same inner radius of r_i.

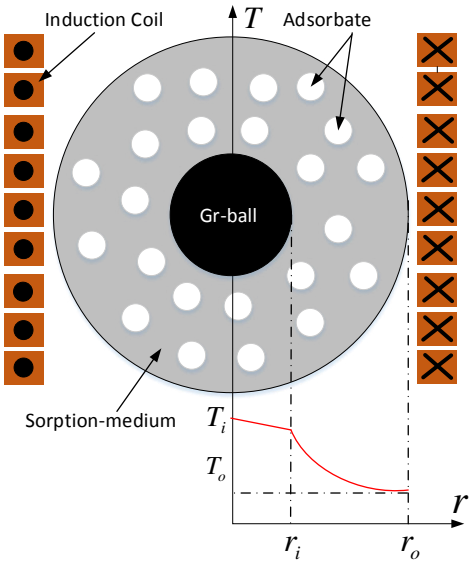

Figure 6.2: Electromagnetic mathematical model of the modified adsorption reactor with Gr-ball

Therefore the best coordinate system for the given geometry is the spherical coordinates, where the temperature varies mainly in one primary radial direction because of the symmetry and the changing with space-time $T(r,t)$ [125]. The mathematical formulation of this problem can be expressed in the spherical container as seen **E**q. 6. 16.

$$\frac{1}{r^2}.\frac{\partial}{\partial r}\left(\lambda_S.r^2\frac{\partial T_S}{\partial r}\right)+\frac{1}{r^2}.\frac{\partial}{\partial r}\left(\lambda_{Gr}.r^2\frac{\partial T_{Gr}}{\partial r}\right)+\dot{g}=[\rho.C.\frac{\partial T}{\partial t}]_{S-medium}+[\rho.C.\frac{\partial T}{\partial t}]_{Gr-ball} \tag{6.16}$$

The Fourier **E**q. 6.16 describes the transient heat transfer process through the adsorption reactor (together Gr-ball and S-medium). The heat source density $\dot{g}$, induced by eddy currents per unit time in a unit volume, must provide the required energy which is absorbed by S-medium in order to desorb the refrigerant CH_3OH. It can be shown that, for the great majority of IH-systems, it is possible to simply the mathematical model further by some typical assumptions.

6.5.1 Boundary and initial conditions

The temperature distribution in the S-medium depends on the conditions at the boundaries of the medium as well as the heat transfer mechanism inside the medium.

1- Interface boundary conditions

The adsorption reactor consists of two different materials (the S-medium and the Gr-ball), and the solution of the heat transfer problem in this reactor requires the specification of the boundary conditions at the interface. The interface boundary conditions considered were based on the following requirements [125]:

- Two materials in contact must have the same temperature with change of the time at the area of contact.

$$T_{Gr}(r_i,t)=T_S(r_i,t) \tag{6.17}$$

The interface between the Gr-ball and S-medium is maintained at constant temperature of maximal temperature T_{max} as a result of the electromagnetic induction occurring inside the Gr-ball.

- The interface can't store any energy, and thus the heat flux on the two sides of an interface must be the same.

$$-\lambda_{Gr}\frac{\partial T_{Gr}(r_i,t)}{\partial r} = -\lambda_S\frac{\partial T_S(r_i,t)}{\partial r} \tag{6.18}$$

2- Specified temperature boundary conditions

$$T_{Gr}(r_i,t) = T_S(r_i,t) = T_{max} \tag{6.19}$$

3- Initial conditions

The spherical adsorption reactor is subjected to specified temperature on its boundaries.

$$T_S(r_o,0) = T_o = T_{amb} \tag{6.20}$$

$$T_S(r_i,0) = T_i = T_{max} \tag{6.21}$$

where T_o and T_i are specified temperatures at the outer surface of spherical container (ambient temperature) and interface between the Gr-ball and S-medium.

4- Heat flux boundary conditions

During the desorption process the walls of the adsorption reactor are defined as an adiabatic wall by setting a zero heat flux condition. Therefore, the temperature or the heat flux remains constant at any location through the balls.

$$\frac{\partial T_S}{\partial r} = 0 \tag{6.22}$$

5- Heat generation

The efficient eddy current computation has to be performed in order to obtain the source term to be plugged into the heat equation. Heat generation is usually expressed per unit volume of the medium, and is denoted by $\dot{g}$, whose unit is W/m^3. In this case, power generation in the Gr-balls of radius r_i can be expressed as $\dot{E}_{gen} = p_v.V_{Gr} = \dot{g}.V_S$. Here V_S is the volume of the spherical S-medium.

The Gr-ball can be considered as a heat generation within the adsorption reactor, because of absorption the induction power inside the Gr-volume and conduction of that into the S-medium. This means the rate of the heat generation $\dot{E}_{gen}$ equals to the rate of heat transfer to the S-medium $\dot{Q}_{req}$. Therefore the temperature of S-medium rises during heat generation as a result of the absorption the generated heat by the medium during transient start up period. This continues until steady conditions (same maximum temperature and minimum adsorbate concentration) are reached. Once the steady operation has been established, the temperature of the medium at any point no longer change. This steady-state energy balance reads as:

$$\dot{E}_{gen} = \dot{Q}_{req} \tag{6.23}$$

$$p_v.V_{Gr} = \dot{g}.V_S \tag{6.24}$$

The volumetric joule losses p_v are given by the expression $p_v = \frac{|\vec{J}|^2}{\sigma}$

$$\dot{g} = \frac{|\vec{J}|^2}{\sigma.\varepsilon_r} \tag{6.25}$$

where ε_r is a new non-dimensional parameter, which is named the aspect ratio and given as:

$$\varepsilon_r = \left(\frac{r_o}{r_i}\right)^3 - 1 \tag{6.26}$$

6- Thermal conductivity

Because the adsorption reactor was filled by adsorption material and methanol as an adsorbate, we can't assume the thermal conductivity as constant, because the thermal conductivity changes with temperature and adsorbate concentration. Therefore it is considered as $\lambda(x, T)$.

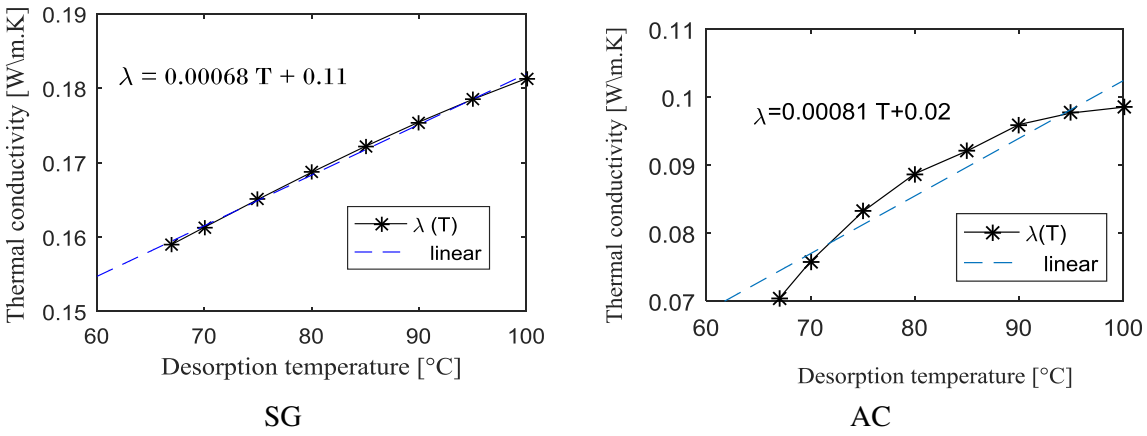

SG AC

Figure 6.3: Variation in the thermal conductivity of the adsorbents with the temperature range

While the variation of thermal conductivity with temperature $\lambda(T)$ and with adsorbate concentration $\lambda(x)$ could be determined, therefore we will use a mean value for the thermal conductivity λ_S and treat it as a constant based on two average values $\lambda_{ave}(T)$ and $\lambda_{ave}(x)$. This is also common practice for other temperature-dependent properties such as the density and a specific heat. Then the mean value can be expresses as follows:

$$\lambda_S = \frac{\lambda_{ave}(T) + \lambda_{ave}(x)}{2} \tag{6.27}$$

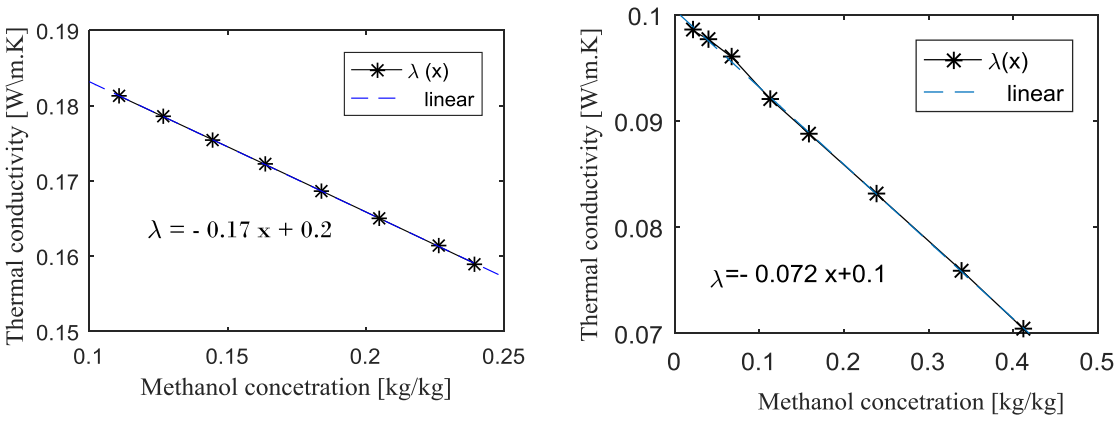

SG AC

Figure 6.4: Variation in the thermal conductivity with the adsorbate concentration

The variation in the thermal conductivity with temperature range based on the **F**ig. 6.3 can approximated as a linear function as follows:

$$\lambda_{SG}(T) = 0.114 + 0.00068\ T \tag{6.28}$$

$$\lambda_{AC}(T) = 0.02 + 0.00081\ T \tag{6.29}$$

The average value of the thermal conductivity in the temperature range between T_i and T_o can be determined from:

$$\lambda_{ave}(T) = \frac{\int_{T_i}^{T_0} \lambda\,(T).\,dT}{T_i - T_0} \tag{6.30}$$

Based on the **F**ig. 6.4, the variation in the thermal conductivity with the adsorbate concentration range is approximated as a linear function as follows:

$$\lambda_{SG}(x) = 0.2 - 0.17\,x_{SG} \tag{6.31}$$

$$\lambda_{AC}(x) = 0.1 - 0.072\,x_{AC} \tag{6.32}$$

The average value of the thermal conductivity in the concentration range can be determined from:

$$\lambda_{ave}(x) = \frac{\int_{x_{max}}^{x_{min}} \lambda(x).\,dx}{x_{max} - x_{min}} \tag{6.33}$$

6.6 Dimensionless system

Under these assumptions (boundary and initial conditions), the Fourier equation (6.16) can be rewritten as:

$$\frac{1}{r^2}.\frac{\partial}{\partial r}\left(\lambda_{tot}.r^2.\frac{\partial T}{\partial r}\right) + \frac{|\vec{j}|^2}{\sigma}.\frac{V_{Gr}}{V_S} = (\rho_S.C_S + \rho_S.C_a.X + \rho_v.C_v + \rho_{Gr}.C_{Gr})\frac{\partial T}{\partial t} + \rho_S.H_{ads}.\frac{\partial x}{\partial t} \tag{6.34}$$

The kinetics of sorption dx/dt is given by:

$$\frac{\partial x}{\partial t} = D_{so}.(x_{eq} - x) \tag{6.35}$$

The dimensionless system is important to know the parameters effect in order to achieve the optimum induction heating and desorption processes. To obtain a non-dimensional system of the model presented, it is necessary to define characteristic values of the parameters which are included in the system of equations (**E**q. 6.34) - (**E**q. 6.35).

These values are as follows: r_i (characteristic radius of the Gr-ball), $\Delta T = T_{des} - T_i$(characteristic temperature), t_{des} (characteristic of desorption time), x_{eq} (characteristic of adsorbate concentration). The relation among the problem parameters and the characteristic numbers can be described as:

$$r = r_i.R, \qquad T = \Delta T.\theta, \quad t = t_{des}.\tau \quad \text{and} \qquad x = x_{eq}.X$$

here, R, θ, τ and X are non-dimensional parameters.

After substitution of these relations into the system of equations (**E**q. 6.34) - (**E**q. 6.35) we obtain the non-dimensional system of equations:

$$\frac{\lambda_{tot}.\Delta T}{r_i^2}.\frac{1}{R^2}.\frac{\partial}{\partial R}\left(R^2.\frac{\partial \theta}{\partial R}\right) + \frac{|\vec{j}|^2}{\sigma}.\varepsilon_r^{-1} = \frac{\Delta T}{t_{des}}.(\rho_S.C_S + \rho_S.C_a.x_{eq}.X + \rho_v.C_v + \rho_{Gr}.C_{Gr})\frac{\partial \theta}{\partial \tau} + \frac{\rho_S.H_{ads}.x_{eq}}{t_{des}}.\frac{\partial X}{\partial \tau},$$

$$\frac{\partial X}{\partial \tau} = D_{so}.t_{des}.(1-X) \tag{6.36}$$

The following non-dimensional parameters C_r, ε, ε_a, ε_v, ε_s and ε_{Gr} are introduced into **E**qs. (6. 36) to normalize the governing equation. Therefore, the resulting non-dimensional equation is as follows:

$$C_r.\frac{1}{R^2}.\frac{\partial}{\partial R}\left(R^2.\frac{\partial \theta}{\partial R}\right) + 1 = \frac{1}{\varepsilon}.\left[(1 + \varepsilon_a X + \varepsilon_v + \varepsilon_{Gr})\frac{\partial \theta}{\partial \tau} + \varepsilon_s.\frac{\partial X}{\partial \tau}\right] \tag{6.37}$$

To know how this equation can be used to support our model, the following groups of the non-dimensional parameters are used in this analysis in order to determine the importance of the parameters.

Conversion ratio C_r is defined as the ratio of the rate of the heat conduction density to the ohmic losses induced by the eddy currents and is given as follow:

$$C_r = \frac{\lambda_{tot}.\Delta T.\varepsilon_r}{p_v.r_i^2} = \frac{\lambda_{tot}.\Delta T.\sigma.\varepsilon_r}{J^2.{r_i}^2} \tag{6.38}$$

Heat transfer effectiveness ε determine the required energy absorbed by the adsorption container per unit volume during the desorption process in order to know the volumetric Joule heat generated in the Gr-ball, with which the eddy currents required can be studied:

$$\varepsilon = \frac{p_v.t_{des}}{\varepsilon_r.\rho_S.C_S.\Delta T} = \frac{J^2.t_{des}}{\varepsilon_r.\rho_S.C_S\sigma.\Delta T} \tag{6.39}$$

The adsorbate number ε_a gives relationships between the specific heat capacity of adsorption material and the specific heat capacity of the adsorbate corresponding to the initial adsorption concentration and given as follows:

$$\varepsilon_a = \frac{C_a.x_{eq}}{C_S} \tag{6.40}$$

The vapor adsorbate number ε_v:

$$\varepsilon_v = \frac{\rho_v.C_v}{\rho_S.C_S} \tag{6.41}$$

The adsorbent number ε_S :

$$\varepsilon_s = \frac{H_{ads}.x_{eq}}{C_S.t_{des}} \tag{6.42}$$

The heat source number ε_{Gr} :

$$\varepsilon_{Gr} = \frac{\rho_{Gr}.C_{Gr}}{\rho_S.C_S} \tag{6.43}$$

6.7 Numerical simulation

Since the design and the investigation of an induction heating system usually relies upon a series of tedious, expensive and long experiments, numerical simulation can be a valuable help in this field. For each problem or family of similar problems, certain software or numerical methods are preferred. No single universal computation method fits and is optimum for solving all induction heating problems [117-120]. The numerical simulation of our induction heating model clearly involves three coupled phenomena: electromagnetism, skin effect and desorption. The solution of the problem by numerical modelling and simulation processes was implemented by the software **A**NSYS **E**lectronics 17.2 (named Maxwell) and **A**NSYS Fluent. Maxwell® is a comprehensive electromagnetic field simulation software package for engineers tasked with designing and analyzing 3D/2D structures, such as motors, actuators, transformers and other electric and electromechanical devices common to automotive, military aerospace and industrial systems. Based on the Finite Element Method, Maxwell can solve static, frequency-domain and time-varying electromagnetic and electric fields [129].

Fig. 6.5a shows the model of the numerical simulation studied in this work using **A**NSYS **E**lectronics. The software **A**NSYS **E**lectronics carried out several measurements for two cases of the induction heating geometries, in order to get a comparison between the different materials (SG and AC) of the

heat generation. **T**ab 6.3 shows the properties of the finite elements method to obtain the numerical model for the simulation procedure.

Model	AC-model	SG-model
Type of elements	Tetrahedra	Tetrahedra
Total number of elements	1186809	1377474
CPU time (h: min)	8:40	8:21

Table 6.3: Properties of the finite elements method to obtain the numerical model for the simulation procedure

It is worth noticing, that the desorption kinetic $\partial x/\partial t$ requires a particularly study through the adsorption reactor which comprises with the adsorbent and the adsorbate, because the physical coefficients of the adsorption medium and the adsorbate concentration change during desorption and induction heating processes. Therefor the thermal problem will be simulated under transient state for an extended period of time.

The temperature distribution at every point throughout the adsorption reactor is simulated by **A**NSYS **F**luent, whereas we have to solve the electromagnetic problem as stationary in time, because the physical coefficients of the Gr-balls don't change under the temperature interval required during the induction heating and desorption processes. **F**ig. 6.5b shows the model of the numerical simulation studied in this work using **A**NSYS **F**luent.

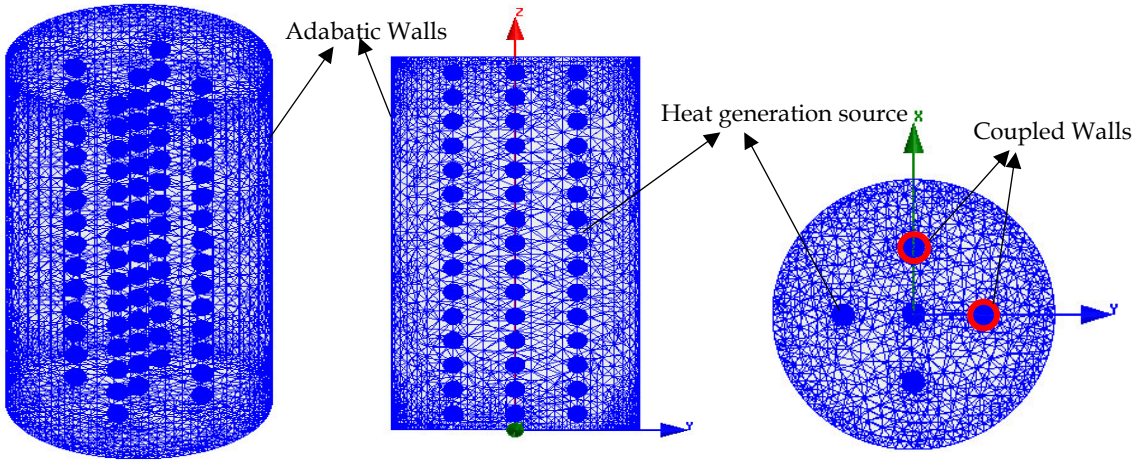

Figure 6.5a: The model of the numerical simulation studied in this work using **A**NSYS **E**lectronics

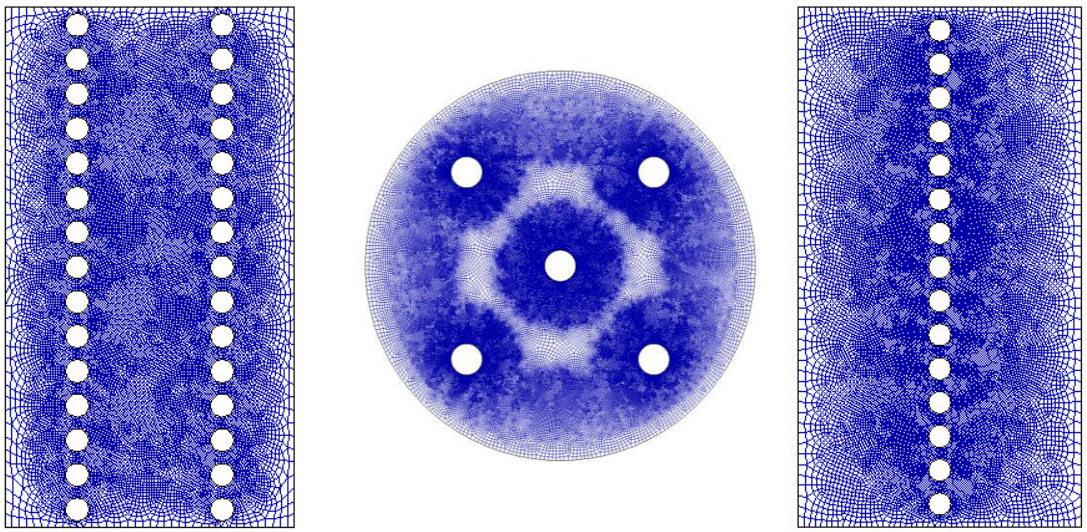

Figure 6.5b: The model of the numerical simulation studied in this work using **A**NSYS **F**luent

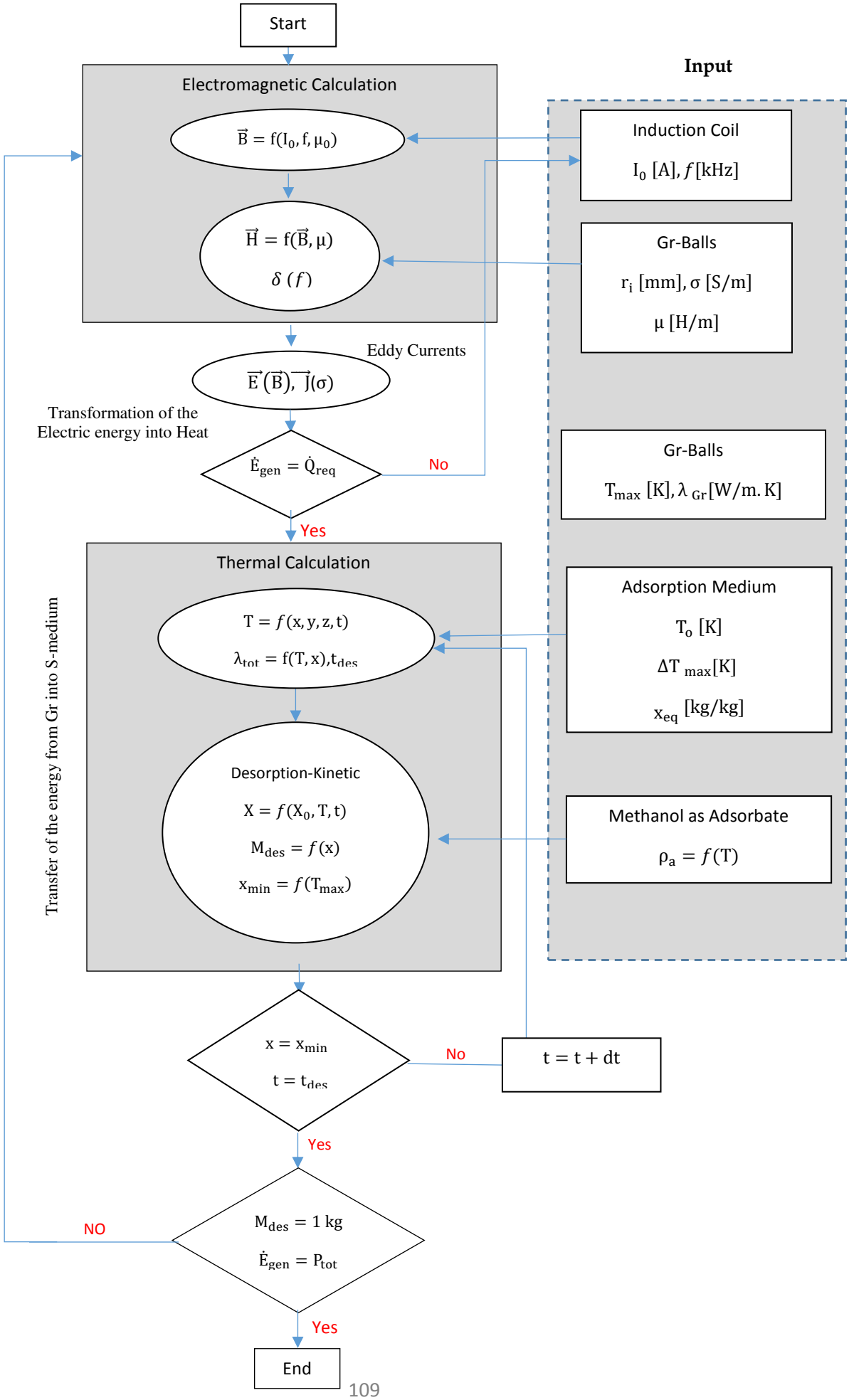

Fig. 6.6: Schematic representation of the simulation procedure

6.8 Results and discussion

6.8.1 Results of the numerical simulation

In order to obtain the numerical simulation we have adopted the schematic representation of the simulation procedure as shown in **F**ig. 6.6 on the basis of the above model.

The numerical simulation using the software **A**NSYS **M**axwell® allows us to investigate the variation of the electric current density $\vec{J}$, the electric field intensity $\vec{E}$, the magnetic flux density $\vec{B}$, the magnetic field intensity $\vec{H}$ and the power density (ohmic losses) p_v, which are induced inside the Gr-balls. Whereas the software **A**NSYS **F**luent can be available help to investigate the temperature distribution at any point and in any cross section of the model during the whole processes of the induction and desorption processes.

The aim of the simulation study is to obtain as smooth a temperature distribution as possible inside the SG-and AC-adsorption reactors using the electromagnetic induction heating technology. So the procedure was the find and determine the appropriate value of the induction coil current, which must be sufficient to obtain the required desorption temperature and also sufficient to achieve the required values of p_v, $\vec{J}$, $\vec{E}$ and $\vec{B}$.

The possibility of studying several skin depths and having several electric currents passing through the induction coil, characterized by different frequencies, have been taken into account. **F**ig. 6.7 shows the relationship between the coil currents studied in the numerical modelling and the values of required induction frequency, which are related to different values of the skin depth.

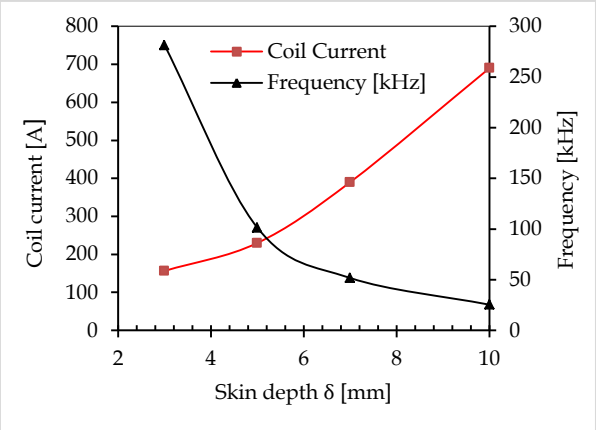

Figure 6.7: Coil current and the frequency as function of the skin peth

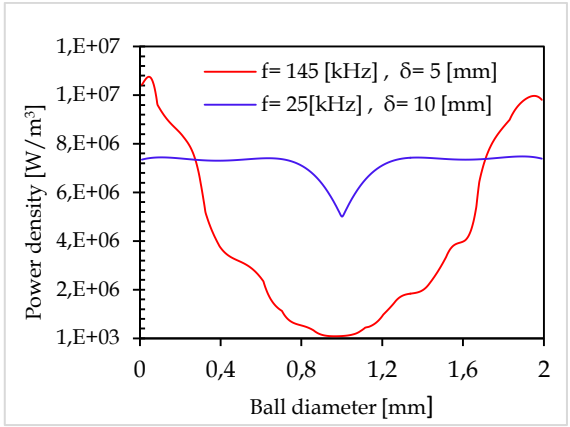

Figure 6.8: Variation of the power density inside the Gr-balls placed in SG-adsorption reactor

The simulation results, which will be present in this work, have been carried out for the skin depth is equal to the ball radius ($\delta = 10$ mm, $f = 25$ kHz), because the power density induced inside the Gr-balls has almost a homogeneity distribution in all dimensions of the Gr-ball, whereas the power density for induction frequency $f = 145$ kHz will be concentrated in the surface layer which is related to $\delta = 5$ mm and decrease from the Gr- ball surface toward its center as shown in **F**ig. 6.8.

The another reason why the simulation procedure is implemented with skin depth equal to the Gr-ball radius is: Based on the analytical results of this study it will be noticed that, the required desorption temperature for a constant value of the power density, can be improved by increasing the skin depth and by decreasing the induction frequency.

6.8.1.1 Temperature field $T(x, y, z, t)$

As shown from last chapter, during the desorption process in order to desorb $1\ kg_{meth}$, the SG-adsorption reactor had to be heated up to the maximal desorption temperature of $T_{des}^{SG} = 100\ °C$, whereas the AC-adsorption reactor only to $T_{des}^{AC} = 84\ °C$.

The numerical study of the temperature field $T(x, y, z, t)$ is necessary to know the homogeneity of the temperature distribution and the impact of the incorporation of the Gr-balls on this distribution. The temperature dependency of all the material properties and the heat transfer parameters are respected in this study. **F**ig. 6.9a exhibits the temperature distribution from our simulation throughout the complete adsorption reactor, which is filled by adsorbent materials.

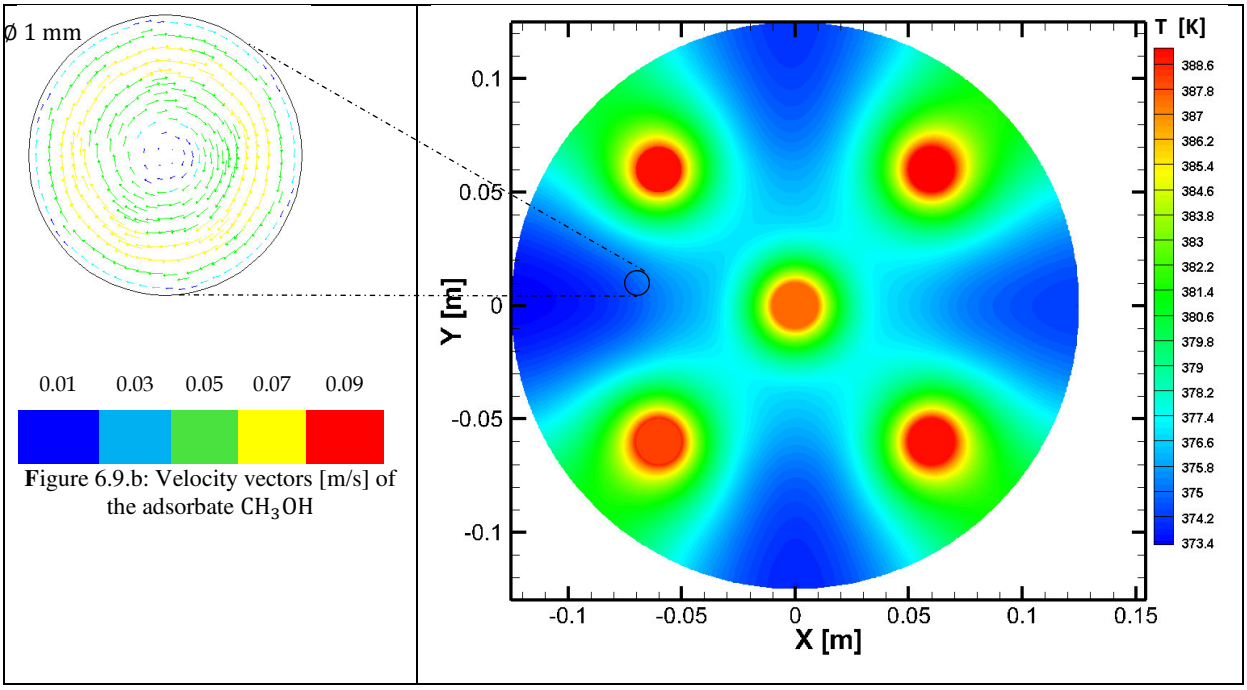

Figure 6.9.b: Velocity vectors [m/s] of the adsorbate CH_3OH

Figure 6.9a: 2D-temperature distribution throughout $x - y$ symmetry plane of the cylindrical SG-adsorption reactor during the desorption process using the electromagnetic induction technology $I_{max} = 690\ A$, $f = 25\ kHz$ and $\delta = r_i = 10\ mm$

It can be seen that the required desorbed temperature of $100\ °C$ is achieved at every location inside the SG-adsorption reactor. The SG-particles, which surround the Gr-balls, have the highest temperature that decreases from the heat source toward the outer boundaries. However the temperature at the farthest point of the balls also reaches the desired desorption temperature. During the desorption process both the temperature of SG-adsorbent particles and temperature of methanol, which loaded on the adsorbent, also rise to the desorption temperature. As a result, the methanol that is used as a refrigerant in the adsorption system, evaporates and leaves from the adsorption reactor. The behavior of methanol has been simulated for circle of 1 mm diameter inside the SG-reactor with coupled wall, which its temperature related to the SG-temperature. **F**ig. 6.9b shows the methanol-behavior, fixing on the SG-particles during desorption process and gives the variation in its velocity resulting from the absorption of the heat by SG-particles. It is observed, that the velocity of the methanol as an adsorbate changes from 0 to $0.06\ m/s$, when its temperature rises from the initial value of $27\ °C$ to the considered desorption value of $100°C$ during the desorption process using the induction heating.

Fig. 6.10 and **F**ig. 6.11 show 2D-temperature distribution throughout $y - z$ symmetry plane and $x - z$ symmetry plane of the cylindrical SG-adsorption reactor during the desorption process using the electromagnetic induction technology.

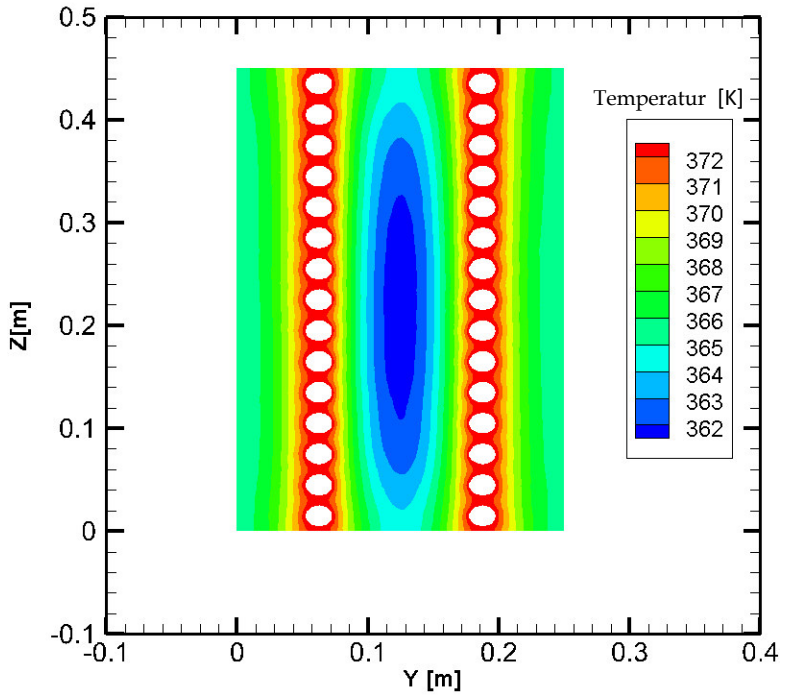

Figure 6.10: 2D-temperature distribution throughout y − z symmetry plane of the cylindrical SG-adsorption reactor during the desorption process using the electromagnetic induction technology

As noticed from the **F**ig. 6.10 and **F**ig. 6.11, the temperature difference between the Gr-ball and the farthest point changes from 67 °C at the start of the desorption process to 15 °C at the end of the process. Consequently, we notice, that the Gr-balls placed inside the adsorption reactor improves both the heat transfer and the desorption process.

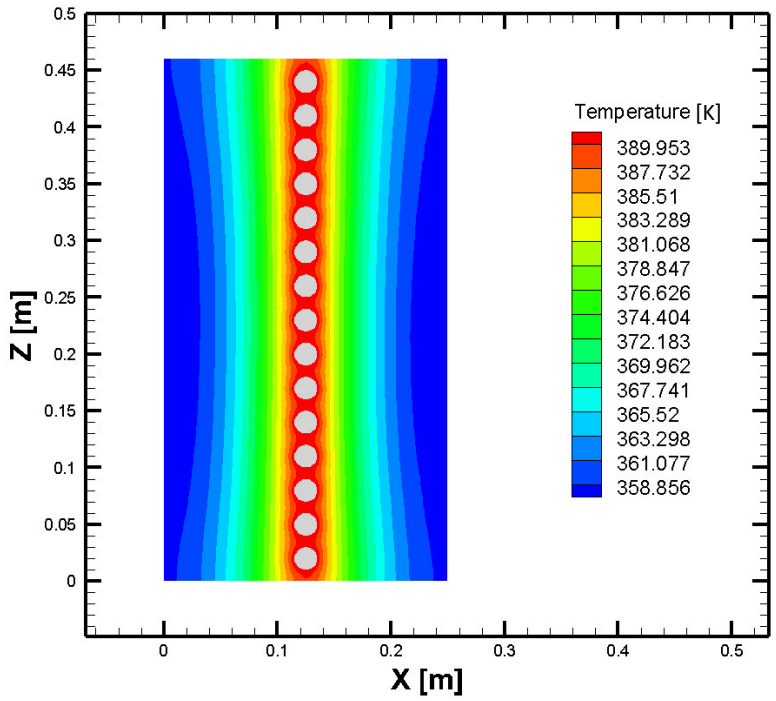

Figure 6.11: 2D-temperature distribution throughout $x - z$ symmetry plane of the cylindrical SG-adsorption reactor during the desorption process using the electromagnetic induction technology

6.8.1.2 Power density p_v $[W/m^3]$

The homogeneous distribution of the desorption temperature throughout the adsorption reactor is resulted by the Gr-balls in which the required Joule heat is generated. The Gr-balls, placed in within the adsorption reactor, where are used to convert the Joule heat induced inside it into the required desorbed energy. Therefore the induced power density (ohmic loss) must be sufficient to obtain the required desorption temperature as presented in the last section. The study to provide the required power density is the main goal of the numerical simulation of the induction heated SG- and AC-adsorption reactor. **F**ig. 6.12 shows the 3D power density distribution of the whole Gr-balls which were placed in the SG-adsorption reactor and also shows 2D distribution of two balls during the induction heating and desorption processes.

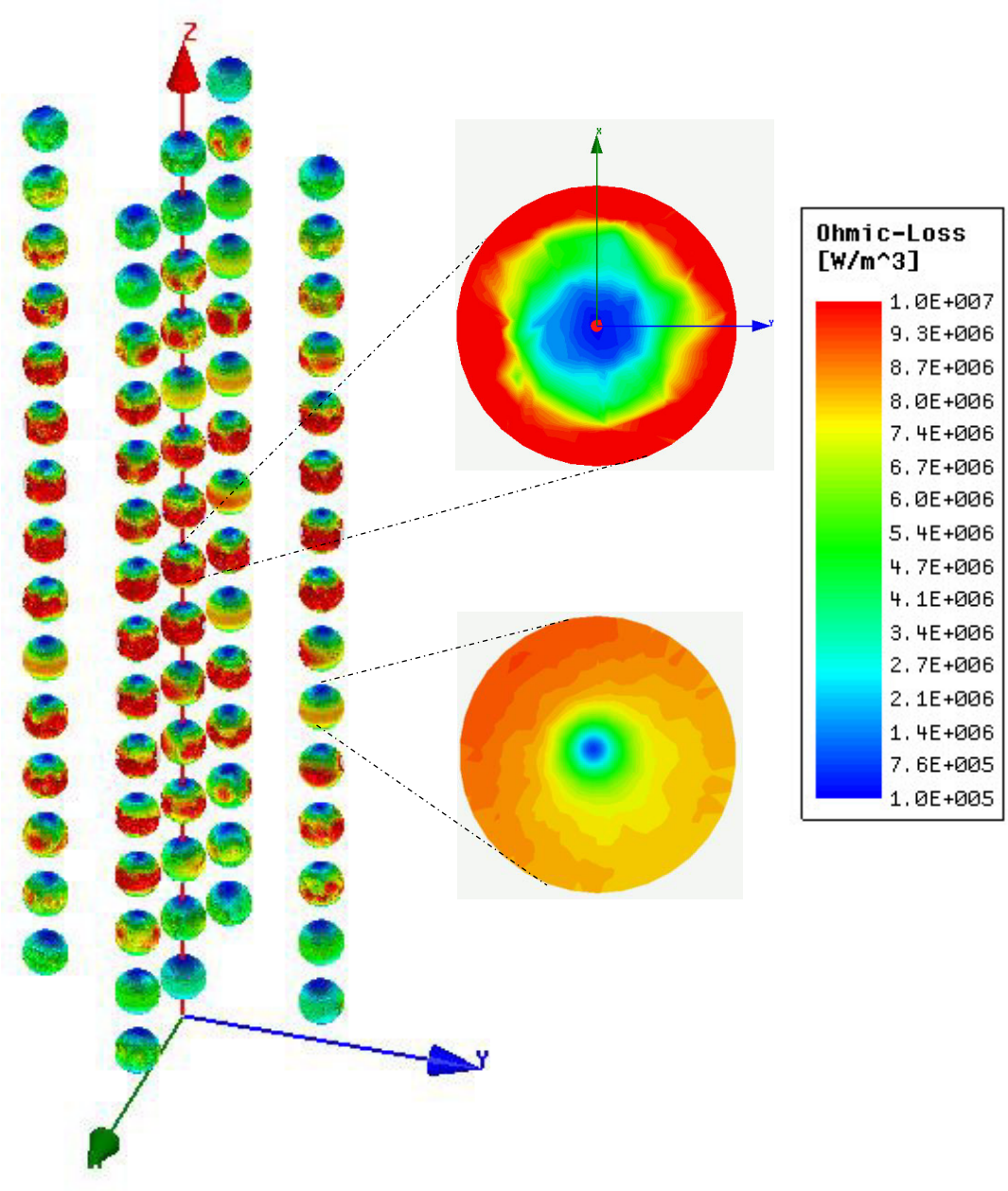

Figure 6.12: 3D and 2D Power density distribution inside the whole Gr-balls placed in the SG-adsorption reactor during the induction heating and desorption processes for $I_{max} = 690$ A , $f = 25$ kHz and $\delta = r_i = 10$ mm

Based on the numerical simulation, it is found, that the required power density, which must be dissipated in the Gr-balls, varies depending on the location of the balls, which corresponds to the magnitude of the magnetic field $\vec{B}$ generated in this location. **F**ig. 6.13 shows the variation of the power density along the *z* axis throughout the SG-adsorption reactor.

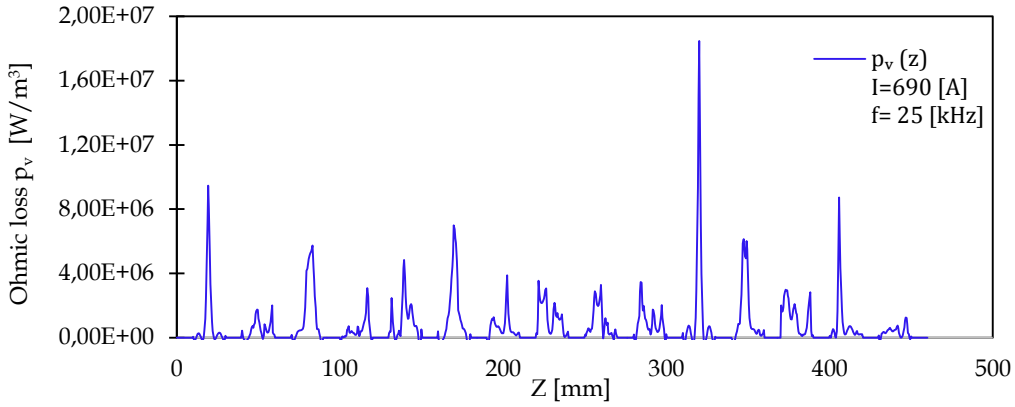

Figure 6.13: Variation of the power density along the z axis throughout the Gr-balls and SG-adsorption reactor for induction coil current $I_{max} = 690\ A$, frequency $f = 25$ kHz and skin depth $\delta = r_i = 10$ mm

Fig. 6.14 shows the power density distribution of the Gr-balls which were placed in the AC-adsorption reactor during the induction heating and desorption processes.

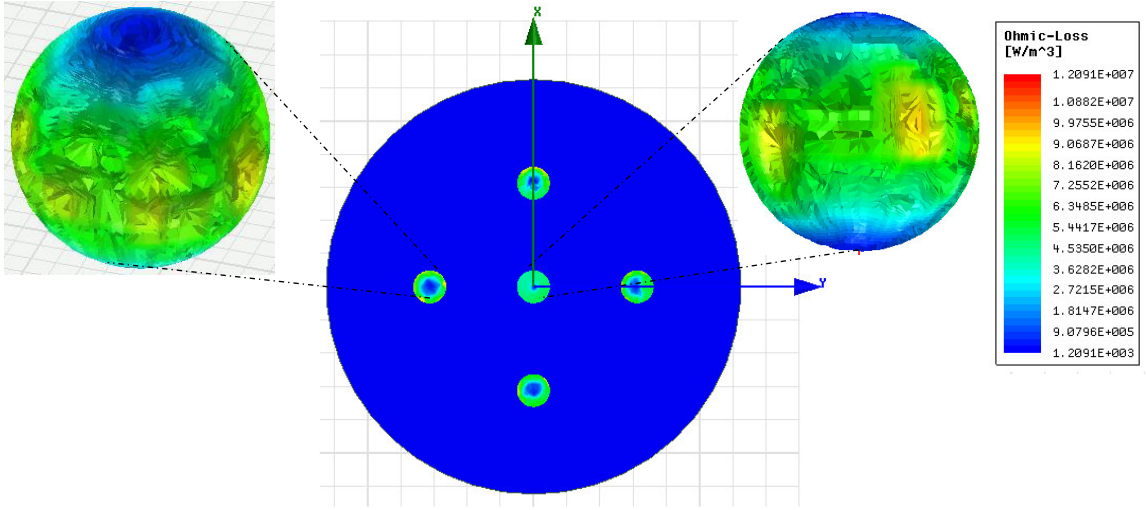

Figure 6. 14: Power density distribution induced inside the Gr-balls placed in AC-adsorption reactor during the induction heating for $I_{max} = 400$ A , $f = 25$ kHz and $\delta = r_i = 10$ mm

The dissipation of the ohmic losses inside the Gr-balls has been simulated and demonstrated as function of the Gr-ball-radius as shown in the **F**ig. 6.15. To provide the required desorbed energy, resulting from the conversion of the volumetric Joule losses, the skin depth is assumed to be equal to the ball radius. **F**ig. 6.15 illustrates an interrelation between the ohmic losses and the ball's diameter. The ohmic losses and the skin depth which is equal to the ball radius are slightiy interrelated. It can be noticed the ohmic losses decreses significantly at the center of the Gr-ball. AS a result, the average value of the power density required, to obtain the desorption process of the SG-and AC-adsorption reactors is equal to 10 and 3 $[MW/m^3]$, respectively.

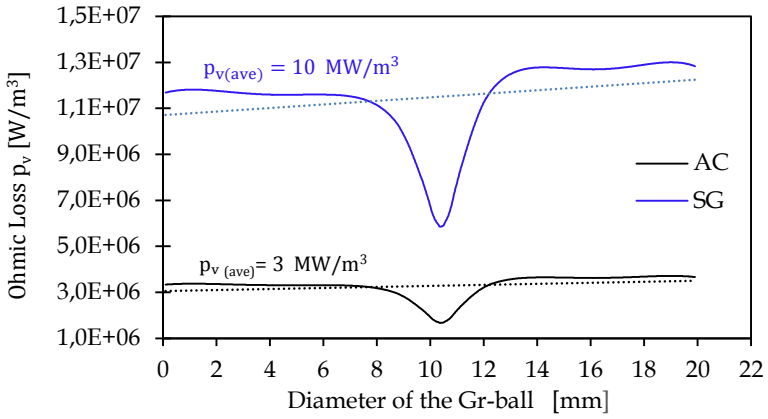

Figure 6.15: Variation of the power density inside the Gr-balls placed in AC- and SG-adsorption reactor during the induction heating for $I_{max}^{SG} = 690$ A , $I_{max}^{AC} = 400$ A, $f = 25$ kHz and $\delta = r_i = 10$ mm

6.8.1.3 Eddy currents density and electric field intensity

The first step of the numerical modelling was to explore the possibility of heating granular silica gel and activated carbon with this technology. The analysis of the electric field $\vec{E}$ was the main reason to use the Gr-balls as a source of heat generation because of the dielectric properties of the adsorption materials such as $\sigma_{SG} = 10^{-12}$ and $\sigma_{AC} = 10^{-3}$ [S/m].

At first, the AC- and SG-adsorption reactors without incorporation of the Gr-balls have been heated using the electromagnetic induction and their models were simulated in our study. It is found, that no electric field can be induced inside the SG-or AC-particles even with high applied values of the coil current, which reaches to 1×10^6 [A]. As noticed from the **F**ig. 6.16, that the induced eddy currents resulting, from applying so much high value of coil current, can't achieve the required Joule heat distribution, which is simulated in last section to obtain the desired desorption process.

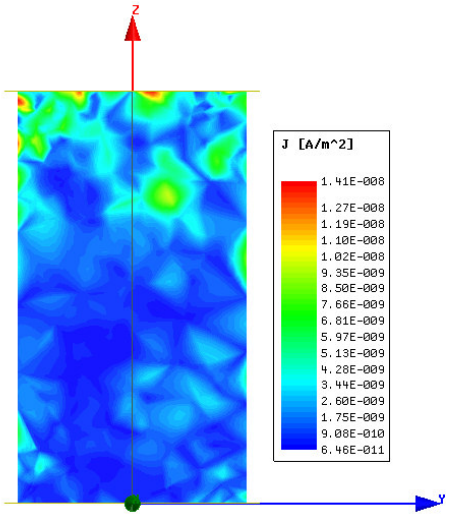

Figure 6.16: Eddy currents density distribution inside the AC-reactor for $I_{max} = 10^6$ A

The required distribution of the power density throughout the whole Gr-balls is caused by the effect of the eddy currents induced in the Gr-balls due to their electric conductivity according to Ampere's and Ohm's laws. Therefore, the electric field intensity must be sufficient to obtain the required desorption temperature corresponding to the power density as simulated in the last section.

The numerical simulation to achieve the required eddy currents and the electric field intensity is another main goal to realize the desired desorption process using the electromagnetic induction technology.

The distribution of the electric field intensity and the eddy currents inside the Gr-balls, plotted on x-y plane of the AC-adsorption reactor, are shown in the **F**ig. 6.17. It is found, that both of the electric

field and the eddy currents decrease close to the center of the Gr-ball. The maximum value of the electric field intensity and the eddy current density are located on the ball edges and estimated to be $5\ [\mathrm{V/m}]$ and $5 \times 10^5\ [\mathrm{A/m^2}]$, respectively. The simulation results of the AC-adsorption reactor is carried out under the assumption that the induction coil and the frequency are $400\ [\mathrm{A}]$ and $25\ [\mathrm{kHz}]$, respectively; this corresponds to the skin depth which is equal to the Gr-ball ($\delta = \mathrm{r_i} = 10\ \mathrm{mm}$).

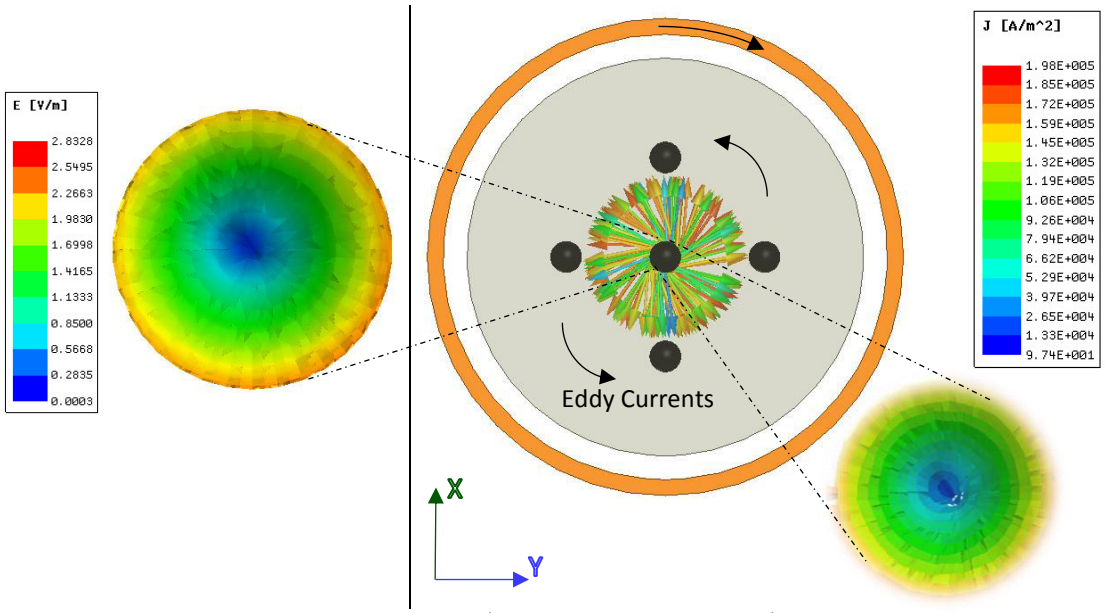

Figure 6.17: Distribution of the electric field intensity $\vec{E}$ and Eddy Currents density $\vec{J}$ inside the Gr-ball, which is placed in AC-adsorption reactor for $\mathrm{I_{max}} = 400\ \mathrm{A}$, $f = 25\ \mathrm{kHz}$ and $\delta = \mathrm{r_i} = 10\ \mathrm{mm}$

The distributional vectors of the electric field and the eddy currents inside the SG-adsorption reactor are demonstrated in the **F**ig. 6.18. The simoulition results of the SG-adsorption reactor based on the Ampere's law show as known that the field lines of the induced electric field are circular and centered on the axis of the balls, i.e. $\mathrm{E}(\mathrm{r}, \mathrm{t})$.

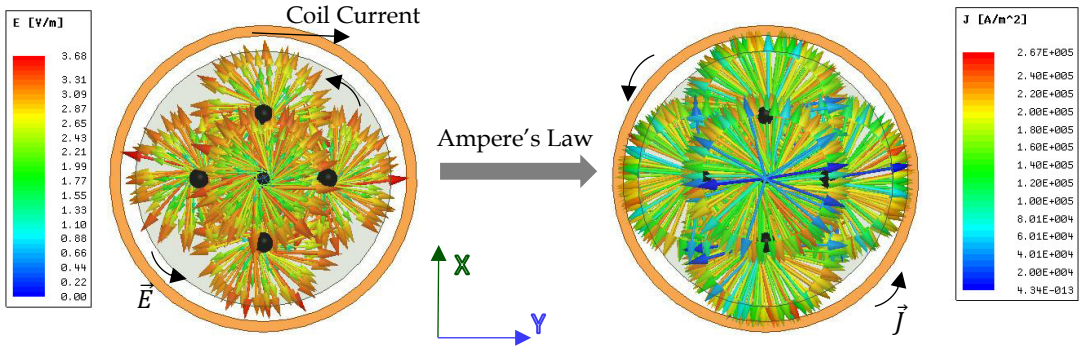

Figure 6.18: Distribution of the electric field intensity $\vec{E}$ and the Eddy Currents density $\vec{J}$ inside the Gr-ball placed in SG-adsorption reactor for $\mathrm{I_{max}} = 690\mathrm{A}$, $f = 25\ \mathrm{kHz}$ and $\delta = \mathrm{r_i} = 10\ \mathrm{mm}$

Fig. 6.19 shows a comparison between AC-and SG adsorption reactors related to the required values of $\vec{\mathrm{J}}$ and $\vec{\mathrm{E}}$ induced. To obtain $84\ ^{\circ}\mathrm{C}$, the desorption temperature of AC-adsorption reactor, the average value of the electric field intensity is estimated to be of $4.5\ [\mathrm{V/m}]$; this can induce an eddy current of $4.5 \times 10^5\ [\mathrm{A/m^2}]$, which is sufficient to provide the required power density. The average

value of the electric field intensity for SG-adsorption reactor is equal to 7 [V/m] and the eddy currents of 7×10^5 [A/m^2], which is sufficient to obtain the desorption temperature of 100 °C.

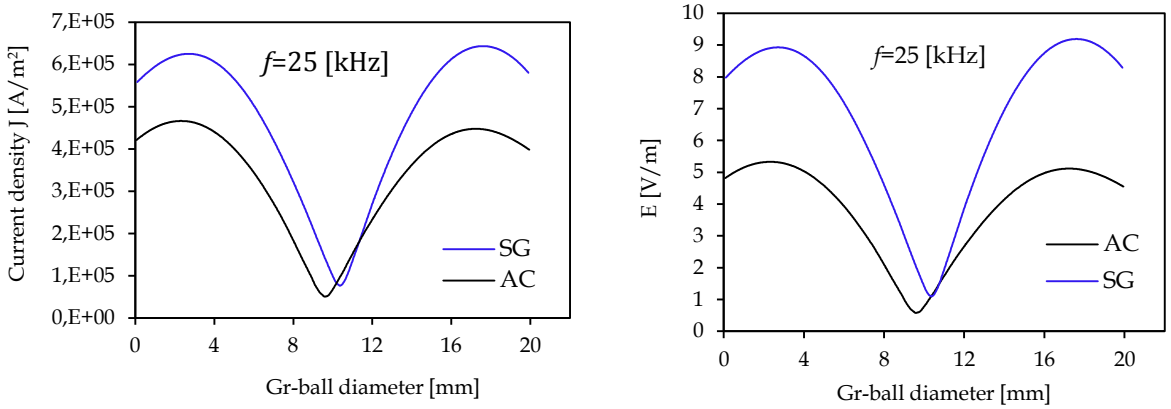

Figure 6.19: Variation of the eddy current density (left) and the electric field intensity (right) inside the Gr-balls placed in AC- and SG-adsorption reactors during the induction heating and the desorption processes for $f = 25$ kHz and $\delta = 10$ mm

There is no electric current density induced, inside the SG-and AC-particles, due to their dielectric properties. Based on the simulation results, it is found that the electric field intensity throughout the SG-and AC-adsorption reactors is equal to zero, therefore the Gr-balls were used inside the adsorption medium, in which induced the Joule heat. **F**ig. 6.20 shows the variation profile of the electric field intensity inside the AC-and SG-adsorption reactors. It can also be noticed, that the value of $\vec{E}$ is equal to zero outside the Gr-balls for SG-and AC-adsorption reactors.

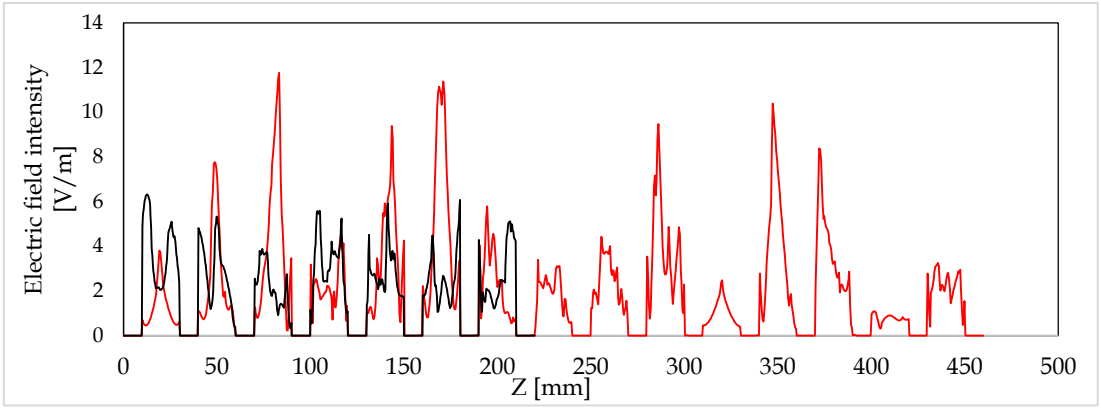

Figure 6.20: Variation of the electric intensity along the *z* axis throughout the SG-and AC-adsorption reactors during the induction heating and the desorption processes for $f = 25$ kHz and $\delta = r_i = 10$ mm

A time varying magnetic flux density induces an electric field intensity according to Faraday's law, therefore the magnetic field would be simulated in the next section.

6.8.1.4 Magnetic field $\vec{B}$

In order to receive the good desorption process and the uniform temperature distribution, it is necessary to know the required magnetic flux density resulting from an induction coil current, which provides a uniform heat through the adsorption reactor. Ampere's Law relates the integrated magnetic field around a closed coil to the electric current passing through the coil. Using Amperes' Law, one can determine the magnetic field associated with a given current $B = f(I)$.

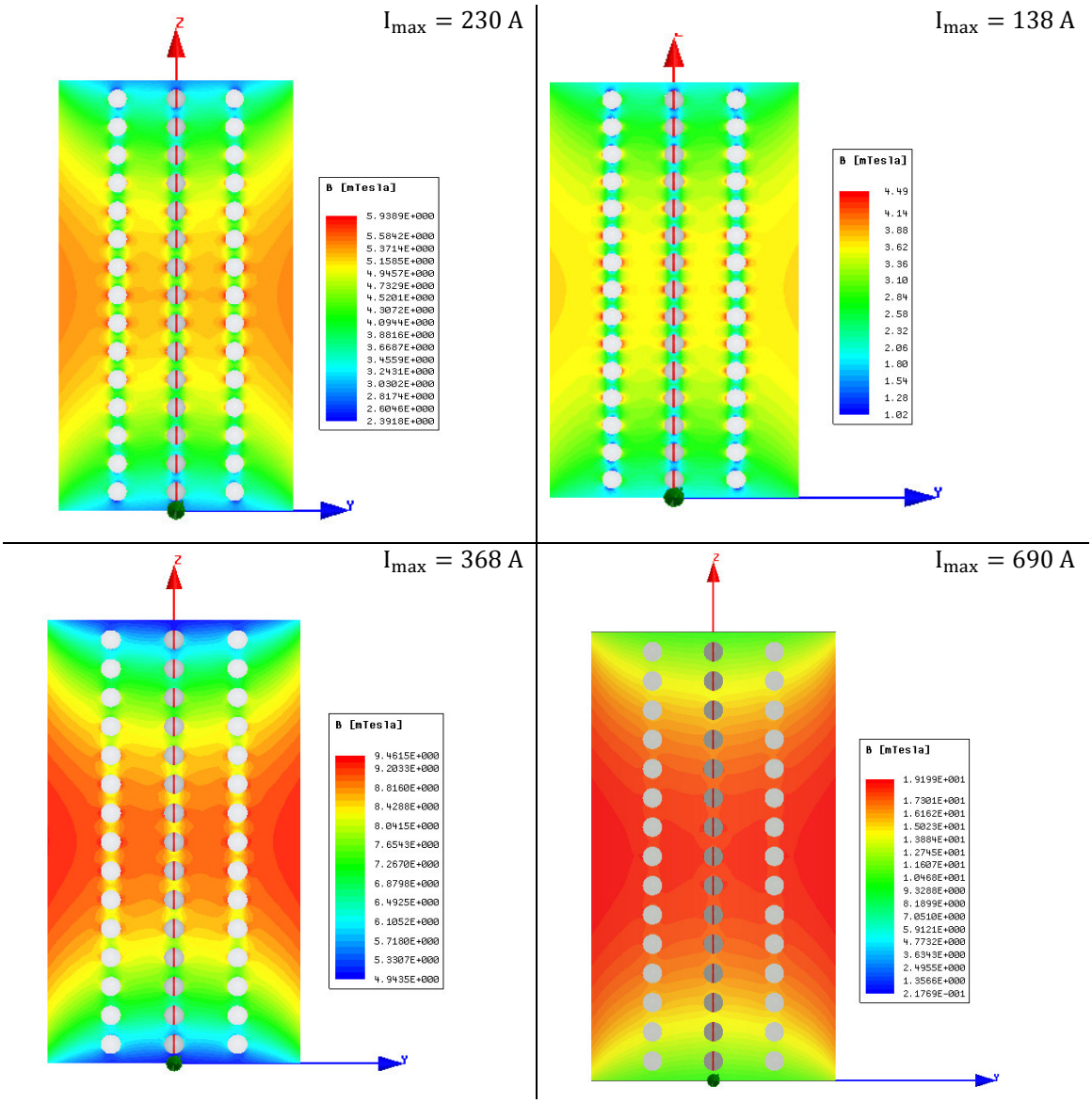

Figure 6.21: Generated magnetic flux density of the Induction heated SG-adsorption reactor with different currents passing the induction coil

The numerical simulation depended on variation the induction coil current to achieve a magnetic flux density which is sufficient to obtain the required desorption temperature, that is equal to 100 °C and 84 °C for SG-reactor and AC-reactor, respectively, resulting from the Joule effect. **F**ig. 6.21 shows the distribution of the magnetic flux density throughout the SG-reactor for different induction coil current of 138, 230, 368 and 690 [A].

The profile of the magnetic flux density is demonstrated along the z-axis of the SG-adsorption reactor and inside the Gr-balls as shown in **F**ig. 6.22. It can be noticed, that the magnetic flux density increases with increasing the induction coil current and reaches its maximum value at the center of the adsorption reactor. The difference of the magnetic flux density between $z = 0$ and $z = 250$ mm is equal to 8 mT for coil current 690 [A].

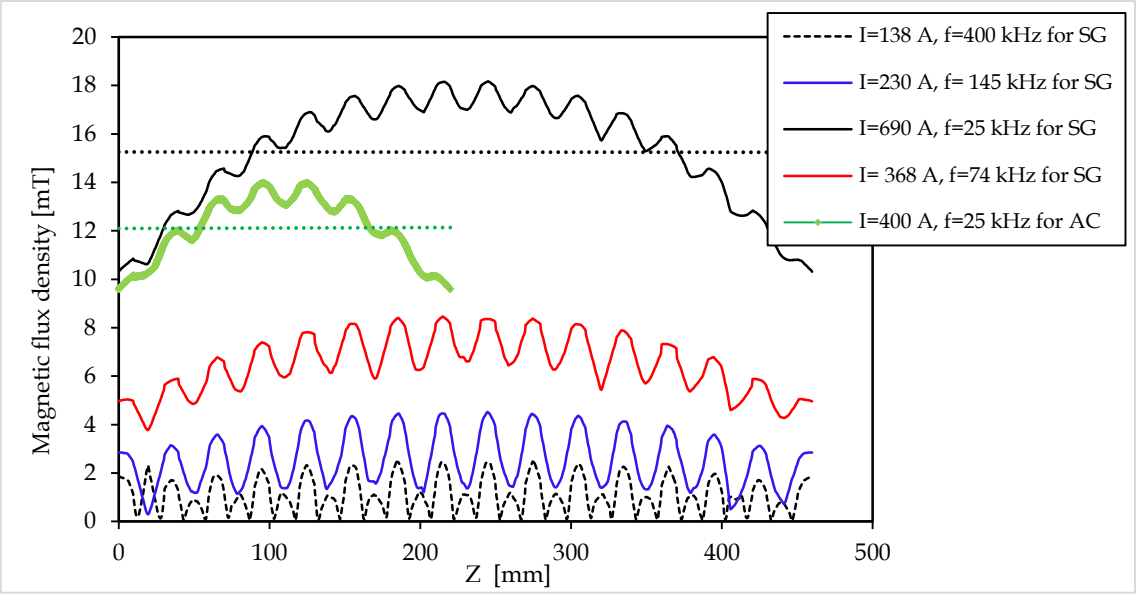

Figure 6.22: Magnetic flux density plot on z axis throughout the Gr-balls and SG-adsorption reactor for different induction coil currents

Based on the simulation results, it is found, that the magnetic flux density generated from coil current of 690 [A] is the required magnetic flux density through the SG-reactor and is estimated to be 15 [mT]; this is sufficient to induce the required Joule heat resulting in from the current density. The distribution of the magnetic field throughout the AC-adsorption reactor has been demonstrated in the **F**ig. 6.23.

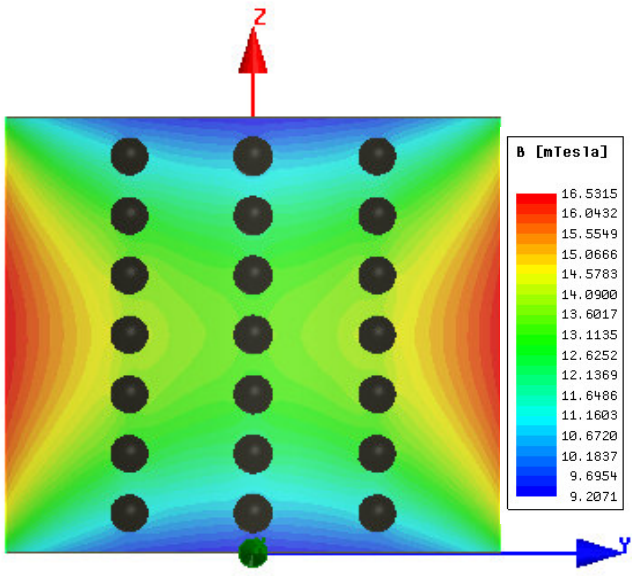

Figure 6.213Magnetic flux density distribution of the induction heated AC-adsorption reactor with induction coil current $I_{max} = 400\ A$ and frequency $f = 25$ kHz

In fact, the magnetic field intensity H[A/m] and magnetic flux density B[T] are linked in a given material, by this equation $B = \mu . H$. **F**ig. 6.24 shows the distribution of the magnetic field intensity throughout the AC- and SG-reactors. This magnetic field intensity is generated by the required induction coil current of 400 [A] and 690 [A] for the AC- and SG-reactors, respectively.

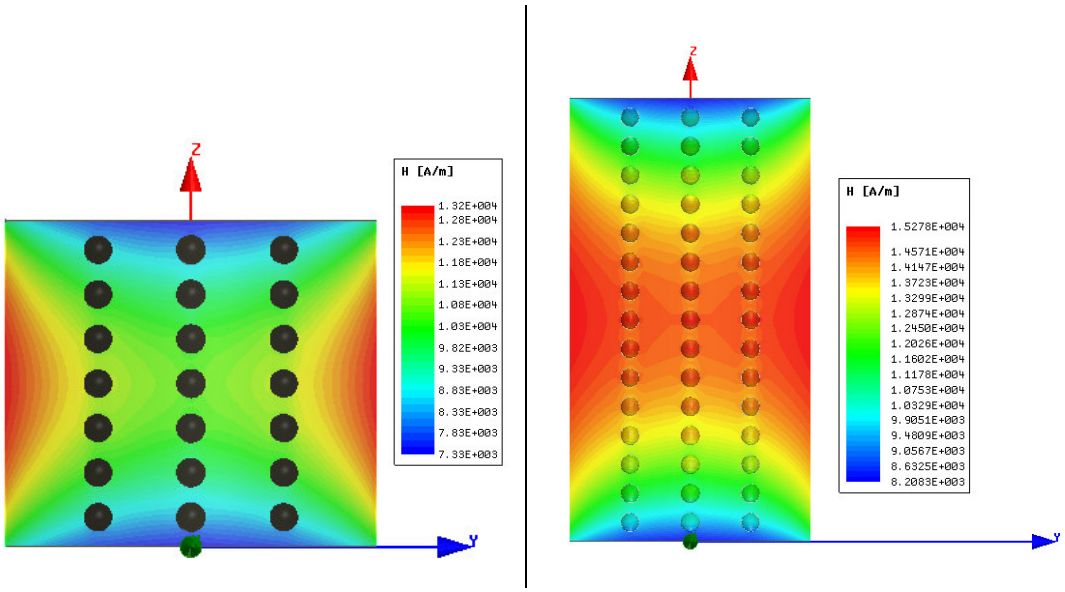

Figure 6.24: Magnetic field intensity distribution of the induction heated AC- and SG-adsorption reactor

6.8.1.5 Comparison between the AC-and AG-reactor using the IH-technology

Tab 6.5 shows the comparison of the obtained simulation results between the SG-and AC-adsorption reactors. It can be noticed, that the numerical simulation results verify from the Gr-balls toward the outer boundaries of the reactor and give a non-homogenous distribution of the p_v, $\vec{j}$, $\vec{E}$ and $\vec{B}$. This can be explained as follows: The parameters p_v, $\vec{j}$ and $\vec{E}$ vary depending on the location of the balls inside the adsorption reactors, which correspond to the magnitude of the magnetic field $\vec{B}$ generated in this location.

Parameter	AC-adsorption reactor	SG-adsorption reactor
Inductor current frequency [kHz]	25	25
Maximum current [A]	400	690
Magnetic flux density [mT]	$9 \div 16$	$10 \div 19$
Electric field intensity [V/m]	$1.4 \div 5$	$1.7 \div 8.7$
Eddy current density [A/m^2]	$1.06 \div 5 \times 10^5$	$1.2 \div 8 \times 10^5$
Power density [MW/m^3]	$1.8 \div 6$	$5 \div 12$

Table 6.5: Comparison of the obtained simulation results between the SG-and AC-adsorption reactor

6.8.2 Results of the analytical modeling

Understanding the dimensionless numbers ε, C_r and ε_r, derived from our analysis of the above mentioned mathematical model, are critical for obtaining the optimal electromagnetic and the heat transfer processes in the adsorption reactors studied using the IH-technology. Therefore we have been studying their variations and their effects on the design parameters of this system.

6.8.2.1 Effect of the heat transfer effectiveness ε

Analyzing the factor ε is crucial to determine the required amount of the energy, absorbed by the adsorption medium, resulting in from the Joule effect in order to know the appropriate eddy currents, which must be induced in the Gr-balls to achieve the needed desorption temperature. Another

importance of the dimensionless number ε is critical for reduction of the energy consumption corresponding to $\varepsilon = 1$.

Based on the analytical results it is found, that the desorption process using the induction heat takes a short time duration while increasing the power density induced in the Gr-balls, but the induced power density, may be greater than the required when $\varepsilon > 1$. Therefore, the adsorption induction heating system in this case is considered as a noneconomic system.

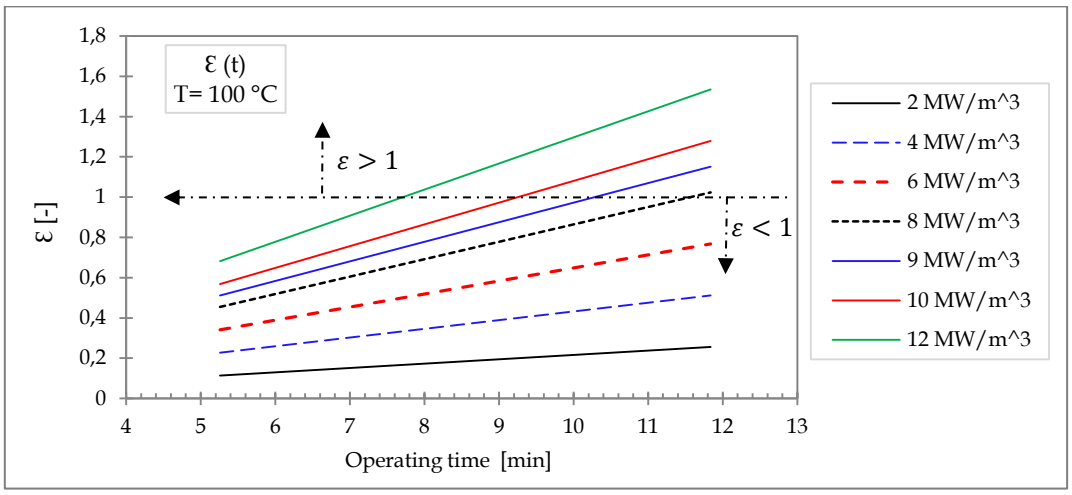

Figure 6.25: Effectiveness ε as a function of the operating time for different power densities induced under a constant desorption temperature of 100 °C to desorb 1 kg_{meth} from the SG-adsorption reactor

The required joule heat can be determined based on the desirable value of $\varepsilon = 1$ and the needed desorption temperature. **F**ig. 6.25 shows the heat transfer effectiveness ε as a function of the operating time for different values of the power density. We notice that the induced power density and the required time are inversely proportional to achieve the same desorption temperature of 100 °C with, $\varepsilon = 1$.

The desorption process becomes worse for $\varepsilon < 1$, because the eddy currents can't induce the required Joule heat. As noticed from the **F**ig. 6.25, the Gr-balls, considering a power density of 4 or 6 [MW/m^3] can't provide the required energy, and the complete desorption process given a power density of 12 [MW/m^3] can't take place before 8 [min], since $\varepsilon < 1$.

6.8.2.2 Effect of the conversion ratio the C_r

The analysis of the effectiveness number ε and the conversion ratio C_r allows us to determine exactly the power density, that is appropriate for our models and must be induced to achieve the required desorption temperature depending on both the $C_r = 1$ and $\varepsilon = 1$.

As shown from the **F**ig. 6.26, the appropriate value of the power density needed to desorb 1 kg_{meth} from the SG-adsorption reactor, is equal to 7.81 [MW/m^3], whereas to desorb the same mass of the adsorbate 1 kg_{meth} from the AC-adsorption reactor requires less value of the power density, which is equal to 2.94 [MW/m^3] .

For operating the IH-system at highest conversion ratio $C_r = 1$ and at optimal the heat transfer effectiveness $\varepsilon = 1$, the AC-adsorption reactor takes longer time about 40 [min] to desorb 1 kg_{meth} in comparison with the SG-adsorption reactor, which takes 11 [min], because the power density, required for desorbing the same mass of 1 kg_{meth}, is higher and estimated to 7.81 [MW/m^3].

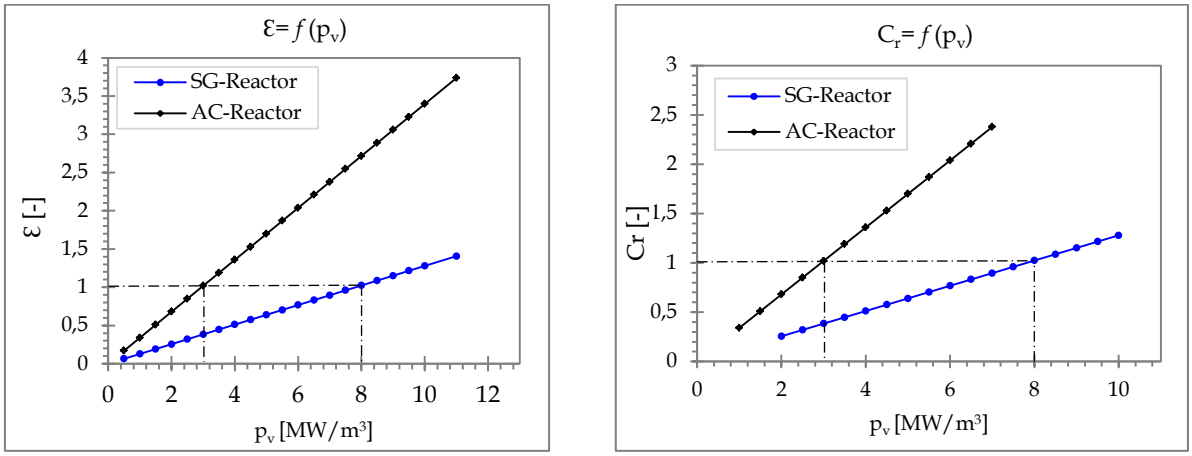

Figure 6.26: Effectiveness ε and the conversion ratio C_r as function of the power density p_v for desorb $M_{des} = 1\ kg_{meth}$ from SG- and AC- adsorption reactors with $T_{des}^{SG} = 100\ °C$ and $T_{des}^{AC} = 84\ °C$

6.8.2.3 Effect of the heat source -material

It is possible based on the knowledge of the C_r number, to choose the appropriate material and the proper size of the balls that are used as a heat source inside the adsorption reactor, because the C_r number is related to the radius r_i, electrical σ and thermal λ conductivities of the heat source (the balls).

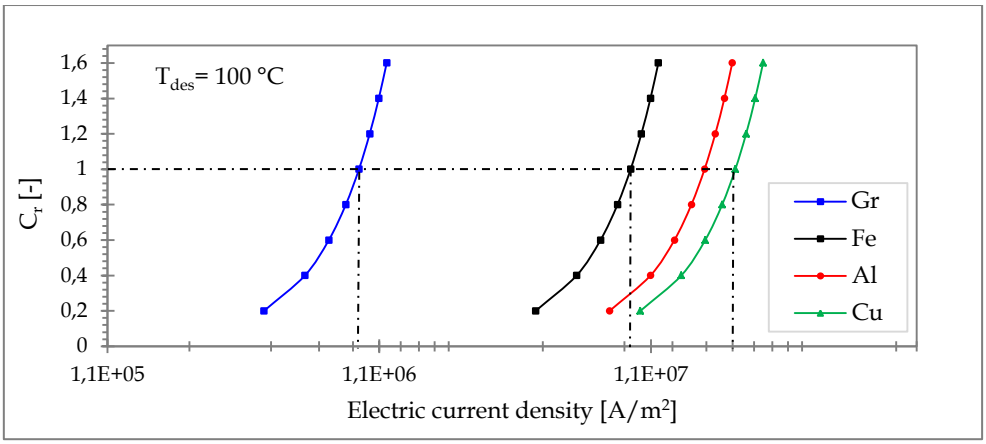

Figure 6.27: Conversion ratio C_r as function of the electric current density for different materials

As noticed from **F**ig. 6.27, the balls made of graphite are better comparing with the balls that made of iron, aluminum or copper, because the Gr-balls could obtain the required desorption temperature of 100 °C at a smaller value of the electric current density $8.84 \times 10^5\ [A/m^2]$ in comparison with the current density induced in the balls, which are made of the another materials. This means using graphite as a heat source reduces the energy consumption.

$p_v = 7.8\ [MW.m^{-3}]$
$\delta = r_i = 10\ [mm]$
$C_r = 1\ [-]$

Ball -Material	Graphite	Iron	Aluminum	Copper
E $[V.m^{-1}]$	8.84	0.88	0.47	0.36
J $[A.m^{-2}]$	8.84E+05	8.84E+06	1.65E+07	2.15E+07
f [Hz]	25330.34	2,53	72.37	42.93

Table 6.6: Comparing between different materials to choose a material of the heat source

If the required power density of $7.8\ [MW/m^3]$ is induced inside balls which are made of the different materials with the same skin depth of $\delta = r_i = 10\ [mm]$ and under the same conversion ratio of $C_r = 1$, it can be seen from **T**ab. 6.6, that the required electric field intensity generated inside Gr-ball is produced from a higher induction frequency, comparing with iron, aluminum and copper. This means that it isn't required high currents, which must be passed the induction coil, with applying high frequency to obtain the electric field

6.8.2.4 Effect of the Gr-ball radius r_i

The possibility of using several sizes of the Gr-balls and the effect of the heat source size on the important factors such as the required power density and the electrical field intensity have been studied based on the analysis of the conversion ratio C_r. The optimum values above mentioned could be determined based on the $C_r = 1$.

The variations of the generated power density and the required electrical field intensity have been demonstrated in the **F**ig. 6.28 for different sizes of the heat source realized by varying the Gr-balls radius r_i. It can be noticed that the size ball has a big effect on the induction heating process, because the factors E and p_v decrease by increasing the ball size.

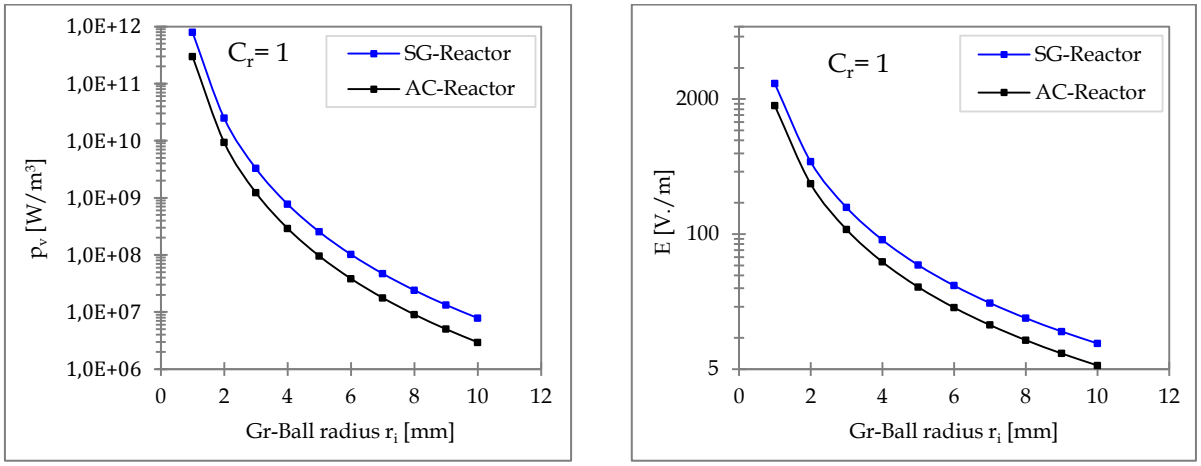

Figure 6.28: Power density and electrical field intensity as function of the heat source geometry (radius of Gr-ball) for desorb $M_{des} = 1\ kg_{meth}$ from SG- and AC- adsorption reactors with $T_{des}^{SG} = 100\ °C$ and $T_{des}^{AC} = 84\ °C$

6.8.2.5 Effect of the skin depth δ and induction frequency *f*

Induction heating technology has another major advantage. At high frequencies, the induced eddy currents flow near the surface of the Gr-balls. This is called the skin effect. The skin depth depends on the frequency and the material properties, while increases with decreasing the frequency as shown in the **F**ig. 6.29.

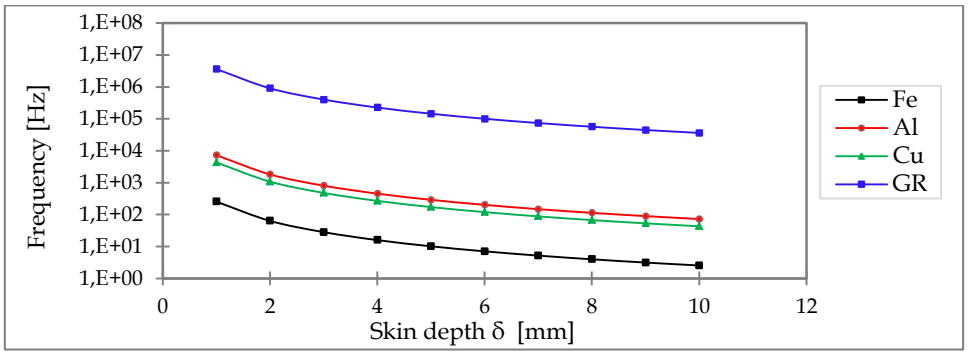

Figure 6.29: Relation between the skin depth and the frequency for different materials

So, by choosing the frequency correctly, one can apply the amount of required heat down to a known depth of the Gr-ball. Therefore, the analytical study of the mentioned mathematical model has included the effect of the skin depth related to the radius of the Gr-ball ($\delta = r_i$).

Fig. 6.30 shows how the induced power density can be reduced with choosing the correct skin depth for the different values of C_r and to achieve the needed desorption temperature of 100 °C throughout the SG-adsorption reactor.

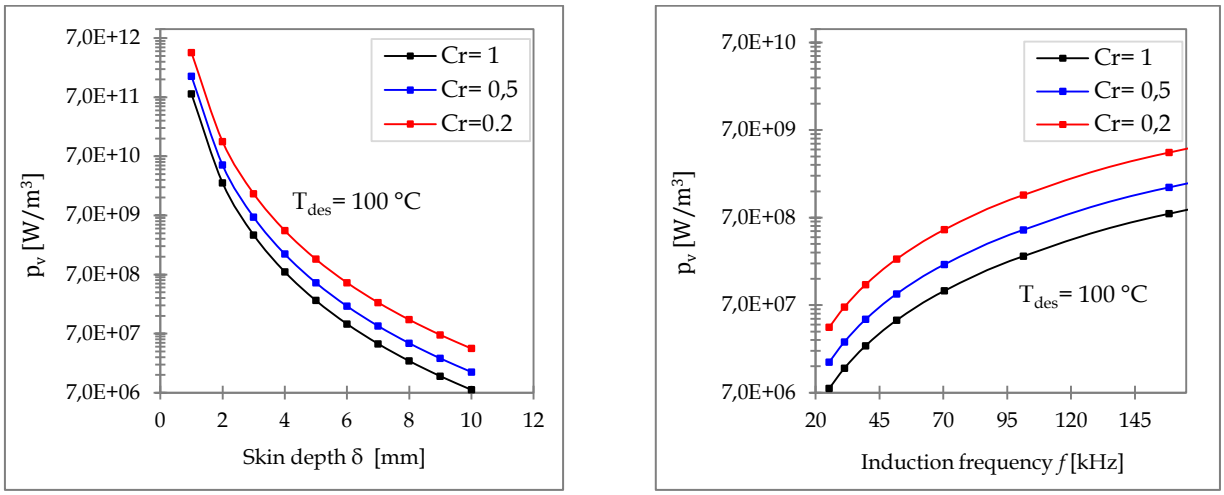

Figure 6.30: Induced power density as function of the skin depth and frequency

The required desorption temperature of SG-adsorption reactor can be achieved under the minimal power density, that can be obtained when ($C_r = 1$) and with ($\delta = r_i$). This means that the skin depth δ [mm] must be equal to the radius of the Gr-ball r_i [mm], because the power density decreases while increasing the skin depth, which is related to the radius of the Gr-ball and the eddy currents concentrate in an area, which is larger with increasing the skin effect.

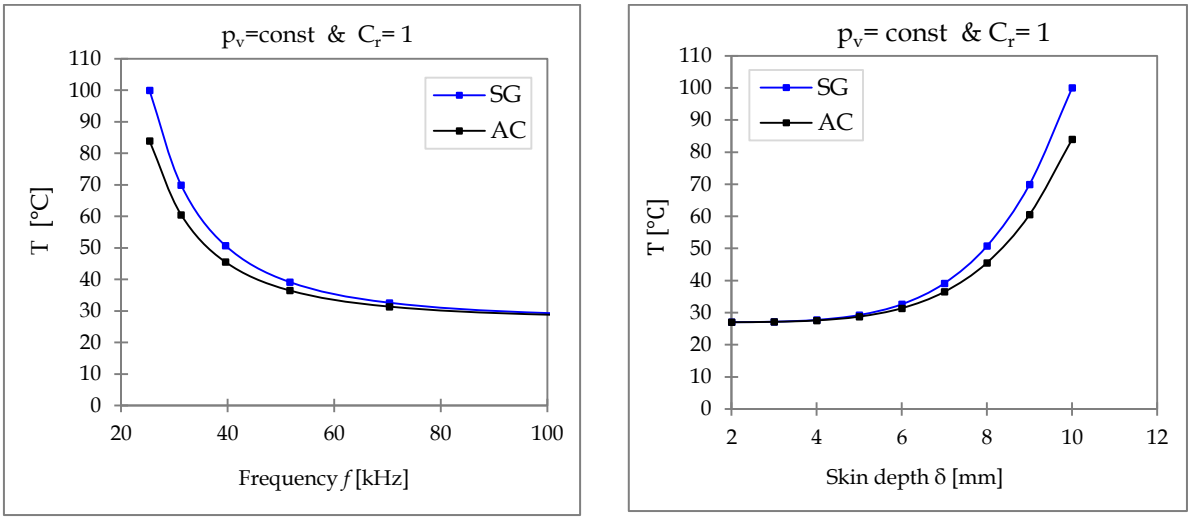

Figure 6.31: Effect of the induction frequency and the skin depth on the required desorption temperature for desorb M_{des} = 1 kg_{meth} from SG- and AC- adsorption reactors

The temperature variation throughout both the SG-and AC-adsorption reactors has been demonstrated in the **F**ig. 6.31 with the variation of the skin depth and the induction frequency. It can be noticed that, the required desorption temperature for a constant value of power density, can be improved by increasing the skin depth and decreasing the induction frequency.

6.8.2.6 Effect of the aspect ratio ε_r

The possibility of using several sizes of the Gr-balls and the ability to heat different amounts of the adsorbent amount M_S [kg] can be taken into account based on the aspect ratio ε_r, which is related to the radius of Gr-ball r_i and the radius of the spherical adsorption reactor r_o. As shown in the **F**ig. 6.32 we notice that, at high values of ε_r, more amount of the adsorbent can be filled by the adsorption reactor.

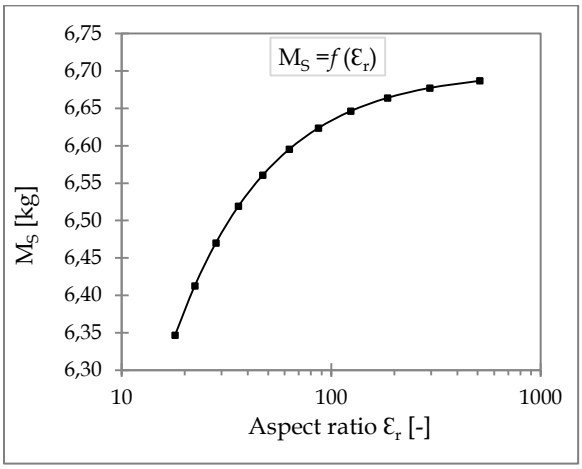

Figure 6.32: Relation between the adsorpent amount M_S and the aspect ratio ε_r

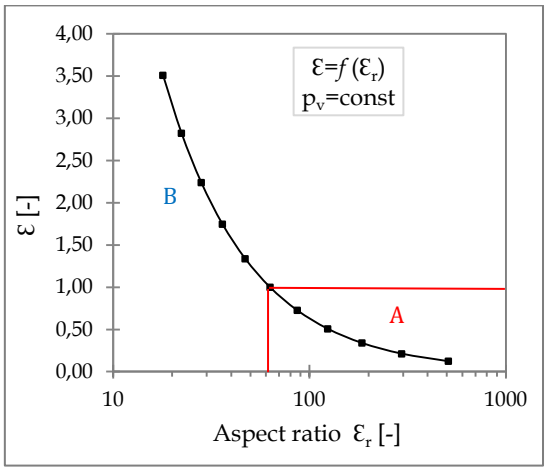

Figure 6.33: Effectiveness ε as function of the aspect ratio ε_r for the same p_v induced and a constat operating time

The change of the aspect ratio ε_r, which depends on the size adsorption reactor, varies both the methanol and the adsorbent amount, for different dimensions of the reactor.

Fig. 6.33 shows how the heat transfers effectiveness changes while increasing the amount of the adsorbent (increasing ε_r) corresponding to the size adsorption reactor. It can be observed, that the heat transfer effectiveness becomes worse by increasing the adsorbent amount (area A, $r_i < 1$cm) by same the power density induced inside the Gr-balls. For $\varepsilon < 1$, desorption process is not complete, i.e., the amount refrigerant desorbed smaller comparing with the adsorption reactor which having $\varepsilon \geq 1$ under the same conditions (area B, $r_i \geq 1$ cm).

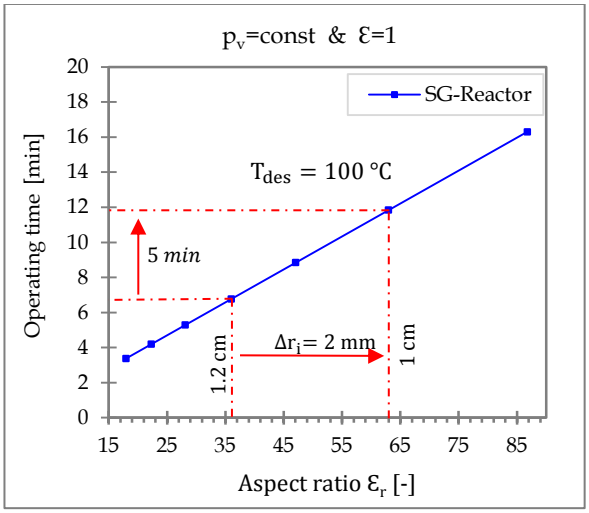

Figure 6.34: Relation between the operating time required and the aspect ratio ε_r for the same power density induced and $\varepsilon = 1$ to obtain the required desorption temperature of $T_{des}^{SG} = 100$ °C

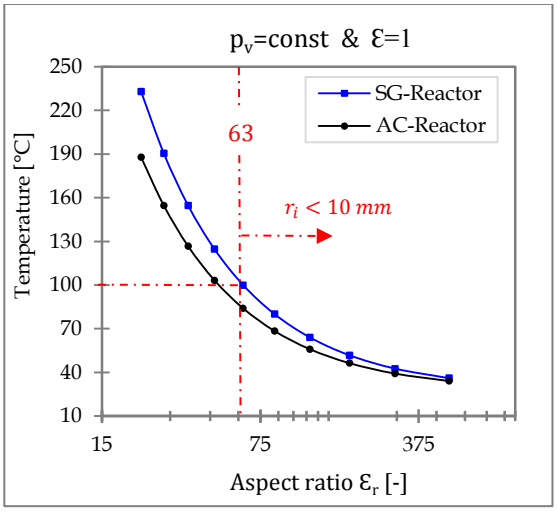

Figure 6.35: Relation between T_{des} and the aspect ratio ε_r for the same desorption time, constant power density and $\varepsilon = 1$

Therefore, the process takes longer time to achieve the complete desorption process to desorb the needed amount of refrigerant by constant power density and for $\varepsilon = 1$, when the aspect ratio increases as shown in **F**ig. 6.34. By decreasing the radius of Gr-balls to about 20 [mm] (increasing ε_r from 36 to 63) for a constant power density and a constant desorption temperature, the duration of desorption process increases about 5 [min] .

To heat a large amount of the adsorbents at same power density and with the same time ($\varepsilon = 1$) we notice from the Fig. **6**.35 that, the adsorption reactors couldn't be heat up to the required desorption temperature after $\varepsilon_r = 63$, because the heat source performed as $r_i < 10$ [mm] can't provide the required heat. This means the power density induced can't able to achieve the desorption temperature required. As shown from **F**ig. 6.35, the maximal desorption temperature obtained with the heat source performed as $r_i = 10$ [mm] for AC-adsorption reactor is 84°C, whereas the SG-adsorption reactor can be heated up to desorption temperature of 100 °C with the same heat source.

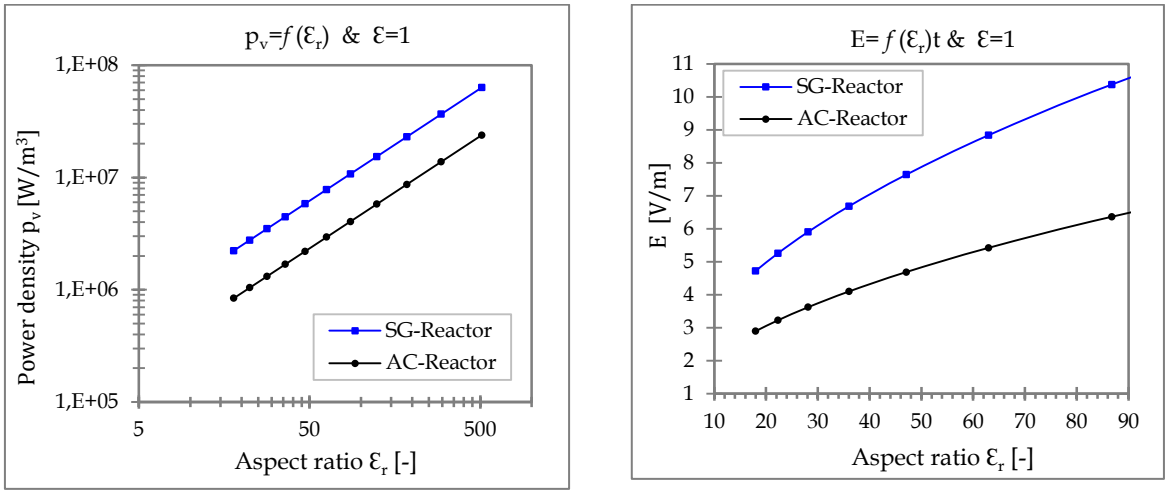

Figure 6.36: Variation of the power density p_v and the electric field intensity with the aspect ratio ε_r for the same desorption time and by $\varepsilon = 1$ to obtain the required desorption temperature of $T_{des}^{SG} = 100$ °C and $T_{des}^{AC} = 84$ °C

In order to obtain the required desorption temperature and to enable the adsorption reactor reaching the minimum value of the adsorbate concentration with the effectiveness $\varepsilon = 1$, the induced power density must be increased while increasing the adsorbent material (increasing ε_r), while the desorption process takes the same time. Therefore, the electric field generated inside the Gr-ball must be also increased. **F**ig. 6.36 shows the variation of the power density required and the electric field intensity induced inside the Gr-ball to achieve the perfect desorption process with $\varepsilon = 1$ and the same desorption time, when the aspect ratio varies.

It can be noticed from **F**ig. 6.36, that by increasing the radius of Gr-balls about 20 [mm] (decreasing ε_r from 63 to 36), the required power density and also the electric field intensity decrease about 3.35 [MW/m^3] and 2.5 [V/m] respectively, but could to obtain the needed desorption temperature because of decrease the adsorbent amount.

6.8.3 Comparison between the analytical and numerical results

The numerical simulation and analytical modelling presented in this work were studied for two IH-systems by using 3.31 kg of activated carbon in the AC- adsorption reactor and 7.95 kg of silica gel in the SG-adsorption reactor.

The analytical results give the certain values of the electric field intensity, power and eddy currents densities, which are induced inside the adsorption reactor and required to desorb 1 kg_{meth}. Whereas the numerical simulation results as shown in **T**ab. 6.5 verify depending on the location of the Gr-balls inside the adsorption reactors, which corresponds to the magnitude of the magnetic field $\vec{B}$ generated in this location. But the comparison study between the analytical and numerical results dependent on finding the mean values of the parameters $p_v, \vec{j}$ and $\vec{E}$ for all the Gr-balls as follows:

$$\overline{p_v} = \frac{1}{i}\left(\sum_1^i p_v(i)\right), \qquad \overline{E} = \frac{1}{i}\left(\sum_1^i E_i\right), \qquad \overline{J} = \frac{1}{i}\left(\sum_1^i J_i\right)$$

here i is the number of the Gr-balls

(a) AC-IH system

Results	Numerical	Analytical	Relativ Error
$M_S(kg)$	3.31	3.31	–
$M_{des}(kg_{meth})$	1	1	–
$E(V.m^{-1})$	4.6	5.43	15.2 %
$J\ (A.m^{-2})$	4.5×10^5	5.43×10^5	17.1 %
$p_v(MW.m^{-3})$	3	2.94	2.04 %

(b) SG-IH system

Results	Numerical	Analytical	Relativ Error
$M_S(kg)$	7.95	7.95	–
$M_{des}(kg_{meth})$	1	1	–
$E(V.m^{-1})$	7.1	8.84	19.6 %
$J\ (A.m^{-2})$	7.2×10^5	8.84×10^5	18.5%
$p_v(MW.m^{-3})$	10	7.82	27.8%

Table 6.8: Comparison between the analytical and numerical results of the SG-and AC-IH systems

Tab 6.8 shows comparison between the obtained analytical and numerical results of both the SG-and AC-adsorption reactors. Based on the simulation results it is found, that the required power density induced inside the Gr-balls placed in the AC-reactor is estimated to 3 $[MW/m^3]$ which is produced by applying current of 400 [A] passing the induction coil at 25 [kHz]. Whereas the required power density induced inside the Gr-balls placed in the SG-reactor is estimated to 10 $[MW/m^3]$ which is produced by applying current of 690 [A] passing the induction coil at 25 [kHz].

It can be noticed from **T**ab. 6.8, that a good agreement have been found between the analytical and numerical results of the SG-and AC-IH systems. The relative error between the analytically and numerically $p_v, \vec{j}$ and $\vec{E}$ of the AC-IH system are 2.04 %, 17.1 % and 15.2 %, respectively. Whereas the relative error between the analytically and numerically $p_v, \vec{j}$ and $\vec{E}$ of the SG-IH system are 27.8 %, 18.5 % and 19.6 %, respectively.

6.9 Summary and conclusions

The purpose of this chapter was the use of electromagnetic induction technology as a new heat source of the adsorption refrigeration system in order to overcome the problems found with conventional methods (thermal heating). Here, inductive heating has been used to desorb the adsorbate CH_3OH loaded within the SG-and AC-particles, i.e. supplying the desorption process with process energy, that the desorption process is the main process of the adsorption systems. So this task dealt with a mathematical modeling and numerical simulation of an induction heating system for two adsorption reactors. The first adsorption reactor was filled by silica gel/methanol and the second by activated carbon/methanol.

To achieve that, a new design for each adsorption reactor was investigated to desorb the same amount of the refrigerant ($1\ kg_{meth}$). Because of the dielectric properties of SG and AC, incorporation of the graphite balls, having a good electrical conductivity, into the adsorption reactors, is used in order to improve the heat transfer process and to save the input energy.

The numerical simulation of our induction heating model clearly involves three coupled phenomena: electromagnetism, skin effect and desorption process (heat transfer). The solution of the problem by numerical modelling and simulation processes was implemented by the software **A**NSYS **E**lectronics 17.2 and **A**NSYS **F**luent.

Obtaining the required desorption temperature to desorb $1\ kg_{meth}$ from each reactor was the main aim of both the mathematical modeling and numerical simulation in this study. So the procedure was to find and determine the appropriate value of the induction coil current, which must be sufficient to obtain the required desorption temperature and also sufficient to achieve the required values of the power density (ohmic losses) p_v, the electric current density $\vec{J}$, the electric field intensity $\vec{E}$ and the magnetic field intensity $\vec{B}$. The following conclusions were drawn from this study:

1. Based on the analytical and numerical investigations, it is found, that the power density, the electric field intensity and the electric current density, which are induced inside the Gr-balls placed in SG-adsorption reactor to desorb $1\ kg_{meth}$ is $50\ \%$ larger than that induced inside the Gr-balls placed in AC-adsorption reactor, which is generated to desorb the same amount of the desorbed refrigerant of $1\ kg_{meth}$.

2. Incorporation of the Gr-balls into the adsorption reactor allows to achieve a homogeneity of the temperature distribution throughout the reactor and allows to obtain the exact temperature distribution needed in the material if required.

3. The analysis of the effectiveness number ε and the conversion ratio C_r allows us to determine exactly the power density, that is appropriate for our models and must be induced to achieve the required desorption temperature depending on both the $C_r = 1$ and $\varepsilon = 1$.

4. Induction heating technology has a major advantage. This is called the skin effect. The skin depth depends on the frequency and the material properties. So, by choosing the frequency correctly, one can apply the amount of required heat down to a known depth of the Gr-ball.

5. Using graphite as a heat source reduces the energy consumption comparing with the balls that are made of iron, aluminum or copper.

6. Desorption process using the induction heat takes short time duration while increasing the power density induced in the Gr-balls.

7. Based on the analytical study it is found, that the required induced power density decreases while increasing the skin depth. Therefore, the numerical simulation has been implemented for the skin depth is equal to the Gr-ball radius, which is the maximum value that can be taken.

8. Using the induction heating is a new process to overcome the problems found with the conventional methods (thermal heating) such as the setup of the adsorption reactor has a complex design, which is composed of tubes of hot water and many fins.

Chapter 7

Design of the Inductive Heating System

7.1 Structure of the inductive heating system

The Induction heating system in this chapter will be designed for two adsorption reactors, which were studied in the fifth chapter using the thermal heating. So that the final purpose is comparing both methods (thermal and induction heating) in terms of the desorption process of the same reactors.
The procedure of the design and analysis of the induction heating system for both the SG-and AC-adsorption reactors is as following:

1. Determine the proper size of the induction coil as a heater (the height, number of the loops and the section-shape of the coil).
2. Analyze the ohmic and inductive resistances of both the work-load and the induction coil in order to know the required input power.
3. Present the magnetic and electric circuit of the IH-system
4. Determine the total power induced inside the Gr-balls, which is required to heat both the SG- and AC-adsorption reactors to the same temperature100 °C and to desorb the same adsorbate amount.

An induction heating system typically consists of four elements. **F**ig. 7.1 shows the main elements of the induction heating system [121].

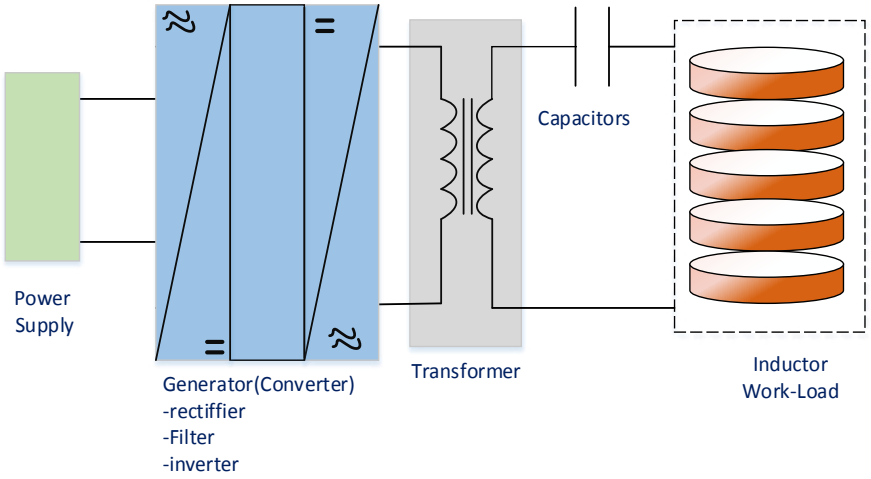

Figure 7.1: Structure of the power supply system for the induction heating system [121]

Power Unit: The power unit of an induction heating system is used to take the mains frequency and increase it to anywhere between $20 \div 900$ [kHz]. The typical output power of a unit reaches to 500 [kW]. This part consists of four elements: Generator; Rectifier; Filter and Inverter.
The alternating current voltage inputs are converted to direct current voltage by the rectifier. This output is then filtered and the voltage output is converted to a high frequency alternating current voltage through the inverter which is connected to the work-head.

Work Head: This contains a combination of capacitor's circuit and transformer and it is used to match the power unit to the work induction coil. The capacitor's circuit consists of the equivalent inductance, which represents the induction coil and the work-materials which be heated.

Work-Load: All of the simulation study and the analysis are based on the work-load which represents in this system Gr-balls and cylindrical adsorption container (together named adsorption reactor).

Induction Coil: The inductor is used to transfer the energy to the work-load. The coil design is one of the most important elements of the system as is a science in itself.

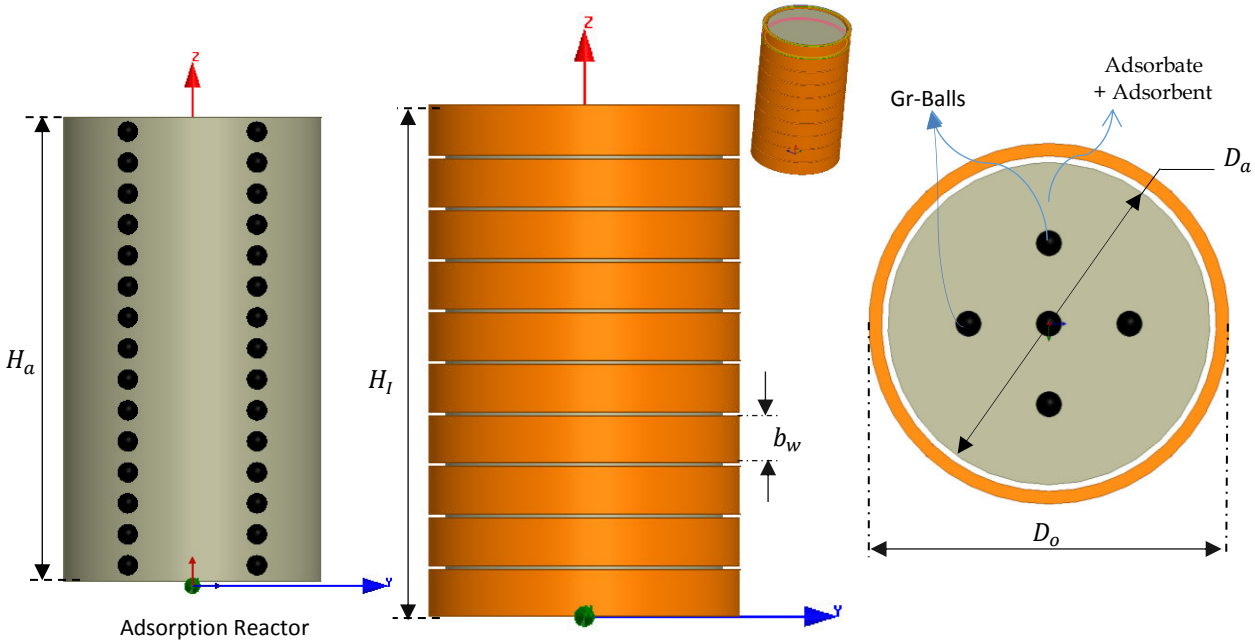

Figure 7.2: The Geometric system presentation of the adsorption reactor with the induction coil

7.2 Analytical model

While the purpose of the heat transfer analysis through the adsorption reactor is to know the required energy adsorbed by the adsorbents SG and AC in order to desorb CH_3OH, it is necessary to determine the proper size of the induction coil as a heater, the maximum rate of the heat losses from the Gr-balls, the ohmic losses in the coil and inside the Gr-balls. In order to study the electrical, electromagnetic and thermal behavior of the induction coil and the adsorption reactor in an induction heating technology, one requires some parameters specifications of the work-materials. **F**ig. 7.2 shows the geometry of the induction heating system studied consisting of the SG-adsorption reactor and the induction coil. **T**ab. 7.1 provides the geometry, thermal and electric properties of the work-load used in the SG-and AC-adsorption reactors which would be considered.

	Parameter	Gr-Ball	AC-Reactor	SG-Reactor	Unit
Work- Load	Shape	Spherical	Cylindrical	Cylindrical	
	Diameter	20	250	250	mm
	Specific Heat Capacity	710	940	850	$J/kg.K$
	Density	2500	2200	750	kg/m^3
	Permeability	1.26	1.26	1.26	$\mu H/m$
	Electric conductivity	10^5	10^{-3}	10^{-13}	S/m
	Thermal Conductivity	168	0.083	0.17	$W/m.K$

Tab. 7.1: Characteristics of the work-load components

The induction heating system in this work would be designed for a new application for desorption process, which is the main process of the adsorption refrigeration system.

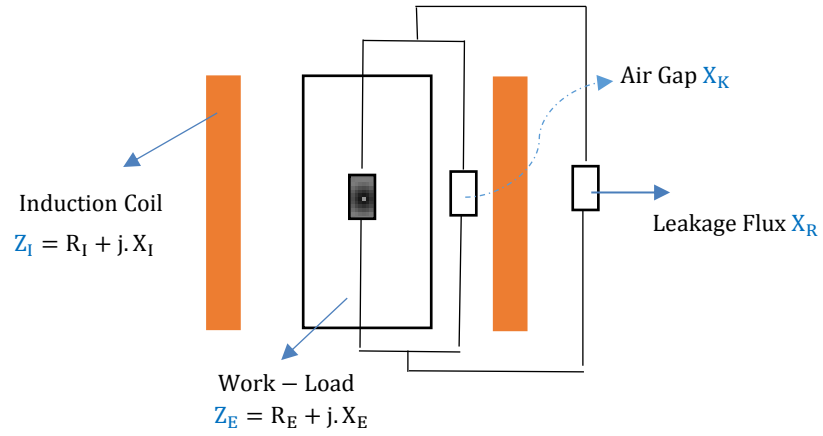

Figure 7.3: Magnetic and electric circuit of the induction heating system studied

The magnetic and electric circuit of the induction heating system studied is shown in **F**ig. 7.3 where the parameter R_E represents the ohmic resistance of the work-load (both the Gr-balls and the adsorption container), R_I is the coil resistance, X_K is the reactance of the air gab, X_I is the coil reactance, X_E is the work-load reactance and X_R the reactance of the leakage flux. **F**ig. 7.4 shows the ohmic and inductive resistances of the induction heating system [118,130].

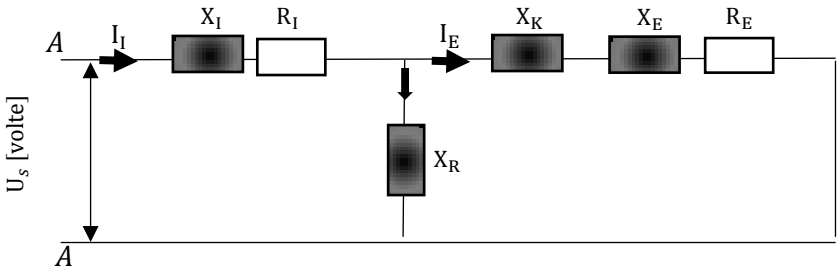

Figure 7.4: Equivalent circuit of the induction heating system studied

In order to know the total power and the input voltage which must be introduced to the induction heating system to achieve the required desorption process, the values of the parameters presented in **F**ig. 7.4 considering correction factors will be analyzed in detail and calculated in this study.

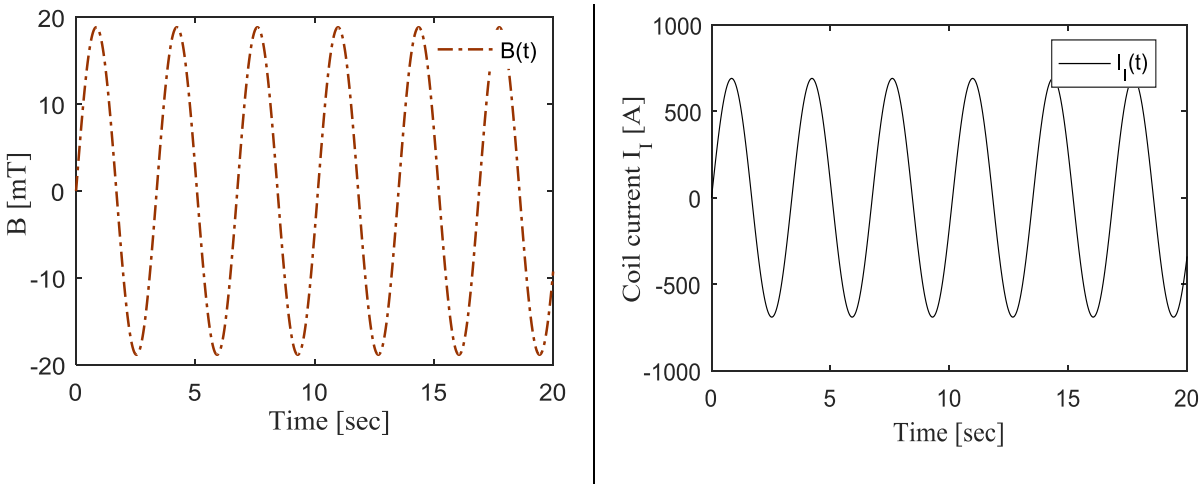

Figure 7.5: Variation of the coil current and the magnetic flux density of the IH-system for both the SG- and AC-adsorption reactors

The alternating current passing the induction coil I_I and the resulted magnetic flux density for both the SG- and AC-induction heating systems are shown in **F**ig. 7.5. So that the induction heating system for the SG- reactor and AC-reactor will be designed and simulated in this study in terms of the same input parameters $I_{I,max} = 690$ [A] and $B_{max} \cong 19$ [mT].

7.2.1 Induction coil design

The induction coil is the heart of the induction heating system. In the literature the coil is designed in various sizes and shapes according to the work-loads for a wide variety of heating operations. The induction coil considered is produced from a rectangular copper hollow profile whose wall thickness depends on the range of the skin depth at the present frequency $S_I(f)$ [130].

where S_I is the thickness of the induction coil rectangular wall.

Tab. 7.2 provides the details of the induction coil used in the IH-system for both the SG-and AC-reactors. The number of coil turns is mainly based on the height of the adsorption reactor and the pitch of windings. It can be easily derived the following expression.

$$N \approx \frac{H_I + P_I}{b_w + P_I}$$

where N, H_I, P_I and b_w are the turns number, the height, the pitch and the winding width of the induction coil, respectively.

	Parameter	Symbol	SG-Reactor	AC-Reactor
Induction Coil	Coil Height	H_I	460 mm	230 mm
	Internal Diameter	D_i	260 mm	260 mm
	External diameter	D_o	280 mm	280 mm
	Coil pitch	P_I	1 mm	1 mm
	Winding width	b_w	45 mm	45 mm
	Conductivity	σ_I	5.8×10^7 S/m	5.8×10^7 S/m
	Number of Turns	N	10	5
	Wall-thickness	S_I	2 mm	2 mm

Tab. 7.2: Results for the induction coil

Since the current flows predominantly in the inner wall of the profile and the wall thickness is small compared to the inner diameter of the coil, the problem can be considered as in a single-sided excited plate. For this case, the following calculation rules can be derived for the elements of the inductor [130-131].

The impedance of the induction coil Z_I is given as following:

$$Z_I = R_I + X_I\, j \tag{7.1}$$

where R_I is the ohmic resistance of the induction coil and given as following:

$$R_I = N^2 . \frac{\pi(2r_I + \delta_I)}{H_I\, \sigma_I\, \delta_I\, k_{cu}} (\varphi_I) \tag{7.2}$$

where δ_I, r_I and σ_I are the skin depth, inner radius and the electric conductivity of the induction coil. k_{cu} is a factor related to the mass of copper used.

The inductive reactance of the induction coil X_I is given as following:

$$X_I = 2\pi f\, K_N N^2 . \mu_0 . \frac{\pi . r_I^2}{H_I} (\Psi_I) \qquad (7.3)$$

The required impedance factors φ and Ψ, which serve to adapt to the given geometry, are shown in **F**ig. 7.6. They are determined as a function of the ratio of wall thickness S_I to skin depth δ_I [130].

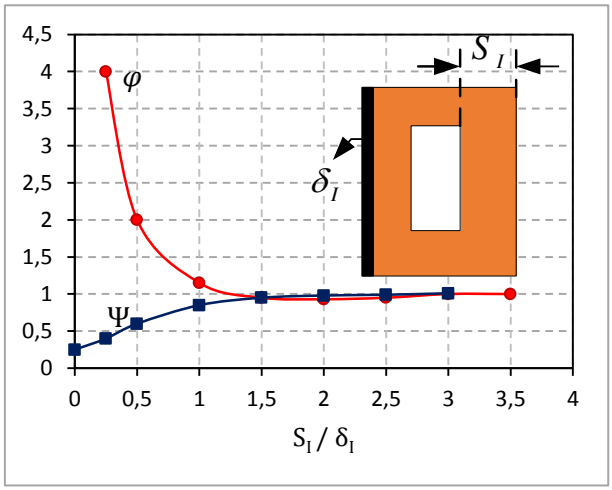

Figure 7.6: correction factors φ and Ψ [130]

The Nagaoka factor K_N is used to correct the inductance of the inductor coil due to the finite length of the coil [131].

The induction coil used for the SG-adsorption reactor is considered as a long coil ($H_I/D_i = 1.7$). So Nagaoka faktor K_N is calculated from Lundin's formula for long coils ($H_I > D_i$) as following:

$$K_N = \frac{[1 + 0.383901(D_i/H_I)^2 + 0.017108(D_i/H_I)^4]}{[1 + 0.258952(D_i/H_I)^2]} - \frac{4\ (D_i/H_I)}{3\pi}$$

Max. Error: 0.0003%.

Whereas the induction coil used for the AC-adsorption reactor is considered as short coil ($H_I/D_i = 0.88$). Lundin's formula for short coils $H_I \leq D_i$ is gives as:

$$K_N = \frac{2}{\pi}(H_I/D_i)\left[\frac{[\ln(4\,D_i/H_I) - 1/2][1 + 0.383901(H_I/D_i)^2 + 0.017108(H_I/D_i)^4]}{[1 + 0.258952(H_I/D_i)^2]} + 0.093842(H_I/D_i)^2 + 0.002029(H_I/D_i)^4 - 0.000801(H_I/D_i)^6\right]$$

Max. Error: 0.0002%.

Tab. 7.3 gives the simulation results of the induction coil, which is used in the induction heating system for both the SG- and AC- adsorption reactors.

	symbol	SG-Reactor	AC-Reactor	Unit
Induction Coil Design	L_I	11.313	5.004	µH
	X_I	1.800	0.796	Ω
	R_I	8.897	4.522	mΩ
	δ_I	0.415	0.415	mm
	K_N	0.780	0.69	-
	I_I	690	690	A

Tab. 7.3: Result for the induction coil

Leakage flux: Most of the magnetic flux, which is produced by the current passing the induction coil, is set up in the core of the induction coil and passes through the particular path that is through the air gap and is utilized in the magnetic circuit. This flux is known as useful flux. As practically it is not

possible that all the flux in the circuit follows a particularly intended path and sets up in the magnetic core and thus some of the flux also sets up around the coil or surrounds the core of the coil, and is not utilized for any work in the magnetic circuit. This type of flux which is not used for any work is called Leakage flux.

It can be notice from the circuit in **F**ig. 3 that, if the current I_E passing through the work-load is close to the induction coil current I_I, the reactance X_R is very large. However, if the magnetic flux is closed in the air, the cross-branch must not be neglected, and the current flowing through the work-load must be smaller than the inductor current. For both the SG-and AC- induction heating system is $H_a < H_I$, so the reactance X_R is calculated as following [130]:

$$X_R = \frac{\omega N^2}{\frac{H_I}{\mu_0 \pi r_I^2}\left(\frac{1}{K_N} - \frac{H_a}{H_I}\right)} \tag{7.4}$$

Air gap: The air gap existing between the induction coil and the adsorption reactor means the magnetic resistance and is noted in the magnetic circuit as reactance of X_K , i.e. reluctance to the magnetic flux density. The reluctance of a magnetic circuit is proportional to the length of the air gap inversely proportional to its cross-sectional area $\pi\,(r_I^2 - r_a^2)$ and a magnetic property of the given material called its permeability. The reactance of the air gap X_K is given as following [130]:

$$X_K = \omega N^2 \pi\,(r_I^2 - r_a^2)\mu_0 . \frac{1}{H_a} \tag{7.5}$$

7.2.2 Work-Load

The work-load (adsorption reactor) considered in this chapter consist of a cylindrical container of nonmagnetic material (SG- or AC- particles) in which Gr-balls are placed as shown in the **F**ig. 7.7.

The work-load can be modeled through its equivalent resistance R_E and inductance X_E. **F**ig. 7.8 illustrates the equivalent circuit of the adsorption reactor. Where R_E is the ohmic's resistance of both the nonmagnetic material R_1 and the Gr-balls R_2 whereas X_E represents the reactance of the nonmagnetic material X_1 and the Gr-balls X_2.

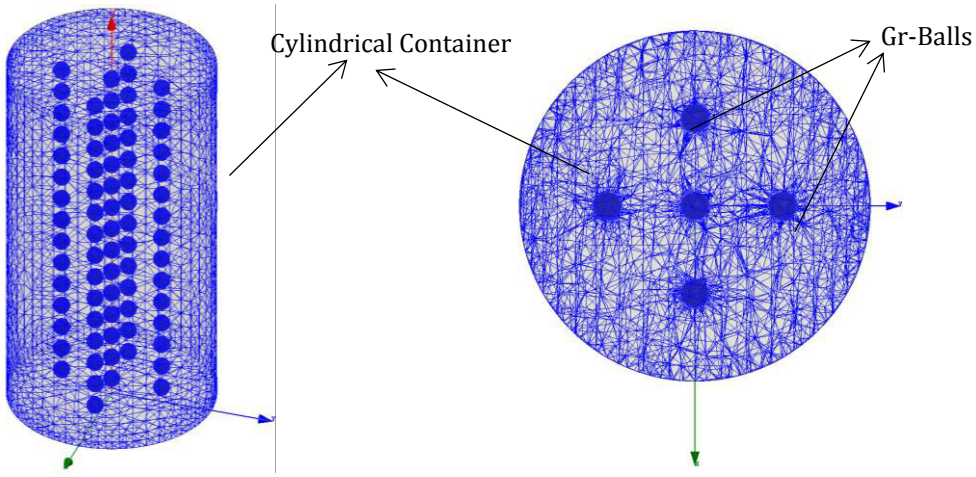

Figure 7.7: The work-load of the induction heating system

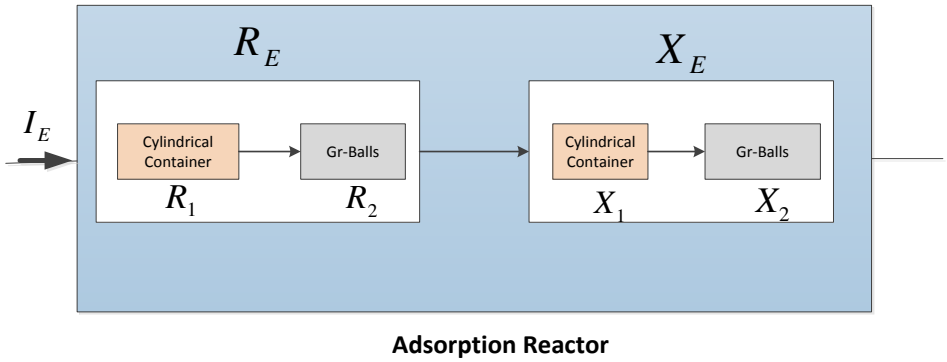

Figure 7.8: Equivalent circuit of the work-load studied

The software **A**NSYS **E**lectronics 17.2 was used for simulation of the magnetic field distribution $\vec{B}$ and to determine the total power P_E induced inside the adsorption reactor in order to know the equivalent circuit of the work-load depending on the following equations.

The resistance of the work-load R_E can be written as follows:

$$R_E = R_1 + R_2 \tag{7.6}$$

$$P_E = P_1 + P_2 = \int_V \frac{1}{\sigma} |\vec{J}|^2 dV = \int_V p_v . dV = R_E . I_E^2 \tag{7.7}$$

where P_E is the useful power induced inside the work-load (Gr-balls and the adsorption medium). P_1 and P_2 are the power induced inside the adsorption medium and the power induced inside the Gr-balls, respectively. Because of dielectric of the cylindrical container (adsorption medium), no power $P_1 = 0$ can be induced inside it, this means $R_1 = 0$.

The inductive reactance of the work-load can be written as follows:

$$X_E = X_1 + X_2 \tag{7.8}$$

$$Q_E = Q_1 + Q_2 = \int_V \frac{1}{\mu} . \omega . |\vec{B}|^2 . dV = X_E . I_E^2 \tag{7.9}$$

where Q_E reactive power of the work-load.

Tab. 7.4 shows the simulation results of the leakage flux reactance X_R, the reactance of the air gap X_K and the results of the equivalent resistance R_E and inductance X_E of the work-load for both the SG- and AC- induction heating systems.

This means that all ohmic resistances and inductive reactances of the occurring elements in the equivalent circuit **F**ig. 7.4 were completely determined.

	symbol	SG-Reactor	AC-Reactor	Unit
Work-Load	R_E	8.734	6.009	mΩ
	X_E	1.207	0.844	Ω
	X_R	7.598	2.342	Ω
	X_K	0.178	0.091	Ω
	I_E	583.6	493.4	A
	δ_E	10	10	mm
	P_E	2975	1463	W

Tab. 7.4: Result for the Work-load

7.2.3 Reduced equivalent circuit

For the sake of simplicity, the equivalent circuit of the induction coil and the work-load are presented as shown in **F**ig. 7.9.

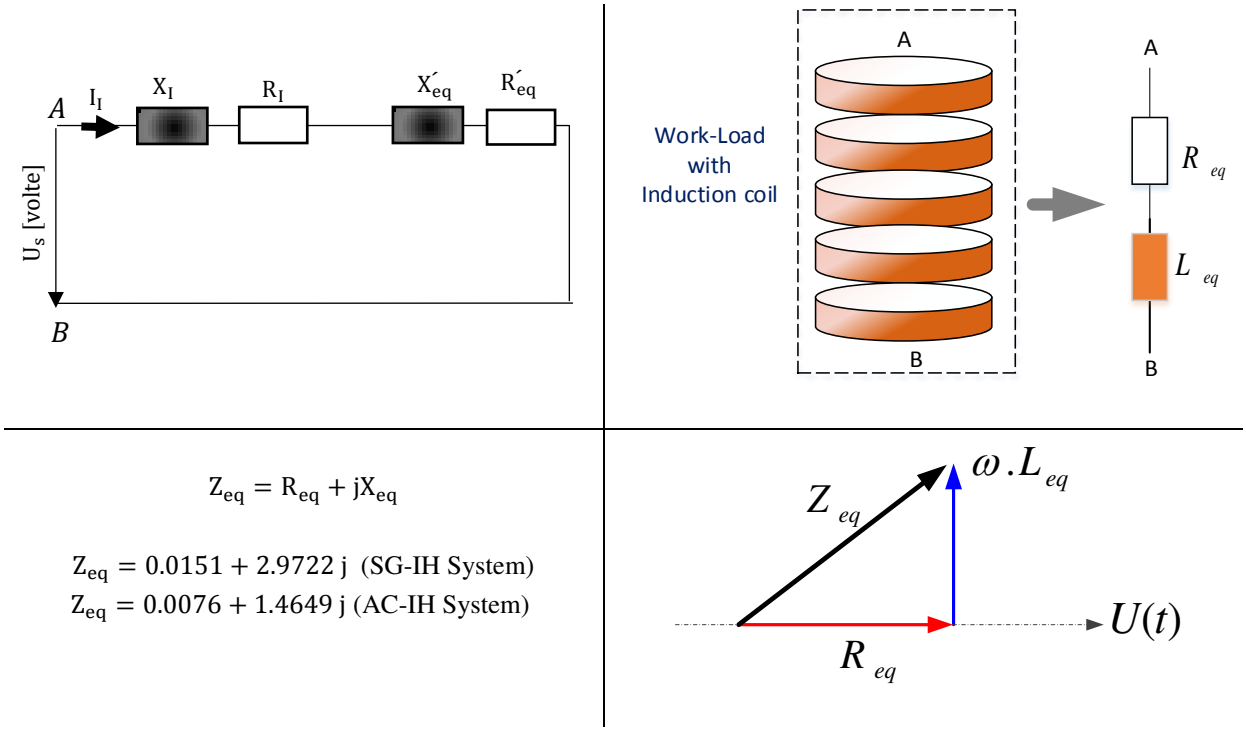

Figure 7.9: Equivalent of the induction coil and the work-load

The impedance of the work − load Z'_{eq} is given as following :

$$Z'_{eq} = R'_{eq} + jX'_{eq},$$

$$Z'_{eq} = \frac{(R_E + j(X_E + X_K))\, jX_R}{R_E + j(X_E + X_K) + jX_R} \tag{7.10}$$

The induction coil, Gr-balls and cylindrical container can be modeled through its equivalent resistance R_{eq} and inductance L_{eq}.

The equivalent impedance Z_{eq} of the IH − circuit is given as following:

$$Z_{eq} = (R'_{eq} + R_I) + (X'_{eq} + X_I)j \tag{7.11}$$

7.2.4 Performance and efficiency

The complex power is the vector sum of the active power P_a [W] and the reactive power Q_r [V. A. R]. The apparent power S[V. A] is the magnitude of the complex power. From all the ohmic and inductive resistances, the apparent power for the induction coil can now be set up as follow [121].

$$S = P_a + jQ_r \;\Rightarrow\; S = I_I^2 . (R_{eq} + jX_{eq}) \tag{7.12}$$

The electrical efficiency is defined as the ratio of the induced power inside the Gr-balls P_E (useful power) to the active power P_a and is denoted by the following equation [121,130]:

$$\eta_{el} = \frac{I_E^2 . R_E}{I_E^2 . R_E + I_I^2 R_I} = \frac{P_E}{P_a} \tag{7.13}$$

Tab. 7.5 shows the simulation results of the equivalent circuit of the induction coil and the work-load. We notice based on these results that both the resistance R_I and the inductance X_I of the induction coil used are bigger than the resistance R'_{eq} and the inductance X'_{eq} of the work-load.

	Symbol	SG-IH System	AC-IH System	Unit
Work-Load + Induction Coil	R'_{eq}	6.2	3.1	mΩ
	X'_{eq}	1.17	0.66	Ω
	R_{eq}	15.1	7.6	mΩ
	X_{eq}	2.97	1.46	Ω
	P_a	7.21	3.88	kW
	Q_r	1415	775	kVAr
	η_{el}	41.25	40.43	%

Table 7.5: Results of the equivalent circuit of the induction coil and the work-load

7.3 Oscillatory circuit

In induction heating system, the eddy currents are induced inside the work-load by a varying magnetic field that is obtained by means of a varying current circulating in the induction coil. Therefore to have a high varying current in the induction coil, the oscillatory circuit, which formed by the induction coil and a capacitor in series or in parallel, is used (series circuit in this study). This oscillatory circuit, also known as resonant circuit tank, is usually fed by a converter [132].

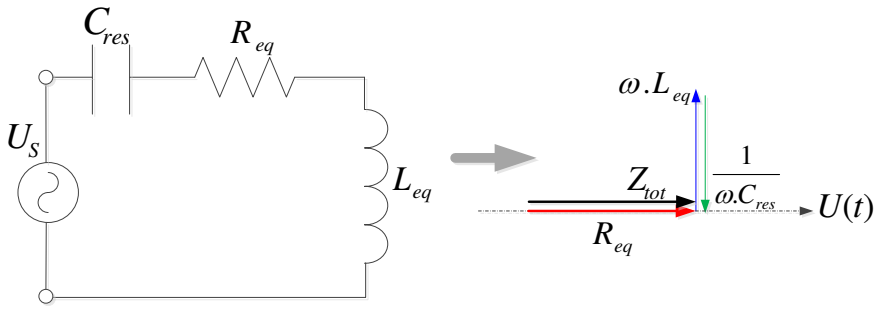

Figure 7.10: Equivalent of series resonant circuit

As shown in **F**ig. 7.10 capacitor is inserted in a circuit to partially compensate for reactive power which consumed by the load. Where R_{eq} and L_{eq} are the resistor and total inductance respectively and C_{res} is the resonant capacitor. Conventionally, capacitors are treated as if they generate reactive power and inductors as if they consume it. If a capacitor and an inductor are placed in parallel or series, then the currents or voltages flowing through the capacitor and the inductor tend to cancel rather than add. This is the fundamental mechanism of the resonant circuit for controlling the power factor. The applied voltage U_S will be the vector of the three components as follows [121]:

$$U_S = R_{eq} . I(t) + L_{eq} . \frac{dI(t)}{dt} + \frac{1}{C_{res}} \int I . dt \tag{7.14}$$

The system impedance is given by expression (7.15). At the resonant frequency, the equivalent impedance is equal simply to a resistor [132].

$$Z_{tot} = \sqrt{R_{eq}^2 + (\omega . L_{eq} - \frac{1}{\omega . C_{res}})^2} \tag{7.15}$$

$$Z_{tot}(f) = R_{eq} \tag{7.16}$$

Tab. 7.6 gives the results for the equivalent oscillatory circuit.

	Symbol	SG-Reactor	AC-Reactor	Unit
Equivalent Circuit	L_{eq}	18.675	9.204	µH
	R_{eq}	15.145	7.600	mΩ
	C_{res}	2.114	4.289	µF
	Z_{tot}	15.145	7.600	mΩ
	f	25.330	25.330	kHz

Tab. 7.6: Results for the equivalent oscillatory circuit

7.4 Transformer

When the voltage is stepped up, the current is stepped down, and vice versa. A simplified circuit of the matching transformer with load can be drawn according to **F**ig. 7.11.

The inverter is connected to transformer and series resonant circuit. This consists of an equivalent inductance representing the induction coil and work-load in series with high-frequency compensating capacitor [132-133].

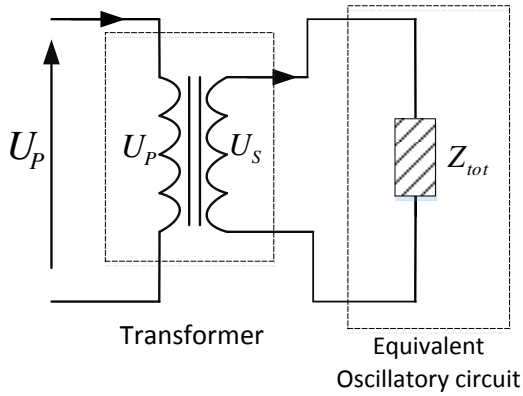

Figure 7.11: Transformer with the equivalent circuit of the induction heating system

The relationship between the voltages in the secondary circuit (the oscillatory circuit) U_s and the primary U_P circuit is determined by the ratio of the turns in each side.

$$\frac{U_s}{U_p} = \frac{N_s}{N_p} \tag{7.17}$$

Here, N_s and N_p represents the turns in the secondary and primary, respectively. Similarly, the relationship between the primary I_p and the secondary current I_s is also given by:

$$\frac{I_p}{I_s} = \frac{N_s}{N_p} \tag{7.18}$$

Fig 7.12 shows the coil current (bleu signal) and voltage (red signal) variations of the secondary circuit studied (the oscillatory circuit) for both the SG- and AC- induction heating systems which are considered in this study.

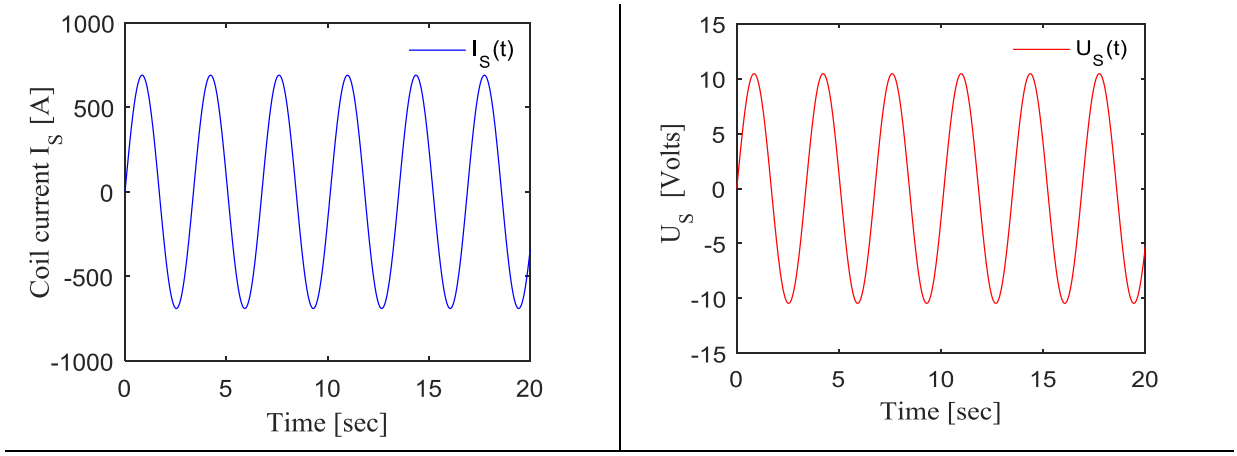

(a) SG-Induction Heating System

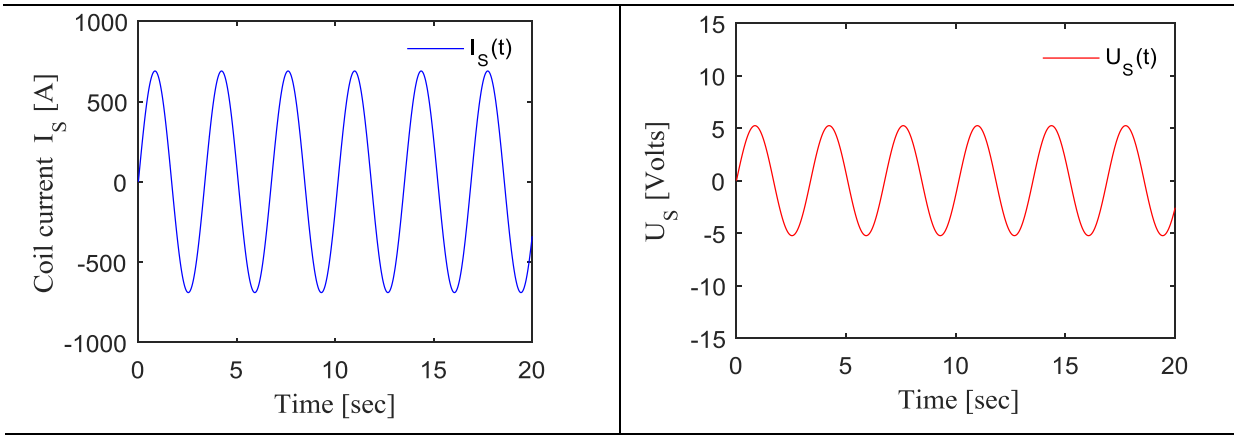

(b) AC-Induction Heating System

Figure 7.12: The coil current (bleu signal) and voltage (red signal) variations of the secondary circuit for both the SG- and AC- induction heating system

The simulation results of the primary and secondary circuits of both the SG- and AC-IH systems are shown in **T**ab. 7.7.

	Symbol	SG-Reactor	AC-Reactor	Unit
Transformer Design	I_S	690	690	A
	I_P	75	75	A
	U_P	96.143	48.18	volte
	U_S	7.210	5.237	volte
	N_P	92	46	turns
	N_S	10	5	turns
	P_{in}	7772.2	3886.1	W

Tab. 7.7: Results for the transformer used

Figure 7.13 shows the input voltage (black signal) and current variations (bleu signal)variations of the primary circuit studied for both the SG- and AC- induction heating system considered in this study.

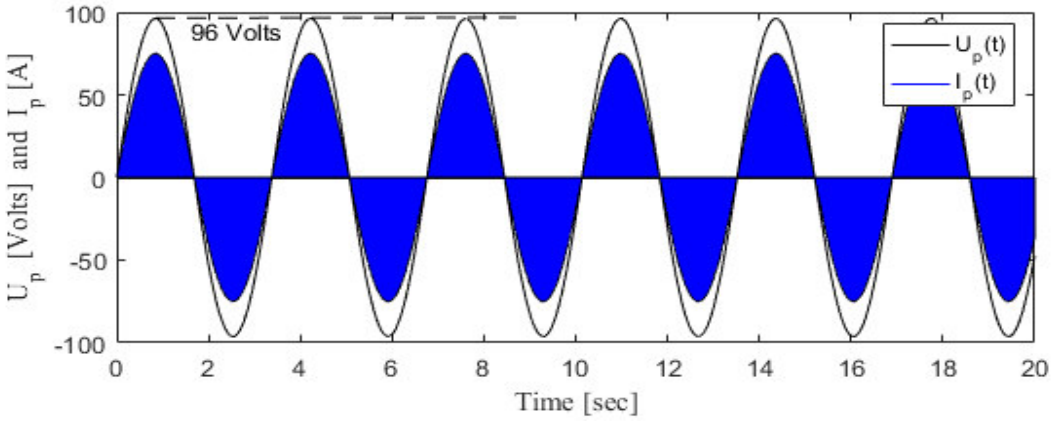

(a) SG-Induction Heating System

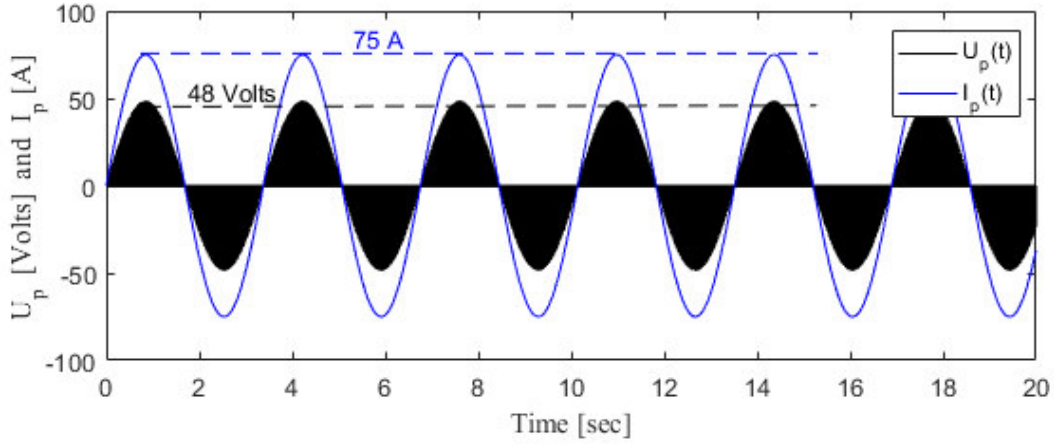

(b) SG-Induction Heating System

Figure 7.13: Input voltage (black signal) and Current variations (bleu signal) of the primary circuit.

7.5 Summary and conclusions

In order to use the induction heating technology as a new heat source to heat the nonmagnetic materials silica gel and activated carbon, it is necessary to study, design and analyze the structure of both the SG- and AC- induction heating systems, which were the main aims of the present chapter. To achieve these aims, the following objectives were implemented:

1. Determine the proper size of two induction coils (the height, number of the loops and the section-shape), which must be appropriate to the SG-and AC-adsorption reactors.
2. Present and analyze the magnetic and electric circuit of both the IH-systems in order to calculate the ohmic and inductive resistances of both the work-load and the induction coil.
3. Study the oscillatory circuit (the secondary circuit) to know the currents I_S and the voltages U_S in order to determine the appropriate currents I_P and the voltages U_p in the primary circuit.
4. Comparison study between the SG- and AC-induction heating systems in terms of the parameters studied (coil design, calculation of the ohmic and inductive resistances, analyze both the secondary and primary circuits).
5. Evaluate of the induction heating system by determining the coil loss, the useful power induced inside the Gr-balls P_E, the active power P_a, the total input power P_{in} and the electrical efficiency for both the SG- and AC- induction heating systems.
6. Develop a simulation computer program using **MATLAB** software.

In terms of desorption, the same amount of methanol from each adsorption reactor, the SG-and AC-reactors must have different sizes and configurations of the induction coil and the adsorption reactor. As shown in **F**ig. 7.14 the size of the SG-reactor has a double size in comparison with AC-reactor and the SG-induction coil has a double height and double turns number in comparison with AC-induction coil. So that the desorption process as in the fourth, fifth and sixth chapters was simulated by using 7.95 kg of silica gel and 1.9 kg of methanol in the SG-adsorption reactor and also by using 3.31 kg of activated carbon and 1.36 kg of methanol in the AC-adsorption reactor.

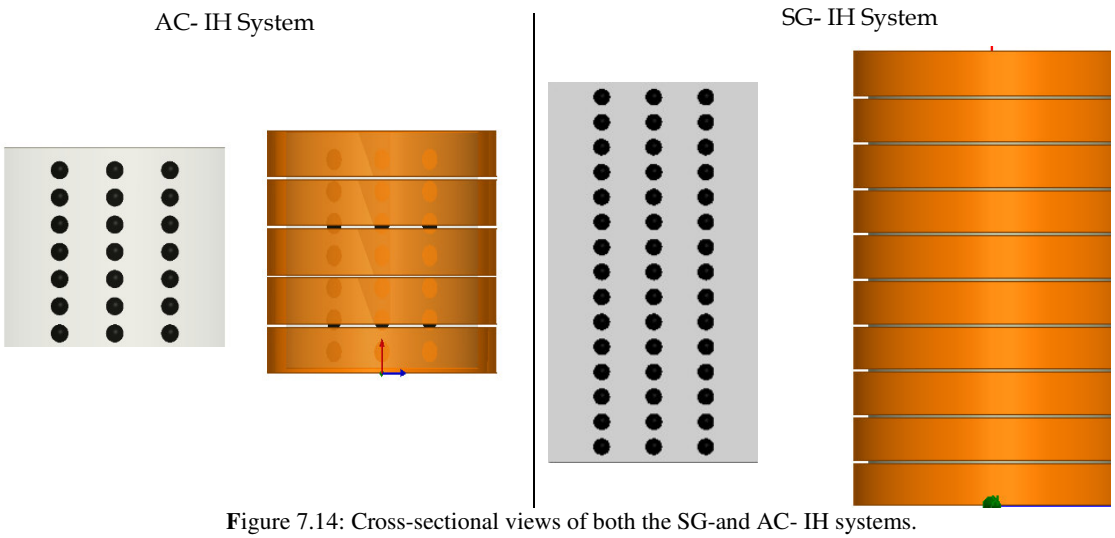

Figure 7.14: Cross-sectional views of both the SG-and AC- IH systems.

In context of desorption process study by applying the same induction current of 690 A passing both the SG-induction coil and AC-induction coil at same induction frequency 25 kHz it is found, that the required useful power for the AC-IH system is less by about 50 % in comparison with the required useful power for the SG-IH system. Although the required useful power of the AC-IH system is lowered by about 50 %, but this power can also achieve more desorbing amount about 1.3 kg at the desorption temperature of 100 °C in comparison with the SG-IH system, which requires double the power and takes about 10 min to desorb 1 kg of methanol at the same temperature 100 °C as shown in **F**ig. 7.15.

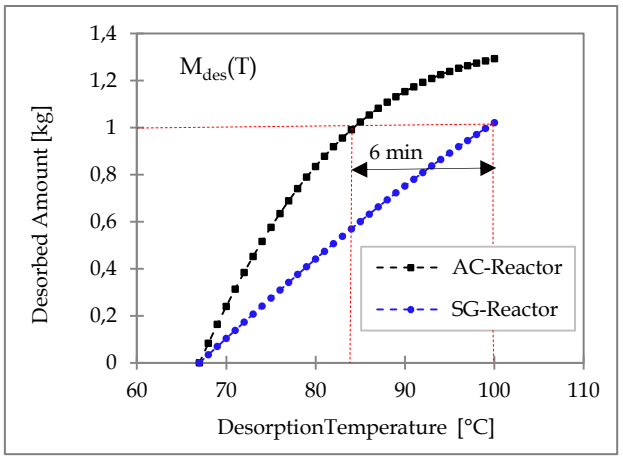

Figure 7.15: Comparison between SG-adsorption reactor and AC-adsorption reactor for the desorbed amount M_{des} at $I_{max} = 690A$, $f = 25$ kHz and $\delta = r_i = 10$ mm

To desorb 1.3 kg of methanol, the AC-reactor takes about 20 min, whereas to desorb 1 kg of methanol with the same applied input power the desorption process takes a lesser duration time of about 16 min.

Fig. 7.16 shows comparison between SG-IH system and AC-IH system for the power flow from the input power unit to the work load.

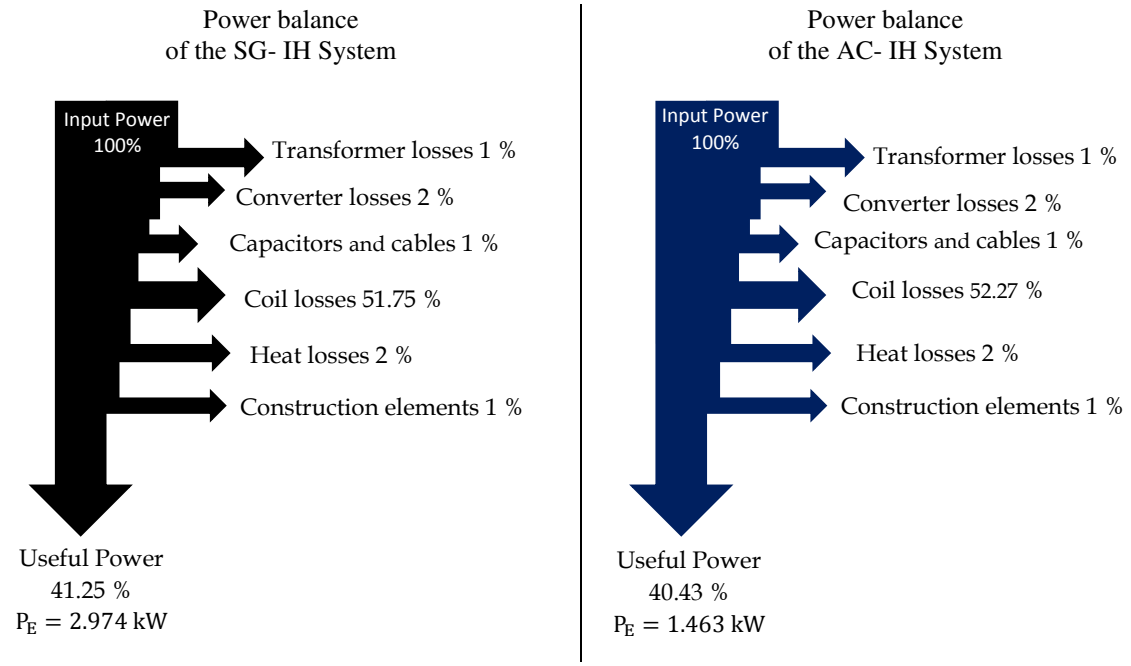

Figure 7.16: Comparison between SG-IH system and AC-IH system for the power balance flow from the power unit to the work load.

It is found based on the simulation results, that the power efficiency of the SG- IH system (41.25%) is slightly larger than that of the AC- IH system (40.43 %). This can be explained by the loss in the induction coil, which is essential factor and depends of the coil dimensions. So that the coil loss of the AC-IH system is slightly larger by about only 0.52 % than that of the SG-IH system. We noticed based on the results of this study that both the resistance and the inductance of the used induction coil are bigger than the resistance and the inductance of the work-load. This means the power loss in the induction coil is more than the useful power induced inside the work-load.

Efficiency of the induction heating system for both the SG- and AC- adsorption reactors is expressed as a total, deducting electrical and heat transfer losses, which are estimated to 7 % of the total input power P_{in} based on the literature. Electrical losses consist in transformer, frequency converter, condenser, wiring, cable and coil. Heat losses in IH system consist of conduction loss of heat through the induction coil walls and radiation loss of heat released from induction coil wall to the ambient.

Chapter 8

Verification, Validation and Comparison

8.1 Introduction

This chapter is devoted to the verification and validation of the Adsorption Ice Production AIP system presented in this work. Currently, the Adsorption Ice Production AIP system does not exist in the literature or in the labor market, this innovative technology works using two different adsorption materials together in one system, thus an experimental set up of ACS 08 system from the manufacturer SorTech AG, which is built in Holzminden (Germany), is done to make validation of some simulation results of the AIP system. But the Adsorption chiller of the SorTech ACS 08 employs silica gel/water as the adsorbent/adsorbate working pair. Therefore, a new numerical program was developed as the same program which has been written for the AIP-system presented in this work, and based on the real data taken from the ACS 08 machine. Here, the simulated data are compared to the measured data of the ACS 08 system which is built in Holzminden and tested by us. The comparison is conducted for the real processes inside the adsorption reactor, the coefficient of performance of the system, the refrigeration capacity and the required time to complete the processes of one cycle.

In addition, the verification of this new technology is investigated currently by comparing the com-AIP system studied in this work with two separate systems: the first system works using one adsorbate/adsorbent pair (silica gel/methanol) in two beds and the second also works using one adsorbate/adsorbent pair (Activated carbon/methanol) also in two beds.

The third part of this chapter presents a comparison between two methods the induction heating and thermal heating of both the SG-and AC-adsorption reactors, which had studied in frame of this work. This comparison will done in terms of the adsorption reactor design, the required input power, the energy consumption per hour, the required desorption time and the losses in both the adsorption reactors in order to desorb the same amount of methanol ($1\,\mathrm{kg_{meth}}$) using the induction heating technology and the conventional method (thermal heating)

8.2 Description of the experiment

Fig. 8.1 shows the thermally driven ACS 08, which has a compact design and is a novel single effect, silica gel/water adsorption chiller with nominal cooling capacity of 7.5 kW, developed by SorTech AG. The system is developed for residential and office buildings as well as other cooling applications. Presently several chillii® solar cooling kits 8 are installed in Germany, Austria, Italy and China. The first experiences of the installed solar cooling systems showed that the chillers and the systems work very well.

The internal structure of the ACS 08 consists of four main components: an evaporator, condenser and two adsorption elements, interchanging periodically between adsorber and desorber function. All hydraulic components, necessary for the internal switchings, are installed inside of the chiller, this allows an easy connection of the chiller to the external three hydraulic circuits (high temperature source HT, heat rejection circuit MT and chilled water circuit LT). Fig. 8.3 presents the operation

phase, of which the upper of the two sorption compartments is currently being desorbed by applying hot water and the lower sorption compartment is working as adsorber, thus taking up the vaporized refrigerant. The refrigerant circle, either fluid or vaporized, is not included in the figure.

Figure 8.1. Adsorption chiller of the SorTech ACS 08 (source: SorTech)

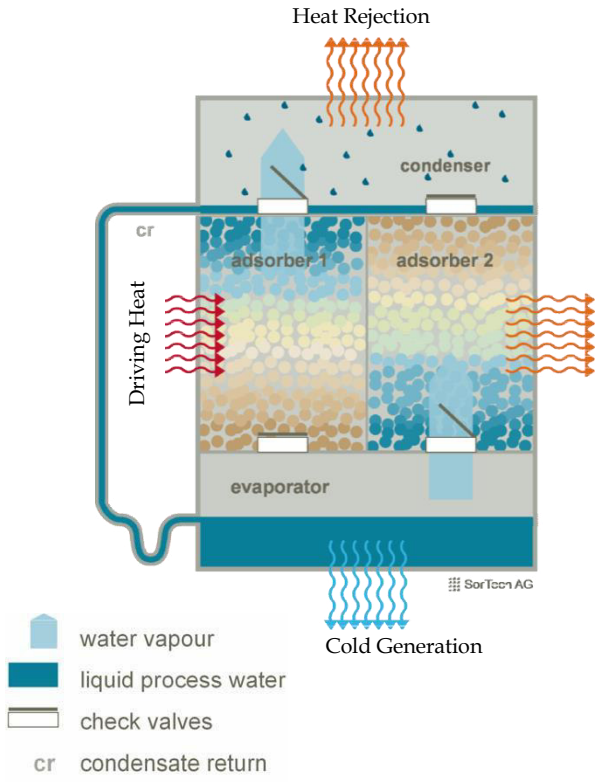

Figure 8.2: Working process of the adsorption chiller (source: SorTech)

8.2.1 Working principle of the adsorption chiller

The working principle of the ACS 08 chiller can be described in four steps as shown in Figs. 8.2 and 8.3.

Step 1: Desorption through heat

Heating water HT coming from the heat source flows into the first heat exchanger (adsorber 1). The adsorbent is dried by heat input. Water vapor is freed from the adsorber 1 and flows into the condenser. When the material is dry, the heat input in the adsorber 1 is stopped and the upper check valve closes.

Step 2: Condensation

The desorbed refrigerant (water vapor) is liquefied in the condenser under heat rejection. In the heat rejection circuit MT the cooling water flowing in the condenser allows to remove the condensation heat.

Step 3: Evaporation

Then, the adsorbate (liquid condensate) flows from the condenser to the evaporator and evaporates there at evaporation temperature. The evaporated adsorbate seizes the heat from chilled water and generates cold, which can be used for air-conditioning (chilled water circuit LT).

Step 4: Adsorption

During the evaporation process the lower check valve to the adsorber 2 opens. After that, the adsorbent (silica gel in adsorber 2), adsorbs the refrigerant (evaporated vapor) that is coming from the evaporator, at which cooling water removes the adsorption heat under heat rejection circuit MT. In order to achieve a continuous cooling production the two adsorbers work in combination, i.e. one adsorber desorbs while the other adsorber generates cold by adsorbing in the meantime.

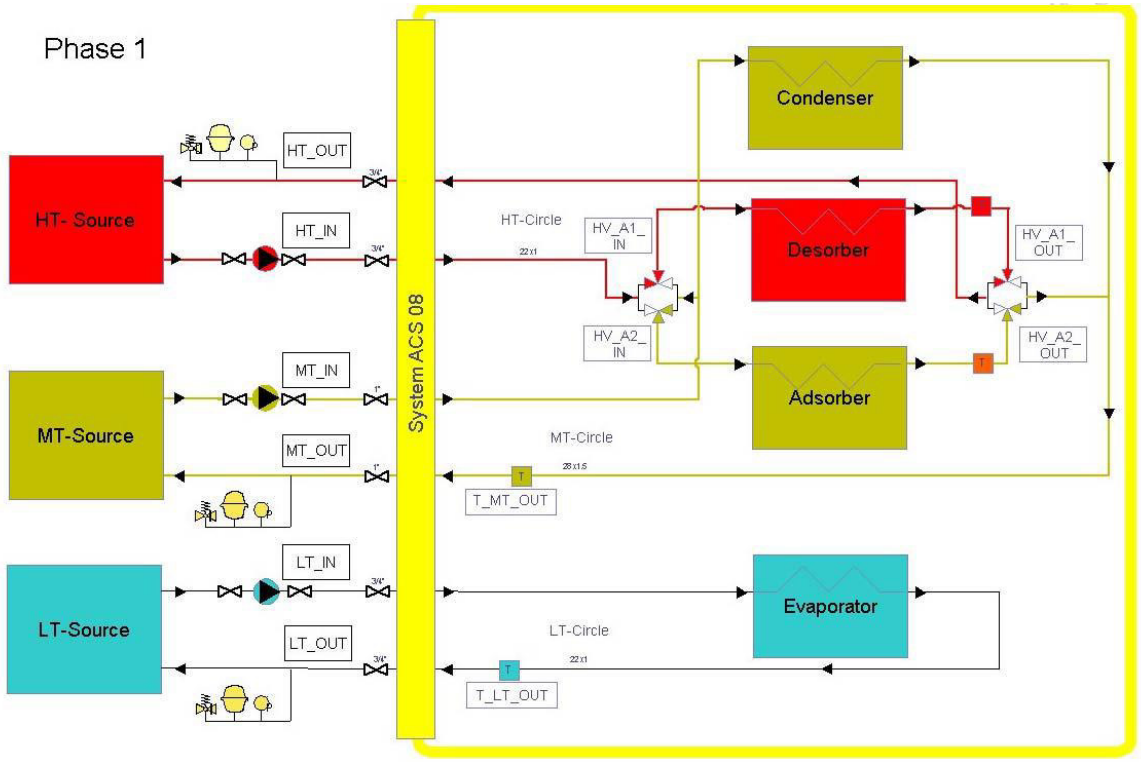

Figure 8.3: Main internal hydraulic components of the SorTech chiller and external connections (Source: SorTech AG)

8.2.2 Adsorbent/Adsorbate working pair

The SorTech chiller uses silica gel as adsorbent. Silica gel is a porous glass with a high capacity of adsorbing water vapor. For that reason, it is used as desiccant in various applications.

Product description: Glassy, hard spherical with high purity of approx. 99.5 % SiO_2 (dry basis) and an internal surface area of approx. 800 [m^2/g]. Because of its very large surface area SG exhibits a high adsorption for water vapor. SG can be reactivated without significantly impairing the efficiency. It is therefore very economical, easy to dispose of without any known adverse effects on the environment.

Standard grain sizes: Spheres Ø 0.5 – 1.5 mm, Ø 1.6– 2.5 mm and Ø 2.0 – 4.0 mm

Formula: $SiO_2 . n\ (H_2O)$ (Amorphous form of silica)

In the ACS 08 machine, the refrigerant is water, which results in the technical task that the machine has to be operated at very low pressures in a vacuum tight containment.

Figure 8.4: Photo of a silica gel coated tube and fin adsorber heat exchanger (source: SorTech)

8.2.3 Operation conditions

Tab. 8.1 summarizes the main technical features of the two chiller products under rated operation conditions. The machine may also be used under other temperature conditions (see as an example the variation of cooling capacity and COP as a function of heat source temperature in **F**ig. 8.7).

	Parameter	**Unit**	**Value**
Driving Heat Circuit	Temperature in/out	°C	72/65
	Volume flow	m^3/h	1.6
	Pressure loss	mbar	230
	Operating pressure max.	bar	4
Heat Rejection Circuit	Temperature in/out	°C	27/32
	Volume flow	m^3/h	3.7
	Pressure loss	mbar	350
	Operating pressure max.	bar	4
Chilled Water Circuit	Temperature in/out	°C	18/15
	Volume flow	m^3/h	2
	Pressure loss	mbar	300
	Operating pressure max.	bar	4
Electricity supply	Voltage	V	230
	Frequency	Hz	50
	Power consumption	W	7
Dimensions	Length	mm	790
	Width	mm	1060
	Height	mm	940
	Weight (empty)	kg	265
	Operating Weight	kg	295

Table 8.1: Technical data for nominal operation conditions of the adsorption Chiller ACS (Source: SorTech AG)

8.3 Description of the simulation Procedure

The analysis of the adsorption system working with silica gel/ water as the working pair has been investigated using a simulation program written in **MATLAB.** This program is designed to analyze the thermodynamic cycle parameters of this technique. The previously of coupled equations (mentioned in the third chapter) is solved by finite difference approximation with a temperature step of one grad Celsius and with a time step of one second.

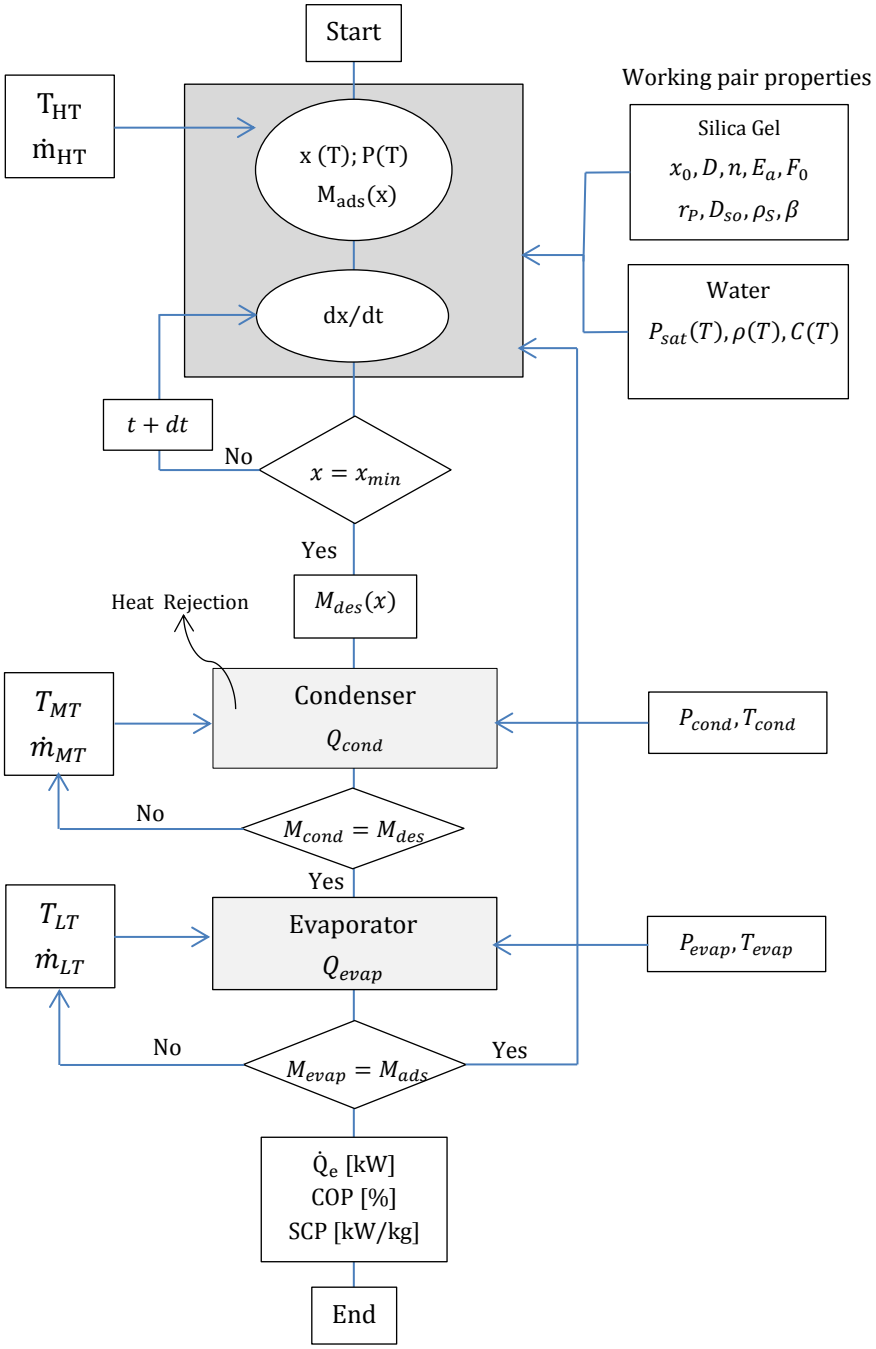

Figure 8.5: Schematic representation of calculation procedure

The numerical code was written and developed to make a comparison between the ACS 08 system existing in Holzminden (Germany) and the numerical code operating with the same working pair silica gel/water depending on the same real working conditions. The boundary conditions used were similar

to the conditions used in ACS 08 system experimental setup tested in Holzminden-laboratory. The simulation uses embedded **Refprop** thermophysical properties of water. The schematic representation of calculation procedure is shown in **F**ig. 8.5.

The investigation focused on the effect of the adsorption reactor temperature, the desorbed refrigerant mass from the adsorption reactor M_{des}, the cycle time t_{cycle} and the coefficient of performance COP as well as the refrigeration capacity $\dot{Q}_e$.

8.4 Comparison between numerical and experimental results

SorTech AG provides a program based on Excel for the calculation of refrigeration capacity and COP under all temperature conditions. The control of the adsorption chiller is managed in a way, that it is easy to operate the machine under partial load. The inner adsorption-desorption cycle of the system is automatically adjusted to the cooling demand. Therefore, under certain temperature conditions there is not a single value but a range of COP and cooling powers under which the machine may be driven.

The relative error $\in_r$ between the experimentally and simulation obtained results was calculated as follows:

$$\in_r = \sqrt{\frac{\sum_{i=1}^{n}(F_{exp}(i) - F_{sim}(i))^2}{\sum_{i=1}^{n}(F_{exp}(i))^2}}$$

Where $F_{exp}(i)$ and $F_{sim}(i)$ are the experimental and simulation results, respectively.

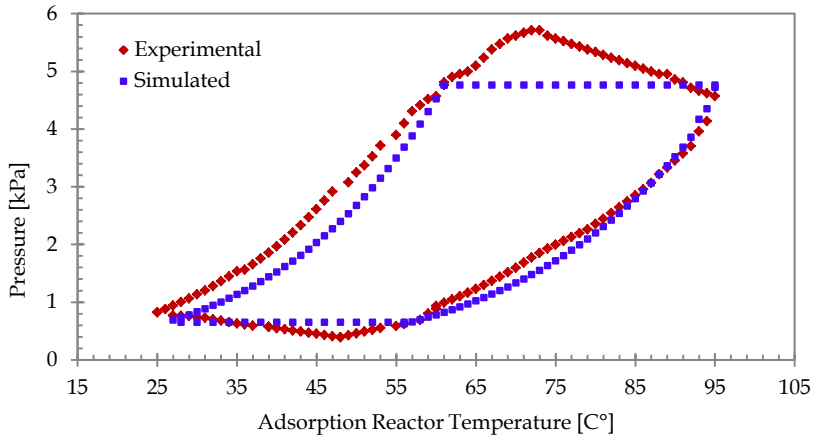

Figure 8.6: Simulated and experimental working processes inside the adsorber/desorber versus the temperature

For all heating and cooling loops the pressure and temperature are recorded and measured by thermometers placed in the adsorber and desorber. **F**ig. 8.6 shows the numerically and experimentally obtained working processes. The processes of one cycle presented as blue-dotted line are more theoretical and simulated based on the key points of the reversible process. In reality as shown in **F**ig. 8.6, the real working operation differs from the simulated because of the following aspects:

- After the circuit starts, the adsorption reactor firstly takes some time in order to change the temperature. Therefore the pressure in the evaporator increases and the pressure in the condenser drops. As a result, the valves (the valve between the evaporator and the adsorber, and the valve between the desorber and condenser) are opened earlier than shown in **F**ig. 8.6 for simulated working processes.

- The heat transfer surfaces are subject to a pinch point, which is varies with performance.
- The mass transfer between vapor and adsorption material is a function of the concentration difference.
- At the valves, pressure losses occur, which are dependent on the flow rate.

In spite of these effects, it can be noticed from **F**ig.8.6, that simulation results agree partly with experimental data. The relative error between the experimentally and numerically desorption and adsorption processes are 1.7% and 0.9 %, respectively.

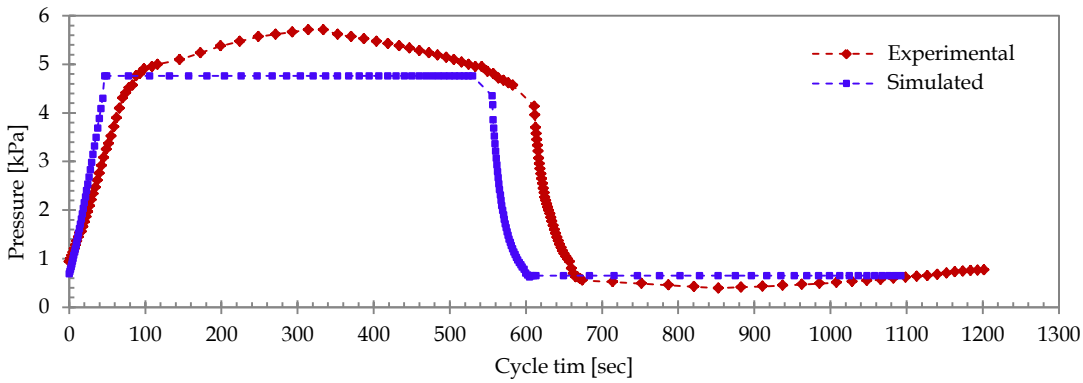

Figure 8.7: Simulated vs experimental pressure in the adsorber/desorber bed.

Fig.8.7 shows the simulated pressure profile versus the measured pressure profile of the adsorber/desorber. Although the desorption and adsorption processes occur as isobaric process, but the experimental pressure was not constant during desorption and adsorption processes because it is affected by temperature fluctuation in the condenser and evaporator, respectively, which is not taken into account in the simulation procedure.

It can be concluded that the simulation achieves one cycle in 1100 s, and good agreement has been found between measured and simulated pressures at pre-heating and pre-cooling processes. Whereas the real working processes takes about 1230s.

In order to quantify the adsorption system performance, the thermal COP (defined as the ratio of chilling output to heat input) and the mean refrigeration capacity over the simulation period are used.

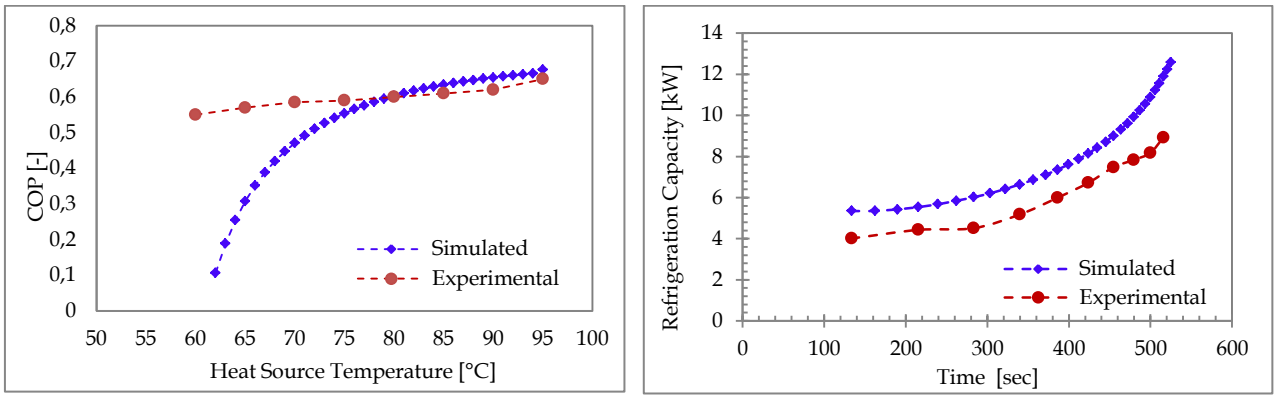

Figure 8.8: Comparison between experimental measurements (blue-dotted lines) and numerical predictions (red-dotted lines) for the coefficient of performance COP and cooling capacity SCP

In **F**ig. 8.8, a comparison between the measured coefficient of performance COP and its result from the simulation is presented with varying heat source temperature, as well as the refrigeration capacity

with operation time. The graphs show that the numerical results follow very similar trends to experimental data. The relative error between the experimentally and numerically COP and SCP are 3.51 % and 8.55 %, respectively.

The maximum absolute error for COP is 27 %, which is observed at 60 °C. The main source of this error of the numerical work is explained as follows:

For the temperature range which is more than 75 °C, the numerically and experimentally results of COP are in good agreement, whereas at low temperature range the difference between the results of COP is about 20 %. This difference is caused by uncertainties of the physical properties used in the numerical model namely adsorbate concentration x [kg/kg], which is simulated based on by Dubinin-Astakhov equation (it is usually used with little error). Furthermore, the desorption process inside the ACS 08 system begins earlier than inside the numerical model. The desorption process in the simulation model does not start before 61 °C this means there is no desorbed refrigerant mass.

8.5 Evaluation of com- Adsorption Ice Production AIP System

In order to assess the effectiveness of com-AIP system proposed on the driving energy required from external heat source Q_{in}, a comparison with two AIP systems is made taking into account the performance COP and the desorbed amount M_{des}. The first system works using silica gel/methanol and the second works using activated carbon/methanol as working pair. The modeling of both the two systems has been simulated also using a **MATLAB** program.

Parameter	Value	Unit
Hot water inlet temperature	100	[°C]
Hot water inlet flow rate	0.232	[kg/sec]
Cooling water inlet temperature	24	[°C]
Cooling water inlet flow rate	0.4	[kg/sec]
Chilled water inlet temperature	15	[°C]

Table 8.2: Standard operating conditions

The comparison with two AIP systems is made under the same operating conditions and the three adsorption reactors are taken the same design (four HTF-tubes and 90 fins). The standard operating conditions are shown in **T**ab 8.2.

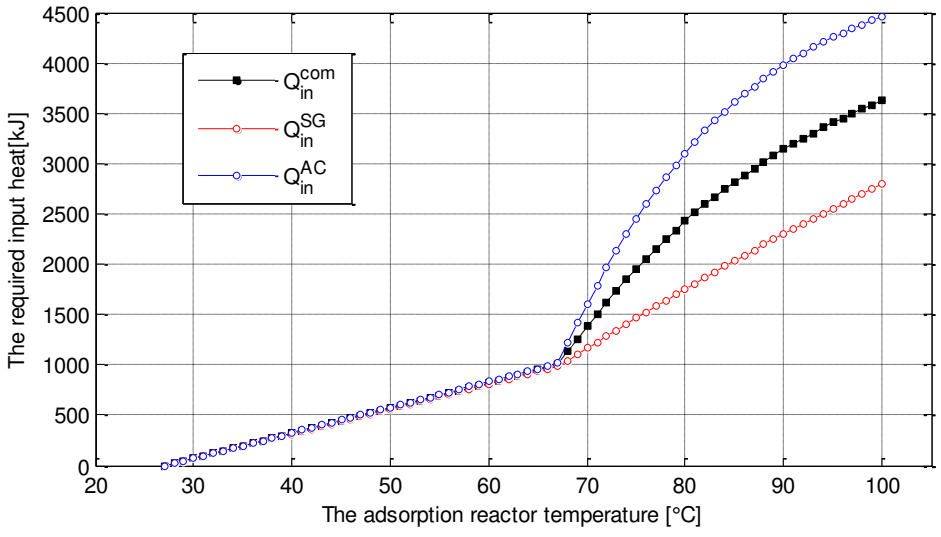

Figure 8.9: The driving energy added to the SG-bed, AC-bed and com-bed during the isosteric preheating and isobaric desorption processes

As shown in the **F**ig. 8.9 the added energy Q_{in}, which is introduced to the com-, SG- and AC-adsorption reactor of these three systems is demonstrated versus the adsorption reactor temperature. The total amount of the required input energy to activate the silica gel adsorption reactor is estimated to 2796 kJ per cycle and to 4460 kJ for activated carbon adsorption reactor.

In comparison with the SG-bed and the AC-bed, we can notice that the driving energy required to activate the novel strategy of com-adsorption reactor is smaller than the required energy in AC-bed and is estimated to be 3628 kJ, and thus it is bigger than the required energy in SG-system but the com-adsorption reactor can produce the double amount of ice because of ability to desorb more amount of the refrigerant under the same operating conditions. The amount of the refrigerant desorbed from the com-adsorption reactor is larger by about 45 % than the desorbed from the SG-reactor.

As noticed from the plot in **F**ig. 8.9, the temperature increases rapidly with respect to the driving energy during the preheating process in comparison with the desorption process. The reason is that all of the energy input to the adsorption bed during the pre-heating process is consumed only in the sensible heating of the bed, whereas, in desorption process, a large portion of energy is consumed during the refrigerant generation process. So that a fraction from the driving energy about 1000 kJ is needed to bring the adsorption reactor up to the starting desorption with temperature of 67 °C.

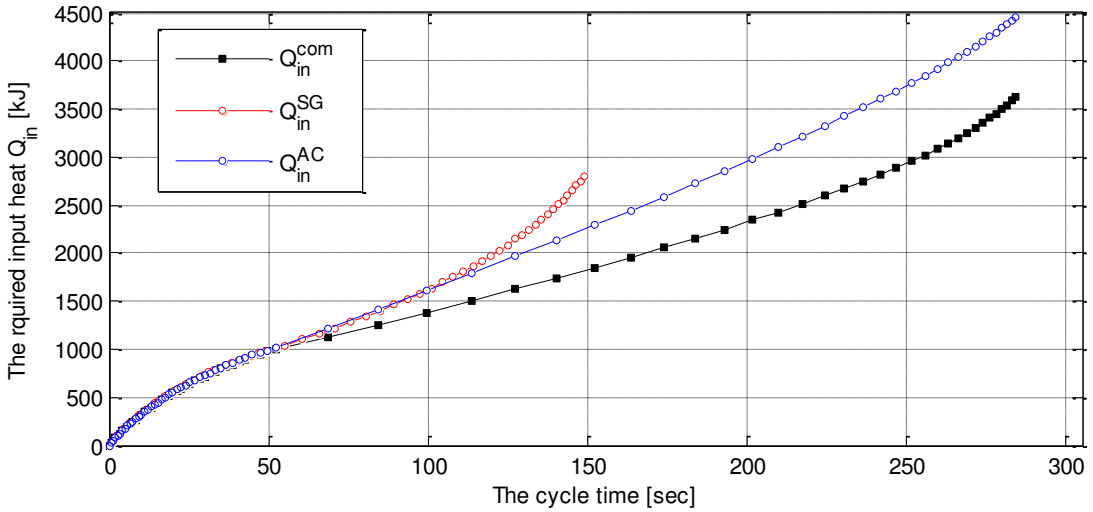

Figure 8.10: The driving energy added to the SG-bed, AC-bed and com-bed during the cycle time

It is interesting to notice from the **F**ig. 8.10 how the driving energy varies with respect to the duration of isosteric and isobaric heating processes over the same range [27 − 100 °C]. As seen in the **F**ig. 8.10 both the com-bed and AC-bed take the same desorption time to heat up and activate the adsorption reactor, but the com-bed adsorption reactor has an advantage compared with the AC- bed that its required driving energy is smaller than the required energy of AC-system. The SG-bed takes about 150 sec to desorb the refrigerant toward the condenser, whereas the com-bed takes about 287 sec to desorb the refrigerant. But the SG-bed adsorption reactor has a disadvantage that it needs higher driving energy during its smaller desorption time compared to com-bed and AC-bed.

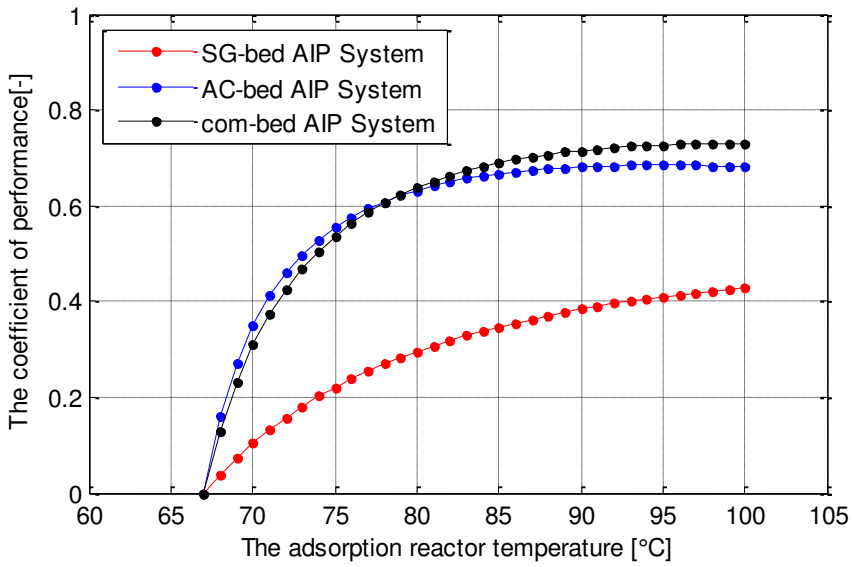

Figure 8.11: Effect of the adsorption reactor temperature on the coefficient of performance COP for the three AIP systems

Fig. 8.11 shows the influence of adsorption reactor temperature on the system COP for the SG-, AC- and com-AIP system. Based on the comparison with the silica gel/methanol AIP system the simulation results showed that, the COP of this novel com-AIP system was improved by 30 % and with activated carbon/methanol AIP system was improved by 7 % .

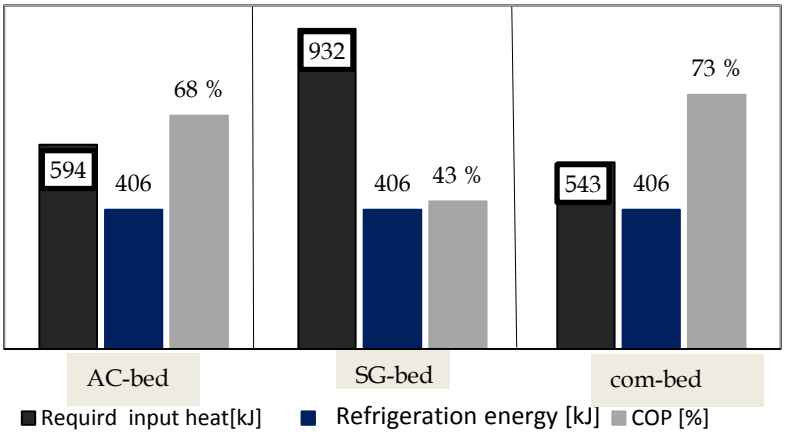

Figure 8.12: Comparison between the three AIP systems, the first is filled only by silica gel/methanol, the second is filled only by activated carbon/methanol and the third is filled by combined adsorbents by silica gel-activated carbon/ methanol

For producing 1 kg of ice from the com-AIP system the refrigeration energy Q_e of all three systems is similar. But the driving energy required by the com-heat exchanger is about 543 kJ per cycle and the performance of the system COP reaches 73 %. Based on the simulation results and the comparison with the AC-AIP system and with SG-AIP system, it has been found that the required input heat by AC-bed is 594 kJ and by SG-bed is 932 kJ under the same operating conditions. This mean that the Q_{in} input heat required from the external heat source of this novel com-heat exchanger could be lowered by 41 % compared with silica gel-methanol AIP system and by 8 % compared with activated carbon-methanol AIP system when the operating conditions were similar.

Due to a lower specific heat capacity C_P of the silica gel particles, faster sorption kinetic of silica gel, smaller density of activated carbon and higher adsorption quantity of the activated carbon particles, the com-adsorption reactor has a higher COP and lower heat input Q_{in} compared to SG-bed and AC-bed.

The importance of the com-AIP system, that the com- adsorption reactor allows using the advantages of physical properties of both the adsorbents SG and AC. As a result of the using this technique the com-adsorption reactor has an important advantage that can save the heat required from the heat source and has efficient performance. This has an important effect on the selection of energy source.

8.6 Comparison between the induction and thermal heating of the adsorption system

The design of the adsorption reactor varies depending on the heating mechanism. In frame of this work, two methods (induction and thermal heating) had been used to heat and activate two adsorption reactors; the first is the SG-adsorption reactor and the second is the AC-adsorption reactor. Both the adsorption reactors using the thermal heating were designed in this work as a heat exchanger. This heat exchanger is composed of flat tubes with rectangular fins and designed in order to desorb/adsorb 1 kg_{meth} of circulated refrigerant mass. The gaps between the fins were filled by the S-medium (adsorbent + adsorbate).

(a) Induction Heating		
Mass of the adsorbent [kg]	7.95	3.31
Mass of the adsorbate[kg]	1.9	1.36
Number of the cylinders	1	1
Number of the Gr-balls	75	35
Number of the inductors	1	1

(b) Thermal Heating		
Mass of the adsorbent [kg]	7.95	3.31
Mass of the adsorbate[kg]	1.9	1.36
Number of the fins	90	90
Number of the HTF-tubes	4	2

Tab. 8.3: Components of the SG- and the AC-adsorption reactors using (a) induction heating (b) thermal heating

Using the induction heating is considered as a new process to overcome the problems found with the conventional method (thermal heating). So that the adsorption reactor using the induction heating in this study has a simple design and consists only of the induction coil (inductor) and the cylindrical container, which is filled with the S-medium. To achieve that, the new design for each adsorption reactor was investigated to desorb the same amount of the refrigerant 1 kg_{meth}.

Because of the dielectric properties of SG and AC, incorporation of the graphite balls, having a good electrical conductivity, into the adsorption reactors, is used in order to improve the heat transfer process and to save the input energy. **T**ab. 8.3a and b show the components of the induction/thermal heating setup for the SG- and the AC-adsorption reactors.

The comparison is implemented to desorb the same amount of the adsorbate (methanol) 1 kg_{meth} from both the SG- and AC adsorption reactors using both the methods of the thermal and induction heating.

Based on the analytical and numerical results presented in the context of this work it can be concluded the comparison between the induction and thermal heating of the adsorption system as following:

It is found by using the induction heating technology, that the required input power of the SG-reactor is estimated to 7.722 kW, and the desorption process takes about 10 min.Whereas the required input power and the desorption time using the thermal heating depends on the HTF-flow nature (Reynolds number). When operating of the SG-reactor in a laminar flow regime (Re = 392), the required input power decreases by about 92.65 % (0.567 kW), but the desorption process requires longer time about 81 min in comparison with the induction heating technology. When the HTF flows with turbulent

flow, both the required input power and desorption time are lowered in comparison with induction heating technology. It is found, when the operating of the SG-reactor in a turbulent flow regime ($\mathrm{Re} = 23511$), the required input power is lowered by about $15\ \%$ $(6.562\ \mathrm{kW})$, and the desorption process requires shorter time about $7\ \mathrm{min}$ in comparison with the IH.

If the SG-reactor works (desorbing$1\ \mathrm{kg_{meth}}$) with the laminar or turbulent flow, the energy consumed per hour is estimated to $0.765\ \mathrm{kWh}$. Whereas using the induction heating technology it is estimated to $1.228\ \mathrm{kWh}$, which is larger by about $37.7\ \%$.

we can explain the reason behind the high value of the energy consumption using the induction heating technology by the loss in the induction coil as follows: the induction coil used in the IH-system consumes more the half of the required input power, because both the resistance and the inductance of the used induction coil are bigger than the resistance and the inductance of the work-load. It is found based on the simulation results, the induction coil used with SG-adsorption reactor (height 460 mm, outer diameter 280 mm and inner diameter 260 mm) consumes about $51.75\ \%$ of the total input power, which is estimated to $4.022\ \mathrm{kW}$. The consumption energy in the induction coil is estimated to $0.67\ \mathrm{kWh}$ during the desorption process.

On the other hand, the metallic constituents (the tubes and fins) used in the adsorption reactor using the thermal heating consumes only $33\ \%$ of the required input power to desorb $1\ \mathrm{kg_{meth}}$. It is found, that the consumption energy by metallic constituents is estimated to $0.257\ \mathrm{kWh}$ during the desorption process using the thermal heating for the laminar and turbulent flow. Consequently, the loss in the metallic constituents using the thermal heating is less by about 61.6 % than the loss in the induction coil used in the induction heating system.

Reynolds number, which is related to the driving temperature $\mathrm{T_{h,in}}$ and velocity $\mathrm{u_z}$ of the HTF, is one of the important factors controlling the heat transfer inside the adsorption reactor using thermal heating method. It was noticed, that Re has an important effect on the desorption process in terms of the required desorption time and required amount of the hot water, which flows through the HTF-tubes. It was found, when operating of the SG-reactor in a turbulent flow regime ($\mathrm{Re} = 23511$), the required desorption time is saved by about more one hour ($95\ \%$), whereas the amount of hot water needed from the heat source in order to achieve completely desorption process (desorbing $1\mathrm{kg_{meth}}$) increases by about $82\ \%$ in comparison with the operating in a laminar flow regime ($\mathrm{Re} = 392$).

Whereas the current passing the induction coil and the power density induced inside the Gr-balls have the important effect on desorption process using the induction heating technology. It is found, that the desorption process takes a short time duration while increasing the power density induced in the Gr-balls, which are used as a heat generation source inside the adsorption reactor. For operating the IH-system at highest conversion ratio $\mathrm{C_r} = 1$ and at optimal the heat transfer effectiveness $\varepsilon = 1$, It was found based on the analytical results, the desorption time is lowerd by about 28 % when the induced power density increase from 8 to 12 $[\mathrm{MW/m^3}]$.

AC-Adsorption reactor	**Induction Heating**	**Thermal Heating**	
		$\mathrm{Re} = 392$	$\mathrm{Re} = 23511$
Total input power [kW]	3.886	0.279	1.467
Consumption energy [kWh]	1.036	0.489	0.489
Required desorption time [min]	16	105	20
Induction coil/Metallic components loss	52.27 %	20.6 %	20.6 %
Energy Source	$\mathrm{I_I} = 690$ A, $\mathrm{f} = 25$ kHz	$\mathrm{T_{h,in}} = 84$ °C, $\mathrm{u_z} = 0.01\ \mathrm{m/s}$	$\mathrm{T_{h,in}} = 84$ °C, $\mathrm{u_z} = 0.6\ \mathrm{m/s}$

Table 8.4: Comparison between the induction and thermal heating of the AC-adsorption system

Tab. 8.4 presents a comparison between the two methods induction and thermal heating in order to desob 1 kg_{meth} from the AC-adsorption reactor.

In comparison between the AC-and SG-reactors using the induction heating technology in order to desorb the same amount of the adsorbate it is found, the required input power and the energy consumption of the AC-reactor can be saved by about 50 % and 15.63 %, respectively.

During the desorption process, the temperature of both the adsorbent and methanol rises to the desorption temperature. As a result, the methanol evaporates and leaves from the adsorption reactor. An assumption (allegation) study was numerically implemented with help the **A**NSYS **F**luent Software. The behavior of methanol (the velocity) has been simulated for circle of 1 mm diameter inside the SG-reactor with coupled wall, which its temperature related to the SG-temperature. **F**ig. 8.13 shows the methanol-behavior, fixing on the SG-particles during desorption process and gives the variation in its velocity resulting from the absorption of the heat by SG-particles.

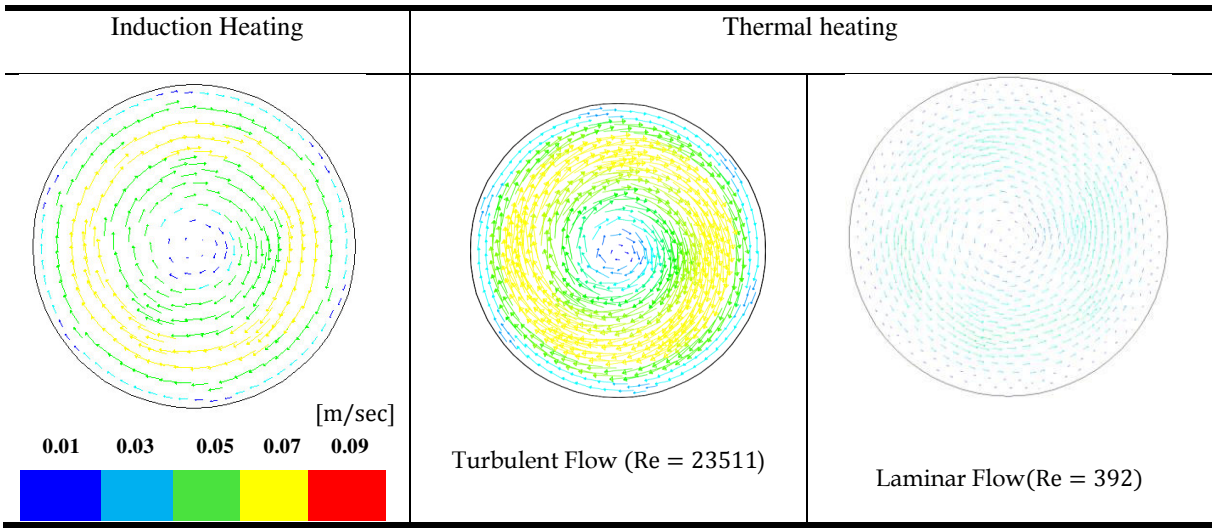

Figure 8.13: Methanol behavior inside the adsorption reactor during the desorption process in case of laminar and turbulent flow

Based on this study when the adsorbent temperature rises from 27 °C to the maximum desorption temperature of 100 °C, it is observed, that the velocity of the methanol as an adsorbate changes from 0 to only 0.03 m/s in the case of laminar flow and from 0 to only 0.08 m/s in the case of turbulent flow. Whereas in the case of using the induction heating the velocity of methanol changes from 0 to 0.06 m/s. Consequently, when the operating in a turbulent flow regime, the methanol can be desorbed from the adsorption material faster in comparison with the laminar flow regime and induction heating method. Therefore, the desorption process with a turbulent regime requires the shortest time.

Chapter 9

Summary, Conclusion and Outlook

In the first part of this thesis, we have theoretically, numerically and thermodynamically investigated a new strategy of two beds adsorption refrigeration system at different operating and boundary conditions. This system utilizes two adsorption materials in one machine and comprises of two adsorption reactors. The adsorption refrigeration system in this work was named the combined **A**dsorption **I**ce **P**roduction system (com-AIP system). The main aims of the present system are: enhancing the amount of ice produced per cycle, producing continuous refrigeration power, improving the cycle time and saving of the required input heat by increasing the desorbed mass. The adsorption thermodynamic cycles of both the SG- and AC-adsorption reactors had been studied in two cases:

1. **First case:** Both the SG-and AC-adsorption reactors were heated to the same desorption temperature and the thermodynamic cycles start at the same time (working simultaneously).
2. **Second case**: Both the SG-and AC-adsorption reactors were heated up to the same level of minimum adsorbate concentration rate and to desorb the same amount of the desorbed refrigerant of $1\ \mathrm{kg_{meth}}$. The thermodynamic cycles were considered to start one after the other.

In the first case the adsorption reactors were taken as same size (number of HTF-tubes and same emptied volume, where the adsorbents are filled). The simulation results showed that $5.34\ \mathrm{kg}$ of ice per cycle could be obtained with a COP of 0.73 under the hot water inlet temperature of $100\ °\mathrm{C}$ whereas the evaporation temperature of $-3\ °\mathrm{C}$. The larger fraction from the produced ice of about $72\ \%$ is produced from the AC-particles whereas the remaining part of the total amount ice produced of $28\ \%$ is created from the SG-particles. This is because of the large adsorption quantity of the activated carbon particles compared to silica gel as adsorbent. This amount of ice produced decreases to $4\ \mathrm{kg}$ with using only silica gel in the adsorption reactor and increases to about $7\ \mathrm{kg}$, if the adsorption reactor is filled with only activated carbon as adsorbent, but in this case the required heat input is about $20\ \%$ higher.

In term of desorption the same amount of methanol, each reactor was filled with a different quantity of the adsorption material to ensure that $1\ \mathrm{kg_{meth}}$ is released. Based on this quantity it is found, that the SG-and AC-reactors must have different sizes and configurations of the heat exchanger. During the desorption process the SG-reactor has to be heated up to the maximal desorption temperature of $100\ °\mathrm{C}$ whereas the AC-reactor only up to $84\ °\mathrm{C}$. Consequently, the required input heat introduced to SG-reactor is estimated to $2.7\ \mathrm{MJ}$, whereas only to $1.7\ \mathrm{MJ}$ in case of the AC-reactor.

If the SG-reactor or the AC-reactor works, the system produces the same mass of ice of 3 kg, but the system attains a coefficient of performance of $66\ \%$, when the AC-reactor works and attains of $44\ \%$, when the SG-reactor works. Therefore the amount of the ice produced from the system estimated to $6\ \mathrm{kg}$ per cycle. Based on the simulation results it is found, that every $1\ \mathrm{kg}$ of silica gel-particles inside the SG-adsorption reactor produces ice mass of $0.38\ \mathrm{kg}$ per cycle under hot water input temperature of $100\ °\mathrm{C}$ and every $1\ \mathrm{kg}$ of activated carbon-particles inside the AC-adsorption reactor produces ice mass of $0.9\ \mathrm{kg}$ per cycle under hot water input temperature of $84\ °\mathrm{C}$.

The new strategy of com-AIP system is completely different from the conventional adsorption reactors, which are filled with one adsorbent in one bed or in two beds. The importance of this strategy of the com-AIP system can be explained as follows:

1. The com-AIP system allows using the advantages of physical properties of both the adsorbents SG and AC. Consequently, this innovative AIP system utilizes effectively low-temperature heat sources of temperature between $65\,°C$ and $100\,°C$ for SG-reactor and between $65\,°C$ and $84\,°C$ for AC-reactor.
2. The adsorption reactor employed by activated carbon as adsorbent can save the required energy about $36\,\%$ and the adsorption reactor employed by silica gel as adsorbent takes a shorter time by about $36\,\%$ compared with AC-reactor to desorb the same mass of refrigerant. This means more produce of ice mass with saving energy.

In order to assess the effectiveness of the com-AIP system proposed, a comparison with two AIP systems was made under the same operating conditions, taking into account the required input energy Q_{in} and coefficient of performance COP. The first system works using silica gel/methanol and the second works using activated carbon/methanol. The modeling of the three systems has been simulated using a **MATLAB** program.

For producing $1\,kg$ of ice from the com-AIP system the refrigeration energy Q_e of all three systems are similar. Based on the simulation results and the comparison with the AC-AIP system and with SG-AIP system, it has been found that the required input heat by AC-bed is $594\,kJ$ and by SG-bed is $932\,kJ$ under the same operating conditions. This means that the input heat required Q_{in} from the external heat source of this novel com-heat exchanger could be lowered by $41\,\%$ compared with silica gel/methanol-AIP system and by $8\,\%$ compared with activated carbon/methanol-AIP system when the operating conditions were similar. Consequently the com-adsorption reactor has an important advantage that can save the heat required from the heat source and have efficient performance.

Also an experimental set up of ACS 08 system from the manufacturer SorTech AG, which is built in Holzminden (Germany), was instrumented to make validation of some simulation results of the AIP system. The simulated data are compared to the measured data of the ACS 08 system. The comparison was conducted for the real processes inside the adsorption reactor, the coefficient of performance of the system, the cooling capacity and the required time to complete the processes of one cycle. A good agreement has been found between measured and simulated data.

The second part of this thesis presented a numerical and analytical investigation of effect of the HTF-flow nature and effect the adsorption reactor design on the desorption process and the performance.

The effect of the HTF-nature has been studied for the same adsorption reactors (SG- and AC-reactors), which were heated to desorb $1kg_{meth}$ of methanol. In order to study the HTF-flow nature effect, the variation of the Reynolds, Nusselt and Biot numbers have been investigated to demonstrate their effects on the temperature distribution through both the reactors. The following conclusions were drawn from this study:

- When operating in a turbulent flow regime, the temperature distribution through the adsorption reactor is higher than in the laminar flow regime.

- It was found based on analysis the Biot number, that the temperature variation inside the adsorption reactor is significant inside the adsorption reactor when $Bi > 1$, so the internal conductive resistance is higher when compared to the external convective resistance, which

can be obtained when the operating in a turbulent flow regime. Whereas it was found by $Bi < 1$ when the operating in a laminar flow regime, that the temperature variation is significantly smaller when comparing to $Bi > 1$.

- Based on the simulation results, it was found, that Nusselt number Nu for different Reynolds number values remains larger than 1, which means more effective convection, because the convective resistance of the heat transfer fluid is less than that the conductive resistance. With $Nu > 1$, the fluid motion enhances heat transfer by advection.

- Regardless of HTF-flow nature, the adsorption reactor requires the same energy consumption per hour.

- It may be concluded that the desorption time is strongly dependent on the HTF-flow nature. So that the desorption process inside the SG-reactor takes shorter time about by 91% when the operating in a turbulent flow regime ($R_e = 23511$) in comparison with the laminar flow regime ($R_e = 392$). Also the required desorption time for the AC-reactor can be saved about 81%.

In the influence study of the HTF-flow nature on the desorption process, the size, installation and composition of both the adsorption reactors including the filled adsorbent amount were kept constant in order to desorb $1kg_{meth}$. Whereas the influence study of the design parameters of the adsorption reactor on the thermal performance of the adsorption system was be investigated by geometrical and thermal study of a set of non-dimensional factors A, F_L, R_G, ξ_{metal}, R_λ and F_S. The analysis of these factors allows us changing the adsorption reactor geometry. Depending on these changes the possibility of absorbing the reactor to different amounts of the adsorption material was taken into account and studied. The influence study of the design parameters of the adsorption reactor had been discussed in the present work with two cases.

1. **First case:** Changing the adsorption reactor geometry at constant adsorbent amount M_S. So that the adsorbent amount remains constant but occupies more space (larger surface).
2. **Second case:** Changing the adsorption reactor geometry but the adsorbent amount changes in order to employ the new spaces, where the adsorbent amount is related to the changed geometry used.

The following conclusions were drawn based on the influence study of the design parameters of the adsorption reactor:

- The same increase of the fin dimensions leads to slight enhancement of COP when $M_S \neq \text{constant}$ but the COP decreases clearly in the first case when $M_S = \text{constant}$. This was explained by analyzing the metal components factor ξ_{metal}. Also in the second case ($M_S \neq \text{constant}$), the adsorption reactor requires more input energy, because this input energy is introduced to activate more amount of the adsorption amount and to desorb more amount of the refrigerant.
- Increasing the area ratio A (increase the fins' dimensions), which is associated with the ability to employ more of the adsorbents amount and adsorbate quantity, leads to increase in the desorbed refrigerant mass M_{des} and leads to an enhancement in the amount of produced ice M_{ice}.
- Increasing the area ratio A by constant adsorbent amount M_S filled between the fins, plays no effect on M_{des} and M_{ice}.

- In opposite of the area ratio A, the increasing adsorbate thickness factor F_S in both the cases ($M_S \neq \text{constant}$ and $M_S = \text{constant}$) leads to clear enhancement in COP. This can be explained by analyzing the metal components factor ξ_{metal}, so that the mass of the used metal components shrinks by increasing the fin spacing (increasing the factor F_S).
- Also in opposite of the area ratio A, the required input heat by increasing the adsorbate thickness factor F_S is lowered in both the cases by about 33 % when $M_S = \text{constant}$ and about 16 % when $M_S \neq \text{constant}$.

Using the electromagnetic induction technology as a new heat source of the adsorption refrigeration system has been also investigated in detail as a main part of this work.

Here, inductive heating has been used to overcome the problems found with conventional methods (thermal heating). So this task dealt with a mathematical modeling and numerical simulation of an induction heating system for the same SG-and AC- adsorption reactors. To achieve that, a new design for each adsorption reactor was investigated to desorb the same amount of the refrigerant ($1\ kg_{meth}$). Because of the dielectric properties of SG and AC, incorporation of the graphite balls, having a good electrical conductivity, into the adsorption reactors, is used in order to improve the heat transfer process and to save the input energy.

The numerical simulation of our induction heating model clearly involves three coupled phenomena: electromagnetism, skin effect and desorption process (heat transfer). The solution of the problem by numerical modelling and simulation processes was implemented by the software **A**NSYS **E**lectronics and **A**NSYS **F**luent. Obtaining the required desorption temperature to desorb $1\ kg_{meth}$ from each reactor was the main aim of both the mathematical modeling and numerical simulation in this study. So the procedure was to find and to determine the appropriate value of the induction coil current, which must be sufficient to obtain the required desorption temperature and also sufficient to achieve the required values of the power density (ohmic losses) p_v, the electric current density $\vec{J}$, the electric field intensity $\vec{E}$ and the magnetic field intensity $\vec{B}$. The following conclusions were drawn from this study:

- Based on the analytical and numerical investigations, it is found, that the power density, the electric field intensity and the electric current density, which are induced inside the Gr-balls placed in SG-adsorption reactor to desorb $1\ kg_{meth}$ is 50 % larger than that induced inside the Gr-balls placed in AC-adsorption reactor.
- Incorporation of the Gr-balls into the adsorption reactor allows achieving homogeneity of the temperature distribution throughout the reactor and allows obtaining the exact needed temperature distribution in the material if required.
- Induction heating technology has a major advantage. This is called the skin effect. The skin depth depends on the frequency and the material properties. So, by choosing the frequency correctly, one can apply the amount of required heat down to a known depth of the Gr-ball. Based on the analytical study it is found, that the required induced power density decreases while increasing the skin depth. Therefore, the numerical simulation had been implemented for the skin depth is equal to the Gr-ball radius, which is the maximum value that can be taken.
- Using graphite as a heat source reduces the energy consumption comparing with the balls that are made of iron, aluminum or copper.
- Desorption process using the induction heating takes short time duration while increasing the power density induced in the Gr-balls.

- Using the induction heating is a new process, problems found with the conventional methods (thermal heating) such as the setup of the adsorption reactor has a complex design, can be overcome.

In order to use the induction heating technology as a new heat source to heat nonmagnetic materials silica gel and activated carbon, it is necessary to study, design and analyze the structure of both the SG- and AC- induction heating systems, which were the main aims in the frame of this work. To achieve these aims, the following objectives were implemented:

1. Determine the proper size of two induction coils (the height, number of the loops and the section-shape of the coil), which must be appropriate to the SG-and AC-adsorption reactors.
2. Present and analyze the magnetic and electric circuit of both the IH-systems in order to calculate the ohmic and inductive resistances of both the work-load and the induction coil.
3. Study the oscillatory circuit (the secondary circuit studied) to know the currents I_S and the voltages U_S in order to determine the appropriate currents I_P and the voltages U_p in the primary circuit.
4. Evaluate of the induction heating system by determining the coil loss, the active power, the useful power induced inside the Gr-balls and the electrical efficiency for both the SG- and AC- induction heating systems.

In term of desorption the same amount of methanol from each adsorption reactor, the SG-and AC-reactors must have different sizes and configurations of the induction coil and the adsorption reactor. The size of the SG-reactor has a double size when compared to AC-reactor and the SG-induction coil has a double height and double turns number when compared to AC-induction coil.

In context of desorption process study by applying the same induction current of 690 [A] passing both the SG-induction coil and AC-induction coil at same induction frequency 25 kHz, in comparison between the AC-and SG-reactors using the induction heating technology it is found, that the required input power and the energy consumption of the AC-reactor can be reduced by about 50 % and 15.63 %, respectively.

It is found based on the simulation results, that the power efficiency of the SG- IH system (41.25%) is slightly larger than that of the AC- IH system (40.43 %). This can be explained by the loss in the induction coil, which is an essential factor that depends of the coil dimensions. So that the coil loss of the AC- IH system is slightly larger about only 0.52 % than that of the AC- IH system. We noticed based on the results of this study that both the resistance and the inductance of the used induction coil are bigger than the resistance and the inductance of the work-load. This means that the power loss in the induction coil is more than the useful power induced inside the work-load.

Depending on the analytical and numerical results presented in the context of this work, a comparison between the induction and thermal heating of the adsorption system was done in the final part of this thesis. If the SG-reactor works (desorbing$1\ \mathrm{kg_{meth}}$) with the laminar or turbulent flow, the energy consumed per hour is estimated to 0.765 kWh. Whereas using the induction heating technology it is estimated to 1.228 kWh, which is larger by about 37.7 %.

The high value of the energy consumption using the induction heating technology can be explained by the high loss in the induction coil used. The induction coil used in the IH-system consumes more the half of the required input power, so that the induction coil used with SG-adsorption reactor consumes about 51.75 % of the total input power, which is estimated to 4.022 kW.

Whereas the metallic constituents (the tubes and fins) used in the adsorption reactor using the thermal heating consumes only 33 % of the required input power to desorb 1 kg_{meth}. Consequently, the loss in the metallic constituents using the thermal heating is less by about 61.6 % than the loss in the induction coil used in the induction heating system.

It is found by using the induction heating technology, that the desorption process inside the SG-reactor takes about 10 min. Whereas the required desorption time using the thermal heating depends on the HTF-flow nature (Reynolds number). When the operating of the SG-reactor in a laminar flow regime ($Re = 392$), the desorption process requires longer time about 81 min. When the HTF flows with turbulent flow, the desorption time is saved in comparison with induction heating technology. It was found, when the operating of the SG-reactor in a turbulent flow regime ($Re = 23511$) the desorption process requires shorter time of about 7 min in comparison with the IH.

Reynolds number has an important effect on the desorption process in terms of the required desorption time and required amount of the hot water, which flows through the HTF-tubes. Whereas the current passing the induction coil and the power density induced inside the Gr-balls have the important effect on desorption process using the induction heating technology.

Outlook

Some recommendations -mainly from the viewpoint of theoretical and thermodynamic analysis- for future work are made in this section.

- A first suggestion is that effort should made to save up the required input energy introduced to both the adsorption reactors, which used in the com-AIP system. So it is recommended for future work to use heat exchanger recovery between the SG-reactor and AC- reactor. Based on the results presented in this work, it is found, that during the desorption process (desorbing the same amount of the adsorbate) the SG-reactor has to be heated up to the maximal desorption temperature of 100 °C whereas the AC-reactor only to 84 °C and because of the faster kinetic desorption of SG-reactor in comparison with AC-reactor, the HTF comes out from the SG-reactor at a temperature higher than the required input temperature into the AC-reactor.

- The new technique of utilize two different adsorbents in one system can be used for another cooling application and for air conditioning, so that it can be another working adsorption pairs. The new strategy of the com-AIP system studied in this work is utilized for is used for freezing application. Therefore, methanol was used as adsorbate with both the adsorption reactors, because methanol has a higher operation pressure compared with water under the same temperature and methanol operates at sub atmospheric pressure; the low-pressure system is suitable to utilize the adsorption cold system as ice maker. For example for the air conditioning system it can be used com-adsorption system consists of two adsorption reactor, the first adsorption reactor is filled by zeolite/water and the second by silica gel/water.

- By using the induction heating technology of the adsorption systems it is recommended to use the induction coil as small sizes because of the high loss in the induction coil. Therefore, the suggestion is using induction heating technology with the adsorption materials having an adsorbate concentration and a high volumetric mass density.

Bibliography

[1]	Industry Study. Commercial Refrigeration Equipment. Source the Freedonia group, Mar 29, 2016. https://www.prnewswire.com/news-releases/the-freedonia-group-us-commercial-refrigeration-equipment-demand-to-exceed-11-billion-300242606.html
[2]	A. Abela, L. Hamilton, R. Hitchin, A. Lewry and Ch. Pout. *Study on Energy Use by Air-Conditioning: Final Report.* BRE Client Report for the Department of Energy & Climate Change, HPR218-1001 - June 2016.
[3]	M. S. Fernandes, G. J. V. N. Brites, J. J. Costa, A. R. Gaspar and V. A. F. Costa. *Review and future trends of solar adsorption refrigeration systems*. Renewable and Sustainable Energy Reviews, 39: 102-123, 2014.
[4]	S. F. PEARSON. *Saving Energy in Refrigeration, Air-Conditioning and Heat-Pump Technology*. IIF-IRD-0427, 2008.
[5]	H. T. Chua, K. Ch. Ng, A. Malek and B. B. Saha. *Modeling the performance of two bed, silica gel-water adsorption chiller*. International Journal of Refrigeration, 22(3): 194-204, 2008.
[6]	A. R. M. Rezk. *Theoretical and experimental investigation of silica gel-water adsorption*. Thesis submitted of the university of Birmingham for the degree of Doctor of Philosophy, 2012.
[7]	J. White. *Literature review on adsorption cooling systems, Latin American and Caribbean*. Journal of Engineering Education 378-884-1-RV, 2013.
[8]	S. J. Gregg and K. S. W. Sing. *Adsorption, surface area and porosity*. 2nd ed. Academic press, London1982.
[9]	R. Farrington and J. Rugh. *Impact of vehicle air-conditioning on fuel economy, tailpipe emissions, and electric vehicle range*. In: Proceeding of the Earth Technologies Forum, Washington, D.C. 2000
[10]	S. Amir and B. Majid. *Assessment of adsorber bed designs in waste-heat driven adsorption cooling system for vehicle air conditioning and refrigeration*. Renewable and Sustainable Energy Reviews 30: 440- 451, 2013.
[11]	Y. Zhao. *Study of activated carbon/methanol adsorption refrigeration tube and system integration*. A thesis submitted of the University of Adelaide for the degree of Doctor of Philosophy, January 2011.
[12]	H.Z. Hasan. *Energy analysis and performance evaluation of the adsorption refrigeration system*. ISRN Mechanical Engineering, Article ID 704340, 14 pages, 2013.
[13]	H. Z. Hasan, A. A. Mohamad, Y. Alyousef and H. A. Al-Ansary. *A review on the equation of state for the working pairs used in adsorption cooling systems*. Renewable and Sustainable Energy Reviews 45, 600-608, 2015.
[14]	I. Solmus, C. Yamali, B. Kafanoglu, D. Baker and A. Caglar. *Adsorption properties of a natural zeolite-water pair for use in adsorption cooling cycles*, Applied Energy 87 (6): 2062-2067, 2010.
[15]	E. Glueckauf. *Formulation for diffusion into spheres and their applications to chromatography*, Trans. Faraday Soc., 51: 1540-1551, 1955
[16]	A. Sakoda and M. Suzuki. *Fundamental study on solar powered adsorption cooling system*, Journal of Chemical Engineering, Japan, 17(1): 52-57, 1984.
[17]	H. T. Chua, K. C. Ng, A. Malek, T. Kashiwage , A. Akisawa and B. B. Saha. *Modeling the performance of two-bed, silica gel-water adsorption chiller*. International journal of refrigeration 22: 194-204, 1999
[18]	S. Jribi, T. Miyazaki, B. B. Saha and S. koyama, *Transient simulation of finned tube type adsorber employing activated carbon-ethanol as adsorbent refrigerant pair*. IIR International Congress of Refrigeration, 575-582, 2015
[19]	G. Cerbe and G. Wilhelms. *Technische Thermodynamik Theoretischer Grundlagen und praktischer Anwendungen*. Carl Hanser Verlag München, 2008.

[20]	F. Dietzel. *Technische Wärmelehre Grundlagen für Ingenieure*. Vogel Verlag und Druck KG, würzburg, 1976.
[21]	A. Dabrowski. *Adsorption- from theory to practice*. Advances in Colloid and Interface Science, 93(1-3): 135-224, 8. October 2001
[22]	G. A. Somorjai. *Principles of Surface Chemistry*, Prentice-Hall, Englewood Cliffs, N. J.1972.
[23]	R.E. Critoph. *Evaluation of alternative refrigerant-adsorbent pairs for refrigeration cycles*. Applied Thermal Engineering, 16: 891-900, 1996.
[24]	M. S. Ahmed and A. A. El-kader shehata. *A review: future of the adsorption working pairs in cooling*. Mechanical engineering department, Sohag university, Egypt.
[25]	M.S. Tswett. *Chromatographic Adsorption Analysis*: Selected Works, Elis Horwood Ltd, 1990.
[26]	E. B. Miller. *The Development of Silica Gel, Refrigerating Engineering.* The American Society of Refrigerating Engineers. 17(4): 103-108, 1929.
[27]	N.V. Keltsev. *Principles of Adsorption Technology in Russian*, WNT, Warsaw, 1980.
[28]	R.M. Barrer. *Zeolites and Clay Minerals*. Academic Press, London, 1978.
[29]	D. W. Breck, W.G. Eversole, R.M. Milton, T.B. Read and T.L. Thomas. *Crystalline Zeolites. I. The Properties of a New Synthetic Zeolite, Type A.* J. Am. Chem. Soc. 78(23): 5963-5972, 1956.
[30]	J. M. Gordona, K.C. Ng, H.T. Chuac and A. Chakraborty. *The electro-adsorption chiller: a miniaturized cooling cycle with applications to micro- electronics*. International Journal of Refrigeration, 25(8): 1025-1033, 2002.
[31]	T. Grof. *Greening of Industry under the Montreal Protocol.* United Nations industrial development organization: Manila: 1-20, 2009.
[32]	The montreal protocol. *ENVIRONMENTAL-INVESTIGATION-AGENCY*. 2011.
[33]	Greenhouse Gas Inventory Based on Data from 2000 through 2006, in the University of Texas at Austin2009.
[34]	V. Hasse, L. Ederberg, and D. Colbourne. *Natural Refrigerants*. Eschborn: German Technical Cooperation, 2008.
[35]	IGT, (1972) Technical feasibility of solid adsorption cooling system, Institute of Gas Technology, Project HC-415, December
[36]	D. I. Tchernev. *Solar Air Conditioning and Refrigeration Systems Utilizing zeolites*. Proceeding of meetings of Commissions E1-E2, Jerusalem, Issued by International Institute of Refrigeration, 209-215, 1979.
[37]	F. Meunier. *Sorption Contribution to Climate Change mitigation*. Proceedings of the International Sorption Heat Pump, Conference, Shanghai. September 24-27, 2002.
[38]	L.W. Wang, R.Z. Wang and R.G. Oliveira. *A review on adsorption working pairs for refrigeration*. Renewable and Sustainable, vol. 13 (3): 518-534, 2009.
[39]	N. C. Srivastava and I. W. Eames. A review of adsorbents and adsorbates in solid-vapour adsorption heat pump systems. Applied Thermal Engineering, 18(19-10): 707-714, 1998.
[40]	K.C.A. Alam, B. B. Saha, Y. T. Kang and T. Kashiwagi. *Heat exchanger design effect on the system performance of silica gel water adsorption system*. International Journal of Heat Mass Transfer, 43 (24): 4419-4431, 2000.
[41]	M. A. Alghoul, M. Y. Sulaim, B. Z. Azmi and M. Abd. Wahab. *Advances on multi-purpose solar adsorption systems for domestic refrigeration and water heating.* Applied Thermal Engineering, 27 (5–6): Pages 813-822, 2007.
[42]	J. White. *A CFD Simulation on How the Different Sizes of Silica Gel Will Affect the Adsorption Performance of Silica Gel*, Modelling and Simulation in Engineering, Hindawi Publishing Corporation. Published online January, Article ID 651434, 2012.
[43]	Y. I. Aristov. *Challenging offers of material science for adsorption heat transformation: A review*. Applied Thermal Engineering, 50(2), 2013.

[44]	J. White. *Computational Fluid Dynamics Modelling and Experimental Study on a Single Silica Gel Type B*, Modelling and Simulation in Engineering, Hindawi Publishing Corporation. Article ID 598479, 2012.
[45]	J. –Y. San and W.-M. Lin. *Comparison among three adsorption pairs for using as the working substances in multi-bed adsorption heat pump*. Applied Thermal Engineering, 28(8-9): 988-977, 2008.
[46]	J. Rouquerol, D. Avnir, C. W. Fairbridge, D. H. Everett, J. H. Haynes, N. Pernicone, J. D. F. Ramsay, K. S. W. Sing and K. K. Unger. *Recommendations for the characterization of porous solids (Technical Report)*. International Union of Pure and Applied Chemistry, 66 (8):1739-1758, 1994.
[47]	Y. Yamada and K. Yano. *Synthesis of monodispersed super-microporous/mesoporous silica spheres with diameters in the low submicron range*. Microporous and Mesoporous Materials, 93(1-3): 190-198, 2006.
[48]	W. S. Loh, I.I. El-Sharkawy, K.C. Ng and B.B. Saha. *Adsorption cooling cycles for alternative adsorbent/adsorbate pairs working at partial vacuum and pressurized conditions*. Applied Thermal Engineering 29: 793-798, 2009.
[49]	X. Guo, W. Hou, W. Ding and Y. Chen. *Synthesis of a novel super-microporous layered material and its catalytic application in the vapor-phase Beckmann rearrangement of cyclohexanone oxime*. Microporous and Mesoporous Materials, 80(1-3): 269-274, 2005.
[50]	Y.-S. Lin, H.-P. Lin, and C.-Y. Mou. *A simple synthesis of well-ordered super-microporous aluminosilicate*. Microporous and Mesoporous Materials, 76(1-3): 203-208, 2004.
[51]	D. Menard and N. Mazet. *Activated carbon monolith of high thermal conductivity for adsorption processes improvement Part A*: *Adsorption step*, Chemical Engineering and Processing, 44(9): 1029–1038, 2005.
[52]	B. B. Saha, I. I. El-Sharkawy, A. Chakraborty and S. Koyama. *Study on an activated carbon fiber–ethanol adsorption chiller. Part II, Performance evaluation*. Internation Journal Refrigeration, 30 (1): 96–102, 2007
[53]	Z. Tamainot-Telto, S. j. Metcalf, R. E. Critoph, Y. Zhong and R. Thorpe. *Carbon-ammonia pairs for adsorption refrigeration applications: ice making, air conditioning and heat pumping*. International Journal of Refrigeration 32(6):1212–1229, 2009.
[54]	Y. Liu and K. C. Leong. *The effect of operating conditions on the performance of zeolite/water adsorption cooling systems*. Technological University Applied Thermal Engineering, 25 (10): 1403–1418, 2005.
[55]	Y. Zhong, R. E. Critoph, R. N. Thorpe, Z. Tamainot-Telto and Y. I. Aristov. *Isothermal sorption characteristics of the BaCl2-NH3 pair in a vermiculite host matrix.* Applied Thermal Engineering, 27(14-15): 2455-2462, 2007.
[56]	S. L. Li, J. Y. Wu, Z. Z. Xia and R. Z. Wang. *Study on adsorption performance of composite adsorbent of CaCl2 and expanded graphite with ammonia as adsorbate*. Energy Conversion and Management, 50(4): 1011-1017, 2009.
[57]	T. X. Li, R. Z. Wang, R. G. Oliveira, J. K. Kiplagat and L. W. Wang. *A combined double-way chemisorption refrigeration cycle based on adsorption and resorption processes*. International Journal of Refrigeration, 32(1): 47-57, 2009.
[58]	S.B. Raffat, C. F. Afonso, A. C. Diveria and D. A, Reay. *Natural refrigerants for refrigeration and air conditioning systems*, Applied Thermal Engineering, 17 (1): 33-42, 1997.
[59]	R. E. Critoph and Y. Zhong. *Review of trands in solid sorption refrigeration and heat pumping technology*. Proc. IMechE Part E: J. Process Mechanical Engeneering, 219, 2005.
[60]	R. E. Critoph. *Adsorption refrigeration and heat pumps, In: Carbon Materials for Advanced Technologies*. Edited by Trimothy D. Burchell, 303-340, PERGAMON, 1999.
[61]	B. B. Saha, K. Habib, I. I. El-Sharkawy and S. Koyama. *Adsorption characteristics and heat of adsorption measurements of R-134a on activated carbon*. International Journal of Refrigeration. 32(7): 1563-1569, 2009.
[62]	A. O. Dieng, and R.Z. Wang. *Literature review on solar adsorption technologies for ice making and air-conditioning purposes and recent developments in solar technology.* Renewable & Sustainable energy reviews,

	5(4): 313-342, 2001
[63]	N. D. Banker, K. Srinivasan and M. Prasad. *Performance analysis of activated carbon + HFC-134a adsorption coolers. Carbon,* 42(1): 117-127, 2004.
[64]	Q. Cui, G. tao, H. Chen, X. Guo and H. Yao. *Environmentally benign working pairs for adsorption refrigeration*. Energy, 30 (2-4): 261-271, 2005.
[65]	Y. Liu and K.C. Leong. *Numerical study of a novel cascading adsorption cycle*. International Journal of Refrigeration, 29(2): 250-259, 2006.
[66]	M. Schicktanz, P. Hügenell and S.K. Henninger. *Evaluation of methanol/activated carbons for thermally driven chillers, part II: The energy balance model*. International Journal of Refrigeration, 35(3): 554-561, 2012.
[67]	C. J. Chen, R. Z. Wang, Z. Z. Xia, J. K. Kiplagat and Z. S. Lu. *Study on a compact silica gel–water adsorption chiller without vacuum valves: Design and experimental study*, Applied Energy, 87(8): 2673–2681, 2010.
[68]	J. H. R. Grisel, S. F. Smeding and R. De Boer. *Waste heat driven silica gel/water adsorption cooling in trigeneration.* Applied Thermal Engineering, Elsevier, 30 (8-9): 1039-1046, 2010.
[69]	R. de Lieto Vollaro, F. Botta, A. de Lieto Vollaro and G. Galli. *Solar cooling system for buildings: thermal analysis of solid absorbents applied in low power adsorption*. Energy and Buildings, 80: 436-440, 2014.
[70]	C. Hai-jun, C. Qun, T. Ying, C. Xiu-jun and Y. Hu-qing. *Attapulgite based LiCl composite adsorbents for cooling and air conditioning applications*. Applied Thermal Engineering. 28(17.18): 2187–2193, 2008.
[71]	A. Dabrowski. *Adsorption-from theory to practice*. Advances in Colloid and Interface Science, 93(1-3): 136-224, 2001.
[72]	D. C. Wang, Z. Z. Xia and J.Y. Wu. *Design and performance prediction of a novel zeolite–water adsorption air conditioner*. Energy Conversion and Management 47(5): 590–610, 2006.
[73]	Y. Z. Lu, R. Z. Wang, S. Jianzhou, Y. X. Xu and J. Y. Wu. *Practical experiments on an adsorption air-conditioner powered by exhausted heat from a diesel locomotive*. Applied Thermal Eng 24(7):1051-1059, 2003.
[74]	L. W. wang, R. Z. Wang, Z. S. Lu, C. J. Chen, K. wang and J. Y. Wu. *The performance of two adsorption ice making test units using activated carbon and a carbon composite as adsorbents*. Carbon 44(13): 2671–2680, 2006.
[75]	D. C. Wang, Y. H. Li, D. Li, Y. Z. Xia and J. P. Zhang. *A review on adsorption refrigeration technology and adsorption deterioration in physical adsorption systems*, Renewable and Sustainable Energy Reviews 14(1): 344–353, 2010.
[76]	L.W. Wang, J.Y. Wu, R.Z. Wang, Y.X. Xu, S.G. Wang and X.R. Li . *Study of the performance of activated carbon–methanol adsorption systems concerning heat and mass transfer*. Applied Thermal Engineering, 23(13): 1605-1617, 2002.
[77]	S. Anirban and K. D. Randip. *Analysis of a continuous activated carbon methanol adsorption refrigeration system*, Proceedings of International Conference on Advances in Mechanical Engineering, COEP, Pune, Maharashtra, India ICAME2013 S12 O1 (Conference Paper), May 29-31, 2013.
[78]	Z. F. Li and k. Sumathy. *A solar powered ice maker with the solid adsorption pair of activated carbon and methanol*, Int. J. Energy Res, 23: 517-527, 1999.
[79]	M. Pones, and J. J. Gulleminot. *Design of an experimental solar-powered solid-adsorption ice maker*. Journal of Solar Energy Engineering, 108(4): 332-337, 1986.
[80]	D. I. Tchernev. *Solar refrigeration utilizing zeolites*, Intersociety Energy Conversion Engineering Conference, 14th, Boston, Mass., August 5-10, Proceedings. Volume 2. (A79-51726 23-44) Washington, D.C., American Chemical Society, 2070-2073, 1979.
[81]	S. Tanaka, T. Hasegawa and T. Waki. *On the integrated solar collector-chiller using the intermittent adsorption cycle*. I.S.E.S. Solar World Congress, August 14-19, Perth, 1983.

[82]	R. P. Kluppel and J. M. A. M. Gurgel. *Solar adsorption cooling using silica gel/water*. Advances In Solar Energy Technology, Vol 3: 2627–2631, 1988.
[83]	N. Medini, B. Marmottant and S. El. Gollia. *Study of a package solar ice maker*. International Journal of Refrigeration, 14(6): 363-367, 1991.
[84]	S. H. Cho and J. N. Kim. *Modeling of a silica gel/water adsorption cooling system*. Energy 17 (9): 829–839, 1992.
[85]	A. Hajji and S. Khalloufi. *Theoretical and experimental investigation of a constant-pressure adsorption process*, International Journal of Heat and Mass Transfer, 38 (18): 3349-3358, 1995.
[86]	K. Oertel and M. Fischer, *Adsorption cooling system for cold storage using methanol/silicagel*. Applied Thermal Engineering, 18 (9-10) 773-786, 1998.
[87]	X. J. Zhang and R. Z.Wang. *A new combined adsorption–ejector refrigeration and heating hybrid system powered by solar energy*. Applied Thermal Engineering, 22(11): 1245-1258, 2002.
[88]	L. Yong and K. Sumathy. *Modeling and simulation of a solar powered two bed adsorption air conditioning system.* Energy Conversion and Management, 45(17): 2761- 2775, 2004.
[89]	E. E. Anyanwu and C. I. Ezekwe. *Design, construction and test run of a solid adsorption solar refrigerator using activated carbon/methanol, as adsorbent/adsorbate pair*. Energy Conversion and Management (44): 2879-2892, 2003.
[90]	N. M. Khattab. *A novel solar-powered adsorption refrigeration module*. Applied Thermal Engineering, 24(17-18): 2747-2760, 2004.
[91]	R. Z. Wang and R. G. Oliveira. *Adsorption refrigeration An Efficient Way to Make Good Use of Waste Heat and Solar Energy*. Progress in Energy and Combustion Science, 32 (4): 424–458, 2006.
[92]	M. A. lambert. *Design of solar powered adsorption heat pump with ice storage*. Applied Thermal Engineering, 27(8-9): 1612-1628, 2007.
[93]	U. Jakob and W. Mittelbach. *Development and Investigation of a Compact silica gel/water adsorption chiller integrated in solar cooling systems***.** VII Minsk, International Seminar, "Heat, Pumps, Refrigerators, Power Sources". Minsk, Belarus, September 8-11
[94]	N.A. A. Qasem and M. A. I. El-Shaarawi. *Thermal analysis and modeling study of an activated carbon solar adsorption icemaker: Dhahran case study*. Energy conversion and Management 100: 310-323, 2015.
[95]	X. Hu and D. D. Do. *Multicomponent Adsorption Kinetics of Hydrocarbons onto Activated Carbon: Effect of Adsorption Equilibrium Equations*. Chem. Eng. Sci., 47(7): 1715-1725, 1992.
[96]	Y. Watabe and M. Yanadori. *Cooling characteristic of adsorption refrigeration apparatus using silica gel-ethanol system*. Kagakii Kogakii Ronbunshu, 20(4): 589-593, 1994.
[97]	B. B. Saha, E. C. Boelman and T. Kashiwagi. *Computational analysis of an advanced adsorption-refrigeration cycle*. Energy, 20(10): 983-994, 1995.
[98]	E. C. Boelman, B. B. Saha, and T. Kashiwagi. *Parametric Study of a Silica Gel-water Adsorption Refrigeration Cycle-the Influence of Thermal Capacitance and Heat Exchanger UA-values* on Cooling Capacity, *Power Density, and COP*. ASHRAE Transactions, 103(1): 139-148, 1997.
[99]	M. Li and R. Z. Wang. *Heat and mass transfer in a flat plate solar solid adsorption refrigeration ice maker*. Renewable Energy 28: 613-622, 2003.
[100]	M. Z. I. Khan, S. Sultan, A. Akisaw and T. Kashiwagi. *Numerical simulation of advanced adsorption refrigeration chiller with mass recovery*. Journal of navel architecture and marine engineering 3: 59-67, 2006.
[101]	E. E. Anyanwu and N. V. Ogueke. *Thermodynamic design procedure for solid adsorption solar refrigerator.* Renewable Energy, 30(1): 81-96, 2005.
[102]	Y. Liu and K. C. leong. *Numerical modeling of a zeolite/water adsorption cooling system with non-constant*

	condensing pressure, International Communications in Heat and Mass Transfer, 35 (5): 618-622, 2008.
[103]	A. El Fadar, A. Mimet and M. Perez-Garcia, *Modelling and performance study of a continuous adsorption refrigeration system driven by parabolic trough solar collector*. Solar Energy, 83(6): 851-861
[104]	N. V. Ogueke and E. E. Anyanwu, *The performance analysis of a solid adsorption solar refrigerator during collector cool-down and refrigerant evaporation/re-adsorption phases.* Journal of Process Mechanical Engineers 223 (1): 11-19, 2009.
[105]	H. Z. Hassan, A. A. Mohamad and R. Bennacer. *Simulation of an adsorption solar cooling system*, Energy, 36(1), 530: 537, 2011.
[106]	G. Zhang, D. C. Wang, J.P. Zhang, Y. P. han and W. Sun. *Simulation of operating characteristics of the silica gel–water adsorption chiller powered by solar energy*, Solar Energy, 85(7): 1469-1478, 2011.
[107]	R. Suleiman, C. Folayan, F. Anafi and D, Kulla, *Transient Simulation of a Flat Plate Solar Powered Adsorption Refrigeration System*. International Journal of Renewable Energy Research-IJRER, 2(2), 2012.
[108]	V. Baiju and C. Muraleedharan . *Performance Prediction of Solar Adsorption Refrigeration System*. International Scholarly Research Network , 2012,Volume 2012, Article ID 102376, 8 pages
[109]	L.X. Gong, R.Z. Wang, Z.Z. Xia and Z.S. Lu. *Experimental study on an adsorption chiller employing Lithium chloride in silica gel and methanol*. International Journal of Refrigeration 35(7): 1950-1957, 2012.
[110]	I. I. El-Sharkawy. M. Hassan, B. B. Saha and M. M. Nasr. *Study on adsorption of methanol onto carbon based adsorbents*. International journal of refrigeration 32(7): 1579-1586, 2009.
[111]	R. D. Goodwin. *Methanol Thermodynamic Properties from 176 to 673 K at pressures to 700 bar*. Thermophysics Division, National Engineering Laboratory, National Bureau of Standards, Colorado 80303, 1987.
[112]	F. Dietzel. *Technische Wärmelehre Grundlagen für Ingenieure*. Vogel Verlag und Druck KG, würzburg, 1976.
[113]	D. B. Riffel, U. Wittstadt. F. Schmidt and A. P. F. Leite. Transient modelling of an adsorber using finned-tube heat exchanger. Int. Journal of Heat and Mass Transfer, 2009.
[114]	D. Surek and S. Stempin. *Technische Strömungsmechanik Für Studium, Examen und praxis*. Springer Vieweg, 2014.
[115]	R. L. Street, G. Z. Watters and J. K. Vennard. *Elementary Fluid Mechanics*. John Wiley & Sons, Inc, 1996.
[116]	P. Bökh and T. Wetzel. Wärmeübertragung, Grundlagen und Praxis. Springer-Verlag Brlin Heidelberg, 2014.
[117]	S. Zinn and S. L. Semiatin. *Elements of Induction Heating - Design, Control, and Applications*. ASM International, Electric Power Research Institute, Metals Park, Ohio, USA, 1988.
[118]	V. Rudnev, D. Loveless and R. Cook. *Handbook of induction heating*, Second Edition, New York, 2017.
[119]	R. Alfred. *History of induction heating and melting*. Essen, Vulkan-Verlag, 2008.
[120]	V. Rudnev, D. Loveless, R. Cook, and M. Black. *Handbook of Induction Heating*. M. Dekker, New York, USA, 2003.
[121]	G. M. Segura. *Induction heating converter's design, control and modeling applied to continuous wire heating.* Doctoral Thesis, Universitat Politecnica de Catalunya, Barcelona, 2012.
[122]	S. Sandar Aung, H. Phyo Wai and N. Nyein Soe. *Design Calculation and Performance Testing of Heating Coil in Induction Surface Hardening machine*. International Journal of Electrical, Computer, Energetic, Electronic and Communication Engineering 2(6), 2008.
[123]	A. Chester and M. Tudbury. *Basics of induction heating.* John F. Rider Publisher, Inc., New York, USA, 1960.
[124]	J. Barglik, A. Smagor and A. smalcerz. *Analysis of coupled electromagnetic and temperature fields in contour induction hardening system for gear wheels*, International Scientific Colloquium, Modelling for

	Electromagnetic processing, Hannover, September 2014.
[125]	F. P. Incropera and D. P. DeWitt. *Fundamentals of Heat and Mass Transfer, Fourth Edition, printed in the United States of America,* 1996.
[126]	[E. Rapoport and Y. Pleshivteva. *Optimal control of induction heating processes*. Taylor & Francis Group, LLC, 2007.
[127]	Jian Tain. *Variable Frequency Asymmetrical PMW for Half-Bridge Resonant Induction Cookers*. Doctoral Thesis. Ilmenau. ISLE (c), 2008.
[128]	F. W. Curist. *High Frequency Induction Heating, first Edition. New York: McGraw-Hill Book Company*. Lindsay Publications Inc, 1987.
[129]	Maxwell 3D User's Guide, Ansoft Corporation. 225 West Station Square Drive Suite 200, Pittsburgh, PA 15219USA 2009.
[130]	U. Lüdtke. *Induktionserwärmung-Energietechnisches Praktikum (Versuchs-Nr.: EEW 2).* Technische Universität Ilmenau Fakultät für Elektrotechnik und Informationstechnik, 2014.
[131]	R. Lundin. *Handbook Formula for the Inductance of a Single-Layer Circular Coil*. Proc. IEEE, Vol. 73, pp. 1428-1429, 1985.
[132]	A. Attab, H. Zeroug and B. Meziane. Resonant Inverter power and coil parameters determination for metal surface hardening, IEEE, METC-0375, 2015.
[133]	S. S. A, H. p. wai and N. N. Soe. Design Calculation and Performance Testing of Heating Coil in Induction Surface Hardening Machine. International Scholarly and Scientific Research & Innovation, 2(6) 2008.

A List of Publications

[1] M. Ali and S. Ajib. Energy Analysis and Modelling Study of Combined Activated Carbon-Silica Gel/Methanol Adsorption Ice Production System. Global Journal of Energy Technology Research Updates, 2016, 3, 1-22.

[2] M. Ali, S. Ajib and Ch. Karcher. Enhancing the amount of cold produce using two different adsorbents together in the Adsorption Ice Production AIP System. Global Journal of Energy Technology Research Updates, 2017, 4, 9-25.

[3] M. Ali, Ch. Karcher and U. Lüdtke. Numerical and Mathematical Modelling of Induction Heating in Adsorption Refrigeration Systems. Workshop Elektroprozesstenik 5.-6. Oktober 2017.

[4] M. Ali, S. Ajib and Ch. Karcher and U. Lüdtke. Numerical and Analytical Modelling of Induction Heating in Silica Gel/Methanol Adsorption Cold Production System. Modern Environmental Science and Engineering, MESE20180507-2, 2018.

Erklärung

Ich versichere, dass ich die vorliegende Arbeit ohne unzulässige Hilfe Dritter und ohne Benutzung anderer als der angegebenen Hilfsmittel angefertigt habe. Die aus anderen Quellen direkt oder indirekt übernommenen Daten und Konzepte sind unter Angabe der Quelle gekennzeichnet.

Bei der Auswahl und Auswertung folgenden Materials haben mir die nachstehend aufgeführten Personen in der jeweils beschriebenen Weise unentgeltlich geholfen:

1. Die fachliche Betreuung der Arbeit erfolgt durch Prof. Dr. Christian Karcher und Prof. Dr. Salman Ajib (Fachgebiet Erneuerbare Energien & dezentrale Energieversorgung Hochschule Ostwestfalen-Lippe / Standort Höxter FB 8 Umweltingenieurwesen und Angewandte Informatik An der Wilhelmshöhe 44; 37671 Höxter).

2. Das wissenschaftliche Gespräch über das Kapitel 7 mit PD Dr.-Ing. habil. Ulrich Lüdtke.

3. Prof. Dr. Wessel Gehlker.
   Praktika Untersuchung an einer Adsorptionskältemaschine: Hochschule Holzminden/ Fachgebiet: Strömungslehre, Heizungs- und Energietechnik.

Weitere Personen waren an der inhaltlich-materiellen Erstellung der vorliegenden Arbeit nicht beteiligt. Insbesondere habe ich hierfür nicht die entgeltliche Hilfe von Vermittlungs-bzw. Beratungsdiensten (Promotionsberater oder anderer Personen) in Anspruch genommen. Niemand hat von mir unmittelbar oder mittelbar geldwerte Leistungen für Arbeiten erhalten, die im Zusammenhang mit dem Inhalt der vorgelegten Dissertation stehen.

Die Arbeit wurde bisher weder im In- noch im Ausland in gleicher oder ähnlicher Form einer Prüfungsbehörde vorgelegt.

Ich bin darauf hingewiesen worden, dass die Unrichtigkeit der vorstehenden Erklärung als Täuschungsversuch bewertet wird und gemäß § 7 Abs. 10 der Promotionsordnung den Abbruch des Promotionsverfahrens zur Folge hat.

Ilmenau, den 04.07.2018

(Ort, Datum) *(Unterschrift)*